Precise Predictions for Higgs Physics in the Next-to-Minimal Supersymmetric Standard Model (NMSSM)

Dissertation zur Erlangung des Doktorgrades
an der Fakultät für Mathematik, Informatik und Naturwissenschaften
Fachbereich Physik der Universität Hamburg

vorgelegt von

Peter Drechsel

geboren am 28.01.1985 in Zwickau

Hamburg
2016

Folgende Gutachter empfehlen die Annahme der Dissertation:

Gutachter der Dissertation und Disputation:	Prof. Dr. Georg Weiglein
	Prof. Dr. Géraldine Servant
Gutachter der Disputation:	Prof. Dr. Peter Schleper
	Dr. Thomas Konstandin
Vorsitzender der Prüfungskommission:	Prof. Dr. Günter Sigl
Tag der Disputation:	20. Januar 2016

Abstract

Within this thesis a precise mass-prediction for the Higgs fields of the Next-to-Minimal Supersymmetric Standard Model (NMSSM) is obtained with Feynman-diagrammatic methods. The results are studied numerically for sample scenarios that are in agreement with current New Physics searches at the LHC. Furthermore a comparison between the obtained results and different calculations is performed as a first step in order to obtain an estimation for the theoretical uncertainties of the Higgs-mass prediction in the NMSSM.

The precise mass-prediction includes the full NMSSM one-loop corrections supplemented with the dominant and sub-dominant two-loop corrections within the Minimal Supersymmetric Standard Model (MSSM). These include contributions at the orders $\mathcal{O}(\alpha_t\alpha_s, \alpha_b\alpha_s, \alpha_t^2, \alpha_t\alpha_b)$, as well as a resummation of leading and subleading logarithms from the top/scalar top sector. Higher-order corrections are essential for the NMSSM in order to provide a Higgs particle that is consistent with the available data, including the observed neutral, $\mathcal{CP}$-even Higgs field with a mass of about 125 GeV. We explored the validity of the applied approximation at the two-loop level and found that it is reliable for a wide range of scenarios within the NMSSM. This is especially true for the mass of the observed (MS)SM-like Higgs field. The result of this work will be included in a future extension of the program `FeynHiggs`.

We also compared our results with the program `NMSSMCalc` that also performs a Feynman-diagrammatic calculation of the Higgs-masses with a slightly different renormalization scheme. The comparison reveals that for the mass of the (MS)SM-like Higgs field the genuine NMSSM-effects induced by the choice of the renormalization scheme are by far minor compared to similar effects observed in the MSSM.

Kurzdarstellung

In dieser Arbeit wird unter Verwendung von Feynman-Diagrammen eine Präzisions-vorhersage für die Massen der Higgs-Felder im Nächstminimalen Supersymmetrischen Standardmodell (NMSSM) erarbeitet. Die Ergebnisse werden numerisch ausgewertet für verschiedene Beispielszenarien, welche im Einklang stehen mit den aktuellen Suchen nach neuer Physik am LHC. Darüber hinaus wird ein Vergleich angestellt zwischen den erhaltenen Ergebnissen und vergleichbaren Berechnungen als ein erster Schritt zur Abschätzung der theoretischen Unsicherheit der Higgs-Massenvorhersage im NMSSM.

Die Präzisionsvorhersage für die Higgsmassen berücksichtigt die vollständigen Ein-schleifen-Korrekturen ergänzt durch führende und nächstführende Zweischleifen-Kor-rekturen aus dem Minimalen Supersymmetrischen Standardmodell (MSSM). Diese beinhalten sowohl Beiträge der Ordnungen $\mathcal{O}(\alpha_t\alpha_s, \alpha_b\alpha_s, \alpha_t^2, \alpha_t\alpha_b)$, als auch eine Re-summation von führenden und nächstführenden Logarithmen aus dem Top/skalaren Top-Sektor. Korrekturen höherer Ordnung sind essentiell für die Existenz eines mit den experimentellen Daten konsistentes Higgs-Feldes im NMSSM. Dies gilt im besonderem Maße für die Masse des beobachteten neutralen, $\mathcal{CP}$-geraden Higgs-Feld mit einer Masse von ungefähr 125 GeV. Wir haben in dieser Arbeit die angewandte Approximation der Zweischleifen-Beiträge untersucht mit dem Ergebnis, dass diese für einen großen Parameterbereich des NMSSM verlässlich ist. Dies gilt in beson-derem Maße für die Masse des beobachteten (MS)SM-artigen Higgs-Feldes. Die Ergebnisse dieser Arbeit werden Teil der zukünftigen Erweiterung des Programms `FeynHiggs` sein.

Darüber hinaus wird unser Ergebnis verglichen mit dem Programm `NMSSMCalc`, welches ebenfalls eine Feynman-diagrammatische Berechnung der Higgs-Massen mit einem leicht verschiedenen Renormierungsschema enthält. Der Vergleich zeigt, dass für die Massenvorhersage des (MS)SM-artigen Higgs-Feldes reine NMSSM-Effekte, erzeugt durch die Wahl des Renormierungsschemas, bedeutend geringer sind als vergleichbare Effekte, die im MSSM beobachtet wurden.

Contents

1 Introduction

The first observation of a Higgs signal in 2012 [1,2] represented a huge success for the description of electroweak symmetry breaking. While the Higgs particle and its role in the process of electroweak symmetry breaking within the Standard Model of particle physics (SM) [3–5] has been postulated almost 50 years earlier by François Englert, Robert Brout and Peter Higgs [6–9], it evaded detection at previous experiments. With the now observed Higgs signal any model, which describes electroweak physics, needs to provide a state that can be identified with it. While within the present experimental uncertainties the properties of the observed state are compatible with the predictions of the SM, many other interpretations are possible as well, in particular as a Higgs boson of an extended Higgs sector.

In the Minimal Supersymmetric Standard Model (MSSM), see e.g. [10,11], the number of particle degrees of freedom is doubled by predicting two scalar partners for all SM fermions, as well as fermionic partners to all bosons. The scalar Higgs sector is extended by an additional Higgs-doublet in order to give mass to all SM fermions. In the $\mathcal{CP}$-conserving MSSM the observed Higgs is a linear combination of the $\mathcal{CP}$-even scalar Higgs fields. For scenarios with one decoupled, heavy $\mathcal{CP}$-even Higgs, the observed state is the lighter of both. Although the mass of the lightest $\mathcal{CP}$-even Higgs field in the MSSM is bound from above by M_Z, the MSSM Higgs-masses receive potentially large higher-order corrections. These corrections can lift the mass up and thus provide a SM-like state with a mass at around the measured value of 125 GeV [12].

The Next-to-Minimal Supersymmetric Standard Model (NMSSM) and its variants [13–19] represent a minimal supersymmetric theory with an extended Higgs sector by one singlet superfield compared to the MSSM. The two additional scalar degrees of freedom mix with the doublet Higgs-fields. However its admixture to the Higgs field observed at around 125 GeV is not allowed to be very large, since it does not couple to the gauge-bosons. As in the MSSM potentially large higher-order corrections appear, that are necessary to provide a SM-like state with appropriate mass. In order to allow for a precise prediction for the Higgs masses in the NMSSM the calculation of higher-order corrections is necessary.

Within the NMSSM several codes exist that calculate the Higgs masses in the pure $\overline{\text{DR}}$ scheme with different two-loop contributions. Amongst these codes SPheno [20, 21] incorporates the most complete results at the two-loop level, including two-loop contributions from the fermion/sfermions, two-loop corrections from the Higgs-sector in the gaugeless limit as well as mixed contributions of both sectors calculated with the results of the effective potential approach as outlined in [22]. The tools FlexibleSUSY [23], NMSSMTools [24, 25] and SOFTSUSY [26–28] include leading (supersymmetric) QCD (SQCD) corrections in the NMSSM from the top-/stop-

/bottom-/sbottom-sectors supplemented by certain MSSM corrections. Also the code `NMSSMCalc` allows to calculate Higgs masses in the NMSSM including leading (S)QCD corrections from the top-/stop-sector. In contrast to the the aforementioned codes the calculation implemented in `NMSSMCalc` [29] is obtained with Feynman-diagrammatic methods with the option to choose between the on-shell and $\overline{\text{DR}}$ renormalisation schemes in the top-/-stop-sector.

The results presented in this thesis will provide an additional calculation with Feynman-diagrammatic methods that will be included in the code `FeynHiggs` [30–36] as a first step to extend this code to the NMSSM, labelled `NMSSM-FeynHiggs` in the following. The presented results differ from the pure $\overline{\text{DR}}$ calculations listed above by the use of a hybrid on-shell/$\overline{\text{DR}}$ renormalisation scheme. From `NMSSMCalc` it differs by approximating the two-loop contributions by their known MSSM counterparts, which are already implemented in `FeynHiggs`. The code `NMSSM-FeynHiggs` will be the only code that includes the resummation of large logarithms and thus improves the results of the Feynman-diagrammatic calculation for heavy supersymmetric partner-fields with masses beyond several TeV [37]. The code `NMSSM-FeynHiggs` will furthermore provide also the wave function normalisation factors of the NMSSM with the employed MSSM approximation for the two-loop contributions. The MSSM approximation of the two-loop contributions yields an accurate mass prediction for (MS)SM-like Higgs-fields for a wide range of parameters. For a light singlet-like Higgs-field the MSSM approximation for the two-loop sfermion-contributions is less reliable for certain parameter regions. However, in these regions two-loop corrections to the singlet mass from the Higgs-sector are expected to be larger than the sfermion contributions of the same loop-level.

Since the calculations implemented in the codes above contain at most partial two-loop contributions an estimate of the unknown higher-order effects is necessary to provide an estimate of the theoretical uncertainties of the Higgs-mass predictions. While such estimations exist for the calculation in the MSSM, see e.g. [32, 38], they are absent for the NMSSM calculation. While a first step for obtaining estimation of theoretical uncertainties for NMSSM Higgs-mass predictions has been performed in [39] for $\overline{\text{DR}}$ codes, the impact of different on-shell/$\overline{\text{DR}}$ renormalisation schemes has not been studied yet. A comparison between the preliminary code `NMSSM-FeynHiggs` and the public code `NMSSMCalc` shows that genuine NMSSM-effects from different prescriptions induce only small higher-order contributions, while a study of partial one-loop corrections suggest that the higher-order effects from missing two-loop contribution can be more significant for certain parameter regions.

Thesis outline

This thesis is structured as follows. In Chapter 2 an overview over the Standard Model and the supersymmetric extensions in form of the MSSM and the NMSSM is given. Chapter 3 will provide details about the treatment of higher-order corrections in supersymmetric theories in general and will discuss regularisation methods, renormalisation schemes, the definition of the wave function normalisation factors as well as the renormalisation group equations. The NMSSM Higgs sector will be discussed

in detail at the one- and two-loop level in Chapter 4. Subsequently the definition of the Higgs masses at higher-orders will be given in Chapter 5, including a description of the used methods and codes. In Chapter 6 the one-loop contributions will be divided into appropriate subsets and discussed separately. At the end of this chapter the discussion is extended to the implications for the two-loop contributions. Chapter 7 will give a brief overview over future implementations of NMSSM calculations into the public codes `FeynHiggs`, `FeynArts` and `FormCalc` based on the presented work. A numerical discussion of the obtained results takes place in Chapter 8. The numerical impact of partial NMSSM-contributions at the one-loop level will be discussed. The employed two-loop MSSM approximation will be compared to the full NMSSM result for the (S)QCD corrections from the top-/stop-sector implemented in `NMSSMCalc`. In the last Chapter 9 a detailed comparison between the codes `NMSSM-FeynHiggs` and `NMSSMCalc` will be presented in order to study higher-order effects induced by different renormalisation prescriptions. The study represents a first attempt to estimate theoretical uncertainties for NMSSM calculations in hybrid on-shell/$\overline{\text{DR}}$ renormalisation schemes. Finally, this thesis will conclude in Chapter 10.

2 The Standard Model and its Supersymmetric Extensions

The development of quantum-field theories (QFTs) during the 20th century provided a powerful tool for the description of elementary particles. They represent a combination of special relativity and quantum theory. At a classical level they connect the particles observed in nature with field degrees of freedom. After canonical quantisation of the theory the field degrees of freedom become operators. Demanding invariance of the action under local, (special) unitary transformations of these degrees of freedom leads to the description of the strong, weak and electromagnetic interactions. The best tested and accepted gauge theory describing these forces is called the Standard Model of Particle Physics (SM) [3–5]. It will be described in this chapter with the conventions used throughout this work. For a more detailed understanding of its properties and the definition of the mentioned quantities, a general $SU(N)$ invariant Yang–Mills theory [40] is discussed in the appendix in sec. A.2. After describing the SM its shortcomings will be outlined to motivate supersymmetric extensions of the SM. The Minimal Supersymmetric Standard Model (MSSM) and the $\mathbb{Z}_3$-invariant Next-to Minimal Supersymmetric Standard Model (NMSSM) will be described in more detail as such extensions and the conventions used in this work. A discussion of a general $SU(N)$ invariant Super Yang–Mills theory is given in the appendix in sec. A.3.

2.1 The Standard Model (SM)

The Standard Model of Particle Physics is a spontaneously broken gauge theory[1]. It successfully unifies the electromagnetic and weak interactions as one electroweak force and contains a description of the the strong interaction. Before spontaneous symmetry breaking the SM is invariant under a local gauge transformation of the groups $U(1)_Y \times SU(2)_\mathrm{L} \times SU(3)_\mathrm{c}$. After the $SU(2)_\mathrm{L} \times U(1)_Y$-symmetry is broken spontaneously to the $U(1)_\mathrm{em}$-symmetry of quantum electrodynamics (QED), massive fields can be described. The underlying procedure of spontaneous symmetry breaking is called the Brout–Englert–Higgs-mechanism (BEH mechanism) [6–9]. After spontaneous symmetry breaking the theory contains three massive vector fields and massive fermions. It is invariant under the group $U(1)_\mathrm{em} \times SU(3)_\mathrm{c}$.

---

[1]At the quantised level it is a BRST-invariant theory as described in sec. A.2.

2.1.1 Gauge Invariance

The generators of the groups $U(1)_Y$, $SU(2)_L$ and $SU(3)_c$ can be expressed by the matrices $Y/2$, $\boldsymbol{\sigma}_a/2$ and $\boldsymbol{\tau}_b/2$. The corresponding charges are called hypercharge, weak isospin and colour. They are called the hypercharge operator, the Pauli- and the Gell-Mann-matrices. Their commutation relations read

$$[Y,Y] = 0, \quad [\boldsymbol{\sigma}_a, \boldsymbol{\sigma}_b] = \mathrm{i}g_w \varepsilon_{abc} \boldsymbol{\sigma}_c, \quad [\boldsymbol{\tau}_a, \boldsymbol{\tau}_b] = \mathrm{i}g_s f_{abc} \boldsymbol{\tau}_c. \tag{2.1}$$

The couplings of the three gauge groups are labelled g_Y, g_w and g_s, ε_{abc} and f_{abc} are the structure constants of $SU(2)_L$ and $SU(3)_c$, respectively. Since $U(1)_Y$ is an abelian group its structure constant is zero. Not all particles in the SM are charged under all three groups. Fermion fields charged under $SU(2)_L$ are denoted by an index L, fields uncharged under this group with an index R. Only quarks are charged under $SU(3)_c$. The 8 gauge bosons of $SU(3)_c$, labelled G_μ^a, describe the gluons, the massless mediators of the strong interaction. Thus $SU(3)_c$ is the gauge group of Quantum Chromodynamics (QCD). The 4 gauge bosons of the $U(1)_Y$ and $SU(2)_L$, labelled B_μ and W_μ^a, can not directly be identified with the mediators of the electroweak interaction. Only their linear combinations describe the observed W- and Z-boson and the photon. To describe the electroweak interaction, the BEH mechanism has to be applied.

2.1.2 Electroweak Symmetry-Breaking

The $SU(2)_L \times U(1)_Y$ invariance introduced in the last section forbids explicit mass terms for both bosons and Dirac-fermions. However, this is in contradiction with observations, since both fermions and gauge bosons of the electroweak interactions are observed as massive particles [41]. This fact hints to a breaking of the $U(1)_Y \times SU(2)_L$ invariance at the weak scale. After the spontaneous breaking a local symmetry under $U(1)_{em}$ has to remain to describe the massless photon of Quantum Electrodynamics (QED).

In the SM the introduced Higgs field is in the fundamental representation of $SU(2)_L$ and decomposed as follows,

$$\Phi = \begin{pmatrix} G^+(x) \\ v + \frac{1}{\sqrt{2}} \left[h(x) + \mathrm{i}G^0(x) \right] \end{pmatrix}. \tag{2.2}$$

Here the $\mathcal{CP}$-even field h is physical and called the Higgs boson. The fields G^+ and G^0 represent the two electrically charged and the one neutral Goldstone modes. The Higgs potential defined in (A.23) for the SM reads

$$V_H^{SM}(\Phi) = \left[-\mu^2 |\Phi|^2 + \lambda |\Phi|^4 \right], \quad \mu, \lambda > 0, \tag{2.3}$$

and thus the vacuum expectation-value obtains the value

$$v = \sqrt{\frac{\mu^2}{2\lambda}}. \tag{2.4}$$

Inserting this value into the kinetic term of the Higgs field (A.25) gives rise to non-zero mass terms for the four vector bosons of $U(1)_Y$ and $SU(2)_{\mathrm{L}}$. However, these massive fields are not observed in nature. They mix into the massless photon field A of QED as well as the massive neutral and charged vector bosons Z_μ and $W_\mu^\pm$ of the weak force. They are obtained by the linear combinations

$$\begin{pmatrix} W_\mu^+ \\ W_\mu^- \end{pmatrix} = \frac{1}{\sqrt{2}} \begin{pmatrix} 1 & -\mathrm{i} \\ 1 & \mathrm{i} \end{pmatrix} \begin{pmatrix} W_{1,\mu} \\ W_{2,\mu} \end{pmatrix}, \quad \begin{pmatrix} Z_\mu \\ A_\mu \end{pmatrix} = \begin{pmatrix} \cos\vartheta_w & -\sin\vartheta_w \\ \sin\vartheta_w & \cos\vartheta_w \end{pmatrix} \begin{pmatrix} W_{3,\mu} \\ B_\mu \end{pmatrix}. \tag{2.5}$$

The conventions follow those of the calculations implemented in the tool `FeynHiggs` [30–36]. It differs from the convention used in [42] by the different sign of the weak mixing angle ϑ_w.

The A-Z mixing is parametrised by the weak mixing angle ϑ_w. This angle can be related to the coupling constants of $U(1)_Y$, $SU(2)_{\mathrm{L}}$ and $U(1)_{\mathrm{em}}$, g_Y, g_w and e, by

$$\sin\vartheta_w \equiv s_w = -\frac{g_Y}{\sqrt{g_Y^2 + g_w^2}}, \quad \cos\vartheta_w \equiv c_w = \frac{g_w}{\sqrt{g_Y^2 + g_w^2}}, \quad e = g_w s_w = g_Y c_w. \tag{2.6}$$

Expressing the mass matrices in analogy to (A.25) reveals only non-vanishing mass terms for the Z- and W-Bosons while the photon remains massless,

$$M_W = M_Z c_w = g_w v, \quad M_A = 0. \tag{2.7}$$

Dirac Fermions and their Mass Terms in the SM

After breaking the $SU(2)_{\mathrm{L}}$ symmetry spontaneously, Dirac mass-terms for the fermions, which would break the $SU(2)_{\mathrm{L}}$ symmetry explicitly otherwise, can be generated by couplings with the Higgs $SU(2)_{\mathrm{L}}$-doublet. In the SM with the assumption of massless neutrinos such couplings exist for the three generations of up- and down-type quarks and leptons, u, d and l. These couplings can be expressed in family space by the 3×3 Yukawa coupling-matrices Y_f and the right- and left-handed spinor fields. With the family indices i and j this reads

$$\mathcal{L}_{\mathrm{Yuk}} = \left(\bar{Q}_L^i \cdot \Phi^C \right) (Y_u)^{ij} \, u_R^j + \left(\bar{Q}_L^i \cdot \Phi \right) (Y_d)^{ij} \, d_R^j + \left(\bar{L}_L^i \cdot \Phi \right) (Y_l)^{ij} \, l_R^j. \tag{2.8}$$

Here $\Phi^C = \mathrm{i}\sigma_3 \phi^*$ represents the charge conjugated Higgs field and the dot denotes the $SU(2)_{\mathrm{L}}$-invariant product given in sec. A.1.3. Replacing the Higgs field by the vacuum expectation-value reveals the mass matrices. For the leptons the mass matrix reads

$$(m_l)^{ij} = v \, (Y_l)^{ij}. \tag{2.9}$$

The quark fields in the theory are not mass eigenstates. Each of the left- and right-handed fields can be transformed into mass eigenstates by a unitary matrix $\boldsymbol{U}_{L/R}^{f}$. Thus the mass matrices for the up- and down-type quarks reads

$$m_u = (U_L^u)^\dagger \, v Y_u U_R^u, \quad m_d = \left(U_L^d\right)^\dagger v Y_d U_R^d. \tag{2.10}$$

The rotation into mass eigenstates leads to the combination

$$V_{\text{CKM}} = (U_L^u)^\dagger \, U_R^d, \tag{2.11}$$

known as the Cabibbo-Kobayashi-Maskawa (CKM) matrix. A complex phase in this matrix provides the only source of $\mathcal{CP}$-violation in the SM. Flavour violation will be neglected in the following, the Yukawa coupling matrices will thus be considered diagonal.

2.1.3 Quantisation

In the SM the functionals C^a mentioned in sec. A.28 are given for the physical vector fields A_μ, Z_μ and $W_\mu^\pm$. Assuming that the primed and unprimed gauge-fixing parameters are chosen equally ($\xi = \xi'$), evaluating (A.28) yields

$$C^A = \partial^\mu A_\mu, \ C^Z = \partial^\mu Z_\mu - \xi_Z M_Z G^0, \ C^\pm = \partial^\mu W_\mu^\pm \mp \mathrm{i}\xi_W M_W G^\pm, \ C^G = \partial^\mu G_\mu. \tag{2.12}$$

The mass matrix for the Goldstone bosons and ghost fields is thus diagonal. The mass parameters of the unphysical ghost fields and Goldstone bosons are equal to the corresponding gauge-boson masses up to a factor ξ_i,

$$M_{G^0}^2 = M_{u^Z}^2 = \xi_Z M_Z^2, \quad M_{G^\pm}^2 = M_{u^W}^2 = \xi_W M_W^2. \tag{2.13}$$

Unless stated otherwise the t'Hooft–Feynman gauge is applied throughout this work, where all gauge-fixing parameters are chosen to be equal to one ($\xi_A = \xi_Z = \xi_W = \xi_G = 1$).

2.1.4 Lagrangian and Particle Content

The covariant derivative of the SM reads

$$\boldsymbol{D}_\mu^{\text{SM}} = \mathbb{1}\partial_\mu + \mathrm{i}\boldsymbol{A}_\mu + \mathrm{i}\boldsymbol{Z}_\mu + \mathrm{i}\boldsymbol{W}_\mu^+ + \mathrm{i}\boldsymbol{G}_\mu \tag{2.14a}$$

with

$$\boldsymbol{A}_\mu = e\left(B_\mu \mathbb{1} + \frac{1}{2}W_{3,\mu}\sigma_3\right), \ \boldsymbol{Z}_\mu = e\left(-B_\mu \mathbb{1} + \frac{c_w}{2s_w}W_{3,\mu}\sigma_3\right), \tag{2.14b}$$

$$\boldsymbol{W}_\mu^\pm = \frac{e}{2s_w}\frac{1}{\sqrt{2}}\left(W_{1,\mu}\sigma_1 \mp W_{2,\mu}\sigma_2\right), \ \boldsymbol{G}_\mu = g_s G_\mu^a \frac{\tau^a}{2}. \tag{2.14c}$$

The full kinetic term for three generations of fermions and the gauge bosons reads

$$\mathcal{L}^{\mathrm{SM}}_{\mathrm{kin.}} = \sum_{i=1}^{3} \left(\bar{Q}^i_L \slashed{D}^{\mathrm{SM}} Q^i_L + \bar{L}^i_L \slashed{D}^{\mathrm{SM}} L^i_L + \bar{u}^i_R \slashed{D}^{\mathrm{SM}} u^i_R + \bar{d}^i_R \slashed{D}^{\mathrm{SM}} d^i_R + \bar{l}^i_R \slashed{D}^{\mathrm{SM}} l^i_R \right)$$
$$+ \mathrm{Tr}\left[\boldsymbol{A}^{\mu\nu} \boldsymbol{A}_{\mu\nu} \right] + \mathrm{Tr}\left[\boldsymbol{Z}^{\mu\nu} \boldsymbol{Z}_{\mu\nu} \right] + \left(\mathrm{Tr}\left[\boldsymbol{W}^{+,\mu\nu} \boldsymbol{W}^-_{\mu\nu} \right] + \mathrm{h.c.} \right) + \mathrm{Tr}\left[\boldsymbol{G}^{\mu\nu} \boldsymbol{G}_{\mu\nu} \right]$$
$$(2.15)$$

with the trace over the gauge indices as defined in (A.22). The left-chiral fermion doublets of quark and lepton/neutrino fields are denoted by

$$Q^i_L = \begin{pmatrix} u^i_L \\ d^i_L \end{pmatrix} \text{ and } L^i_L = \begin{pmatrix} \nu_{l^i,L} \\ l^i_L \end{pmatrix}. \tag{2.16}$$

The right-chiral fields are denoted with small letters u_R, d_R and l_R for the up- and down-quark, and the leptons. Neutrinos are considered massless throughout this work, thus no right-chiral neutrino fields exists.

The Lagrangian of the SM is formed by the sum of the parts mentioned in this section and the appendix A.2,

$$\mathcal{L}^{\mathrm{SM}} = \mathcal{L}^{\mathrm{SM}}_{\mathrm{kin}} + \mathcal{L}^{\mathrm{SM}}_{\mathrm{Yuk}} + \mathcal{L}^{\mathrm{SM}}_{\mathrm{ghost}} + \mathcal{L}^{\mathrm{SM}}_{\mathrm{fix}}. \tag{2.17}$$

It describes the dynamics and interactions of the particles listed in tab. 2.1.

type	field	$Y/2$	I_3	field	group	generators	index
leptons/ neutrinos	L^i_L	$-1/2$	$\pm 1/2$	B_μ	$U(1)_Y$	Y	
	e^i_R	-1	0	W^a_μ	$SU(2)_{\mathrm{L}}$	σ_a	$\{1,2,3\}$
	$\nu_{l^i,L}$	0	$+1/2$	G^a_μ	$SU(3)_{\mathrm{c}}$	τ_a	$\{1,\dots,8\}$

type	field	$Y/2$	I_3	type	field	$Y/2$	$\sigma_3/2$
quarks	Q^i_L	$1/6$	$\pm 1/2$	Higgs	h	$1/2$	$-1/2$
	u^i_R	$2/3$	0				
	d^i_R	$-1/3$	0				

Table 2.1: Matter fields of the SM before electroweak symmetry-breaking. The symbols denote the eigenvalues of the operators for the hypercharge Y and the weak isospin I_3.

2.1.5 Shortcomings of the SM

In spite of the successful description of electroweak and strong interactions the SM fails to provide a description of all phenomena observed in nature, among that it lacks a description of gravity. Due to this shortcoming the SM can be interpreted at most as an effective theory [43] that is only valid up to the scale where gravitational interactions are of relevance. The scale of gravity is usually associated with the Planck scale $M_{\mathrm{P}} = 10^{19}$ GeV. Above this scale a full theory, which includes gravity,

is needed. The couplings of the SM at the electroweak scale associated with M_W would then be predictions of the full theory.

The unified description of the electromagnetic and weak interactions at the weak scale motivates to attempt that a unified description of the electroweak and strong interactions described by a grand unified theory (GUT) exists at a scale $M_{\mathrm{GUT}} < M_{\mathrm{P}}$. The description of the unified interactions would be described by one gauge group. This assumption however implies that the couplings g_Y, g_w and g_s have the same value at M_{GUT}, which is only possible if additional matter is added to the SM [44].

In the treatment of the SM as an effective theory the Higgs mass would be a prediction of the full theory above M_{P}. At M_{P}, the running Higgs mass has to match the Higgs mass in the full theory. If the full theory contains fermions with a mass of $\approx M_{\mathrm{P}}$ that couple to the Higgs, however, their contributions to the Higgs self-energy are proportional to M_{P}^2 and thus would be very large. Since the Higgs mass in the SM was measured with around 125 GeV very large cancellations have to occur between the bare self-energies and their counterterms to arrive at this low mass in the on-shell scheme. This cancellation has to be fine-tuned in order to arrive from contributions of $\mathcal{O}(M_{\mathrm{P}}^2)$ at a mass of the order of $\mathcal{O}(M_Z^2)$. The large gap between the two scales has to be bridged by precise cancellations. Even in the absence of additional, heavy fermions a large gap exists between the mass scales of the SM particles and any new particles with masses around M_{P}. This is know as the "hierarchy problem".

It is implied by astrophysical observations that only 5% of the energy content of the universe is made of SM matter. Dark Matter (DM) and Dark Energy (DE) constitute 27% and 68% [45], respectively, of the matter content of the universe. Any candidate for DM has to be stable on cosmological time scales and is only allowed to interact weakly. None of the SM particles is a viable DM candidate under this constraints[2]. Furthermore, additional sources of $\mathcal{CP}$-violation beyond the single complex phase in the CKM matrix are necessary in order to explain the observed matter-antimatter asymmetry in the universe and to meet the Sakharov conditions [49].

2.2 Minimal Supersymmetric Standard Model

In the Minimal Supersymmetric Standard Model (MSSM) [10, 11] the Poincaré symmetry of the SM is extended by one fermionic generator ($N = 1$ supersymmetry). The gauge groups of the MSSM are identical to the SM. For each fermion in the SM a scalar superpartner, a sfermion, and for each SM boson a fermionic superpartner, a bosino, is thus introduced.

2.2.1 Motivation

Supersymmetric theories cure several shortcomings of non-supersymmetric theories. The hierarchy problem is directly addressed by supersymmetry: Scalar self-energies

---

[2]Although neutrinos are weakly interacting, massive [46, 47] particles, they are too light to account for more than a small fraction of dark matter [48].

are protected against quadratic contributions due to a non-renormalisation theorem [50–55]. This property is preserved in softly-broken supersymmetric theories like the MSSM [56], if the difference between the mass of the heavier fermions and their superpartners is smaller than or of the order of the Higgs mass. The invariance of a theory under local supersymmetry provides a connection to general relativity [57].

As an extension of the SM, in the MSSM a unification of the three gauge-couplings g_Y, g_w and g_s at a scale M_{GUT} is possible. In this case the superpartner masses are typically of several TeV.

In addition the MSSM can provide a possible cold dark matter candidate. If the lightest supersymmetric partner field is stable, electrically neutral and only weakly charged it can serve as a candidate for non-baryonic dark matter [58,59].

For certain scenarios it is possible starting from universal boundary condition on the high scale to arrive at a negative value of the squared Higgs mass $m_h^2(M_{\mathrm{SUSY}})$ at the mass scale of the supersymmetric partner fields M_{SUSY}, which leads to radiative electroweak symmetry-breaking [60]. In such scenarios the Higgs potential obtains a non-zero vacuum expectation-value that leads to spontaneous breaking of the electroweak symmetry.

2.2.2 Chiral Superfields for SM Fields

For each SM fermion a chiral superfield, denoted with a hat, is introduced, which contains the left- and right-handed SM fermion in the Weyl representation and its superpartners as component fields. The introduced fields and components are outlined in tab. 2.2. The scalar superpartners are denoted by an additional letter s in front of the name of its SM partner. E.g. the partners of the top are called stops.

field	scalar	fermion	field	scalar	fermion
$\hat{Q}_i$	$\tilde{Q} = \left(\tilde{u}_L^i, \tilde{d}_L^i\right)^{\mathrm{T}}$	$Q = \left(u_L^i, d_L^i\right)^{\mathrm{T}}$	$\hat{u}_i$ $\hat{d}_i$	$\tilde{u}_R^i$ $\tilde{d}_R^i$	u_R^i d_R^i
$\hat{L}_i$	$\tilde{L} = \left(\tilde{\nu}_L^i, \tilde{l}_L^i\right)^{\mathrm{T}}$	$L = \left(\nu_L^i, l_L^i\right)^{\mathrm{T}}$	$\hat{l}_i$	$\tilde{l}_R^i$	l_R^i

Table 2.2: Superfields and their component fields the MSSM with generation index i. In the left table the $SU(2)_{\mathrm{L}}$-doublet superfields are given, in the right table the $SU(2)_{\mathrm{L}}$-singlet superfields. The fermionic component fields are two-component Weyl-spinors. Since neutrinos are considered massless throughout this work, superfields for right handed neutrino fields are absent.

2.2.3 Super Gauge-Invariance

The vector superfield $\boldsymbol{V}$ can be expressed with the generators of the gauge groups,

$$\boldsymbol{V} = g_Y B \frac{Y}{2} + g_w W_a \frac{\boldsymbol{\sigma}_a}{2} + g_s G_b \frac{\boldsymbol{\tau}_b}{2}. \tag{2.18}$$

The left- and right-chiral field strength can be decomposed in the same way due to its construction from $\boldsymbol{V}$. The vector superfields B, W_a and G_b contain the component field as outlined in tab. 2.3.

group	field	vector	fermion
$U(1)_Y$	B	B_μ	$\widetilde{B}$
$SU(2)_{\mathrm{L}}$	W_a	W_a^μ	$\widetilde{W}_a$
$SU(3)_{\mathrm{c}}$	G_b	G_b^μ	$\widetilde{G}_b$

Table 2.3: Component fields of the vector superfields in the MSSM. The fermionic components for the superfields of $U(1)_Y$, $SU(2)_{\mathrm{L}}$ and $SU(3)_{\mathrm{c}}$ are called the bosino, the winos and the gluinos.

2.2.4 Electroweak Symmetry-Breaking and Soft-Breaking Terms

Two different Higgs doublets are needed to obtain the mass terms for the SM fermions given in (2.8), since a term mixing chiral and anti-chiral superfields is not allowed in the superpotential given in eq. (A.49). The two Higgs superfields will be called $\hat{H}_1$ and $\hat{H}_2$ and carry the hypercharge Y of -1 and 1, respectively. The term in the superpotential for these fields in the MSSM is given by

$$W_{\mathrm{Higgs}}^{\mathrm{MSSM}} = \mu \; \hat{\mathcal{H}}_2 \cdot \hat{\mathcal{H}}_1. \tag{2.19}$$

The D-terms from the kinetic term and the F-terms contribute to the Higgs potential. If the scalar component fields of $\hat{\mathcal{H}}_1$ and $\hat{\mathcal{H}}_2$ are to obtain non-vanishing vacuum expectation-values v_1 and v_2 it is necessary to add the soft breaking terms,

$$\mathcal{L}_{\mathrm{soft}}^{\mathrm{Higgs,\ MSSM}} = -m_1^2 \left|\mathcal{H}_1\right|^2 - m_2^2 \left|\mathcal{H}_2\right|^2 - \left[b_{12}\mu\left(\mathcal{H}_2 \cdot \mathcal{H}_1\right) + \mathrm{h.c.}\right]. \tag{2.20}$$

With these additions the Higgs potential of the MSSM is given by

$$V_{\mathrm{H}}^{\mathrm{MSSM}} = m_1^2 \left|\mathcal{H}_1\right|^2 + m_2^2 \left|\mathcal{H}_2\right|^2 + \mu\left(\mathcal{H}_2 \cdot \mathcal{H}_1\right) + \left[b_{12}\mu\left(\mathcal{H}_2 \cdot \mathcal{H}_1\right) + \mathrm{h.c.}\right]$$
$$+ \frac{1}{8}\left(g_1^2 + g_2^2\right)\left(\left|\mathcal{H}_1\right|^2 + \left|\mathcal{H}_2\right|^2\right)^2 + \frac{1}{2}g_2^2 \left|\mathcal{H}_1^\dagger \mathcal{H}_2\right|^2. \tag{2.21}$$

The scalar components $\mathcal{H}_1$ and $\mathcal{H}_2$ can be expanded around their vacuum expectation-values by

$$\mathcal{H}_1 = \begin{pmatrix} v_1 + \frac{1}{\sqrt{2}}\left(\phi_1 - i\chi_1\right) \\ -\phi_1^- \end{pmatrix}, \quad \mathcal{H}_2 = \begin{pmatrix} \phi_2^+ \\ v_2 + \frac{1}{\sqrt{2}}\left(\phi_2 + i\chi_2\right) \end{pmatrix}. \tag{2.22}$$

Here the fields ϕ_i are the $\mathcal{CP}$-even, χ_j the $\mathcal{CP}$-odd and $\phi_k^\pm$ the charged scalar fields. The sum $v^2 = v_1^2 + v_2^2$ of the squared values for v_1 and v_2 is determined by the minimisation conditions of the Higgs potential. The Higgs-sector fields and the Higgs

potential will be discussed for the Next-to-Minimal Supersymmetric Standard Model (NMSSM) in sec. 2.3. Both doublets contribute to the masses of the gauge bosons, that read

$$M_W = M_Z c_w = g_w \sqrt{v_1^2 + v_2^2}. \tag{2.23}$$

Mass Terms for Fermions and Sfermions in the MSSM

The field $\mathcal{H}_2$ gives mass to the up-type fermions/sfermions, the field $\mathcal{H}_1$ gives mass to the down-type fermions/sfermions and leptons/sleptons. The superpotential for these mass terms is given by

$$W_{\text{Yukawa}} = \sum_{i=1}^{3} \left(\hat{Q}_{\text{L}}^i \cdot \hat{H}_2 \right) Y_u \hat{u}_{\text{R}}^i - \left(\hat{Q}_{\text{L}}^i \cdot \hat{H}_1 \right) Y_d \hat{d}_{\text{R}}^i - \left(\hat{L}_{\text{L}}^i \cdot \hat{H}_1 \right) Y_l \hat{l}_{\text{R}}^i. \tag{2.24}$$

The Yukawa matrices for the MSSM can be written in terms of the ratio between the vacuum expectation-values and the SM matrices,

$$Y_u = Y_u^{(\text{SM})} \frac{1}{\sin \beta}, \quad Y_{d,l} = Y_{d,l}^{(\text{SM})} \frac{1}{\cos \beta}, \quad \tan \beta = \frac{v_2}{v_1}. \tag{2.25}$$

The introduction of additional soft-breaking terms for the sfermions allow them to have different masses than their SM counterparts. They read

$$\mathcal{L}_{\text{soft}}^{\text{scalar}} =$$
$$- \sum_{i=1}^{3} \left(M_{\tilde{Q}_L^i}^2 \left| \tilde{Q}_L^i \right|^2 + M_{\tilde{u}_R^i}^2 \left| \tilde{u}_R^i \right|^2 + M_{\tilde{d}_R^i}^2 \left| \tilde{b}_R^i \right|^2 + M_{\tilde{L}_L^i}^2 \left| \tilde{L}_L^i \right|^2 + M_{\tilde{l}_R^i}^2 \left| \tilde{l}_R^i \right|^2 \right)$$
$$- \sum_{i=1}^{3} \left[A_u^i Y_u^i \left(\tilde{Q}_L^i \cdot H_2 \right) \left(\tilde{u}_R^i \right)^* + A_d^i Y_d^i \left(\tilde{Q}_L^i \cdot H_1 \right) \left(\tilde{d}_R^i \right)^* + A_l^i Y_l^i \left(\tilde{L}_l^i \cdot H_1 \right) \left(\tilde{l}_R^i \right)^* + \text{h.c.} \right]. \tag{2.26}$$

The parameters $M_{\tilde{Q}_L^i}$ and $M_{\tilde{L}_L^i}$ are the soft mass terms for the partners of the left-handed quarks, leptons and neutrinos, while $M_{\tilde{u}_R^i}$, $M_{\tilde{d}_R^i}$ and $M_{\tilde{l}_R^i}$ are the soft masses for the superpartners of the right-handed up- and down-type quarks and leptons. The parameters A_u^i, A_d^i and A_l^i denote the trilinear breaking terms for the up- and down-type squarks and sfermions. The superscript i is the generation index.

The soft breaking terms for the gauginos of $U(1)_Y$, $SU(2)_{\text{L}}$ and $SU(3)_{\text{c}}$ read

$$\mathcal{L}_{\text{soft}}^{\text{fermion}} = -\frac{1}{2} \left(M_1 \tilde{B} \tilde{B} + M_2 \tilde{W}^a \tilde{W}^a + M_3 \tilde{G}^b \tilde{G}^b + \text{h.c.} \right). \tag{2.27}$$

The aforementioned soft parameters can in general be complex. Since only the $\mathcal{CP}$-conserving case will be discussed in this work, they are considered to be real.

2.2.5 R-**Parity**

An additional constraint on the number of allowed vertices is applied by introducing a global symmetry, the R-symmetry [61, 62]. It acts on the Grassmann coordinates in superfields,

$$\Phi\big(x, \vartheta, \bar\vartheta\big) \to \mathrm{e}^{(\mathrm{i}\alpha R)}\Phi\big(x, \mathrm{e}^{\mathrm{i}\alpha R_\Phi}\vartheta, \mathrm{e}^{-\mathrm{i}\alpha R_\Phi}\bar\vartheta\big). \tag{2.28}$$

The eigenvalues R_Φ are integer numbers, the angle α is an arbitrary real constant; the eigenvalue of a product of superfields is the sum of all eigenvalues. R-parity is a special case for $\alpha = \pi$. The eigenvalues for an SM component field are defined as 1, while the eigenvalues of the corresponding superpartner components are defined as -1. Demanding R-parity conservation forbids vertices that enable the violation of lepton- and baryon-number conservation.

2.2.6 **Lagrangian and Particle Content**

For each chiral and vector superfield a kinetic term as given in (A.48) exists in the MSSM,

$$\begin{aligned}
\mathcal{L}_{\text{kin}}^{\text{MSSM}} &= \mathcal{L}_{\text{kin,chir}}^{\text{MSSM}} + \mathcal{L}_{\text{kin,vec}}^{\text{MSSM}} + \mathcal{L}_{\text{kin,Higgs}}^{\text{MSSM}} \\
\mathcal{L}_{\text{kin,chir}}^{\text{MSSM}} &= \int \mathrm{d}^2\vartheta\mathrm{d}^2\bar\vartheta \sum_{i=1}^{3} \Big(\hat{Q}_i^\dagger \mathrm{e}^{2\boldsymbol{V}}\hat{Q}_i + \hat{u}_i^\dagger \mathrm{e}^{2\boldsymbol{V}}\hat{u}_i + \hat{d}_i^\dagger \mathrm{e}^{2\boldsymbol{V}}\hat{d}_i + \hat{L}_i^\dagger \mathrm{e}^{2\boldsymbol{V}}\hat{L}_i + \hat{e}_i^\dagger\, \mathrm{e}^{2\boldsymbol{V}}\hat{e}_i\Big) \\
\mathcal{L}_{\text{kin,Higgs}}^{\text{MSSM}} &= \int \mathrm{d}^2\vartheta\mathrm{d}^2\bar\vartheta \sum_{n=1}^{2} \hat{H}_n^\dagger \mathrm{e}^{2\boldsymbol{V}}\hat{H}_n, \quad \mathcal{L}_{\text{kin,vec}}^{\text{MSSM}} = \Big(\int \mathrm{d}^2\vartheta\, \boldsymbol{\mathcal{W}}_\alpha\boldsymbol{\mathcal{W}}^\alpha + \text{h.c.}\Big). \tag{2.29}
\end{aligned}$$

The terms from the superpotential of the MSSM are given by

$$\mathcal{L}_{\text{Suppot}}^{\text{MSSM}} = \int \mathrm{d}^2\vartheta\, W^{\text{MSSM}} + \text{h.c.}, \quad W^{\text{MSSM}} = W_{\text{Yukawa}} + W_{\text{Higgs}}^{\text{MSSM}}. \tag{2.30}$$

The Lagrangian for the MSSM is the sum of the aforementioned parts,

$$\mathcal{L}^{\text{MSSM}} = \mathcal{L}_{\text{kin}}^{\text{MSSM}} + \mathcal{L}_{\text{Suppot}}^{\text{MSSM}} + \mathcal{L}_{\text{soft}}^{\text{MSSM}} + \mathcal{L}_{\text{ghost}}^{\text{SM}} + \mathcal{L}_{\text{fix}}^{\text{SM}} \tag{2.31}$$

The unphysical ghost and the gauge parts are identical to the ones used in the SM. For the ghost and gauge-fixing parts only the contributions from the SM are considered in the R_ξ-gauge. The Goldstone bosons of the MSSM are linear combinations of the charged and $\mathcal{CP}$-odd scalar states from the Higgs doublets.

2.2.7 **Shortcomings of the MSSM**

However, the most severe shortcoming of supersymmetric extensions of the SM represents the fact that so far neither a superpartner field nor an additional Higgs field have been observed [41]. The search for superpartner fields remains as an important task for contemporary and future experiments.

The dimensionful parameter μ appears as a free parameter in the superpotential of the MSSM. In the SM all dimensionful parameters can be connected to electroweak symmetry-breaking, which also fixes their order to $\mathcal{O}(M_Z)$. An association between μ and electroweak symmetry-breaking as in the SM would conceptually be preferable. This is called the μ-problem.

The tree-level mass m_h^{tree} of the lightest $\mathcal{CP}$-even Higgs is bound from above by the Z-mass,

$$\left(m_h^{\text{tree}}\right)^2 < M_Z^2 \cos^2 2\beta. \tag{2.32}$$

In order to lift its value up to 125.1 GeV [12] large higher-order corrections are necessary. While this is possible, especially for scenarios with a large mass splitting between the stop superpartners, this re-introduces a "little hierarchy problem" between the masses of the two stops.

2.3 Next-to-Minimal Supersymmetric Standard Model

The NMSSM and its variants [13–19] represent a minimal supersymmetric theory with an extended Higgs sector. In the $\mathbb{Z}_3$-invariant NMSSM an additional chiral superfield $\hat{S}$, that is a singlet under all gauge groups, is added to the MSSM with a modified NMSSM superpotential. Its interactions are defined solely by the NMSSM superpotential. The singlet superfield adds a $\mathcal{CP}$-even and -odd Higgs field to the theory. The fermionic component of $\hat{S}$ serves as an additional neutralino.

2.3.1 Motivation

In the NMSSM two shortcomings of the MSSM are addressed directly: It solves the μ-problem and increases the upper bound for the mass of the lightest, doublet-like Higgs field compared to the MSSM.

The μ-term in the NMSSM is dynamically generated by an additional gauge-singlet scalar field that receives a vacuum expectation-value by electroweak symmetry-breaking. Thus in the initial superpotential no dimensionful parameter is present, as in the SM.

The upper bound on the tree-level mass m_h^{tree} of the lightest $\mathcal{CP}$-even doublet-Higgs field is lifted in the NMSSM compared to the MSSM by the new Higgs self-coupling parameter λ,

$$\left(m_h^{\text{tree}}\right)^2 < M_Z^2 \cos^2 2\beta + \lambda^2 v^2 \sin^2 2\beta. \tag{2.33}$$

In the NMSSM the magnitude of higher-order corrections necessary to lift the mass of the SM-like Higgs to its measured value is therefore decreased compared to the MSSM.

2.3.2 Differences to the Minimal Supersymmetric Standard Model

Compared to the superpotential of the MSSM (2.19) only the second part, which describes the interaction between the extended Higgs and Neutralino sectors is changed. Several possibilities exist to implement the singlet superfield $\hat{S}$. A good overview can be found in [17]. For this work only the $\mathbb{Z}_3$-invariant NMSSM will be discussed. This symmetry only allows terms with three superfields in the superpotential. The Superpotential of the $\mathbb{Z}_3$-invariant NMSSM reads

$$W_{\text{NMSSM}} = W_{\text{Yukawa}} + W_{\text{Higgs}}^{\text{NMSSM}}, \quad W_{\text{Higgs}}^{\text{NMSSM}} = \lambda\hat{S}\left(\hat{H}_2 \cdot \hat{H}_1\right) + \frac{1}{3}\kappa\hat{S}^3. \tag{2.34}$$

The parameters λ and κ are free parameters of the NMSSM and considered real in the $\mathcal{CP}$-conserving NMSSM. The new singlet fields are unable to couple to SM fermions and therefore do not affect their masses. The scalar component of the field $\hat{S}$ can acquire a vacuum expectation-value v_s, around which it can be expanded as

$$\mathcal{S} = v_s + \frac{1}{\sqrt{2}}\left(\phi_s + \mathrm{i}\chi_s\right). \tag{2.35}$$

The value v_s gives rise to an effective μ-term in the superpotential,

$$\lambda\hat{S}\left(\hat{H}_2 \cdot \hat{H}_1\right) = \mu_{\text{eff}}\,\hat{H}_2 \cdot \hat{H}_1 + \text{excitations},\ \ \mu_{\text{eff}} = \lambda v_s. \tag{2.36}$$

In the MSSM the quartic couplings between the components of the doublet Higgs fields $\mathcal{H}_1$ and $\mathcal{H}_2$ are determined solely by D-terms. They are proportionally to the squared of gauge couplings. In the NMSSM additional quartic coupling terms proportional to λ^2 are introduced due to F-terms from the superpotential. For the singlet all D-terms vanish. Its quartic couplings are determined solely by F-terms and thus λ and κ.

Compared to the soft breaking terms of the MSSM given in (2.26) only the last term involving the interaction between the Higgs fields is subject to a change in the NMSSM. For the new parameters λ and κ new breaking parameters A_λ and A_κ are introduced, and the scalar component of $\hat{S}$ receives a soft mass parameter m_s,

$$\begin{aligned} \mathcal{L}_{\text{soft}}^{\text{Higgs, NMSSM}} = &-m_1^2\left|\mathcal{H}_1\right|^2 - m_2^2\left|\mathcal{H}_2\right|^2 - m_s^2\left|\mathcal{S}\right|^2 \\ &-\left[\lambda A_\lambda \mathcal{S}\left(\mathcal{H}_2 \cdot \mathcal{H}_1\right) + \frac{1}{3}\kappa A_\kappa \mathcal{S}^3 + \text{h.c.}\right]. \end{aligned} \tag{2.37}$$

In the $\mathcal{CP}$-conserving NMSSM the new soft-breaking parameters are real. The Higgs potential of the NMSSM is given by the aforementioned parts and D-term contributions. It reads

$$\begin{aligned} V_{\text{H}}^{\text{NMSSM}} = &m_1^2\left|\mathcal{H}_1\right|^2 + m_2^2\left|\mathcal{H}_2\right|^2 + m_s^2\left|\mathcal{S}\right|^2 + \lambda^2\mathcal{S}^2\left(\left|\mathcal{H}_1\right|^2 + \left|\mathcal{H}_2\right|^2\right) \\ &+\left|\lambda\left(\mathcal{H}_2 \cdot \mathcal{H}_1\right) + \kappa\mathcal{S}^2\right|^2 + \left[\lambda A_\lambda\left(\mathcal{H}_2 \cdot \mathcal{H}_1\right) + \frac{1}{3}\kappa A_\kappa\mathcal{S}^3\text{h.c.}\right] \end{aligned}$$

$$+ \frac{1}{8} \left(g_1^2 + g_2^2 \right) \left(|\mathcal{H}_1|^2 + |\mathcal{H}_2|^2 \right)^2 + \frac{1}{2} g_2^2 \left| \mathcal{H}_1^\dagger \mathcal{H}_2 \right|^2 . \tag{2.38}$$

2.3.3 Lagrangian

The Lagrangian of the NMSSM is identical to the one of the MSSM given in (2.31) up to the different superpotential and the additional kinetic term for the singlet superfield,

$$
\begin{aligned}
\mathcal{L}_{\text{Suppot}}^{\text{NMSSM}} &= \int \mathrm{d}^2\vartheta \; W^{\text{NMSSM}} + \text{h.c.} \\
\mathcal{L}_{\text{kin,Higgs}}^{\text{NMSSM}} &= \int \mathrm{d}^2\vartheta \mathrm{d}^2\bar{\vartheta} \left(\sum_{n=1}^{2} \hat{H}_n^\dagger \mathrm{e}^{2\boldsymbol{V}} \hat{H}_n + \hat{S}^\dagger \hat{S} \right).
\end{aligned}
\tag{2.39}
$$

Note that the singlet superfield is not coupled to the vector superfields.

2.3.4 Masses of Gauginos, Higgsinos and Sfermions

The superpartner fields of the SM fields as obtained directly from the superfields are not observable. They can mix and have to be expressed in the mass basis. In the following the mass matrices for the superpartner fields will be given in the conventions of [31, 33] for the real case. Instead of the gauge couplings and the vacuum expectation-values of the Higgs fields the result is expressed in terms of the gauge boson masses and μ_{eff} where applicable.

Charginos

Charginos are mixed from the charged Higgsino and Winos. They obtain a Dirac mass-term. The mass matrix for the fields in the interaction basis reads

$$\mathbf{X} = \begin{pmatrix} M_2 & \sqrt{2} M_W \sin\beta \\ \sqrt{2} M_W \cos\beta & \mu_{\text{eff}} \end{pmatrix} . \tag{2.40}$$

It can be diagonalised by a biunitary transformation

$$\mathbf{X}^{(\text{diag})} = \mathbf{U}_{\chi^+}^* \mathbf{X} \mathbf{V}_{\chi^-}^\dagger = \text{diag}\{m_{\chi_1}, m_{\chi_2}\} . \tag{2.41}$$

A numerical singular value decomposition on $\mathbf{X}$ yields numerical results for the positive and real singular values, which can be identified with the two chargino masses. The decomposition also yields results for the matrices $\mathbf{U}$ and $\mathbf{V}$.

Neutralinos

The superpartner fields of the singlet mix with the other neutral gauginos and higgsinos. Thus there are five neutralinos in the NMSSM. Their mass matrix in

the interaction basis reads

$$\mathbf{Y} = \begin{pmatrix} M_1 & 0 & -M_Z s_W \cos\beta & M_Z s_W \sin\beta & 0 \\ 0 & M_2 & M_Z c_W \cos\beta & -M_Z c_W \sin\beta & 0 \\ -M_Z s_W \cos\beta & M_Z c_W \cos\beta & 0 & -\mu_{\text{eff}} & \lambda v_2 \\ M_Z s_W \sin\beta & -M_Z c_W \sin\beta & -\mu_{\text{eff}} & 0 & \lambda v_1 \\ 0 & 0 & \lambda v_2 & \lambda v_1 & -\sqrt{2}\kappa v_s \end{pmatrix}. \tag{2.42}$$

It can be diagonalised by a unitary transformation $\mathbf{N}_{\chi^0}$ by

$$\mathbf{Y}^{(\text{diag})} = \mathbf{N}_{\chi^0}^* \mathbf{Y} \mathbf{N}_{\chi^0}^\dagger = \text{diag}\Big\{m_{\chi_1^0}, m_{\chi_2^0}, m_{\chi_3^0}, m_{\chi_4^0}, m_{\chi_5^0}\Big\}. \tag{2.43}$$

Since $\mathbf{Y}$ is a 5×5 matrix, $\mathbf{N}_{\chi^0}$ is of the same rank. Since $\mathbf{Y}$ is hermitian, it can be diagonalised with only one unitary matrix $\mathbf{N}$. The numerical values for the mixing matrix and the neutralino masses are obtained by performing a numerical singular value decomposition on $\mathbf{Y}$.

Sfermions

The sfermions are mixed between the superpartners of the right- and left-handed SM fermions. The mass matrix for the fields in the interaction basis reads

$$\mathbf{M}_{\tilde{f}} = \begin{pmatrix} M_{\tilde{f}_{\text{L}}}^2 + m_f^2 + M_Z^2 \cos 2\beta (I_3^f - Q_f s_W^2) & m_f X_f \\ m_f X_f & M_{\tilde{f}}^2 + m_f^2 + M_Z^2 \cos 2\beta Q_f s_W^2 \end{pmatrix}, \tag{2.44}$$

with $(f, \tilde{f}, \tilde{f}_{\text{L}}) \in \{(u, \tilde{u}, \tilde{q}), (d, \tilde{d}, \tilde{q}), (e, \tilde{e}, \tilde{l})\}$ and $X_f = (A_f - \mu_{\text{eff}}\, t_{\tilde{f}}(\beta))$, where $t_{\tilde{f}}(\beta) = \tan\beta$ for sleptons and down-type squarks and $t_{\tilde{f}}(\beta) = \cot\beta$ for up-type squarks. The symbols I_3^f and Q_f denote the weak isospin and electric charge of the corresponding SM fermion.

Since the sfermion mass matrix is hermitian, it can be diagonalised by a unitary 2×2 matrix $\mathbf{U}_{\tilde{f}}$ given by

$$\mathbf{M}_{\tilde{f}}^{(\text{diag})} = \mathbf{U}_{\tilde{f}} \mathbf{M}_{\tilde{f}} \mathbf{U}_{\tilde{f}}^\dagger = \text{diag}\Big\{m_{\tilde{f}_1}^2, m_{\tilde{f}_2}^2\Big\}. \tag{2.45}$$

Throughout this work the mixing matrix will be parametrised by the real mixing angle $\theta_{\tilde{f}}$,

$$\mathbf{U}_{\tilde{f}} = \begin{pmatrix} \cos\theta_{\tilde{f}} & \sin\theta_{\tilde{f}} \\ -\sin\theta_{\tilde{f}} & \cos\theta_{\tilde{f}} \end{pmatrix}, \tag{2.46}$$

that depends on the mass hierarchy between the two stop masses. The elements of

the mixing matrix elements fulfil the relation

$$\left(\mathbf{U}_{\tilde{f}}\right)_{11}\left(\mathbf{U}_{\tilde{f}}\right)_{12} = \frac{m_f X_f}{m_{\tilde{f}_1}^2 - m_{\tilde{f}_2}^2}. \tag{2.47}$$

The mass eigenstates are given by

$$m_{\tilde{f}_{1,2}}^2 = m_f^2 + \frac{1}{2}\left[M_{\tilde{f}}^2 + m_f^2 + I_3^f M_Z^2 \cos 2\beta \right.$$
$$\left. \mp \sqrt{M_{\tilde{f}}^2 - M_{\tilde{f}}^2 + M_Z^2 \cos 2\beta(I_3^f - Q_f s_W^2) + 4_{,f}^2 \left|A_f - \mu_{\text{eff}}\, t_{\tilde{f}}(\beta)\right|^2}\right]. \tag{2.48}$$

2.3.5 Higgs Masses

The Higgs potential V_H contains all terms in the Lagrangian that emerge from terms proportional to arbitrary powers of Higgs fields. It is formed from by contributions from both the superpotential and the Kähler potential (A.48). Since $\hat{S}$ transforms as a singlet, the D-terms of the Higgs sector remain identical to the ones from the MSSM. In this work the vacuum expectation-values of the Higgs doublets (2.22) and the singlet (2.35), v_1, v_2 and v_s, are only allowed to be real. Rearranging V_H by powers of the fields leads to

$$V_{\mathrm{H}} = \ldots - T_{\phi_1}\phi_1 - T_{\phi_2}\phi_2 - T_{\phi_S}\phi_S \tag{2.49}$$
$$+ \frac{1}{2}\left(\phi_1, \phi_2, \phi_S\right)\mathbf{M}_{\phi\phi}\begin{pmatrix}\phi_1\\\phi_2\\\phi_S\end{pmatrix} + \frac{1}{2}\left(\chi_1, \chi_2, \chi_S\right)\mathbf{M}_{\chi\chi}\begin{pmatrix}\chi_1\\\chi_2\\\chi_S\end{pmatrix} + \left(\phi_1^-, \phi_2^-\right)\mathbf{M}_{\phi^\pm\phi^\pm}\begin{pmatrix}\phi_1^+\\\phi_2^+\end{pmatrix}$$
$$+ \cdots.$$

The coefficients linear in the fields are the tadpole coefficients. The ones bilinear in the fields are the mass matrices $\mathbf{M}_{\phi\phi}$, $\mathbf{M}_{\chi\chi}$ and $\mathbf{M}_{\phi^\pm\phi^\pm}$. In eq. (2.49) the Higgs potential is given in the interaction basis with the fields ϕ_i and $\phi_j^\pm$. A unitary transformation has to be applied in order to obtain physical fields in the mass basis. For the $\mathcal{CP}$-conserving case the mixing into mass eigenstates can be described at lowest order by the unitary transformations

$$\begin{pmatrix}H_1\\H_2\\H_3\end{pmatrix} = \mathbf{U}_{e(0)}\begin{pmatrix}\phi_1\\\phi_2\\\phi_s\end{pmatrix}, \quad \begin{pmatrix}A_1\\A_2\\G^0\end{pmatrix} = \mathbf{U}_{o(0)}\begin{pmatrix}\chi_1\\\chi_2\\\chi_s\end{pmatrix}, \quad \begin{pmatrix}H^\pm\\G^\pm\end{pmatrix} = \mathbf{U}_{c(0)}\begin{pmatrix}\phi_1^\pm\\\phi_2^\pm\end{pmatrix}. \tag{2.50}$$

The new fields correspond to the five neutral Higgs bosons H_i and A_j, the charged pair $H^\pm$ and the Goldstone bosons G^0 and $G^\pm$. For the interaction fields the Higgs mass-matrices are not diagonal. They are diagonalised at tree-level by the matrices $\mathbf{U}_{\{e,o,c\}(0)}$,

$$\mathbf{U}_{e(0)}\mathbf{M}_{\phi\phi}\mathbf{U}_{e(0)}^\dagger = \text{diag}\left(m_{H_1}^2, m_{H_2}^2, m_{H_3}^2\right), \tag{2.51a}$$

$$\mathbf{U}_{o(0)}\mathbf{M}_{\chi\chi}\mathbf{U}_{o(0)}^{\dagger} = \mathrm{diag}\left(m_{A_1}^2, m_{A_2}^2, 0\right), \tag{2.51b}$$

$$\mathbf{U}_{c(0)}\mathbf{M}_{\phi^{\pm}\phi^{\pm}}\mathbf{U}_{c(0)}^{\dagger} = \mathrm{diag}\left(m_{H^{\pm}}^2, 0\right), \tag{2.51c}$$

without the contributions from gauge-fixing sector. The explicit discussion of the Higgs mass-matrices and tadpoles will be given in chapter 4.

2.3.6 MSSM-Limit

The MSSM can be obtained as a limit of the NMSSM for

$$\lambda \to 0, \ \kappa \to 0, \ \mu_{\mathrm{eff}} = \mathrm{const.}, \ \frac{\lambda}{\kappa} = \mathrm{const.} \tag{2.52}$$

If κ maintains a finite value in this limit, the singlet and singlino sector decouples from the remaining fields. The result is the MSSM with a self-interacting singlet and singlino sector.

3 Higher-Order Corrections

The S-matrix element for the transition of an initial state labelled i into a final state labelled f can be written as

$$S_{fi} = \delta_{fi} + \mathrm{i}\,(2\pi)^4\,\delta^{(4)}(p_i - p_f)\mathcal{M}_{fi} \tag{3.1}$$

with the Kronecker-delta δ_{ij} and the invariant matrix element $\mathcal{M}_{fi}$. The four dimensional delta-function $\delta^{(4)}$ ensures momentum conservation between the initial and final states. An expansion of $\mathcal{M}_{fi}$ can be performed in powers of the appearing couplings. For a theory with one coupling g this expansion reads

$$\mathcal{M}_{fi} = \sum_{n=1}^{\infty} g^n \mathcal{M}_{fi}^{(n)}. \tag{3.2}$$

Each $\mathcal{M}_{fi}^{(n)}$ relates to a calculation at fixed order and is gauge-invariant independently. They involve the description of intermediate states that take part in the process $i \to f$. While the four dimensional delta-function in (3.1) secures momentum conservation for the external states, the momenta of the intermediate states are not necessarily fully determined by momentum-conservation. In order to consider these momenta consistently it is necessary to integrate over all possible values. The integration over all possible momenta leads to non well-defined expressions. In order to address this problem these integrals have to be regularised. By applying this procedure the integrals become well-defined quantities. This process is always connected to the introduction of an unphysical scale μ_r, that drops out only if the invariant matrix element $\mathcal{M}_{fi}$ is calculated at all orders. After regularisation it is possible for renormalisable theories to apply a renormalisation procedure that ensures that each of the $\mathcal{M}_{fi}^{(n)}$ remains well-defined after the regularisation procedure is reversed.

3.1 Regularisation

Several methods exist for regularisation. Amongst the most common ones are dimensional regularisation (DREG) [63, 64] and dimensional reduction (DRED) [65].

3.1.1 Dimensional Regularisation (DREG)

In order to regularise the divergent integrals all 4-dimensional quantities in the calculation are treated as D-dimensional objects, where D is an arbitrary real number, usually expressed as $D = 4 - 2\epsilon$ with the arbitrary real number ϵ. The limit $\epsilon \to 0$ restores the result in 4 dimensions. The change in dimensionality affects the measure

in integrations over momentum and spatial coordinates. For the bare invariant action of a theory with the coupling g and scalar field Ψ with mass m this leads to[1]

$$S = \mu_r^{D-4} \int \mathrm{d}^D x \, \mathcal{L}(g, m, \Psi). \tag{3.3}$$

In order to keep the dimension $\hbar$ for the invariant action the scale μ_r has to be absorbed by a redefinition of the couplings and fields of the theory.

The potentially ultraviolet-divergent loop-integrals in momentum space are well defined quantities in D dimensions. The one-loop integral of a function F over the momentum k can be expressed as a polynomial in ϵ,

$$\int \frac{\mathrm{d}^4 k}{(4\pi)^4} F(k) \rightarrow \mu_r^{4-D} \int \frac{\mathrm{d}^D k}{(4\pi)^D} F(k) = \Delta a_\Delta + a_0 + \epsilon a_1 + \mathcal{O}\!\left(\epsilon^2\right), \tag{3.4}$$

with the real coefficients a and the typical divergent factor Δ, which reads for dimensional regularisation

$$\Delta = \frac{1}{\epsilon} - \gamma_E + \ln 4\pi. \tag{3.5}$$

Here γ_E is the Euler-Mascheroni constant. The first term in eq. (3.5) corresponds to the divergent contribution in $D = 4$ dimensions. The remaining constant terms are introduced by performing the integration in D-dimensions. Any terms proportional to negative powers of ϵ have to cancel in the calculation of physical quantities. Any terms proportional to positive powers of ϵ vanish for $D \rightarrow 0$, but can cancel their power in ϵ with divergent terms in calculations beyond one-loop order.

One major disadvantage of dimensional regularisation is its explicit breaking of supersymmetry. Treating vector fields in D dimensions leads to D bosonic degrees of freedom, while the number of fermionic degrees of freedom remains unchanged. In a vector superfield consequently the number of fermionic degrees of freedom is not equal to the number of the degrees of freedom of the vector component-field, as supersymmetry requires. In order to avoid this problem either supersymmetric counterterms can be introduced [66,67] or a supersymmetry conserving regularisation method can be used.

3.1.2 Dimensional Reduction (DRED)

In this procedure only the momenta of the calculations are treated as D-dimensional objects, while the vector-fields remain 4-dimensional. The difference to dimensional regularisation only appears in fixed order calculations. At one-loop order the expansion in terms of ϵ outlined in eq. (3.4) remains unchanged. Dimensional reduction will be applied to all calculations performed in this work.

It has been shown that DRED conserves supersymmetry at one-loop order [64].

---

[1]Eq. (3.3) is understood for the bare quantities. With the notation of sec. 3.2 it reads $S_0 = \mu_r^{D-4} \int \mathrm{d}^D x \, \mathcal{L}_0(g_0, m_0, \Psi_0)$.

As of today the supersymmetry conserving properties of DRED at two-loop order are only known for special cases. For the calculations and results in this work the supersymmetry conserving property of DRED has been explicitly checked in [68].

3.2 Renormalisation

Renormalisation is a two-step process. At first a renormalisation transformation has to be applied to all fields and independent parameters of the theory. This introduces new parameters, the renormalisation constants. Their explicit form has to be fixed in a second step.

The renormalisation transformations for independent parameters of a theory with fields Ψ_0, coupling g_0 and mass m_0 read

$$g_0 \to g + \delta g, \quad m_0 \to m + \delta m, \quad \Psi_0 \to \sqrt{Z_\Psi}\Psi = \left(1 + \frac{1}{2}\delta Z_\Psi\right)\Psi \qquad (3.6)$$

The quantities with the subscript zero are the parameters and fields that are called unrenormalised or bare. The quantities without subscript are called renormalised. The quantities denoted with a δ are the renormalisation constants. Applying this procedure to the Lagrangian generates new terms that are denoted by $\mathcal{L}$ and $\delta\mathcal{L}$. While $\mathcal{L}$ depends only on the renormalised parameters and fields, the counterterm Lagrangian $\delta\mathcal{L}$ depends also on the renormalisation constants,

$$\mathcal{L}_0(g_0, m_0, \Psi_0) \to \mathcal{L}(g, m, \Psi) + \delta\mathcal{L}(g, m, \Psi; \ \delta g, \delta m, \delta Z_\Psi) = \hat{\mathcal{L}}(g, m, \Psi; \ \delta g, \delta m, \delta Z_\Psi). \tag{3.7}$$

Both $\mathcal{L}$ and $\delta\mathcal{L}$ are independent of the bare couplings and fields.

For the renormalisation of a vector field V in a gauge theory the gauge-fixing parameter ξ_V also has to be renormalised,

$$\xi_V \to \xi_V \left(1 + \frac{1}{2}\delta Z_{\xi_V}\right). \tag{3.8}$$

The divergent part of the counterterm for ξ_V, however, is fixed by gauge-symmetry relations of the theory [69] to

$$\delta\xi_V|^{\text{div.}} = \delta Z_V|^{\text{div.}}. \tag{3.9}$$

Here δZ_V is the field renormalisation constant for the vector field V.

In a second step after applying the renormalisation transformations the renormalisation constants have to be defined. Only after this step the renormalised parameters of the theory have a physical meaning. The divergent contributions of the renormalisation constants is defined such that the contributions from $\delta\mathcal{L}$ cancel all appearing regularised ultraviolet-divergences in physical observables. The finite contributions of the renormalisation constants can be defined arbitrarily in each renormalisation scheme. However, the physical meaning of the renormalised param-

eters is dependent on the finite contributions of their renormalisation constants and thus on the renormalisation scheme. For a fixed-order calculation, however, different renormalisation schemes can lead to different results. Two common renormalisation schemes, the on-shell and $\overline{\text{MS}}$-/$\overline{\text{DR}}$-scheme, are described in the following section.

3.2.1 On-Shell Scheme

It is possible to define the renormalisation constants for masses and fields such that the renormalised mass-parameters are the parameters of the classical Lagrangian. Furthermore it ensures, that in- and outgoing particles maintain correct in-shell properties. This scheme is called on-shell scheme. Depending on the Lorentz structure of the fields the on-shell conditions have a different form. An overview over this procedure in the SM can be found in [42][2]. Here the renormalisation conditions that are necessary for this work will be presented in their general form.

Scalar Fields

The on-shell renormalisation conditions for a single complex scalar field ϕ with the tree-level mass-parameter M_ϕ read

$$\text{Re}\hat{\Gamma}_{\phi^\dagger\phi}\left(k^2\right)\Big|_{k^2=M_\phi^2} \overset{!}{=} 0, \quad \lim_{k^2\to M_\phi^2}\frac{1}{k^2-M_\phi^2}\hat{\Gamma}_{\phi^\dagger\phi}\left(k^2\right) \overset{!}{=} 1. \tag{3.10}$$

The corresponding renormalised two-point functions at one-loop order reads

$$\text{i}\hat{\Gamma}_{\phi\phi}\left(k^2\right) = \text{i}\left(k^2-M_\phi^2\right) + \text{i}\Sigma_{\phi^\dagger\phi}\left(k^2\right) + \text{i}\left(k^2-M_\phi^2\right)\frac{1}{2}\left(\delta Z_\phi^\dagger + \delta Z_\phi\right) - \text{i}\delta M_\phi^2 \tag{3.11}$$

with the unrenormalised self energy $\Sigma_{\phi^\dagger\phi}(k^2)$ and the square of the external momentum k^2. The renormalisation conditions lead to expressions for the renormalisation constants appearing in eq. (3.11) that read

$$\delta M_\phi^{2,\text{OS}} = \text{Re}\Sigma_{\phi^\dagger\phi}\left(M_\phi^2\right), \quad \delta Z_\phi^{\text{OS}} = -\frac{\partial}{\partial k^2}\Sigma_{\phi^\dagger\phi}\left(k^2\right)\Big|_{k^2=M_\phi^2}. \tag{3.12}$$

The on-shell conditions in eq. (3.10) are formulated for an unstable particle. For a stable particle it is sufficient to impose both conditions only for the real part of the two-point functions instead.

Vector Fields

For the renormalisation of a vector field V with mass M_V the on-shell conditions read

$$\text{Re}\hat{\Gamma}_{\mu\nu}^V(q)\varepsilon^\nu(q)\Big|_{q^2=M_V^2} \overset{!}{=} 0, \quad \lim_{q^2\to M_V^2}\frac{1}{q^2-M_V^2}\text{Re}\hat{\Gamma}_{\mu\nu}^V\left(q\right)\varepsilon^\nu(q) \overset{!}{=} 0 \tag{3.13}$$

---

[2]Note the different sign convention for the weak angle between the reference and the calculation presented here. Furthermore the results in this reference only accounts for stable particles.

with the polarisation vector ε and momentum q of the external field. The corresponding renormalised two-point function at one-loop order reads

$$
\begin{aligned}
\mathrm{i}\hat{\Gamma}_{\mu\nu}^{V}(q) = \quad & \\
-\,\mathrm{i} & \left[\left(g_{\mu\nu} - \frac{q_\mu q_\nu}{q^2}\left(1 - \xi_V\right) \right) q^2 - g_{\mu\nu} M_V^2 \right] - \mathrm{i} \left[\left(g_{\mu\nu} - \frac{q_\mu q_\nu}{q^2} \right) \Sigma_{\mathrm{T}}^{V}(q^2) + \frac{q_\mu q_\nu}{q^2} \hat{\Sigma}_{\mathrm{L}}^{V}(q^2) \right] \\
-\,\frac{\mathrm{i}}{2} & \left[\left(g_{\mu\nu} - \frac{q_\mu q_\nu}{q^2}\left(1 - \xi_V\right) \right) q^2 - g_{\mu\nu} M_V^2 \right] \left(\delta Z_V^\dagger + \delta Z_V \right) \\
+\,\mathrm{i} & \left(g_{\mu\nu}\delta M_V^2 + \xi_V \frac{q_\mu q_\nu}{2} \delta Z_{\xi_V} \right).
\end{aligned}
\tag{3.14}
$$

with the unrenormalised transversal and longitudinal self energies $\Sigma_{\mathrm{T}}^{V}(q^2)$ and $\Sigma_{\mathrm{L}}^{V}(q^2)$. Since $q_\mu \varepsilon^\mu = 0$ this fixes only the mass and field renormalisation constants. They read

$$
\delta M_V^{2,\mathrm{OS}} = \mathrm{Re}\,\Sigma_{\mathrm{T}}^{V}\!\left(M_V^2\right), \quad \delta Z_V^{\mathrm{OS}} = -\frac{\partial}{\partial q^2}\mathrm{Re}\,\Sigma_{\mathrm{T}}^{V}\!\left(M_V^2\right)
\tag{3.15}
$$

Fermion Fields

For the renormalisation of a fermion field ψ with mass m_ψ the on-shell conditions read

$$
\mathrm{Re}\,\hat{\Gamma}_{\psi\psi}(p)u(p)\Big|_{q^2 = m_\psi^2} \overset{!}{=} 0, \qquad \lim_{p^2 \to m_\psi^2} \frac{\slashed{p} - m_\psi}{p^2 - m_\psi^2}\mathrm{Re}\,\hat{\Gamma}_{\psi\psi}\left(p\right) u(p) \overset{!}{=} \mathrm{i}u(p).
\tag{3.16}
$$

with the spinors u of the external field. The corresponding renormalised two-point function at one-loop order reads

$$
\mathrm{i}\hat{\Gamma}_{\psi\psi}(p) = \mathrm{i}(\slashed{p} - m_\psi) + \mathrm{i}\Sigma_{\psi\psi}(p) + \mathrm{i}(\slashed{p} - m_\psi)\delta Z_\psi - \mathrm{i}\delta m_\psi
\tag{3.17}
$$

with the unrenormalised self energy $\Sigma_{\psi\psi}$, which can be decomposed as

$$
\begin{aligned}
\Sigma_{\psi\psi}(p) &= \slashed{p}\,\Sigma_{\psi\psi}^{(\slashed{p})}(p) + m_\psi \Sigma_{\psi\psi}^{(S)}(p) \\
&= \slashed{p}\left[P_{\mathrm{L}}\Sigma_{\psi\psi}^{(\slashed{p},L)}(p) + P_{\mathrm{R}}\Sigma_{\psi\psi}^{(\slashed{p},R)}(p) \right] + m_\psi \left[P_{\mathrm{L}}\Sigma_{\psi\psi}^{(S,L)}(p) + P_{\mathrm{R}}\Sigma_{\psi\psi}^{(S,R)}(p) \right]
\end{aligned}
\tag{3.18}
$$

in electroweak theory. This leads to the mass renormalisation constants given by

$$
\delta m_\psi^{\mathrm{OS}} = \frac{1}{2}\mathrm{Re}\left[\Sigma_{\psi\psi}^{(\slashed{p},L)}(p) + \Sigma_{\psi\psi}^{(\slashed{p},R)}(p) + \Sigma_{\psi\psi}^{(S,L)}(p) + \Sigma_{\psi\psi}^{(S,R)}(p) \right]_{\slashed{p} = m_\psi}.
\tag{3.19a}
$$

For the field renormalisation constants of the left- and right-handed field in the on-shell scheme this yields

$$
\delta Z_\psi^{\mathrm{L,OS}} = -\mathrm{Re}\,\Sigma_{\psi\psi}^{(\slashed{p},L)}\!\left(p^2\right) - m_\psi^2 \left[\frac{\partial}{\partial p^2}\mathrm{Re}\left(\Sigma_{\psi\psi}^{(\slashed{p})}\!\left(p^2\right) + \Sigma_{\psi\psi}^{(S)}\!\left(p^2\right) \right) \right]_{p^2 = m_\psi^2}
\tag{3.19b}
$$

$$\delta Z_\psi^{\mathrm{R,OS}} = -\mathrm{Re}\Sigma_{\psi\psi}^{(\not{p},R)}\!\left(p^2\right) - m_\psi^2 \left[\frac{\partial}{\partial p^2}\mathrm{Re}\left(\Sigma_{\psi\psi}^{(\not{p})}\!\left(p^2\right) + \Sigma_{\psi\psi}^{(S)}\!\left(p^2\right)\right)\right]_{p^2=m_\psi^2}. \qquad (3.19c)$$

3.2.2 $\overline{\mathrm{MS}}$-/$\overline{\mathrm{DR}}$-Scheme

The $\overline{\mathrm{MS}}$-scheme denotes a modified minimal subtraction (MS) scheme using dimensional regularisation. In this scheme the renormalisation constants absorb only the divergent part and the constants that appear in the typical divergent factor given in eq. (3.5). The $\overline{\mathrm{DR}}$ renormalisation scheme refers to $\overline{\mathrm{MS}}$ with dimensional reduction as the regularisation procedure. Since only the $\overline{\mathrm{DR}}$ renormalisation scheme is used in the following, the superscript $\overline{\mathrm{MS}}$ will be dropped. In D dimensions a renormalisation constant reads at one-loop order

$$\delta g^{\overline{\mathrm{DR}}} = \Delta \cdot c, \quad c = \mathrm{const.} \qquad (3.20)$$

The relation between the $\overline{\mathrm{DR}}$ and on-shell counterterms can be obtained via1

$$\delta m_\phi^{2,\mathrm{OS}} = \delta m_\phi^{2,\overline{\mathrm{DR}}} + \delta m_\phi^{2,\mathrm{OS}}\Big|^{\mathrm{fin.}}, \quad \delta Z_\phi^{\mathrm{OS}} = \delta Z_\phi^{\overline{\mathrm{DR}}} + \delta Z_\phi^{\mathrm{OS}}\Big|^{\mathrm{fin.}} \qquad (3.21)$$

Here the finite contributions to the renormalisation constants do not contain contributions proportional to Δ. It is, however, not necessary to obtain the full on-shell renormalisation constants to determine $\overline{\mathrm{DR}}$ renormalisation constants. Since only the divergent part is necessary, any renormalisation condition imposed to a vertex function that involves the renormalisation constant is sufficient.

3.2.3 Conversion between Renormalisation Schemes

If it is necessary to transform a renormalised quantity from renormalisation scheme I to another renormalisation scheme II, the transformation can be performed by starting from the bare parameter which is equal in both schemes. The bare parameter can then be expressed by the renormalised parameters and the renormalisation constants of both schemes according to

$$g_0 = g^I + \delta g^I = g^{II} + \delta g^{II}. \qquad (3.22)$$

Thus the renormalised parameter in scheme I, g^I, can be expressed by the renormalised in scheme II, g^{II}, as

$$g^I = g^{II} + \left(\delta g^{II} - \delta g^I\right) = g^{II} + \Delta_g. \qquad (3.23)$$

The difference between the renormalisation constants in both schemes yields a finite shift Δ_g.

3.3 Wave Function Normalisation Factors

In order to ensure the independence of the S-matrix from the field normalisation, each external leg of a stable field ϕ in amputated Green-functions has to enter the calculation with a factor $\sqrt{Z_\phi}$. The factor Z_ϕ is given by the residuum of the full propagator

$$\mathrm{i}Z_\phi = \mathrm{Res}_{\mathcal{M}^2}[\Delta_{\phi\phi}] = \lim_{\mathrm{p}^2 \to \mathcal{M}^2} \left[\left(\mathrm{p}^2 - \mathcal{M}^2 \right) \Delta_{\phi\phi}\left(\mathrm{p}^2 \right) \right], \tag{3.24}$$

where $\mathcal{M}^2$ is the (real) pole of the full propagator. This is a result of the Lehmann–Symanzik–Zimmermann (LSZ) theorem [70]. At lowest order $Z_\phi = 1$ holds. In the on-shell renormalisation the field renormalisation constant of ϕ is chosen such that this relation holds also at higher-orders.

For the Higgs-fields fields h_i, that are unstable and can mix with each other, on-shell renormalisation conditions given in eq. (3.10) have to be imposed for all two-point functions involving fields h_i in order to ensure that the normalisation factors for the fields h_i are identical to one. However, for the calculation in this work each Higgs-doublet and the Higgs Higgs-singlet field receives one field renormalisation constant that is fixed in the $\overline{\mathrm{DR}}$-scheme. Thus the wave function normalisation factors Z_i the Higgs-fields h_i are not equal to one at higher-orders. Furthermore the wave function normalisation factors form a non-unitary matrix $\hat{\mathbf{Z}}_h$, that relates the $\hat{h}_i$ with the fields h_i,

$$\begin{pmatrix} \hat{h}_1 \\ \hat{h}_2 \\ \hat{h}_3 \end{pmatrix} = \hat{\mathbf{Z}}_h \begin{pmatrix} h_1 \\ h_2 \\ h_3 \end{pmatrix} \tag{3.25}$$

The fields h_i are the tree-level Higgs-fields in the mass basis. The fields $\hat{h}_i$ can be interpreted with physical, asymptotically free fields. The matrix $\hat{\mathbf{Z}}_h$ is non-diagonal and accounts for higher-order corrections to the mixing of the interaction states. If all fields were renormalised in the on-shell scheme, the matrix $\hat{\mathbf{Z}}_h$ would be the unity matrix.

The elements of the $\hat{\mathbf{Z}}_h$-matrix are obtained with the full propagator-matrix $\mathbf{\Delta}_{hh}(k^2)$, that is related to the inverse of the matrix of the renormalised two-point functions, $\hat{\mathbf{\Gamma}}_{hh}(k^2)$,

$$\left[\hat{\mathbf{\Gamma}}_{hh}(k^2) \right]_{ij} = \left(p^2 - m_{h_i}^2 \right) \delta_{ij} + \hat{\Sigma}_{h_i h_j}\left(p^2 \right) \tag{3.26}$$

by

$$\mathbf{\Delta}_{hh}(k^2) = \mathrm{i} \left[\hat{\mathbf{\Gamma}}_{hh}(k^2) \right]^{-1}. \tag{3.27}$$

With the results for the renormalised self-energies $\Sigma_{h_i h_j}(k^2)$ the inverse propagator

matrix can be calculated as

$$\left[\hat{\mathbf{\Gamma}}_{hh}(k^2)\right]_{ij} = \left(k^2 - m_{h_i}^2\right)\delta_{ij} + \hat{\Sigma}_{h_i h_j}\left(k^2\right). \tag{3.28}$$

With the result of [71, 72] the matrix elements of $\hat{\mathbf{Z}}$ read

$$\left[\hat{\mathbf{Z}}_h(k^2)\right]_{ij}^a = \frac{1}{\sqrt{\hat{Z}_i^a}}\, \mathrm{Res}_{\mathcal{M}_a^2}\left[\Delta_{h_i h_j}\left(k^2\right)\right] = \sqrt{\hat{Z}_i^a}\left[\frac{\Delta_{h_i h_j}(k^2)}{\Delta_{h_i h_j}(k^2)}\right]_{p^2=\mathcal{M}_a^2}, \tag{3.29}$$

where $\mathcal{M}_a^2$ denotes on of the complex poles of the propagator-matrix and

$$\hat{Z}_i^a = \mathrm{Res}_{\mathcal{M}_a^2}\left[\Delta_{h_i h_i}\left(k^2\right)\right]. \tag{3.30}$$

With this relations the matrix $\hat{\mathbf{Z}}_h$ can be written as

$$\hat{\mathbf{Z}}_h = \begin{pmatrix} \sqrt{\hat{Z}_1^1} & \sqrt{\hat{Z}_1^1}\hat{Z}_{12}^1 & \sqrt{\hat{Z}_1^1}\hat{Z}_{13}^1 \\ \sqrt{\hat{Z}_2^2}\hat{Z}_{21}^2 & \sqrt{\hat{Z}_2^2} & \sqrt{\hat{Z}_2^2}\hat{Z}_{23}^2 \\ \sqrt{\hat{Z}_3^3}\hat{Z}_{31}^3 & \sqrt{\hat{Z}_3^3}\hat{Z}_{32}^3 & \sqrt{\hat{Z}_3^3} \end{pmatrix}. \tag{3.31}$$

All matrix elements that contribute to $\hat{h}_a$ are considered to be evaluated at the complex pole $\mathcal{M}_a^2$, assuming that $\mathrm{Re}(\mathcal{M}_1^2) < \mathrm{Re}(\mathcal{M}_2^2) < \mathrm{Re}(\mathcal{M}_3^2)$. If no off-diagonal of the full propagator matrix $\mathbf{\Delta}_{hh}(k^2)$, the matrix $\hat{\mathbf{Z}}_h$ is diagonal. In this special case its entries correspond to the Z-factors of the LSZ-theorem, but evaluated at the complex pole for unstable particles. In this case no higher-order mixing-effects are considered in $\hat{\mathbf{Z}}_h$. The inclusion of off-diagonal entries of $\mathbf{\Delta}_{hh}(k^2)$ relates to including higher-order mixing-effects due to the inversion of the non-diagonal matrix $\mathbf{\Gamma}_{hh}(k^2)$.

With this definition of the wave function normalisation matrix $\hat{\mathbf{Z}}_h$ the diagonal elements of the inverse propagator-matrix have on-shell properties if the matrix $\hat{\mathbf{Z}}_h$ is applied for both external legs

$$\lim_{k^2 \to \mathcal{M}_i^2} \frac{1}{k^2 - \mathcal{M}_i^2}\left(\hat{\mathbf{Z}} \cdot \hat{\mathbf{\Gamma}}_{hh} \cdot \hat{\mathbf{Z}}^{\mathrm{T}}\right)_{ii} = 1. \tag{3.32}$$

The analogue procedure can be used to obtain the wave function normalisation factors for the $\mathcal{CP}$-odd Higgs-fields. For an extensive discussion of the wave normalisation functions see [73].

3.3.1 Relation between physical Fields and Fields in the interaction Basis

Only the matrix $\hat{\mathbf{Z}}$ can determine the admixture of a certain mass eigenstate h_a to the physical fields $\hat{h}$ at higher-orders. For the admixture of the fields ϕ_1, ϕ_2 and ϕ_s

to the physical fields $\hat{h}$ can be obtained by

$$\begin{pmatrix} \hat{h}_1 \\ \hat{h}_2 \\ \hat{h}_3 \end{pmatrix} = \hat{\mathbf{Z}}_h \begin{pmatrix} h_1 \\ h_2 \\ h_3 \end{pmatrix} = \hat{\mathbf{Z}}_h \mathbf{U}_{e(0)} \begin{pmatrix} \phi_1 \\ \phi_2 \\ \phi_s \end{pmatrix} \tag{3.33}$$

Depending on the loop-order of the higher-order contribution in the inverse propagator-matrix we define

$$\mathbf{U}_{e(n)} := \hat{\mathbf{Z}}_h^{(n)} \mathbf{U}_{e(0)}, \tag{3.34}$$

where $\hat{\mathbf{Z}}_h^{(n)}$ denotes the wave function normalisation matrix obtained with two-point functions including correction up to the n-th loop-order. However, $\hat{\mathbf{Z}}_h^{(n)}$ contains corrections of a higher loop-orders due to mixing effects as explained above.

The $\hat{\mathbf{Z}}$-matrix was not available for the numerical results presented in this work. Thus we will use an approximate result for $\mathbf{U}_{e(n)}$ instead, that is obtained by the singular value decomposition of the inverted propagator-matrix close to zero momentum, to illustrate the singlet-admixture to the physical fields in certain numerical scenarios.

3.4 Renormalisation Group Equation

Any result for a physical observables must be independent of the renormalisation prescription. The renormalisation group equation (RGE) [74, 75] describes this by depicting the independence of renormalised vertex functions of renormalisation points [69]. In dimensional regularisation this translates to the independence of the unphysical regularisation scale μ_r. The total derivative of a renormalised vertex function $\hat{\Gamma}^{(n)}$ with n external scalar fields Ψ as described in sec. 3.2 with respect to the regularisation scale μ_r has to vanish,

$$\begin{aligned} 0 &= \mu_r \frac{\mathrm{d}}{\mathrm{d}\mu_r} \hat{\Gamma}^{(n)}(p_k; g, m; \mu_r) \\ &= \mu_r \left(\frac{\partial}{\partial \mu_r} + \frac{\partial g}{\partial \mu_r} \frac{\partial}{\partial g} + \frac{\partial m}{\partial \mu_r} \frac{\partial}{\partial m} + \frac{n}{2} \frac{1}{Z_\Psi} \frac{\partial Z_\Psi}{\partial \mu_r} \right) \hat{\Gamma}^{(n)}(p_k; g, m; \mu_r). \end{aligned} \tag{3.35}$$

The coefficients in front of the derivatives in eq. (3.35) define the β-function

$$\beta(g, m; \mu_r) = \lim_{\epsilon \to 0} \mu_r \frac{\partial}{\partial \mu_r} g(g_0, m_0, \epsilon; \mu_r), \tag{3.36}$$

the anomalous dimension

$$\gamma(g, m; \mu_r) = -\lim_{\epsilon \to 0} \frac{1}{2Z_\Psi} \mu_r \frac{\partial}{\partial \mu_r} Z_\Psi(g_0, m_0, \epsilon; \mu_r) \tag{3.37}$$

and the renormalisation-group coefficient for the mass term

$$\gamma_m(g, m; \mu_r) = -\lim_{\epsilon \to 0} \frac{1}{m} \mu_r \frac{\partial}{\partial \mu_r} m(g_0, m_0, \epsilon; \mu_r), \tag{3.38}$$

where ϵ is defined as in the previous sections.

Renormalisation Group Evolution

Before applying the limes $\epsilon \to 0$ to the β-function, eq. (3.36) presents a differential equation for the finite part of the coupling g,

$$\mu_r \frac{\partial}{\partial \mu_r} g(\mu_r) = \beta + \mathcal{O}(\varepsilon) = \sum_{n=1}^{\infty} g^n(\mu_r) \beta_g^{(n)} + \mathcal{O}(\varepsilon), \tag{3.39}$$

where $\beta_g^{(n)}$ represents the β-function of g at n-th order divided by $g^n(\mu_r)$. By solving this equation the finite value of g can be obtained at any scale for a given initial condition μ_0. Including the one-loop β-function leads to the running coupling including all leading logarithms in the scale μ_r, including the two-loop β-function leads to the incorporation of next-to-leading logarithms, etc.

Construction of divergent Counterterm Contributions

Due to the structure of the coefficient

$$\mu_r^{D-4} = e^{\ln \mu_r^{2\epsilon}} = 1 + \epsilon \ln \mu_r^2 + \mathcal{O}\left(\epsilon^2\right) \tag{3.40}$$

in eq. (3.4) the typical divergent factor appears with the same coefficient c,

$$c\mu_r^{4-D}\Delta = c\Delta + c \ln \mu_r^2 + \mathcal{O}(\epsilon). \tag{3.41}$$

Thus the identity

$$\mu_r^2 \frac{\partial}{\partial \mu_r^2} \equiv \frac{\partial}{\partial \ln \mu_r^2} = \frac{\partial}{\partial \Delta} \tag{3.42}$$

holds at one-loop order. Thus the divergent part of an unrenormalised quantity can be expressed by β-functions and anomalous dimensions,

$$g^{(1)} = \Delta \beta^{(1)} + \text{finite} \tag{3.43a}$$

$$Z^{(1)} = \Delta \gamma^{(1)} + \text{finite} \tag{3.43b}$$

$$m^{(1)} = \Delta m^{(0)} \gamma_m^{(1)} + \text{finite}. \tag{3.43c}$$

The superscript (0) denotes tree-level parameters. From these expressions the $\overline{\text{DR}}$ renormalisation constants can be obtained by

$$g^{(1)} - \delta g^{(1),\overline{\text{DR}}} \stackrel{!}{=} \text{finite} \;\Rightarrow\; \delta g^{(1),\overline{\text{DR}}} = \Delta \beta^{(1)} \tag{3.44a}$$

$$Z^{(1)} - \delta Z^{(1),\overline{\mathrm{DR}}} \stackrel{!}{=} \text{finite} \ \Rightarrow \ \delta Z^{(1),\overline{\mathrm{DR}}} = \Delta\gamma^{(1)} \tag{3.44b}$$

$$m^{(1)} - \delta m^{(1),\overline{\mathrm{DR}}} \stackrel{!}{=} \text{finite} \ \Rightarrow \ \delta m^{(1),\overline{\mathrm{DR}}} = \Delta m^{(0)}\gamma_m^{(1)} \tag{3.44c}$$

for a given scale μ_{r}.

4 Higgs-Sector of the NMSSM

The mass M_Ψ of a complex field Ψ with total width Γ_Ψ is defined according to the real part of the complex pole $\mathcal{M}_\Psi^2 = M_\Psi^2 - \mathrm{i}\mathcal{M}_\Psi^2\Gamma_{\Psi1}$ of the renormalised, full propagator. For this value the inverse propagator, the renormalised two-point function $\hat{\Gamma}_{\Psi^\dagger\Psi}$ as given in eq. (3.11), vanishes,

$$\hat{\Gamma}_{\Psi^\dagger\Psi} = \frac{\delta^2\hat{\mathcal{L}}}{\delta\Psi^\dagger\delta\Psi}, \quad \hat{\Gamma}_{\Psi^\dagger\Psi}\left(k^2\right)\big|_{k^2=\mathcal{M}_\Psi^2} = 0. \tag{4.1}$$

The two-point function receives higher-order corrections. If the parameter m_Ψ^2 is independent, a renormalisation condition can be applied to $\hat{\Gamma}_{\Psi^\dagger\Psi}$ directly and the pole mass can be renormalised independently. If m_Ψ^2 is a dependent quantity no independent renormalisation condition can be imposed on $\hat{\Gamma}_{\Psi^\dagger\Psi}$. The pole mass can then be predicted in terms the independent parameters.

For the determination of the pole mass it is necessary to obtain the Higgs propagator-matrices and tadpole coefficients expressed by the independent parameters. In a next step the counterterms for Higgs mass-matrices are obtained by applying the renormalisation transformation for the independent parameters. After that the renormalisation constants are fixed by independent renormalisation conditions.

The results outlined in this section are obtained in the same convention as used for calculations of the corresponding quantities in the MSSM, e.g. [31, 33, 35], that are included in `FeynHiggs`. The analytic results for the MSSM mass matrix elements and their counterterms as given in [31] have been verified in the MSSM limit defined in eq. (2.52) for the real case. Further checks have been performed with the analytic NMSSM results given in [76].

4.1 Higgs Mass-Matrices and Tadpole Coefficients

In this section the explicit expressions for the tadpole coefficients and Higgs mass-matrices are given together with the relations between the chosen set of independent parameters. The initial set of independent parameters and the chosen set for the calculation are shown in tab. 4.1.

4.1.1 Tree-Level expression in terms of the initial Set of Parameters

In the $\mathcal{CP}$-conserving NMSSM the Higgs mass-matrices, $\mathbf{M}_{\phi\phi}$, $\mathbf{M}_{\chi\chi}$ and $\mathbf{M}_{\phi^\pm\phi^\pm}$, are hermitian 3×3 and 2×2 matrices respectively. Their independent entries read for

Kähler potential	super-potential	vacuum expectation-values	soft breaking parameters
g_1, g_2	λ, κ	v_1, v_2, v_s	$T_{\phi_1}, T_{\phi_2}, T_{\phi_s}, m_1, m_2, m_s, A_\lambda, A_\kappa$
$\updownarrow$	$\updownarrow$	$\updownarrow$	$\updownarrow$
M_W, M_Z	λ, κ	$\tan\beta, v, \mu_{\text{eff}}$	$T_{h_1}, T_{h_2}, T_{h_3}, M_{H^\pm}^2, A_\kappa$

Table 4.1: Set of independent parameters of the NMSSM Higgs-potential V_{H} as given in eq. (2.38) listed by their origin (first row) versus the final choice of independent parameters (second row). The arrows denote parameters that are replaced in the specified sectors.

the $\mathcal{CP}$-even fields

$$(\mathbf{M}_{\phi\phi})_{11} = \widetilde{m}_1^2 + \lambda^2 v_2^2 + \frac{1}{4}\left(g_1^2 + g_2^2\right)\left(3v_1^2 - v_2^2\right) \tag{4.2a}$$

$$(\mathbf{M}_{\phi\phi})_{22} = \widetilde{m}_2^2 + \lambda^2 v_1^2 + \frac{1}{4}\left(g_1^2 + g_2^2\right)\left(3v_2^2 - v_1^2\right) \tag{4.2b}$$

$$(\mathbf{M}_{\phi\phi})_{33} = m_s^2 + \lambda^2\left(v_1^2 + v_2^2\right) - 2\lambda\kappa v_1 v_2 + 6\kappa^2 v_s^2 + 2\kappa v_s A_\kappa \tag{4.2c}$$

$$(\mathbf{M}_{\phi\phi})_{12} = -\mu_{\text{eff}}B + 2\lambda^2 v_1 v_2 - \frac{1}{2}\left(g_1^2 + g_2^2\right)v_1 v_2 \tag{4.2d}$$

$$(\mathbf{M}_{\phi\phi})_{13} = -\frac{v_2}{v_s}\mu_{\text{eff}}B + \lambda v_s\left(2\lambda v_1 - \kappa v_2\right) \tag{4.2e}$$

$$(\mathbf{M}_{\phi\phi})_{23} = -\frac{v_1}{v_s}\mu_{\text{eff}}B + \lambda v_s\left(2\lambda v_2 - \kappa v_1\right), \tag{4.2f}$$

for the $\mathcal{CP}$-odd fields

$$(\mathbf{M}_{\chi\chi})_{11} = \widetilde{m}_1^2 + \lambda^2 v_2^2 - \frac{1}{4}\left(g_1^2 + g_2^2\right)\left(v_1^2 - v_2^2\right) \tag{4.3a}$$

$$(\mathbf{M}_{\chi\chi})_{22} = \widetilde{m}_2^2 + \lambda^2 v_1^2 - \frac{1}{4}\left(g_1^2 + g_2^2\right)\left(v_2^2 - v_1^2\right) \tag{4.3b}$$

$$(\mathbf{M}_{\chi\chi})_{33} = m_s^2 + \lambda^2\left(v_1^2 + v_2^2\right) + 2\lambda\kappa v_1 v_2 + 2\kappa^2 v_s^2 - 2\kappa v_s A_\kappa \tag{4.3c}$$

$$(\mathbf{M}_{\chi\chi})_{12} = -\mu_{\text{eff}}B \tag{4.3d}$$

$$(\mathbf{M}_{\chi\chi})_{13} = -\frac{v_2}{v_s}\mu_{\text{eff}}B + 2\lambda\kappa v_2 v_s \tag{4.3e}$$

$$(\mathbf{M}_{\chi\chi})_{23} = \frac{v_1}{v_s}\mu_{\text{eff}}B - 2\lambda\kappa v_1 v_s \tag{4.3f}$$

and for the charged fields

$$(\mathbf{M}_{\phi^\pm\phi^\pm})_{11} = \widetilde{m}_1^2 + \frac{1}{4}g_1^2\left(v_1^2 - v_2^2\right) + \frac{1}{4}g_2^2\left(v_1^2 + v_2^2\right) \tag{4.4a}$$

$$(\mathbf{M}_{\phi^\pm\phi^\pm})_{22} = \widetilde{m}_2^2 + \frac{1}{4}g_1^2\left(v_2^2 - v_1^2\right) + \frac{1}{4}g_2^2\left(v_2^2 + v_1^2\right) \tag{4.4b}$$

$$(\mathbf{M}_{\phi^\pm\phi^\pm})_{12} = -\mu_{\text{eff}}B + \lambda^2 v_1 v_2 - \frac{1}{2}g_2 v_1 v_2, \tag{4.4c}$$

where $\widetilde{m}_{\phi_i}^2 = m_{\phi_i}^2 + \lambda^2 v_s^2$ and $\mu_{\text{eff}} B = \lambda v_s (\kappa v_s + A_\lambda)$. The Higgs mass-matrices are diagonalised according to eq. (2.51).

4.1.2 Tree-Level expressions in terms of the chosen Set of Parameters

For the determination of NMSSM Higgs-masses at higher orders all appearing independent parameters have to be renormalised. At one-loop order only the twelve independent parameters from the Higgs potential V_{H} given in eq. (2.38) enter the calculation. While their number is fixed, the set of independent parameters can in principle be chosen arbitrarily. In practice choices are constrained due to numerical stability and sensitivity of masses, e.g. in the neutralino-/chargino-sector, to the soft-breaking parameters.

Parameters from the Kähler Potential

The gauge-boson masses, M_W and M_Z, and the SM vacuum expectation-value v are known and fixed [77–79], while the remaining parameters only appear in the NMSSM- and a subset also in the MSSM-calculation. The Higgs mass-matrices have to be expressed by the chosen set of independent parameters and thus the relations between them and the initial parameters are necessary.

Vacuum Expectation Values

The relation between the v_1, v_2 and v is given by

$$v_1^2 + v_2^2 = v^2. \tag{4.5}$$

Thus the two vacuum expectation-values of the doublet fields can also be expressed by their ratio,

$$\tan \beta = \frac{v_2}{v_1}, \quad v_1 = v \cos \beta, \ v_2 = v \sin \beta. \tag{4.6}$$

The relation between the vacuum expectation-values and the gauge-boson masses are stated in eq. (2.23), the relation between the singlet vacuum expectation-value and the effective μ-parameter μ_{eff} is given in eq. (2.36).

Charged Higgs Mass

The relation between the trilinear breaking parameter A_λ or $\mu_{\text{eff}} B$, and the charged Higgs mass at lowest order is obtained by diagonalising the charged Higgs mass-matrix $\mathbf{M}_{\phi^\pm \phi^\pm}$ from eq. (4.4a). With the real angle β_c and the ansatz

$$\mathbf{U}_{c(0)} = \begin{pmatrix} -\sin \beta_c & \cos \beta_c \\ \cos \beta_c & \sin \beta_c \end{pmatrix} \tag{4.7}$$

the masses of the charged Higgs and unphysical Goldstone pair read

$$M_{H^\pm}^2 = (\mathbf{M}_{\phi^\pm\phi^\pm})_{11} \sin^2\beta_c + (\mathbf{M}_{\phi^\pm\phi^\pm})_{22} \cos^2\beta_c - 2(\mathbf{M}_{\phi^\pm\phi^\pm})_{12} \sin\beta_c \cos\beta_c \quad (4.8a)$$

$$M_{G^\pm}^2 = (\mathbf{M}_{\phi^\pm\phi^\pm})_{11} \cos^2\beta_c + (\mathbf{M}_{\phi^\pm\phi^\pm})_{22} \sin^2\beta_c + 2(\mathbf{M}_{\phi^\pm\phi^\pm})_{12} \sin\beta_c \cos\beta_c \quad (4.8b)$$

The explicit value for β_c can be obtained by the requirement that the mass of the charged Goldstone pair depends only on the tadpole coefficients and thus vanishes at tree-level for the contribution from the Higgs sector. In general there are also contributions from the gauge-fixing term. In case of β, $\beta_c \in [0, 2\pi)$ this is true, if $\beta_c = \beta$, which yields

$$M_{H^\pm}^2 = -\frac{1}{\sqrt{2}v} \left(\frac{\sin^2\beta}{\cos\beta} T_{\phi_1} + \frac{\cos^2\beta}{\sin\beta} T_{\phi_2} \right) \frac{\mu_{\text{eff}}B}{\sin\beta\cos\beta} + M_W^2 + \lambda^2 v^2 \quad (4.9a)$$

$$M_{G^\pm}^2 = -\frac{1}{\sqrt{2}v} (T_{\phi_1}\cos\beta + T_{\phi_2}\sin\beta) \quad (4.9b)$$

By solving eq. (4.9a) for $\mu_{\text{eff}}B$ one obtains

$$\mu_{\text{eff}}B = \frac{1}{\sqrt{2}v} \left(\sin^3\beta\, T_{\phi_1} + \cos^3\beta\, T_{\phi_2} \right) + \left(M_{H^\pm}^2 - M_W^2 + \lambda^2 v^2 \right) \sin\beta\cos\beta. \quad (4.10)$$

It hast to be pointed out that the angle β_c is not an independent parameter and consequently will not receive a counterterm.

Tadpole Coefficients

The tadpole coefficients in the interaction basis are defined as the first derivatives of the Higgs potential with respect to the Higgs fields taken in the classical minimum, where all fields vanish. In order to obtain a stable minimum all first derivatives with respect to the Higgs fields have to vanish,

$$T_{\phi_i} = \left. \frac{\partial}{\partial\phi_i} V_{\text{H}} \right|_{\phi_l,\chi_m,\phi_n^\pm=0} \overset{!}{=} 0 \quad (4.11a)$$

$$T_{\chi_i} = \left. \frac{\partial}{\partial\chi_i} V_{\text{H}} \right|_{\phi_l,\chi_n,\phi_n^\pm=0} \overset{!}{=} 0 \quad (4.11b)$$

$$T_{\phi_i^\pm} = \left. \frac{\partial}{\partial\phi_i^\pm} V_{\text{H}} \right|_{\phi_l,\chi_n,\phi_n^\pm=0} \overset{!}{=} 0. \quad (4.11c)$$

They are related to the tadpole coefficients in the mass basis for in the mass basis T_{h_i}, by

$$\begin{pmatrix} T_{h_1} \\ T_{h_2} \\ T_{h_3} \end{pmatrix} = \mathbf{U}_{e(0)} \begin{pmatrix} T_{\phi_1} \\ T_{\phi_2} \\ T_{\phi_s} \end{pmatrix} \quad \text{and} \quad \begin{pmatrix} T_{\phi_1} \\ T_{\phi_2} \\ T_{\phi_s} \end{pmatrix} = \mathbf{U}_{e(0)}^\dagger \begin{pmatrix} T_{h_1} \\ T_{h_2} \\ T_{h_3} \end{pmatrix}. \quad (4.12)$$

For the tree-level calculation all tadpole coefficients are zero, but they receive higher-order corrections. Thus it is necessary to treat them as non-vanishing quantities and neglect them only after their renormalisation transformations are applied. In order to shorten the following expressions, the tadpole coefficients in the interaction basis will be used in the following.

In the NMSSM with real parameters the conditions (4.11b) and (4.11c) are always fulfilled due to $\mathcal{CP}$- and charge-conservation. However, this is not true for conditions (4.11a). In order to fulfil these conditions for the $\mathcal{CP}$-even fields it is necessary to choose three free parameters, normally the soft Higgs-masses m_i, such that the tadpoles for the $\mathcal{CP}$-even fields vanish. If conditions (4.11a) are fulfilled, the soft Higgs-masses are given by

$$\widetilde{m}_1 = -\frac{T_{\phi_1}}{\sqrt{2}v_2} + \frac{v_2}{v_1}\mu_{\text{eff}}B - \lambda^2 v_2^2 + \frac{1}{4}\left(g_1^2 + g_2^2\right)\left(v_2^2 - v_1^2\right) \tag{4.13a}$$

$$\widetilde{m}_2 = -\frac{T_{\phi_2}}{\sqrt{2}v_1} + \frac{v_1}{v_2}\mu_{\text{eff}}B - \lambda^2 v_1^2 + \frac{1}{4}\left(g_1^2 + g_2^2\right)\left(v_1^2 - v_2^2\right) \tag{4.13b}$$

$$m_s^2 = -\frac{T_{\phi_s}}{\sqrt{2}v_s} + \frac{v_1 v_2}{v_s^2}\mu_{\text{eff}}B - \lambda^2\left(v_1^2 + v_2^2\right) + \lambda\kappa v_1 v_2 - 2\kappa^2 v_s^2 - \kappa v_s A_\kappa, \tag{4.13c}$$

The expressions for the soft-breaking parameters given in eq. (4.13) in terms of the new set of independent parameters read

$$\widetilde{m}_1 = -\frac{T_{\phi_1}}{\sqrt{2}v\sin\beta} + \mu_{\text{eff}}B\tan\beta - \lambda^2 v^2 \sin^2\beta + \frac{1}{4}M_Z^2\left(\sin^2\beta - \cos^2\beta\right) \tag{4.14a}$$

$$\widetilde{m}_2 = -\frac{T_{\phi_2}}{\sqrt{2}v\cos\beta} + \mu_{\text{eff}}B\cot\beta - \lambda^2 v^2 \cos^2\beta + \frac{1}{4}M_Z^2\left(\cos^2\beta - \sin^2\beta\right) \tag{4.14b}$$

$$m_s^2 = -\frac{\lambda T_{\phi_s}}{\sqrt{2}\mu_{\text{eff}}} + \left(\mu_{\text{eff}}B\frac{\lambda^2 v^2}{\mu_{\text{eff}}^2} + \lambda\kappa v^2\right)\sin\beta\cos\beta - \lambda^2 v^2 - 2\frac{\kappa^2}{\lambda^2}\mu_{\text{eff}}^2 + \frac{\kappa}{\lambda}\mu_{\text{eff}}A_\kappa. \tag{4.14c}$$

Higgs Mass-Matrices

In the final set of independent parameters the Higgs mass-matrix elements for the $\mathcal{CP}$-even fields read

$$(\mathbf{M}_{\phi\phi})_{11} = \frac{1}{\sqrt{2}v}\left(-\frac{1 - \sin^4\beta}{\cos\beta}T_{\phi_1} + \cos^2\beta\sin\beta\,T_{\phi_2}\right)$$
$$+ \left(M_{H^\pm}^2 - M_W^2 + \lambda^2 v^2\right)\sin^2\beta + M_Z^2\cos^2\beta \tag{4.15a}$$

$$(\mathbf{M}_{\phi\phi})_{22} = \frac{1}{\sqrt{2}v}\left(\sin^2\beta\cos\beta\,T_{\phi_1} - \frac{1 - \cos^4\beta}{\sin\beta}T_{\phi_2}\right)$$
$$+ \left(M_{H^\pm}^2 - M_W^2 + \lambda^2 v^2\right)\cos^2\beta + M_Z^2\sin^2\beta \tag{4.15b}$$

$$(\mathbf{M}_{\phi\phi})_{33} = \frac{\lambda}{\sqrt{2}\mu_{\text{eff}}} \left[-T_{\phi_s} + \frac{\lambda v}{\mu_{\text{eff}}} \sin\beta\cos\beta \left(\sin^3\beta \, T_{\phi_1} + \cos^3\beta \, T_{\phi_2} \right) \right]$$
$$+ \frac{\lambda^2 v^2}{\mu_{\text{eff}}^2} \sin^2\beta\cos^2\beta \left(M_{H^\pm}^2 - M_W^2 + \lambda^2 v^2 \right) \tag{4.15c}$$
$$- \lambda\kappa v^2 \sin\beta\cos\beta + 4\frac{\kappa^2}{\lambda^2}\mu_{\text{eff}}^2 + \frac{\kappa}{\lambda}\mu_{\text{eff}}A_\kappa$$

$$(\mathbf{M}_{\phi\phi})_{12} = -\frac{1}{\sqrt{2}v} \left(T_{\phi_1}\sin^3\beta + T_{\phi_2}\cos^3\beta \right)$$
$$- \left(M_{H^\pm}^2 - M_W^2 + \lambda^2 v^2 + M_Z^2 \right) \sin\beta\cos\beta \tag{4.15d}$$

$$(\mathbf{M}_{\phi\phi})_{13} = -\frac{\lambda}{\sqrt{2}\mu_{\text{eff}}} \sin\beta \left(\sin^3\beta \, T_{\phi_1} + \cos^3\beta \, T_{\phi_2} \right)$$
$$+ \frac{\lambda v}{\mu_{\text{eff}}} \left(M_{H^\pm}^2 - M_W^2 + \lambda^2 v^2 \right) \sin^2\beta\cos\beta \tag{4.15e}$$
$$- \kappa v \sin\beta\mu_{\text{eff}} + 2\lambda v \cos\beta\mu_{\text{eff}}$$

$$(\mathbf{M}_{\phi\phi})_{23} = -\frac{\lambda}{\sqrt{2}\mu_{\text{eff}}} \cos\beta \left(\sin^3\beta \, T_{\phi_1} + \cos^3\beta \, T_{\phi_2} \right)$$
$$+ \frac{\lambda v}{\mu_{\text{eff}}} \left(M_{H^\pm}^2 - M_W^2 + \lambda^2 v^2 \right) \cos^2\beta\sin\beta \tag{4.15f}$$
$$- \kappa v \cos\beta\mu_{\text{eff}} + 2\lambda v \sin\beta\mu_{\text{eff}},$$

for the $\mathcal{CP}$-odd fields the Higgs mass-matrix elements read

$$(\mathbf{M}_{\chi\chi})_{11} = \frac{1}{\sqrt{2}v} \left(-\frac{1-\sin^4\beta}{\cos\beta}T_{\phi_1} + \cos^2\beta\sin\beta \, T_{\phi_2} \right)$$
$$+ \left(M_{H^\pm}^2 - M_W^2 + \lambda^2 v^2 \right) \sin^2\beta \tag{4.16a}$$

$$(\mathbf{M}_{\chi\chi})_{22} = \frac{1}{\sqrt{2}v} \left(\sin^2\beta\cos\beta \, T_{\phi_1} - \frac{1-\cos^4\beta}{\sin\beta}T_{\phi_2} \right)$$
$$+ \left(M_{H^\pm}^2 - M_W^2 + \lambda^2 v^2 \right) \cos^2\beta \tag{4.16b}$$

$$(\mathbf{M}_{\chi\chi})_{33} = \frac{\lambda}{\sqrt{2}\mu_{\text{eff}}} \left[-T_{\phi_s} + \frac{\lambda v}{\mu_{\text{eff}}} \sin\beta\cos\beta \left(\sin^3\beta \, T_{\phi_1} + \cos^3\beta \, T_{\phi_2} \right) \right]$$
$$+ \frac{\lambda^2 v^2}{\mu_{\text{eff}}^2} \sin^2\beta\cos^2\beta \left(M_{H^\pm}^2 - M_W^2 + \lambda^2 v^2 \right) \tag{4.16c}$$
$$+ 3\lambda\kappa v^2 \sin\beta\cos\beta - 3\frac{\kappa}{\lambda}\mu_{\text{eff}}A_\kappa$$

$$(\mathbf{M}_{\chi\chi})_{12} = -\frac{1}{\sqrt{2}v} \left(T_{\phi_1}\sin^3\beta + T_{\phi_2}\cos^3\beta \right) - \left(M_{H^\pm}^2 - M_W^2 + \lambda^2 v^2 \right) \sin\beta\cos\beta \tag{4.16d}$$

$$(\mathbf{M}_{\chi\chi})_{13} = -\frac{\lambda}{\sqrt{2}\mu_{\text{eff}}} \sin\beta \left(\sin^3\beta \, T_{\phi_1} + \cos^3\beta \, T_{\phi_2} \right)$$
$$- \frac{\lambda v}{\mu_{\text{eff}}} \left(M_{H^\pm}^2 - M_W^2 + \lambda^2 v^2 \right) \sin^2\beta\cos\beta + 3\kappa v \sin\beta\mu_{\text{eff}} \tag{4.16e}$$

$$
\begin{aligned}
(\mathbf{M}_{\chi\chi})_{23} = {}& \frac{\lambda}{\sqrt{2}\mu_{\mathrm{eff}}} \cos\beta \left(\sin^3\beta\, T_{\phi_1} + \cos^3\beta\, T_{\phi_2} \right) \\
&+ \frac{\lambda v}{\mu_{\mathrm{eff}}} \left(M_{H^\pm}^2 - M_W^2 + \lambda^2 v^2 \right) \cos^2\beta \sin\beta - 3\kappa v \cos\beta \mu_{\mathrm{eff}}.
\end{aligned}
\tag{4.16f}
$$

Obtaining the Goldstone Bosons

In the (unphysical) charged Higgs sector the charged Goldstone pair $G^\pm$ is obtained with the rotation matrix given in eq. (4.7) with $\beta_c = \beta$. When rotating the mass matrix $\mathbf{M}_{\chi\chi}$ of the $\mathcal{CP}$-odd Higgs-fields into the mass basis the neutral Goldstone boson must only contain admixtures of the doublet fields. Thus the mixing matrix in the $\mathcal{CP}$-odd sector can be decomposed as

$$
\mathbf{U}_{o(0)} = \mathbf{U}_{o(0)}^{(a)} \mathbf{U}_{o(0)}^{(G)},
\tag{4.17a}
$$

where the second matrix rotates the doublet fields such that the the Goldstone boson is obtained and the first matrix rotates the remaining $\mathcal{CP}$-odd fields such that the physical fields are obtained,

$$
\mathbf{U}_{o(0)} \begin{pmatrix} \chi_1 \\ \chi_2 \\ \chi_s \end{pmatrix} = \mathbf{U}_{o(0)}^{(a)} \mathbf{U}_{o(0)}^{(G)} \begin{pmatrix} \chi_1 \\ \chi_2 \\ \chi_s \end{pmatrix} = \mathbf{U}_{o(0)}^{(a)} \begin{pmatrix} a_1 \\ a_2^{(s)} \\ G^0 \end{pmatrix} = \begin{pmatrix} A_1 \\ A_2 \\ G^0 \end{pmatrix}.
\tag{4.17b}
$$

After the first rotation the field a_1 is purely doublet and the field $a_2^{(s)}$ is purely singlet like. The singlet field is demixed from the remaining, MSSM-like field a_1 and the Goldstone boson. For the mass matrix this leads to

$$
\begin{aligned}
\mathbf{U}_{o(0)} \mathbf{M}_{\chi\chi} \mathbf{U}_{o(0)}^\dagger &= \mathbf{U}_{o(0)}^{(a)} \mathbf{U}_{o(0)}^{(G)} \mathbf{M}_{\chi\chi} \left(\mathbf{U}_{o(0)}^{(G)} \right)^\dagger \left(\mathbf{U}_{o(0)}^{(a)} \right)^\dagger \\
&= \mathbf{U}_{o(0)}^{(a)} \mathbf{M}_{aa} \left(\mathbf{U}_{o(0)}^{(a)} \right)^\dagger \\
&= \mathrm{diag}\{ m_{A_1}^2, m_{A_2}^2, 0 \}.
\end{aligned}
\tag{4.17c}
$$

Both matrices $\mathbf{U}_{o(0)}^{(a)}$ and $\mathbf{U}_{o(0)}^{(G)}$ are rotations with one angle. This allows the ansatz

$$
\mathbf{U}_{o(0)}^{(G)} = \begin{pmatrix} -\sin\beta_n & \cos\beta_n & 0 \\ 0 & 0 & 1 \\ \cos\beta_n & \sin\beta_n & 0 \end{pmatrix}.
\tag{4.18}
$$

As β_c the real mixing angle β_n is not an independent parameter and does not need to be renormalised. The value for β_n can be fixed by the condition that the Goldstone-boson mass,

$$
M_{G^0} = (\mathbf{M}_{\chi\chi})_{11} \cos^2\beta_n + (\mathbf{M}_{\chi\chi})_{22} \sin^2\beta_n + 2 (\mathbf{M}_{\chi\chi})_{12} \sin\beta_n \cos\beta_n,
\tag{4.19}
$$

depends only on on tadpole coefficients and vanishes at tree-level. In case of $\beta,\ \beta_n \in [0, 2\pi)$ this is true, if $\beta_n = \beta$.

With the mixing matrices given in eqs. (4.7) and (4.18) for the charged and $\mathcal{CP}$-odd Higgs sector the Goldstone bosons are obtained only from the doublet fields as

$$G^{\pm} = -\phi_1^{\pm} \cos\beta + \phi_2^{\pm} \sin\beta \tag{4.20a}$$

$$G^0 = -\chi_1 \cos\beta + \chi_2 \sin\beta, \tag{4.20b}$$

as in the MSSM for the same sign conventions in the Higgs doublets as given in eq. (2.22).

4.2 Renormalisation of the Higgs Potential

The renormalisation transformation for the Higgs potential reads

$$V_{\mathrm{H}} \rightarrow V_{\mathrm{H}} + \delta V_{\mathrm{H}} \tag{4.21}$$

with the dependent counterterm δV_{H}. It enters the renormalised two-point functions (4.1) in the form

$$i\hat{\Gamma}_{\Psi_i^{\dagger}\Psi_j}\left(k^2\right) = \tag{4.22}$$

$$ik^2\delta_{ij}\left[1 + \frac{1}{2}\left(\delta Z_{\Psi_i}^{\dagger} + \delta Z_{\Psi_j}\right)\right] + i\Sigma_{\Psi_i^{\dagger}\Psi_j}\left(k^2\right) - i\left[\frac{\delta^2}{\delta\Psi_i^{\dagger}\delta\Psi_j}\left(V_{\mathrm{H}} + \delta V_{\mathrm{H}}\right)\right]_{\Psi_l^{\dagger}=\Psi_m=0}$$

where Ψ denotes any scalar Higgs field with the field renormalisation constant δZ_{Ψ}. The self-energy for the according external fields is denoted by $\Sigma_{\Psi_i^{\dagger}\Psi_j}(k^2)$. From the definition of V_{H} in eq. (2.49) the contributions from the Higgs potential and its counterterm can be read off

$$(V_{\mathrm{H}})_{\Psi_i^{\dagger}\Psi_j} \equiv \left[\frac{\delta^2 V_{\mathrm{H}}}{\delta\Psi_i^{\dagger}\delta\Psi_j}\right]_{\Psi_l^{\dagger}=\Psi_m=0} = (\mathbf{M}_{\Psi\Psi})_{ij} \tag{4.23}$$

$$(\delta V_{\mathrm{H}})_{\Psi_i^{\dagger}\Psi_j} \equiv \left[\frac{\delta^2 (\delta V_{\mathrm{H}})}{\delta\Psi_i^{\dagger}\delta\Psi_j}\right]_{\Psi_l^{\dagger}=\Psi_m=0} = (\mathbf{M}_{\Psi\Psi})_{ij}\frac{1}{2}\left(\delta Z_{\Psi_i}^{\dagger} + \delta Z_{\Psi_j}\right) + (\delta\mathbf{M}_{\Psi\Psi})_{ij}, \tag{4.24}$$

where $\mathbf{M}_{\Psi\Psi}$ denotes the mass matrix for the fields Ψ with the counterterm mass-matrix $\delta\mathbf{M}_{\Psi\Psi}$. In this section the counterterm mass-matrices will be given explicitly.

4.2.1 Renormalisation Transformations for independent Parameters at One-Loop Order

Compared to the MSSM, the number of independent parameters that enter the Higgs mass calculation at one-loop order is increased in the NMSSM. In the MSSM one-loop calculation only $\tan\beta$ and the charged Higgs mass $M_{H^{\pm}}^2$ (or the mass of the single

$\mathcal{CP}$-odd Higgs field M_A^2) need to be renormalised, all other parameters drop out[1]. The additional parameters that have to be renormalised in the NMSSM are the new NMSSM specific parameters λ, κ and A_κ, as well as the vacuum expectation-value v, that does not drop out as in the MSSM.

The renormalisation transformation for the set of independent parameters read

$$
\begin{aligned}
T_{h_1} &\to T_{h_1} + \delta T_{h_1}, & \tan\beta &\to \tan\beta + \delta\tan\beta \\
T_{h_2} &\to T_{h_2} + \delta T_{h_2} & \mu_{\text{eff}} &\to \mu_{\text{eff}} + \delta\mu_{\text{eff}} \\
T_{h_s} &\to T_{h_s} + \delta T_{h_s} & v &\to v + \delta v \\
M_Z^2 &\to M_Z^2 + \delta M_Z^2 & \lambda &\to \lambda + \delta\lambda \\
M_W^2 &\to M_W^2 + \delta M_W^2 & \kappa &\to \kappa + \delta\kappa \\
M_{H^\pm}^2 &\to M_{H^\pm}^2 + \delta M_{H^\pm}^2 & A_\kappa &\to A_\kappa + \delta A_\kappa.
\end{aligned}
\tag{4.25}
$$

The tadpole counterterms in the mass basis are connected to the counterterms in the interaction basis in the same way as the tadpole coefficients by

$$
\begin{pmatrix} \delta T_{h_1} \\ \delta T_{h_2} \\ \delta T_{h_3} \end{pmatrix} = \mathbf{U}_{e(0)} \begin{pmatrix} \delta T_{\phi_1} \\ \delta T_{\phi_2} \\ \delta T_{\phi_s} \end{pmatrix} \quad \text{and} \quad \begin{pmatrix} \delta T_{\phi_1} \\ \delta T_{\phi_2} \\ \delta T_{\phi_s} \end{pmatrix} = \mathbf{U}_{e(0)}^\dagger \begin{pmatrix} \delta T_{h_1} \\ \delta T_{h_2} \\ \delta T_{h_3} \end{pmatrix}.
\tag{4.26}
$$

4.2.2 Explicit Counterterms for the Higgs Mass-Matrices in the interaction Basis

The counterterms for the mass matrices (4.15) of the $\mathcal{CP}$-even and -odd Higgs fields read in the interaction basis

$$
\mathbf{M}_{\phi\phi} \to \mathbf{M}_{\phi\phi} + \delta\mathbf{M}_{\phi\phi} \tag{4.27a}
$$

$$
\mathbf{M}_{\chi\chi} \to \mathbf{M}_{\chi\chi} + \delta\mathbf{M}_{\chi\chi} \tag{4.27b}
$$

They read in components

$$
\delta\mathbf{M}_{\phi\phi} = \begin{pmatrix} \delta m_{\phi_1\phi_1}^2 & \delta m_{\phi_1\phi_2}^2 & \delta m_{\phi_1\phi_s}^2 \\ \delta m_{\phi_2\phi_1}^2 & \delta m_{\phi_2\phi_2}^2 & \delta m_{\phi_2\phi_s}^2 \\ \delta m_{\phi_s\phi_1}^2 & \delta m_{\phi_s\phi_2}^2 & \delta m_{\phi_s\phi_s}^2 \end{pmatrix} \tag{4.28a}
$$

$$
\delta\mathbf{M}_{\chi\chi} = \begin{pmatrix} \delta m_{\chi_1\chi_1}^2 & \delta m_{\chi_1\chi_2}^2 & \delta m_{\chi_1\chi_s}^2 \\ \delta m_{\chi_2\chi_1}^2 & \delta m_{\chi_2\chi_2}^2 & \delta m_{\chi_2\chi_s}^2 \\ \delta m_{\chi_s\chi_1}^2 & \delta m_{\chi_s\chi_2}^2 & \delta m_{\chi_s\chi_s}^2 \end{pmatrix}. \tag{4.28b}
$$

In order to obtain the Higgs mass-matrix counterterms the renormalisation transformations given in eq. (4.25) have to be applied to the tree-level mass-matrices given in eq. (4.15) and (4.16).

This yields for the components of the counterterm matrix in the interaction basis

---

[1]The gauge couplings appear with a coefficient v and thus are expressed in terms of the gauge-boson masses.

for the $\mathcal{CP}$-even fields

$$\delta m_{\phi_1\phi_1}^2 = \frac{1}{\sqrt{2}v}\left(-\frac{1-\sin^4\beta}{\cos\beta}\delta T_{\phi_1} + \cos^2\beta\sin\beta\,\delta T_{\phi_2}\right)$$
$$+ \left[\delta M_{H^\pm}^2 - \delta M_W^2 + 2\lambda v\left(\delta\lambda v + \lambda\delta v\right)\right]\sin^2\beta + \delta M_Z^2\cos^2\beta$$
$$+ 2(M_{H^\pm}^2 + \lambda^2 v^2 - M_W^2 - M_Z^2)\sin\beta\cos^3\beta\,\delta\tan\beta \tag{4.29a}$$

$$\delta m_{\phi_2\phi_2}^2 = \frac{1}{\sqrt{2}v}\left(\sin^2\beta\cos\beta\,\delta T_{\phi_1} - \frac{1-\cos^4\beta}{\sin\beta}\delta T_{\phi_2}\right)$$
$$+ \left[\delta M_{H^\pm}^2 - \delta M_W^2 + 2\lambda v\left(\delta\lambda v + \lambda\delta v\right)\right]\cos^2\beta + \delta M_Z^2\cos^2\beta$$
$$+ 2(M_{H^\pm}^2 + \lambda^2 v^2 - M_W^2 - M_Z^2)\cos\beta\sin^3\beta\,\delta\tan\beta \tag{4.29b}$$

$$\delta m_{\phi_s\phi_s}^2 = \frac{\lambda}{\sqrt{2}\mu_{\text{eff}}}\left[-\delta T_{\phi_s} + \frac{\lambda v}{\mu_{\text{eff}}}\sin\beta\cos\beta\left(\sin^3\beta\,\delta T_{\phi_1} + \cos^3\beta\,\delta T_{\phi_2}\right)\right]$$
$$+ \frac{\lambda^2 v^2}{\mu_{\text{eff}}^2}\sin^2\beta\cos^2\beta\left[\delta M_{H^\pm}^2 - \delta M_W^2 + 2\lambda v\left(\delta\lambda v + \lambda\delta v\right)\right]$$
$$+ \frac{\lambda^2 v^2}{\mu_{\text{eff}}^2}\left(M_{H^\pm}^2 - M_W^2 + \lambda^2 v^2\right)\sin^2\beta\cos^2\beta\cdot$$
$$\left[2\left(\frac{\delta\lambda}{\lambda} - \frac{\delta\mu_{\text{eff}}}{\mu_{\text{eff}}}\right) + \frac{\delta v^2}{v^2} + 2\left(\cos^2\beta - \sin^2\beta\right)\frac{\delta\tan\beta}{\tan\beta}\right]$$
$$+ 8\frac{\kappa^2}{\lambda^2}\mu_{\text{eff}}^2\left(\frac{\delta\kappa}{\kappa} - \frac{\delta\lambda}{\lambda} + \frac{\delta\mu_{\text{eff}}}{\mu_{\text{eff}}}\right) + \frac{\kappa}{\lambda}\mu_{\text{eff}}A_\kappa\left(\frac{\delta\kappa}{\kappa} - \frac{\delta\lambda}{\lambda} + \frac{\delta\mu_{\text{eff}}}{\mu_{\text{eff}}} + \frac{\delta A_\kappa}{A_\kappa}\right) \tag{4.29c}$$

$$\delta m_{\phi_1\phi_2}^2 = -\frac{1}{\sqrt{2}v}\left(\sin^3\beta\,\delta T_{\phi_1} + \cos^3\beta\,\delta T_{\phi_2}\right)$$
$$- \left[\delta M_{H^\pm}^2 - \delta M_W^2 + 2\lambda v\left(\delta\lambda v + \lambda\delta v\right)\right]\sin\beta\cos\beta$$
$$- \left(M_{H^\pm}^2 - M_W^2 + \lambda^2 v^2\right)\cos^2\beta\left(\cos^2\beta - \sin^2\beta\right)\delta\tan\beta \tag{4.29d}$$

$$\delta m_{\phi_1\phi_s}^2 = -\frac{\lambda}{\sqrt{2}\mu_{\text{eff}}}\sin\beta\left(\sin^3\beta\,\delta T_{\phi_1} + \cos^3\beta\,\delta T_{\phi_2}\right)$$
$$+ \frac{\lambda v}{\mu_{\text{eff}}}\sin^2\beta\cos\beta\left[\delta M_{H^\pm}^2 - \delta M_W^2 + 2\lambda v\left(\delta\lambda v + \lambda\delta v\right)\right]$$
$$+ \frac{\lambda v}{\mu_{\text{eff}}}\left(M_{H^\pm}^2 - M_W^2 + \lambda^2 v^2\right)\sin^2\beta\cos\beta\cdot$$
$$\left[\frac{\delta\lambda}{\lambda} - \frac{\delta\mu_{\text{eff}}}{\mu_{\text{eff}}} + \frac{1}{2}\frac{\delta v^2}{v^2} + \left(2\cos^2\beta - \sin^2\beta\right)\frac{\delta\tan\beta}{\tan\beta}\right]$$
$$- \kappa v\sin\beta\mu_{\text{eff}}\left(\frac{\delta\mu_{\text{eff}}}{\mu_{\text{eff}}} + \frac{\delta\kappa}{\kappa} + \frac{1}{2}\frac{\delta v^2}{v^2} + \cos^2\beta\frac{\delta\tan\beta}{\tan\beta}\right)$$
$$+ 2\lambda v\cos\beta\mu_{\text{eff}}\left(\frac{\delta\lambda}{\lambda} + \frac{\delta\mu_{\text{eff}}}{\mu_{\text{eff}}} + \frac{1}{2}\frac{\delta v^2}{v^2} + \sin\beta\cos\beta\,\delta\tan\beta\right) \tag{4.29e}$$

$$\delta m^2_{\phi_2\phi_s} = -\frac{\lambda}{\sqrt{2}\mu_{\text{eff}}}\cos\beta\left(\sin^3\beta\;\delta T_{\phi_1}+\cos^3\beta\;\delta T_{\phi_2}\right)$$
$$+\frac{\lambda v}{\mu_{\text{eff}}}\sin^2\beta\cos\beta\left[\delta M^2_{H^\pm}-\delta M^2_W+2\lambda v\left(\delta\lambda v+\lambda\delta v\right)\right]$$
$$+\frac{\lambda v}{\mu_{\text{eff}}}\left(M^2_{H^\pm}-M^2_W+\lambda^2 v^2\right)\sin^2\beta\cos\beta\cdot$$
$$\left[\frac{\delta\lambda}{\lambda}-\frac{\delta\mu_{\text{eff}}}{\mu_{\text{eff}}}+\frac{1}{2}\frac{\delta v^2}{v^2}+\left(\cos^2\beta-2\sin^2\beta\right)\frac{\delta\tan\beta}{\tan\beta}\right]$$
$$-\kappa v\cos\beta\mu_{\text{eff}}\left(\frac{\delta\mu_{\text{eff}}}{\mu_{\text{eff}}}+\frac{\delta\kappa}{\kappa}+\frac{1}{2}\frac{\delta v^2}{v^2}+\sin\beta\cos\beta\;\delta\tan\beta\right)$$
$$+2\lambda v\sin\beta\mu_{\text{eff}}\left(\frac{\delta\lambda}{\lambda}+\frac{\delta\mu_{\text{eff}}}{\mu_{\text{eff}}}+\frac{1}{2}\frac{\delta v^2}{v^2}+\cos^2\beta\frac{\delta\tan\beta}{\tan\beta}\right) \tag{4.29f}$$

and for components of the counterterm matrix in the interaction basis for the $\mathcal{CP}$-odd fields

$$\delta m^2_{\chi_1\chi_1} = \frac{1}{\sqrt{2}v}\left(-\frac{1-\sin^4\beta}{\cos\beta}\delta T_{\phi_1}+\cos^2\beta\sin\beta\;\delta T_{\phi_2}\right)$$
$$+\left[\delta M^2_{H^\pm}-\delta M^2_W+2\lambda v\left(\delta\lambda v+\lambda\delta v\right)\right]\sin^2\beta$$
$$+2(M^2_{H^\pm}+\lambda^2 v^2-M^2_W)\sin\beta\cos^3\beta\;\delta\tan\beta \tag{4.30a}$$

$$\delta m^2_{\chi_2\chi_2} = \frac{1}{\sqrt{2}v}\left(\sin^2\beta\cos\beta\;\delta T_{\phi_1}-\frac{1-\cos^4\beta}{\sin\beta}\delta T_{\phi_2}\right)$$
$$+\left[\delta M^2_{H^\pm}-\delta M^2_W+2\lambda v\left(\delta\lambda v+\lambda\delta v\right)\right]\cos^2\beta$$
$$+2(M^2_{H^\pm}+\lambda^2 v^2-M^2_W)\cos\beta\sin^3\beta\;\delta\tan\beta \tag{4.30b}$$

$$\delta m^2_{\chi_s\chi_s} = \frac{\lambda}{\sqrt{2}\mu_{\text{eff}}}\left[-\delta T_{\phi_s}+\frac{\lambda v}{\mu_{\text{eff}}}\sin\beta\cos\beta\left(\sin^3\beta\;\delta T_{\phi_1}+\cos^3\beta\;\delta T_{\phi_2}\right)\right]$$
$$+\frac{\lambda^2 v^2}{\mu^2_{\text{eff}}}\sin^2\beta\cos^2\beta\left[\delta M^2_{H^\pm}-\delta M^2_W+2\lambda v\left(\delta\lambda v+\lambda\delta v\right)\right]$$
$$+\frac{\lambda^2 v^2}{\mu^2_{\text{eff}}}\left(M^2_{H^\pm}-M^2_W+\lambda^2 v^2\right)\sin^2\beta\cos^2\beta\cdot$$
$$\left[2\left(\frac{\delta\lambda}{\lambda}-\frac{\delta\mu_{\text{eff}}}{\mu_{\text{eff}}}\right)+\frac{\delta v^2}{v^2}+2\left(\cos^2\beta-\sin^2\beta\right)\frac{\delta\tan\beta}{\tan\beta}\right]$$
$$+8\frac{\kappa^2}{\lambda^2}\mu^2_{\text{eff}}\left(\frac{\delta\kappa}{\kappa}-\frac{\delta\lambda}{\lambda}+\frac{\delta\mu_{\text{eff}}}{\mu_{\text{eff}}}\right)+\frac{\kappa}{\lambda}\mu_{\text{eff}}A_\kappa\left(\frac{\delta\kappa}{\kappa}-\frac{\delta\lambda}{\lambda}+\frac{\delta\mu_{\text{eff}}}{\mu_{\text{eff}}}+\frac{\delta A_\kappa}{A_\kappa}\right)$$
$$\tag{4.30c}$$

$$\delta m^2_{\chi_1\chi_2} = -\frac{1}{\sqrt{2}v}\left(\sin^3\beta\;\delta T_{\phi_1}+\cos^3\beta\;\delta T_{\phi_2}\right)$$
$$-\left[\delta M^2_{H^\pm}-\delta M^2_W+2\lambda v\left(\delta\lambda v+\lambda\delta v\right)\right]\sin\beta\cos\beta$$
$$-\left(M^2_{H^\pm}-M^2_W+\lambda^2 v^2\right)\cos^2\beta\left(\cos^2\beta-\sin^2\beta\right)\delta\tan\beta \tag{4.30d}$$

$$\delta m^2_{\chi_1\chi_s} = -\frac{\lambda}{\sqrt{2}\mu_{\mathrm{eff}}}\sin\beta\left(\sin^3\beta\ \delta T_{\phi_1} + \cos^3\beta\ \delta T_{\phi_2}\right)$$
$$+\frac{\lambda v}{\mu_{\mathrm{eff}}}\sin^2\beta\cos\beta\left[\delta M^2_{H^\pm} - \delta M^2_W + 2\lambda v\left(\delta\lambda + \lambda\delta v\right)\right]$$
$$+\frac{\lambda v}{\mu_{\mathrm{eff}}}\left(M^2_{H^\pm} - M^2_W + \lambda^2 v^2\right)\sin^2\beta\cos\beta\ \cdot$$
$$\left[\frac{\delta\lambda}{\lambda} - \frac{\delta\mu_{\mathrm{eff}}}{\mu_{\mathrm{eff}}} + \frac{1}{2}\frac{\delta v^2}{v^2} + \left(2\cos^2\beta - \sin^2\beta\right)\frac{\delta\tan\beta}{\tan\beta}\right] \qquad (4.30\mathrm{e})$$
$$-\kappa v\sin\beta\mu_{\mathrm{eff}}\left(\frac{\delta\mu_{\mathrm{eff}}}{\mu_{\mathrm{eff}}} + \frac{\delta\kappa}{\kappa} + \frac{1}{2}\frac{\delta v^2}{v^2} + \cos^2\beta\frac{\delta\tan\beta}{\tan\beta}\right)$$
$$+2\lambda v\cos\beta\mu_{\mathrm{eff}}\left(\frac{\delta\lambda}{\lambda} + \frac{\delta\mu_{\mathrm{eff}}}{\mu_{\mathrm{eff}}} + \frac{1}{2}\frac{\delta v^2}{v^2} + \sin\beta\cos\beta\ \delta\tan\beta\right)$$

$$\delta m^2_{\chi_2\chi_s} = -\frac{\lambda}{\sqrt{2}\mu_{\mathrm{eff}}}\cos\beta\left(\sin^3\beta\ \delta T_{\phi_1} + \cos^3\beta\ \delta T_{\phi_2}\right)$$
$$+\frac{\lambda v}{\mu_{\mathrm{eff}}}\sin^2\beta\cos\beta\left[\delta M^2_{H^\pm} - \delta M^2_W + 2\lambda v\left(\delta\lambda + \lambda\delta v\right)\right]$$
$$+\frac{\lambda v}{\mu_{\mathrm{eff}}}\left(M^2_{H^\pm} - M^2_W + \lambda^2 v^2\right)\sin^2\beta\cos\beta\ \cdot$$
$$\left[\frac{\delta\lambda}{\lambda} - \frac{\delta\mu_{\mathrm{eff}}}{\mu_{\mathrm{eff}}} + \frac{1}{2}\frac{\delta v^2}{v^2} + \left(\cos^2\beta - 2\sin^2\beta\right)\frac{\delta\tan\beta}{\tan\beta}\right] \qquad (4.30\mathrm{f})$$
$$-\kappa v\cos\beta\mu_{\mathrm{eff}}\left(\frac{\delta\mu_{\mathrm{eff}}}{\mu_{\mathrm{eff}}} + \frac{\delta\kappa}{\kappa} + \frac{1}{2}\frac{\delta v^2}{v^2} + \sin\beta\cos\beta\ \delta\tan\beta\right)$$
$$+2\lambda v\sin\beta\mu_{\mathrm{eff}}\left(\frac{\delta\lambda}{\lambda} + \frac{\delta\mu_{\mathrm{eff}}}{\mu_{\mathrm{eff}}} + \frac{1}{2}\frac{\delta v^2}{v^2} + \cos^2\beta\frac{\delta\tan\beta}{\tan\beta}\right)$$

4.2.3 Explicit Counterterms for the Higgs Mass-Matrices in the mass Basis

For the calculation the counterterms have to be transformed into the mass basis, where the renormalisation transformation for the diagonalised mass matrices read

$$\mathbf{M}_{hh} \rightarrow \mathbf{M}_{hh} + \delta\mathbf{M}_{hh} \qquad (4.31\mathrm{a})$$
$$\mathbf{M}_{AA} \rightarrow \mathbf{M}_{AA} + \delta\mathbf{M}_{AA}, \qquad (4.31\mathrm{b})$$
$$\mathbf{M}_{H^\pm G^\pm} \rightarrow \mathbf{M}_{H^\pm G^\pm} + \delta\mathbf{M}_{H^\pm G^\pm}. \qquad (4.31\mathrm{c})$$

The components of the counterterm matrices in the mass basis are obtained by rotating the counterterm mass matrices in the interaction basis in the same way as the tree-level mass-matrices (2.51),

$$\delta\mathbf{M}_{hh} = \mathbf{U}_{e(0)}\ \delta\mathbf{M}_{\phi\phi}\ \mathbf{U}^\dagger_{e(0)} = \begin{pmatrix} \delta m^2_{h_1 h_1} & \delta m^2_{h_1 h_2} & \delta m^2_{h_1 h_3} \\ \delta m^2_{h_2 h_1} & \delta m^2_{h_2 h_2} & \delta m^2_{h_2 h_3} \\ \delta m^2_{h_3 h_1} & \delta m^2_{h_3 h_2} & \delta m^2_{h_3 h_3} \end{pmatrix} \qquad (4.32\mathrm{a})$$

$$\delta\mathbf{M}_{AA}, = \mathbf{U}_{o(0)}\,\delta\mathbf{M}_{\chi\chi}\,\mathbf{U}_{o(0)}^{\dagger} = \begin{pmatrix} \delta m^2_{A_1 A_1} & \delta m^2_{A_1 A_2} & \delta m^2_{A_1 G_0} \\ \delta m^2_{A_2 A_1} & \delta m^2_{A_2 A_2} & \delta m^2_{A_2 G_0} \\ \delta m^2_{G_0 A_1} & \delta m^2_{G_0 A_2} & \delta m^2_{G_0 G_0} \end{pmatrix} \tag{4.32b}$$

$$\delta\mathbf{M}_{H^{\pm}G^{\pm}} = \mathbf{U}_{c(0)}\delta\mathbf{M}_{\phi^{\pm}\phi^{\pm}}\mathbf{U}_{c(0)}^{\dagger} = \begin{pmatrix} \delta m^2_{H^{\pm}H^{\pm}} & \delta m^2_{H^{\pm}G^{\pm}} \\ \delta m^2_{G^{\pm}H^{\pm}} & \delta m^2_{G^{\pm}G^{\pm}} \end{pmatrix}. \tag{4.32c}$$

In the charged sector the only relevant counterterm matrix-element reads

$$\delta m^2_{H^{\pm}H^{\pm}} = \delta M^2_{H^{\pm}}, \tag{4.33}$$

since the charged Higgs-boson mass is renormalised after the rotation into the mass basis. For the $\mathcal{CP}$-odd counterterm matrix the rotation can be performed in two steps as described for the tree-level mass matrix in eq. (4.17),

$$
\begin{aligned}
\mathbf{U}_{o(0)}\delta\mathbf{M}_{\chi\chi}\mathbf{U}_{o(0)}^{\dagger} &= \\
= \mathbf{U}_{o(0)}^{(a)}\mathbf{U}_{o(0)}^{(G)}\delta\mathbf{M}_{\chi\chi}\left(\mathbf{U}_{o(0)}^{(G)}\right)^{\dagger}\left(\mathbf{U}_{o(0)}^{(a)}\right)^{\dagger} &= \begin{pmatrix} \delta m^2_{\chi_1\chi_1} & \delta m^2_{\chi_1\chi_2} & \delta m^2_{\chi_1\chi_s} \\ \delta m^2_{\chi_2\chi_1} & \delta m^2_{\chi_2\chi_2} & \delta m^2_{\chi_2\chi_s} \\ \delta m^2_{\chi_s\chi_1} & \delta m^2_{\chi_s\chi_2} & \delta m^2_{\chi_s\chi_s} \end{pmatrix} \\
= \mathbf{U}_{o(0)}^{(a)}\delta\mathbf{M}_{aa}\left(\mathbf{U}_{o(0)}^{(a)}\right)^{\dagger} &= \begin{pmatrix} \delta m^2_{a_1 a_1} & \delta m^2_{a_1 a_2} & \delta m^2_{a_1 G^0} \\ \delta m^2_{a_2 a_1} & \delta m^2_{a_2 a_2} & \delta m^2_{a_2 G^0} \\ \delta m^2_{G^0 a_1} & \delta m^2_{G^0 a_2} & \delta m^2_{G^0 G^0} \end{pmatrix} \\
= \delta\mathbf{M}_{AA} &= \begin{pmatrix} \delta m^2_{A_1 A_1} & \delta m^2_{A_1 A_2} & \delta m^2_{A_1 G^0} \\ \delta m^2_{A_2 A_1} & \delta m^2_{A_2 A_2} & \delta m^2_{A_2 G^0} \\ \delta m^2_{G^0 A_1} & \delta m^2_{G^0 A_2} & \delta m^2_{G^0 G^0} \end{pmatrix}. \tag{4.34}
\end{aligned}
$$

In the first rotation the singlet counterterms are demixed from the doublet counterterms similar to the fields as described in eqs. (4.17).

Although the charged and neutral Goldstone fields obtain a mass term $\xi_W M_W^2$ and $\xi_Z M_Z^2$ by the gauge-fixing term, they are considered to be renormalised such that do not contribute to the counterterm construction.

4.2.4 Field Renormalisation

For the field renormalisation, which is necessary to obtain finite Green-functions for arbitrary values of the external momentum, a single renormalisation constant is given to each Higgs doublet and the singlet,

$$\mathcal{H}_1 \to \left(\mathbb{1} + \frac{1}{2}\delta Z_{\mathcal{H}_1}\right)\mathcal{H}_1, \quad \mathcal{H}_2 \to \left(\mathbb{1} + \frac{1}{2}\delta Z_{\mathcal{H}_2}\right)\mathcal{H}_2, \quad \mathcal{S} \to \left(\mathbb{1} + \frac{1}{2}\delta Z_{\mathcal{S}}\right)\mathcal{S}. \tag{4.35}$$

In the mass basis the field renormalisation in the $\mathcal{CP}$-even and $\mathcal{CP}$-odd sectors reads

$$\begin{pmatrix} h_1 \\ h_2 \\ h_3 \end{pmatrix} \to \left[\mathbb{1} + \frac{1}{2}\delta\mathcal{Z}_{hh}\right]\begin{pmatrix} h_1 \\ h_2 \\ h_3 \end{pmatrix} = \left[\mathbb{1} + \frac{1}{2}\begin{pmatrix} \delta Z_{h_1 h_1} & \delta Z_{h_1 h_2} & \delta Z_{h_1 h_3} \\ \delta Z_{h_2 h_1} & \delta Z_{h_2 h_2} & \delta Z_{h_2 h_3} \\ \delta Z_{h_3 h_1} & \delta Z_{h_3 h_2} & \delta Z_{h_3 h_3} \end{pmatrix}\right]\begin{pmatrix} h_1 \\ h_2 \\ h_3 \end{pmatrix} \tag{4.36a}$$

$$\begin{pmatrix} A_1 \\ A_2 \\ G^0 \end{pmatrix} \rightarrow \left[\mathbb{1} + \frac{1}{2}\delta\mathscr{Z}_{AA} \right] \begin{pmatrix} A_1 \\ A_2 \\ G^0 \end{pmatrix} = \left[\mathbb{1} + \frac{1}{2} \begin{pmatrix} \delta Z_{A_1 A_1} & \delta Z_{A_1 A_2} & \delta Z_{A_1 G^0} \\ \delta Z_{A_2 A_1} & \delta Z_{A_2 A_2} & \delta Z_{A_2 G^0} \\ \delta Z_{G^0 A_1} & \delta Z_{G^0 A_2} & \delta Z_{G^0 G^0} \end{pmatrix} \right] \begin{pmatrix} A_1 \\ A_2 \\ G^0 \end{pmatrix}.$$

$$(4.36b)$$

The renormalisation constants defined in the interaction basis according to eqs. (4.35) are related to the renormalisation constants in the mass basis from by

$$\delta\mathscr{Z}_{hh} = \mathbf{U}_{e(0)} \begin{pmatrix} \delta Z_{\mathcal{H}_1} & 0 & 0 \\ 0 & \delta Z_{\mathcal{H}_2} & 0 \\ 0 & 0 & \delta Z_{\mathcal{S}} \end{pmatrix} \mathbf{U}_{e(0)}^\dagger \tag{4.37a}$$

$$\delta\mathscr{Z}_{AA} = \mathbf{U}_{o(0)} \begin{pmatrix} \delta Z_{\mathcal{H}_1} & 0 & 0 \\ 0 & \delta Z_{\mathcal{H}_2} & 0 \\ 0 & 0 & \delta Z_{\mathcal{S}} \end{pmatrix} \mathbf{U}_{o(0)}^\dagger. \tag{4.37b}$$

Since the all fields of $\mathcal{H}_1$, $\mathcal{H}_2$ and $\mathcal{S}$, the on-shell conditions can not be fulfilled for all physical fields at the same time, which leads to non-trivial wave function normalisation-constants.

4.3 Renormalisation Conditions

For the one-loop calculation the chosen set independent parameters from the Higgs potential V_{H} given in tab. 4.1 has to be renormalised. In this section the explicit form of their counterterms given in eq. (4.25) will be fixed. An overview over the chosen renormalisation schemes for the independent parameters is given in tab. 4.2. In order

on-shell scheme:	M_W, M_Z, $M_{H^\pm}($, T_{h_1}, T_{h_2}, $T_{h_s})$
$\overline{\mathrm{DR}}$ scheme:	λ, κ, $\tan\beta$, v, μ_{eff}, A_κ

Table 4.2: Chosen renormalisation schemes for the set of independent parameters. The on-shell scheme for the tadpole coefficient means they are renormalised to their classical value, which is zero in the minimum of the Higgs potential V_{H}

to maintain compatibility with earlier calculations in the MSSM as implemented in `FeynHiggs`, the MSSM-Parameters are renormalised according to the conventions of this code. An overview over employed renormalisation schemes in the MSSM with real parameters can be found in [80]. All parameters that are genuine to the NMSSM-calculation are chosen to be renormalised in the $\overline{\mathrm{DR}}$ scheme at the specified renormalisation scale of the Higgs-mass calculation. In `FeynHiggs` this scale is typically the mass of the top-quark.

4.3.1 MSSM(-like) Parameters

The SM gauge bosons and the charged Higgs masses are renormalised on-shell,

$$\delta M_W^2 = \mathrm{Re}\Sigma_\mathrm{T}^{WW}\left(M_W^2\right), \quad \delta M_Z^2 = \mathrm{Re}\Sigma_\mathrm{T}^{ZZ}\left(M_Z^2\right), \quad \delta M_W^2 = \mathrm{Re}\Sigma_{H^\pm H^\pm}\left(M_{H^\pm}^2\right). \quad (4.38)$$

As the tadpole coefficients are required to vanish to ensure the minimisation of the Higgs potential, their renormalisation constants follow from

$$T_{h_i}^{(1)} + \delta T_{h_i} = 0, \quad i \in \{1, 2, 3\} \quad (4.39)$$

where $T_{h_i}^{(1)}$ denotes the tadpole contributions at one-loop order[2]. The conditions (4.39) yield

$$\delta T_{h_i} = -T_{h_i}^{(1)}, \quad i \in \{1, 2, 3\}. \quad (4.40)$$

For the field renormalisation constants the $\overline{\mathrm{DR}}$-scheme is chosen

$$\delta Z_{\mathcal{H}_1} = -\frac{\partial}{\partial k^2}\Sigma_{\phi_1\phi_1}\bigg|^{\mathrm{div}}, \quad \delta Z_{\mathcal{H}_2} = -\frac{\partial}{\partial k^2}\Sigma_{\phi_2\phi_2}\bigg|^{\mathrm{div}}, \quad \delta Z_{\mathcal{S}} = -\frac{\partial}{\partial k^2}\Sigma_{\phi_s\phi_s}\bigg|^{\mathrm{div}} \quad (4.41)$$

The field renormalisation constants completely drop out in the determination of the Higgs-boson masses at one-loop order. They only enter via residual higher-order effects as a consequence of the iterative numerical determination of the propagator poles described in sect. 5.2. The $\overline{\mathrm{DR}}$ scheme for the field renormalisation constants is convenient in order to avoid the possible occurrence of unphysical threshold effects. Higgs bosons appearing as external particles in a physical process of course have to obey proper on-shell conditions as discussed in sec. 3.3.

Based on the field renormalisation constants the $\overline{\mathrm{DR}}$ scheme is adopted for $\tan\beta$

$$\delta\tan\beta = \frac{1}{2}\left(\delta Z_{\mathcal{H}_2} - \delta Z_{\mathcal{H}_2}\right)\tan\beta \quad (4.42)$$

Since clear experimental signals for supersymmetry are a absent, a manifestly process independent renormalisation condition as in eq. (4.42) is convenient. For calculations in the MSSM this definition yields numerically stable results [81–83]. This scheme also is gauge-independent at the one-loop level both in the MSSM [83] and NMSSM [84, 85].

4.3.2 Parameters genuine to the NMSSM Calculation

In the MSSM only the renormalisation constants of the W-boson mass, δM_W^2, the charged Higgs mass, $\delta M_{H^\pm}^2$, and $\delta\tan\beta$ enter the one-loop calculation together with the tadpole counterterms. In the NMSSM more renormalisation constants enter. These constant are not all genuine to the NMSSM. Genuine to the NMSSM are λ, κ,

---

[2]Although the singlet tadpole coefficient is not MSSM-like it is mentioned along its MSSM counterparts, since it is renormalised in the same way.

A_κ and the tadpole of the singlet field T_{ϕ_s}. Besides the tadpole, that is renormalised as its MSSM counterpart, they are renormalised in the $\overline{\mathrm{DR}}$ scheme. The parameters not genuine to the NMSSM the vacuum expectation-value v and μ_{eff}. They do not drop out in the tree-level NMSSM calculation like for the MSSM calculation. In particular the $\overline{\mathrm{DR}}$ renormalisation of v has repercussion on the charge renormalisation, since they are directly related to each other. This relation will be discussed in the following section in greater detail.

4.4 Renormalisation of the electromagnetic Coupling Constant α

In the NMSSM calculation of Higgs masses the SM vacuum expectation-value v does not drop out of the tree-level calculation. Thus an additional independent parameter has to be renormalised, either v or the electromagnetic coupling constant α, which are related by

$$v^2 = \frac{2s_w^2 M_W^2}{4\pi\alpha}. \tag{4.43}$$

The weak mixing angle is not an independent parameter in the presented calculation, where the gauge-boson masses are treated as independent parameters. The weak mixing angle is related to them by eq. (2.7).

Applying a renormalisation transformation to the parameters s_w and α,

$$\alpha \to \alpha\left(1 + \delta Z_\alpha\right), \quad s_w^2 \to s_w^2 + \delta s_w^2 \tag{4.44}$$

to eq. (4.43) yields

$$\delta v^2 = \frac{2s_w^2 M_W^2}{4\pi\alpha}\left(\frac{\delta s_w^2}{s_w^2} + \frac{\delta M_W^2}{M_W^2} - \delta Z_\alpha\right). \tag{4.45}$$

Considering δM_W^2 and subsequently δs_w^2 already fixed by on-shell conditions for the gauge-boson masses as outlined in sec. 4.3.1, where the dependent counterterm for the sine of the weak mixing angle is given by

$$\delta s_w^2 = -c_w^2\left(\frac{\delta M_W^2}{M_W^2} - \frac{\delta M_Z^2}{M_Z^2}\right), \tag{4.46}$$

either δZ_α or δv in eq. (4.45) can be fixed by an independent renormalisation condition (and the other counterterm is then a dependent quantity).

In this section a motivation for the chosen $\overline{\mathrm{DR}}$ renormalisation scheme for v will be given together with a description of the implications for the renormalisation of α and the applied reparametrisation procedure.

4.4.1 Motivation for a $\overline{\text{DR}}$ renormalised v

The renormalisation prescription [76] where δZ_α is fixed by renormalising e,

$$e \rightarrow e\left(1 + \delta Z_e\right), \quad \delta Z_\alpha = 2\delta Z_e, \tag{4.47}$$

in the static limit results in a non-$\overline{\text{DR}}$ renormalisation for δv. Here δZ_e is the counterterm of the charge renormalisation within the NMSSM according to the static (Thomson) limit,

$$\delta Z_e = \frac{1}{2}\Pi^{\gamma\gamma}(0) + \frac{s_w}{c_w}\frac{\Sigma_T^{\gamma Z}(0)}{M_Z^2} , \tag{4.48}$$

and $\Pi^{\gamma\gamma}(0)$, $\Sigma_T^{\gamma Z}(0)$ are the derivative of the transverse part of the photon self-energy and the transverse part of the photon–Z self-energy at zero momentum transfer, respectively. It is important to stress that the sign convention for the weak mixing-angle differs from the standard convention found in the literature for the SM, e.g. in [42, 69], which changes the sign in front of $\Sigma_T^{\gamma Z}(0)$ in eq. (4.48).

For the self-energies in the Higgs sector δv enters the counterterms for the renormalised Higgs potential in eq. (4.21) with coefficients involving λ and κ, like

$$\delta m_{\phi_s\phi_{\{1,2\}}}^2 \supset -\kappa\mu_{\text{eff}}\left\{\sin\beta, \cos\beta\right\}\left(\delta v + \ldots\right), \tag{4.49}$$

for the self-energies with each an external doublet and singlet field. The ellipsis in eq. (4.49) denote other renormalisation constants that are fixed in the $\overline{\text{DR}}$-scheme and thus do not contribute with a finite part. However, a finite contribution from δv would lead to a κ-dependence of all loop contributions to δv, in particular also of the corrections from the fermions and sfermions (while the fermion and sfermion contributions to the unrenormalised self-energy are κ-independent). A finite contribution from δv would furthermore imply the rather artificial feature that a self-energy involving an external gauge singlet field would receive a counterterm contribution involving the renormalisation constant δZ_e for the electric charge. We therefore prefer to use the $\overline{\text{DR}}$-scheme for the renormalisation of v, which means that we use a scheme where δZ_e is a dependent counterterm. This leads to the relation

$$\delta Z_e^{\text{dep}} = \frac{1}{2}\left[\frac{\delta s_w^2}{s_w^2} + \frac{\delta M_W^2}{M_W^2} - \frac{\delta v^2}{v^2}\right] , \tag{4.50}$$

which implies

$$\delta Z_e^{\text{dep}}\bigg|^{\text{fin}} = \frac{1}{2}\left[\frac{\delta s_w^2}{s_w^2} + \frac{\delta M_W^2}{M_W^2}\right]^{\text{fin}} \tag{4.51}$$

for the finite part of δZ_e^{dep}. In this scheme the numerical value for the electric charge e (and accordingly for α) is determined indirectly via eq. (4.51). In order to avoid a non-standard numerical value for α in our numerical results, a two-step procedure is

applied: In the first step a $\overline{\text{DR}}$ renormalisation for v is applied as outlined above. As a second step this result is reparametrised in terms of a suitably chosen expression for α. By default we use the same convention as for the MSSM result that is implemented in `FeynHiggs`, namely the expression for the electric charge in terms of Fermi's constant G_F, in order to facilitate the comparison between the `FeynHiggs` result in the MSSM and our new result in the NMSSM. For the numerical comparison with `NMSSMCalc` $\alpha(M_Z)$ will be used instead. The procedure of the reparametrisation is outlined in the following section.

4.4.2 Reparametrisation of α

Because of the equality of the bare couplings, the couplings g^I and g^{II} in two different renormalisation schemes are in general related to each other by

$$g^I \left(1 + \delta Z_g^I \right) = g^{II} \left(1 + \delta Z_g^{II} \right) \ . \tag{4.52}$$

The corresponding shift in the numerical values of the coupling definitions is obtained from the finite difference of the two counterterms, $\Delta \equiv g^{II} \delta Z_g^{II} - g^I \delta Z_g^I$. Accordingly, a reparametrisation from the numerical value of the coupling used in scheme I to the one of scheme II can be performed via

$$g^I = g^{II} + \Delta \ . \tag{4.53}$$

Since Δ is of one-loop order, its insertion into a tree-level expression generates a term of one-loop order, etc.

In our calculation the reparametrisation of the electromagnetic coupling is only necessary up to the one-loop level, since all corrections of two-loop and higher order that we are going to incorporate have been obtained in the gauge-less limit (some care is necessary regarding the incorporation of the MSSM-type contributions of $\mathcal{O}(\alpha_t^2)$, see [86, 87]). At this order the shift Δ can simply be expressed as $\Delta = g^{II} \left(\delta Z_g^{II} - \delta Z_g^I \right)$. Specifically, for the reparametrisation of the electromagnetic coupling constant in terms of G_F the parameter shift Δ_{G_F} reads

$$\Delta_{G_F} = e \left(\delta Z_e - \delta Z_e^{\text{dep}} - \frac{1}{2} \Delta r^{\text{NMSSM}} \right) \ . \tag{4.54}$$

Here δZ_e is the counterterm of the charge renormalisation within the NMSSM according to the static (Thomson) limit as given in eq. (4.48). The counterterm δZ_e^{dep} has been defined in eq. (4.50), and for the quantity Δr^{NMSSM} we use the result of [88] (see also [89]). The numerical value for the electromagnetic coupling e in this parametrisation is obtained from the Fermi constant in the usual way as $e = 2 M_W s_w \sqrt{G_F \sqrt{2}}$.

Similarly, for the reparametrisation of the electromagnetic coupling defined in the

previous section in terms of $\alpha(M_Z)$ the parameter shift $\Delta_{\alpha(M_Z)}$ reads

$$\Delta_{\alpha(M_Z)} = e\left(\delta Z_e - \delta Z_e^{\text{dep}} - \frac{1}{2}\Delta\alpha\right) . \tag{4.55}$$

The numerical value of e in this parametrisation is obtained from $\alpha(M_Z) = \alpha(0)/(1-\Delta\alpha)$, and $\alpha(0)$ is the value of the fine-structure constant in the Thomson limit. The quantity $\Delta\alpha$ will be discussed when $\Delta_{\alpha(M_Z)}$ will be described in more detail for the comparison with the code NMSSMCalc in sec. 8.1.3.

4.4.3 Reparametrisation of the NMSSM Higgs-Sector

The reparametrisation of the NMSSM Higgs-sector leads to additional terms of one-loop order that are added the mass matrices at tree-level,

$$\mathbf{M}_{\Psi\Psi}^2 \to \mathbf{M}_{\Psi\Psi}^2 + \Delta\mathbf{M}_{\Psi\Psi}^2, \quad \Psi \in \{\phi,\ \chi\}. \tag{4.56}$$

The matrix $\Delta\mathbf{M}_{\Psi\Psi}^2$ is proportional to the finite shift Δ_α and vanishes in the MSSM-limes. Its components read for the $\mathcal{CP}$-even sector in the interaction basis

$$\left(\Delta\mathbf{M}_{\phi\phi}^2\right)_{11} = \lambda^2 v^2 \sin^2\beta\ \Delta_\alpha, \tag{4.57a}$$

$$\left(\Delta\mathbf{M}_{\phi\phi}^2\right)_{22} = \lambda^2 v^2 \cos^2\beta\ \Delta_\alpha, \tag{4.57b}$$

$$\left(\Delta\mathbf{M}_{\phi\phi}^2\right)_{33} = \left(2\frac{\lambda^4 v^4}{\mu_{\text{eff}}^2}\sin^2\beta\cos^2\beta - \lambda\kappa v^2 \sin\beta\cos\beta\right)\Delta_\alpha, \tag{4.57c}$$

$$\left(\Delta\mathbf{M}_{\phi\phi}^2\right)_{12} = -\lambda^2 v^2 \sin\beta\cos\beta\ \Delta_\alpha, \tag{4.57d}$$

$$\left(\Delta\mathbf{M}_{\phi\phi}^2\right)_{13} = \left(3\frac{\lambda^3 v^3}{\mu_{\text{eff}}}\sin\beta 2\cos\beta - \kappa v\mu_{\text{eff}}\sin\beta + 2\lambda v\mu_{\text{eff}}\cos\beta\right)\frac{\Delta_\alpha}{2}, \tag{4.57e}$$

$$\left(\Delta\mathbf{M}_{\phi\phi}^2\right)_{23} = \left(3\frac{\lambda^3 v^3}{\mu_{\text{eff}}}\cos^2\beta\sin\beta - \kappa v\mu_{\text{eff}}\cos\beta + 2\lambda v\mu_{\text{eff}}\sin\beta\right)\frac{\Delta_\alpha}{2}, \tag{4.57f}$$

and for the $\mathcal{CP}$-odd sector they read

$$\left(\Delta\mathbf{M}_{\chi\chi}^2\right)_{11} = \lambda^2 v^2 \sin^2\beta\ \Delta_\alpha, \tag{4.58a}$$

$$\left(\Delta\mathbf{M}_{\chi\chi}^2\right)_{22} = \lambda^2 v^2 \cos^2\beta\ \Delta_\alpha, \tag{4.58b}$$

$$\left(\Delta\mathbf{M}_{\chi\chi}^2\right)_{33} = \left(2\frac{\lambda^4 v^4}{\mu_{\text{eff}}^2}\sin^2\beta\cos^2\beta + 3\lambda\kappa v^2 \sin\beta\cos\beta\right)\Delta_\alpha, \tag{4.58c}$$

$$\left(\Delta\mathbf{M}_{\chi\chi}^2\right)_{12} = -\lambda^2 v^2 \sin\beta\cos\beta\ \Delta_\alpha, \tag{4.58d}$$

$$\left(\Delta\mathbf{M}_{\chi\chi}^2\right)_{13} = \left(-3\frac{\lambda^3 v^3}{\mu_{\text{eff}}}\sin^2\beta\cos\beta + 3\kappa v\mu_{\text{eff}}\sin\beta\right)\frac{\Delta_\alpha}{2}, \tag{4.58e}$$

$$\left(\Delta\mathbf{M}_{\chi\chi}^2\right)_{23} = \left(3\frac{\lambda^3 v^3}{\mu_{\text{eff}}}\cos^2\beta\sin\beta - 3\kappa v\mu_{\text{eff}}\cos\beta\right)\frac{\Delta_\alpha}{2}. \tag{4.58f}$$

The shift-matrix $\Delta \mathbf{M}^2_{\Psi\Psi}$ is transformed into the mass basis by the unitary transformations $\mathbf{U}_{\{e,o\}(0)}$ at lowest order,

$$\Delta \mathbf{M}^2_{hh} = \mathbf{U}_{e(0)} \Delta \mathbf{M}^2_{\phi\phi} \mathbf{U}^\dagger_{e(0)}, \quad \Delta \mathbf{M}^2_{AA} = \mathbf{U}_{o(0)} \Delta \mathbf{M}^2_{\chi\chi} \mathbf{U}^\dagger_{o(0)}. \tag{4.59}$$

4.5 Analytic Tests of the Renormalisation Scheme

Including $\overline{\text{DR}}$ renormalisation constants does not influence the Higgs-mass predictions, which depend only on finite higher-order contributions. However, including $\overline{\text{DR}}$ renormalisation constants presents a non-trivial test for the calculation. It involves all NMSSM vertices that enter the Higgs-mass calculation. This test is of particular importance for the genuine NMSSM couplings that are not present in the MSSM.

The presented calculations of higher-order corrections in the Higgs sector were performed semi-automatically. In order to generate the unrenormalised higher-order corrections the NMSSM was implemented into a model file for the tool `FeynArts` [90]. The implementation of the NMSSM is performed in the mass basis, expressed by the vertices in the interaction basis and generic mixing matrices for the superpartner fields. The model file is based on an automatically generated NMSSM model file obtained by an early version of `Sarah` [91]. The model file itself was already used for previous NMSSM studies [92] in which not all sectors relevant to the Higgs-mass calculation were involved, and thus the model file was only partially tested. Thus further testing and improvement of this model file was advisable and necessary.

In order to have a simple and elegant check for $\overline{\text{DR}}$ renormalised NMSSM specific parameters κ, λ and A_κ, the one-loop β-functions have been recovered from their counterterms as described in sec. 3.4. The β-functions and anomalous (field) dimensions γ of the NMSSM are well-known, see [17, 93, 94], for a more general treatment see [84, 85, 95–97]. The one-loop β functions are unique for a given theory. In particular they are independent of the basis in which they are calculated. Hence a calculation in the interaction basis for the Higgs-, higgsino- and gaugino-sectors is applied. In this approach, where no mixing between any fields in these sectors occurs, the calculation obtains a simple structure and is thus feasible to be performed analytically. In the mass basis the presence of several mixing matrices makes an analytic calculation unwieldy. For the NMSSM calculation with the help of `FeynArts` and `FormCalc` the calculation in the interaction basis is performed as in the mass basis, but with all mixing matrices set identical to the unity matrix. The outlined approach is spelled out for the one-loop calculation. It makes extensive use of reduced set of couplings between the singlet/singlino field and the remaining field spectrum. An extension to two-loop order is possible, but retrieving the divergences from the β-functions and anomalous dimensions is more involving.

4.5.1 Feynman-Rules and higher-order Corrections in the Interaction Basis

In the interaction basis both diagonal and non-diagonal entries of the mass matrices can give rise to tree-level vertices between two different fields, which reads for scalars Ψ_i

$$\Gamma_{\Psi_i\Psi_j}\left(p^2\right) = \mathrm{i}\left[p^2\delta_{ij} - \left(\mathcal{M}_{\Psi\Psi}\right)_{ij}\right].\tag{4.60}$$

If the fields in the interaction basis are considered massive, the diagonal entries of the mass matrices are included in the propagator and do not give rise to additional vertices,

$$\Gamma_{\Psi_i\Psi_j}\left(p^2\right) = \mathrm{i}\underbrace{\left(p^2 - \left[\mathcal{M}_{\Psi\Psi}\right]_{ii}\right)\delta_{ij}}_{\text{inverse propagator}} - \mathrm{i}\underbrace{\left(\mathcal{M}_{\Psi\Psi}\right)_{ij}\left(1 - \delta_{ij}\right)}_{\text{vertex}}.\tag{4.61}$$

In terms of Feynman rules this reads as a propagator and a mass-vertex

$$\Psi_i \;\text{-------}\; \Psi_j \quad = \frac{\mathrm{i}\delta_{ij}}{p^2 - \left(\mathcal{M}_{\Psi\Psi}\right)_{ii}}\tag{4.62a}$$

$$\Psi_i \;\text{----}\bullet\text{----}\; \Psi_j \quad = \mathrm{i}\left(\mathcal{M}_{\Psi\Psi}\right)_{ij}\left(1 - \delta_{ij}\right)\;.\tag{4.62b}$$

These vertices give rise to an infinite number of Feynman diagrams that contribute to higher-order corrections at each order separately. From these new diagrams, however, only a very small number is divergent and needs to be considered in order to obtain the divergent part at each order. The analogous procedure gives rise to similar new Feynman rules for the fermion fields in the interaction basis, in particular for the higgsinos. In the following the divergent contribution of higher-order corrections to fermion self-energies and trilinear couplings between three scalars, and two fermions and one scalar will be outlined. The potentially divergent diagrams will be identified.

Self-Energies

In the interaction basis an infinite number of diagrams contributes to the self-energy Σ at one-loop order,

$$\Sigma\left(p^2\right) = \text{---}\bigcirc\text{---} + \text{---}\bigcirc\text{---} + \text{---}\bigcirc\text{---} + \dots$$
$$= \text{---}\bigcirc\text{---} + \text{---}\bigcirc\text{---} + \text{finite}.\tag{4.63}$$

The diagrams expressed by the ellipses contain more than one two-point vertex. However, power-counting reveals that only the first two diagrams are potentially

divergent, while all remaining diagrams are finite.

Three-Point Function for three Scalars $\Gamma_{\phi\phi\phi}$

The one-loop diagrams contributing to a triple scalar vertex include pure fermion or scalar loops,

$$\Gamma^{(1)}_{\phi\phi\phi} = \quad + \quad + \quad + \quad + \dots \qquad (4.64)$$

Again, the diagrams expressed by the ellipses contain more than one two-point vertex. The second diagram with the scalar triangle loop is finite, while the other depicted diagrams are power-counting divergent.

Three-Point Function for two fermions and one Scalar $\Gamma_{\phi\psi\bar\psi}$

The contributing one-loop diagrams to a vertex with two fermions and one scalar are

$$\Gamma^{(1)}_{\phi\psi\bar\psi} = \quad + \quad + \dots \qquad (4.65)$$

The only power-counting divergent diagram is the second one, containing one scalar and two fermion propagators. Diagrams with one or more two-point vertices are finite.

4.5.2 Renormalisation Conditions for λ, κ, A_κ and μ_{eff}

The parameter μ_{eff} will be fixed by renormalising the two-point function in the neutralino/higgsino sector, while the remaining parameters are renormalised by vertex functions. The renormalisation conditions for the renormalised two- and three-point functions,

$$\hat{\Gamma}_{\tilde{h}_1\bar{\tilde{h}}_2} = -\mathbf{Y}_{34} + \delta\mathbf{Y}_{34} + \Sigma_{\tilde{h}_1\bar{\tilde{h}}_2}, \quad \hat{\Gamma}_{\Psi\Psi\Psi} = \hat{\Gamma}^{(0)}_{\Psi\Psi\Psi} + \delta\hat{\Gamma}_{\Psi\Psi\Psi} + \hat{\Gamma}^{(1)}_{\Psi\Psi\Psi}, \qquad (4.66)$$

where the index Ψ denotes any external field and the superscripts 0 and 1 denote tree-level and one-loop quantities, read

$$\hat{\Gamma}_{\tilde{h}_1\bar{\tilde{h}}_2}\Big|^{\text{div}} = \hat{\Gamma}_{\tilde{h}_s\bar{\tilde{h}}_s\phi_s}\Big|^{\text{div}} = \hat{\Gamma}_{\tilde{h}^\pm\bar{\tilde{h}}^\pm\phi_s}\Big|^{\text{div}} = \hat{\Gamma}_{\phi_s\phi_s\phi_s}\Big|^{\text{div}} = 0. \qquad (4.67)$$

The tree-level quantities for the vertex functions read

$$\mathbf{Y}_{34} = -\mu_{\text{eff}}, \qquad (4.68a)$$

$$\Gamma^{(0)}_{\tilde{h}_s\bar{\tilde{h}}_s\phi_s} = -\sqrt{2}\kappa\left(P_L + P_R\right) = -\sqrt{2}\kappa, \qquad (4.68b)$$

$$\Gamma^{(0)}_{\tilde{h}^\pm\bar{\tilde{h}}^\pm\phi_s} = -\frac{\lambda}{\sqrt{2}}\left(P_L + P_R\right) = -\frac{\lambda}{\sqrt{2}}, \qquad (4.68c)$$

$$\Gamma^{(0)}_{\phi_s \phi_s \phi_s} = -\sqrt{2} \left(\kappa A_\kappa + 6 \frac{\kappa^2}{\lambda} \mu_{\text{eff}} \right). \tag{4.68d}$$

After applying the renormalisation transformations to these equations and using the result of [84, 85],

$$\left[\frac{\delta \mu_{\text{eff}}}{\mu_{\text{eff}}} - \frac{\delta \lambda}{\lambda} \right]^{\text{div}} = \frac{1}{2} \delta Z_{\phi_s} \Big|^{\text{div}}, \tag{4.69}$$

one obtains the following expressions for the renormalisation constants

$$\delta \mu_{\text{eff}} = - \left[\mu_{\text{eff}} \frac{1}{2} \left(\delta Z_{\tilde{h}_1} + \delta Z_{\tilde{h}_2}^\dagger \right) + \Sigma_{\tilde{h}_1 \bar{\tilde{h}}_2} \right]^{\text{div.}} \tag{4.70a}$$

$$\delta \kappa = - \frac{1}{\sqrt{2}} \left[\Gamma^{(1)}_{\tilde{h}_s \bar{\tilde{h}}_s \phi_s} + \sqrt{2} \Gamma^{(0)}_{\tilde{h}_s \bar{\tilde{h}}_s \phi_s} \left(\delta Z_{\tilde{\phi}_s} + \frac{1}{2} \delta Z_{\phi_s} \right) \right]^{\text{div}} \tag{4.70b}$$

$$\delta \lambda = \sqrt{2} \left[\Gamma^{(1)}_{\tilde{h}^\pm \bar{\tilde{h}}^\pm \phi_s} - \frac{1}{2} \Gamma^{(0)}_{\tilde{h}^\pm \bar{\tilde{h}}^\pm \phi_s} \left(\delta Z_{\tilde{h}^\pm}^{\text{L}} + \delta Z_{\tilde{h}^\pm}^{\text{L}} + \delta Z_{\phi_s} \right) \right]^{\text{div}} \tag{4.70c}$$

$$\delta A_\kappa = \frac{1}{\sqrt{2}\kappa} \left[\Gamma^{(1)}_{\phi_s \phi_s \phi_s} - \frac{3}{2} \Gamma^{(0)}_{\phi_s \phi_s \phi_s} \delta Z_{\phi_s} \right]^{\text{div}} - A_\kappa \frac{\delta \kappa}{\kappa} + 6 \frac{\kappa^2}{\lambda} \mu_{\text{eff}} \left(2 \frac{\delta \kappa}{\kappa} + \frac{1}{2} \delta Z_{\phi_s} \right). \tag{4.70d}$$

According to eq. (3.19b) the field renormalisation constant for the neutral higgsinos, which are Majorana fermions, are given in the $\overline{\text{DR}}$-scheme by

$$\delta Z_{\tilde{h}_i}^{\text{L}} = \delta Z_{\tilde{h}_i}^{\text{R}} = \delta Z_{\tilde{h}_i} = \left[\Sigma_{\tilde{h}_i \bar{\tilde{h}}_i}^{(\not{p})} (0) \right]^{\text{div}}, \quad i \in \{1, 2\}. \tag{4.71}$$

For the charged higgsino, which is a Dirac fermion, the $\overline{\text{DR}}$ field renormalisation constants read

$$\delta Z_{\tilde{h}^\pm}^{\text{L}} = - \left[\Sigma_{\tilde{h}^\pm \bar{\tilde{h}}^\pm}^{(\not{p}, L)} \left(\mu_{\text{eff}}^2 \right) \right]^{\text{div}}, \quad \delta Z_{\tilde{h}^\pm}^{\text{R}} = - \left[\Sigma_{\tilde{h}^\pm \bar{\tilde{h}}^\pm}^{(\not{p}, R)} \left(\mu_{\text{eff}}^2 \right) \right]^{\text{div}}. \tag{4.72}$$

Since only the divergent parts of higher-order contributions are necessary, only a subset of all contributing one-loop diagrams in the interaction basis has to be considered They will be discussed explicitly in the following section.

4.5.3 Diagrams with mixed Propagators

For the renormalisation conditions above two additional diagrams are necessary in order to express the neutral and charged higgsino self-energies and the one-loop corrections to the three-scalar vertex in terms of diagrams in the interaction basis.

Self-Energies

In the neutral higgsino sector only one power-counting divergent diagram with one two-point vertex exists which is given in eq. (4.63). It is, however, finite and does

not contribute to the determination of the $\overline{\text{DR}}$ field-renormalisation of the neutral higgsino.

Also for the charged higgsino only one diagram with one two-point vertex is power-counting divergent. The diagram is indeed divergent, but the divergence is independent of the external momentum $\not{p}$ and p^2. Thus it does not contribute to $\Sigma^{(\not{p})}_{\tilde{h}_i \bar{\tilde{h}}_i}(0)$ and subsequently does not contribute to the field renormalisation constants of the charged higgsino.

Higher-Order Corrections to $\Gamma_{\phi_s \phi_s \phi_s}$

For the higher-order corrections to the vertex function $\Gamma_{\phi_s \phi_s \phi_s}$ one diagram with a two-point vertex has to be evaluated. Since the singlet does neither couple to the SM fermions nor to the gaugino fields at tree-level,

$$\Gamma^{(0)}_{\phi_s f \bar{f}} = \Gamma^{(0)}_{\phi_s \widetilde{W}^\pm \widetilde{W}^\pm} = \Gamma^{(0)}_{\phi_s \widetilde{B} \widetilde{B}} = 0, \tag{4.73}$$

those fields cannot appear as internal fields in the diagram. Additionally the couplings to the neutral higgsinos are severely constrained with only one non-vanishing vertex to both different neutral higgsinos, see eq. (4.68c). The coupling to two charged higgsinos does not vanish, but no two-point vertex exists for the charged higgsino. The only divergent diagram reads

$$\Gamma^{(1,\text{mix})}_{\phi_s \phi_s \phi_s} = \quad \phi_s \quad \tilde{h}_2 \quad \tilde{h}_1 \quad \phi_s \quad \tilde{h}_2 \quad \tilde{h}_1 \quad \phi_s \quad . \tag{4.74}$$

Due to the simple coupling structure of the singlet to the higgsinos the divergent contribution of this graph can be easily calculated via the box diagram,

$$\mathrm{i}\Gamma^{(1)}_{\phi_s \phi_s \phi_s \phi_s} = \quad \phi_s \quad \widetilde{\phi}_2 \quad \phi_s \quad \widetilde{\phi}_1 \quad \widetilde{\phi}_1 \quad \phi_s \quad \widetilde{\phi}_2 \quad \phi_s \tag{4.75}$$

by replacing one vertex $\Gamma^{(0)}_{\phi_s \tilde{h}_1 \tilde{h}_2} = \lambda/\sqrt{2}$ with the two-point vertex $\Gamma^{(0)}_{\tilde{h}_1 \tilde{h}_2} = -\mu_{\text{eff}}$,

$$\mathrm{i}\Gamma^{(1,\text{mix})}_{\phi_s \phi_s \phi_s}\Big|^{\text{div}} = \left[\frac{\Gamma^{(0)}_{\tilde{h}_1 \tilde{h}_2}}{\Gamma^{(0)}_{\phi_s \tilde{h}_1 \tilde{h}_2}} \mathrm{i}\Gamma^{(1)}_{\phi_s \phi_s \phi_s \phi_s} \right]^{\text{div}} = -\sqrt{2}\frac{\mu_{\text{eff}}}{\lambda}\left[\mathrm{i}\Gamma^{(1)}_{\phi_s \phi_s \phi_s \phi_s} \right]^{\text{div}}. \tag{4.76}$$

4.5.4 Explicit Expressions for $\delta\mu_{\text{eff}}$, $\delta\lambda$, $\delta\kappa$ and δA_κ

After the calculation of all relevant diagrams eqs. (4.70) yield the analytic results

$$\frac{\delta\kappa}{\kappa} = \frac{\Delta}{16\pi^2} 3 \left(\kappa^2 + \lambda^2\right) \tag{4.77a}$$

$$\delta A_\kappa = \frac{\Delta}{16\pi^2} 6 \left(\lambda^2 A_\lambda + \kappa^2 A_\kappa\right) \tag{4.77b}$$

$$\frac{\delta\mu_{\text{eff}}}{\mu_{\text{eff}}} = \frac{\Delta}{16\pi^2} \left(\frac{1}{2}\left(3Y_t^2 + 3Y_b^2 + Y_\tau^2\right) + \lambda^2 - \frac{\alpha}{c_w^2 s_w^2}\left(1 + 2c_w^2\right)\right) \tag{4.77c}$$

$$\frac{\delta\lambda}{\lambda} = \frac{\Delta}{16\pi^2} \left(\frac{1}{2}\left(3Y_t^2 + 3Y_b^2 + Y_\tau^2\right) + \kappa^2 + 2\lambda^2 - \frac{\alpha}{c_w^2 s_w^2}\left(1 + 2c_w^2\right)\right). \tag{4.77d}$$

The results are given in the original set of independent parameters as present in the Higgs potential (2.38) to enable an easier comparison with the β-functions given in [17]. Both results agree with each other[3]. In order to test the consistency of the model file the higher-order corrections for additional vertices between three fields were successfully checked for finiteness with the methods described in this section.

These tests included all three-point vertices at one-loop order with three $\mathcal{CP}$-even Higgs bosons and all remaining singlet-higgsino-Higgs vertices,

$$\hat{\Gamma}_{\phi_i \phi_j \phi_k} = \Gamma^{(0)}_{\phi_i \phi_j \phi_k} + \Gamma^{(1)}_{\phi_i \phi_j \phi_k} + \delta\Gamma_{\phi_i \phi_j \phi_k} = \text{finite}, \tag{4.78a}$$

$$\hat{\Gamma}_{\tilde{h}_i \tilde{h}_s \phi_j} = \Gamma^{(0)}_{\tilde{h}_i \tilde{h}_s \phi_j} + \Gamma^{(1)}_{\tilde{h}_i \tilde{h}_s \phi_j} + \delta\Gamma_{\tilde{h}_i \tilde{h}_s \phi_j} = \text{finite}, \tag{4.78b}$$

where $\{i, j, k\} \in \{1, 2, s\}$ and

$$\delta\Gamma_{\Psi_l \Psi_m \Psi_n} = \delta g_{\Psi_l \Psi_m \Psi_n} + \frac{1}{2}\left(\delta Z_{\Psi_l} + \delta Z_{\Psi_m} + \delta Z_{\Psi_n}\right)\Gamma^{(0)}_{\Psi_l \Psi_m \Psi_n}. \tag{4.78c}$$

Here the symbols Ψ_l denote Higgs- or higgsino-fields, and δg contains no field renormalisation constants.

---

[3] In [17] the β-functions for an additional supersymmetry conserving μ-parameter and λ^2 are given. The result for μ_{eff} is identical to the result for μ, while the one-loop result for λ is related by $\beta_\lambda = \beta_{\lambda^2}/2$.

5 Calculation of Higgs Masses

The determination of NMSSM Higgs-masses was performed as a first step of an extension of the public tool `FeynHiggs` [30–36] for the NMSSM with real parameters. This extension consists of a full one-loop calculation in the NMSSM supplemented by two-loop contributions from the MSSM that are already implemented in `FeynHiggs`. Thus the presented calculation was performed by using the same diagrammatic methods with a mixed on-shell and $\overline{\text{DR}}$ renormalisation scheme as was used for the calculations implemented in FeynHiggs. The NMSSM- and MSSM-calculations should thus yield identical results for the Higgs-masses in the MSSM-limit.

In this chapter the definition of the Higgs pole-masses will be given. Furthermore the chapter will provide descriptions of the tools and methods used in the calculation and numerical evaluation of the obtained results for the Higgs pole-masses.

5.1 Pole-Mass Definition

The pole mass m_{pole} of an unstable scalar field ϕ is determined by the real part of the complex pole $\mathcal{M}$ of the full propagator, which is given in the ϕ^3-theory by

$$\mathrm{i}\Delta_{\phi\phi}\!\left(p^2\right) = \quad p \text{———} p$$

$$+ \sum_{n=1}^{\infty} \left(p \text{—}\bigcirc\text{—} p \right)^n \cdot \left(p \text{———} p \right)^{n+1}$$

$$+ \sum_{n=1}^{\infty} \left(p \text{—}\ominus\text{—} p + p \text{—}\ocirc\text{—} p \right)^n \cdot \left(p \text{———} p \right)^{n+1}$$

$$+ \ldots \tag{5.1}$$

where the scalar field ϕ is always denoted by a solid line. The first diagram in eq. (5.1) denotes the tree-level propagator, the second line contains all renormalised one-loop diagrams and the third line all renormalised two-loop diagrams[1]. The ellipses denote diagrams of higher-order. Summed up the full propagator reads

$$\hat{\Delta}_{\phi\phi}\!\left(p^2\right) = \frac{1}{p^2 - m_\phi^2 + \hat{\Sigma}(p^2)}, \tag{5.2}$$

---

[1]Tadpole contributions are considered to be already renormalised and absorbed by the tadpole counterterm contributions.

where m_ϕ denotes the tree-level mass-parameter of the field ϕ. The renormalised higher-order corrections are expressed by the renormalised self-energy $\hat{\Sigma}$,

$$\hat{\Sigma}\left(p^2\right) = \sum_{n=1}^{\infty} \hat{\Sigma}^{(n)}\left(p^2\right) = \hat{\Sigma}^{(1)}\left(p^2\right) + \hat{\Sigma}^{(2)}\left(p^2\right) + \ldots \tag{5.3}$$

with

$$\hat{\Sigma}^{(1)}\left(p^2\right) = p \,-\!\!\bigcirc\!\!-\, p \;, \quad \hat{\Sigma}^{(2)}\left(p^2\right) = p \,-\!\!\ominus\!\!-\, p \;+ p \,-\!\!\text{\large$\circ$}\!\!-\, p \;. \tag{5.4}$$

At the pole $\mathcal{M}^2$ of the full propagator the inverse propagator vanishes. This means the renormalised two-point function vanishes at $\mathcal{M}^2$,

$$\mathrm{i}\hat{\Delta}_{\phi\phi}^{-1}\left(\mathcal{M}^2\right) = \hat{\Gamma}_{\phi\phi}\left(\mathcal{M}^2\right) = \mathcal{M}^2 - m_\phi^2 + \hat{\Sigma}\left(\mathcal{M}^2\right) = 0. \tag{5.5}$$

After obtaining the complex pole by solving eq. (5.5) it can be decomposed into the pole mass and the total width Γ_ϕ of the particle ϕ

$$\mathcal{M}^2 = m_{\text{pole}}^2 - \mathrm{i}m_{\text{pole}}\Gamma_\phi. \tag{5.6}$$

In the NMSSM the Higgs bosons mix with each other resulting in a propagator matrix with several poles $\mathcal{M}_i^2$. The pole condition given in eq. (5.5) is then translated into

$$\det\left[\hat{\Gamma}_{\phi\phi}\left(k^2\right)\right]_{k^2 = \mathcal{M}_i^2} = 0. \tag{5.7}$$

5.1.1 Self-Energy Contributions

The renormalised self-energies in the $\mathcal{CP}$-even and -odd sectors are evaluated by taking into account the full contributions from the NMSSM at one-loop order and as an approximation, the contributions from the MSSM at two-loop order,

$$\hat{\Sigma}_{\Psi\Psi}\left(k^2\right) \approx \left.\hat{\Sigma}_{\Psi\Psi}^{(1)}\left(k^2\right)\right|^{\text{NMSSM}} + \left.\hat{\Sigma}_{\Psi\Psi}^{(2)}\left(k^2\right)\right|_{k^2=0}^{\text{MSSM}}, \quad \Psi\Psi \in \{hh, AA\}. \tag{5.8}$$

The two-loop self-energies are taken directly as a numerical result from `FeynHiggs`. For the final implementation the momentum dependence of the term of $\mathcal{O}(\alpha_t\alpha_s)$ [98] will be included as well.

5.2 Pole-Mass Determination in the NMSSM Higgs-Sector

The masses of the NMSSM Higgs bosons are obtained from the complex poles of the full propagator-matrix. The inverse propagator-matrix for the three $\mathcal{CP}$-even Higgs

bosons h_i from eq. (2.50) is a 3×3 matrix that reads

$$\mathrm{i}\hat{\Delta}_{hh}^{-1}\left(k^2\right) = \hat{\Gamma}_{hh}\left(k^2\right). \tag{5.9}$$

Here $\mathcal{M}_{hh}$ denotes the diagonalised mass matrix of the $\mathcal{CP}$-even Higgs fields at tree-level and $\hat{\Sigma}_{h_i h_j}$ denotes their renormalised self-energy corrections,

$$\hat{\Gamma}_{hh}\left(k^2\right) = \begin{pmatrix} k^2 - m_{h_1}^2 + \hat{\Sigma}_{h_1 h_1}(k^2) & \hat{\Sigma}_{h_1 h_2}(k^2) & \hat{\Sigma}_{h_1 h_3}(k^2) \\ \hat{\Sigma}_{h_2 h_1}(k^2) & k^2 - m_{h_2}^2 + \hat{\Sigma}_{h_2 h_2}(k^2) & \hat{\Sigma}_{h_2 h_3}(k^2) \\ \hat{\Sigma}_{h_3 h_1}(k^2) & \hat{\Sigma}_{h_3 h_2}(k^2) & k^2 - m_{h_2}^2 + \hat{\Sigma}_{h_3 h_3}(k^2) \end{pmatrix} \tag{5.10}$$

The three complex poles $\mathcal{M}_i$ of the propagator in the $\mathcal{CP}$-even Higgs sector are given by the values of the external momentum k^2 for which the determinant of the inverse propagator-matrix vanishes,

$$\det\left[\hat{\Gamma}_{hh}\left(k^2\right)\right]_{k^2 = \mathcal{M}_i^2} \overset{!}{=} 0, \ i \in \{1, 2, 3\}. \tag{5.11}$$

For the $\mathcal{CP}$-odd sector the inverse propagator matrix reads

$$\mathrm{i}\hat{\Delta}_{AA}^{-1}\left(k^2\right) = \hat{\Gamma}_{AA}\left(k^2\right). \tag{5.12}$$

Here $\mathcal{M}_{AA}$ denotes the diagonalised mass matrix of the $\mathcal{CP}$-odd Higgs fields at tree level and $\hat{\Sigma}_{AA}$ denotes their renormalised self-energy corrections,

$$\hat{\Gamma}_{AA}\left(k^2\right) = \begin{pmatrix} k^2 - m_{A_1}^2 + \hat{\Sigma}_{A_1 A_1}(k^2) & \hat{\Sigma}_{A_1 A_2}(k^2) & \hat{\Sigma}_{A_1 G^0}(k^2) \\ \hat{\Sigma}_{A_2 A_1}(k^2) & k^2 - m_{A_2}^2 + \hat{\Sigma}_{A_2 A_2}(k^2) & \hat{\Sigma}_{A_2 G^0}(k^2) \\ \hat{\Sigma}_{G^0 A_1}(k^2) & \hat{\Sigma}_{G^0 A_2}(k^2) & k^2 + \hat{\Sigma}_{G^0 G^0}(k^2) \end{pmatrix}. \tag{5.13}$$

The Higgs–Goldstone mixing contributions and the self-energy of the neutral Goldstone-boson, $\hat{\Sigma}_{G^0 A_i}(k^2)$ and $\hat{\Sigma}_{G^0 G^0}(k^2)$, are of subleading two-loop order and are thus neglected. In the pole determination the Goldstone-boson is considered massless. Besides the trivial propagator-pole at $k^2 = 0$, the remaining poles are determined as in the $\mathcal{CP}$-even sector.

5.3 Incorporation of One-Loop Contributions

The one-loop diagrams were generated with `FeynArts 3.9` [90] by using the private NMSSM model-file mentioned in the previous chapter. The amplitudes were subsequently calculated with `FormCalc 7.4`[2] [102]. For both tools the computer algebra software `Mathematica` [103] was used. After obtaining analytic expres-

---

[2]The versions of both tools were the current versions of the time of the calculation, while several updates for `FormCalc` have been released in the meantime [99–101].

sions for the higher-order corrections the renormalisation scheme was implemented in `Mathematica`. Finiteness of renormalised self-energies was checked analytically for the fermions/sfermion contributions and numerically for the remaining Higgs- and gauge-sector contributions in `Mathematica`. Since computer-algebra software tends to be relatively slow for processing numerical evaluations, the analytic results were converted into `Fortran` code. This was performed partly with the help of the export features of `FormCalc`. Due to the better numerical performance the numerical evaluation of the finite results was performed completely in a self-developed `Fortran` code using the `Fortran` library of `LoopTools 2.12` [104] to evaluate the one-loop diagrams.

5.3.1 Implementation of complex Momentum-Dependence

`LoopTools` does not allow the evaluation of loop functions for complex momenta. In order to attribute this shortcoming for the determination of complex poles, the self-energies are expanded around the real part of the complex momentum

$$\Sigma\big(p^2\big) \approx \Sigma\big(p_r^2\big) + \mathrm{i}p_i^2 \frac{\mathrm{d}}{\mathrm{d}p_r^2}\Sigma\big(p_r^2\big), \quad p^2 = p_r^2 + \mathrm{i}p_i^2. \tag{5.14}$$

The approximation performed by truncating the series has been tested to create no significant error [105] for many parameters.

5.3.2 Reparametrisation

For the determination of $\Delta r^{\mathrm{NMSSM}}$ a `Fortran`/`Mathematica`-routine based on the result of [88] has been used. Contributions from the reparametrisation are added as a momentum independent shift to the inverse propagator-matrices,

$$\Gamma_{\Psi\Psi}\big(k^2\big) = \big(\mathbb{1}k^2 - \mathbf{M}_{\Psi\Psi}^2\big) + \Delta\mathbf{M}_{\Psi\Psi}^2 + \hat{\Sigma}_{\Psi\Psi}\big(k^2\big), \quad \Psi \in \{h, A\}. \tag{5.15}$$

For the reparametrisation to $\alpha(M_Z)$ the value $\Delta_{\alpha(M_Z)}$ no additional input from an external code is necessary, since $\Delta\alpha$ is a constant value.

5.3.3 Implementation of the Pole Determination at One-Loop Order

The pole determination is performed numerically by an iterative procedure. It starts by performing an eigenvalue decomposition on the loop-corrected mass matrix

$$\mathbf{M}_{hh}^{(1)}(k^2) = \mathbf{M}_{hh} - \hat{\Sigma}_{hh}^{(1)}\big(k^2\big), \quad \mathbf{M}_{hh}^{(1)}(k^2) = \mathbf{M}_{hh}^{(1)}(k^2) + \hat{\Sigma}_{hh}^{(2)}\big(k^2\big) \tag{5.16}$$

for a given (complex) momentum argument $k_{(n)}^2$. The obtained eigenvalues $\widetilde{\mathcal{M}}_i^2(k_{(n)}^2)$ are stored. Since the pole condition given in eq. (5.11) can be written with the

complex poles $\mathcal{M}_i^2$ as

$$0 \overset{!}{=} \prod_{i=1}^{3} \left\{ k_{(n)}^2 - \mathcal{M}_i^2 \right\}, \tag{5.17}$$

the quantity

$$d_{(n)} = \left| k_{(n)}^2 - \widetilde{\mathcal{M}}_i^2 \left(k_{(n)}^2 \right) \right| \tag{5.18}$$

is calculated, where i is fixed for the algorithm. If $d_{(n)} > 10^{-9}$, the determinant will not be considered as vanishing. Then a new momentum will be defined as

$$k_{(n+1)}^2 = \widetilde{\mathcal{M}}_i^2 \left(k_{(n)}^2 \right) \tag{5.19}$$

and $d_{(n+1)}$ will be calculated. This procedure is repeated until $d_{(m)} \lesssim 10^{-9}$ or a given number of 50 iterations reached. In the first case the last value for the momentum is considered the as the complex pole. In the the second case the routine is considered as unsuitable for the task, since it found no converging result. However, the algorithm has proven to be viable for a wide range of parameters.

The procedure has to be executed for all different poles. The tree-level masses are a good choice as starting conditions for finding all poles,

$$k_{(0)}^2 = m_{h_i}^2, \tag{5.20}$$

since the algorithm tends to find the pole closest to the starting condition [73].

5.4 Incorporation of Two-Loop Contributions

The renormalised two-loop self-energies are taken as a numerical result from `FeynHiggs` `2.10.2`. They are passed to the `Fortran` code containing the one-loop results, where they are converted into the mass basis of the NMSSM and subsequently added to the one-loop self-energies of the NMSSM. In this section the available two-loop corrections implemented in `FeynHiggs` for the MSSM are described together with the description of their implementation into the NMSSM results.

5.4.1 `FeynHiggs`

`FeynHiggs` [30–36] is a package for the prediction of Higgs observables in the real and complex MSSM. For the Higgs-boson masses it includes the full MSSM one-loop and partial two-loop contributions. In the $\mathcal{CP}$-conserving, real MSSM the included two-loop corrections are of $\mathcal{O}(\alpha_s \alpha_t, \alpha_t^2, \alpha_s \alpha_b, \alpha_t \alpha_b)$, for an overview see [32], in the complex MSSM the implemented contributions are of $\mathcal{O}(\alpha_s \alpha_t, \alpha_t^2)$ [31, 35, 36]. Furthermore it includes a resummation of large logarithms that can appear for large scale differences in the calculation [30] and momentum-dependent two-loop contributions of $\mathcal{O}(\alpha_t \alpha_s)$ for the MSSM with real parameters [98]. Also included in `FeynHiggs` are higher-order

corrections Δ_b to the bottom Yukawa-coupling [106,107]. In all calculations the stop-masses are considered to be renormalised on-shell. The top-mass is also renormalised on-shell, but a reparametrisation to the $\overline{\text{MS}}$-mass of the top quark is available as an option.

For this work the NMSSM predictions include the MSSM two-loop corrections without momentum-dependence and without Δ_b-corrections. In the MSSM the momentum-dependence at two-loop order has a minor effect of less than 1 GeV for the mass of the light, SM-like Higgs field in the scenarios considered in [98] and can increase up to the experimental uncertainty [12]. The Δ_b-corrections also remain very small for the scenarios discussed in this work. Both features are thus neglected for this work, but will be available in the public NMSSM-version of `FeynHiggs`.

5.4.2 Conversion of the MSSM Self-Energies

The MSSM self-energies from `FeynHiggs` have to be converted into self-energies in the mass basis off the NMSSM. All necessary parameters for this procedure are provided by `FeynHiggs`.

In the $\mathcal{CP}$-even sector the two-loop MSSM-corrections are provided by `FeynHiggs` in the MSSM mass-basis of the fields h and H

$$\hat{\Sigma}_{e,hH}^{(\text{MSSM})} = \begin{pmatrix} \hat{\Sigma}_{hh}^{(2)} & \hat{\Sigma}_{hH}^{(2)} \\ \hat{\Sigma}_{Hh}^{(2)} & \hat{\Sigma}_{HH}^{(2)} \end{pmatrix} \tag{5.21}$$

together with the lowest-order mixing matrix $\mathbf{U}_{e(0)}^{(\text{MSSM})}$ that relates h and H with the fields ϕ_1 and ϕ_2 in the interaction basis,

$$\begin{pmatrix} h \\ H \end{pmatrix} = \mathbf{U}_{e(0)}^{(\text{MSSM})} \begin{pmatrix} \phi_1 \\ \phi_2 \end{pmatrix}, \quad \mathbf{U}_{e(0)}^{(\text{MSSM})} = \begin{pmatrix} -\sin\alpha & \cos\alpha \\ \cos\alpha & \sin\alpha \end{pmatrix}. \tag{5.22}$$

Since the two-loop self-energies are taken in the limit of vanishing external momenta, the momentum argument of the self-energies is suppressed in this section.

In the $\mathcal{CP}$-odd sector only one self-energy and the mixing matrix for the $\mathcal{CP}$-odd Higgs field A is given,

$$\hat{\Sigma}_{o,AG}^{(\text{MSSM})} = \begin{pmatrix} \hat{\Sigma}_{AA}^{(2)} & 0 \\ 0 & 0 \end{pmatrix} \tag{5.23}$$

together with the lowest-order mixing matrix $\mathbf{U}_{o(0)}^{(\text{MSSM})}$ that relates A and the neutral Goldstone boson G with the fields χ_1 and χ_2 in the interaction basis,

$$\begin{pmatrix} A \\ G \end{pmatrix} = \mathbf{U}_{o(0)}^{(\text{MSSM})} \begin{pmatrix} \chi_1 \\ \chi_2 \end{pmatrix}, \quad \mathbf{U}_{o(0)}^{(\text{MSSM})} = \begin{pmatrix} -\sin\beta & \cos\beta \\ \cos\beta & \sin\beta \end{pmatrix}. \tag{5.24}$$

The MSSM self-energy corrections in the interaction basis are obtained by

$$\hat{\Sigma}_{e,\phi\phi}^{(\text{MSSM})} = \left(\mathbf{U}_{e(0)}^{(\text{MSSM})}\right)^{\dagger} \hat{\Sigma}_{e,hH}^{(\text{MSSM})} \mathbf{U}_{e(0)}^{(\text{MSSM})} = \begin{pmatrix} \hat{\Sigma}_{\phi_1\phi_1}^{(\text{MSSM})} & \hat{\Sigma}_{\phi_1\phi_2}^{(\text{MSSM})} \\ \hat{\Sigma}_{\phi_2\phi_1}^{(\text{MSSM})} & \hat{\Sigma}_{\phi_2\phi_2}^{(\text{MSSM})} \end{pmatrix} \tag{5.25}$$

$$\hat{\Sigma}_{e,\chi\chi}^{(\text{MSSM})} = \left(\mathbf{U}_{o(0)}^{(\text{MSSM})}\right)^{\dagger} \hat{\Sigma}_{o,AG}^{(\text{MSSM})} \mathbf{U}_{o(0)}^{(\text{MSSM})} = \begin{pmatrix} \hat{\Sigma}_{\chi_1\chi_1}^{(\text{MSSM})} & \hat{\Sigma}_{\chi_1\chi_2}^{(\text{MSSM})} \\ \hat{\Sigma}_{\chi_2\chi_1}^{(\text{MSSM})} & \hat{\Sigma}_{\chi_2\chi_2}^{(\text{MSSM})} \end{pmatrix} \tag{5.26}$$

and are subsequently rotated into the NMSSM mass-basis with the mixing matrices of the NMSSM,

$$\hat{\Sigma}_{hh}^{(2)}\Big|^{\text{MSSM}} = \mathbf{U}_{e(0)} \begin{pmatrix} \hat{\Sigma}_{\phi_1\phi_1}^{(\text{MSSM})} & \hat{\Sigma}_{\phi_1\phi_2}^{(\text{MSSM})} & 0 \\ \hat{\Sigma}_{\phi_2\phi_1}^{(\text{MSSM})} & \hat{\Sigma}_{\phi_2\phi_2}^{(\text{MSSM})} & 0 \\ 0 & 0 & 0 \end{pmatrix} \mathbf{U}_{e(0)}^{\dagger} = \begin{pmatrix} \hat{\Sigma}_{h_1h_1} & \hat{\Sigma}_{h_1h_2} & \hat{\Sigma}_{h_1h_3} \\ \hat{\Sigma}_{h_2h_1} & \hat{\Sigma}_{h_2h_2} & \hat{\Sigma}_{h_2h_3} \\ \hat{\Sigma}_{h_3h_1} & \hat{\Sigma}_{h_3h_2} & \hat{\Sigma}_{h_3h_3} \end{pmatrix} \tag{5.27}$$

$$\hat{\Sigma}_{AA}^{(2)}\Big|^{\text{MSSM}} = \mathbf{U}_{o(0)} \begin{pmatrix} \hat{\Sigma}_{\chi_1\chi_1}^{(\text{MSSM})} & \hat{\Sigma}_{\chi_1\chi_2}^{(\text{MSSM})} & 0 \\ \hat{\Sigma}_{\chi_2\chi_1}^{(\text{MSSM})} & \hat{\Sigma}_{\chi_2\chi_2}^{(\text{MSSM})} & 0 \\ 0 & 0 & 0 \end{pmatrix} \mathbf{U}_{o(0)}^{\dagger} = \begin{pmatrix} \hat{\Sigma}_{A_1A_1} & \hat{\Sigma}_{A_1A_2} & 0 \\ \hat{\Sigma}_{A_2A_1} & \hat{\Sigma}_{A_2A_2} & 0 \\ 0 & 0 & 0 \end{pmatrix}. \tag{5.28}$$

The two-loop contributions to the Goldstone boson self-energies are neglected.

5.4.3 Renormalisation Scheme and On-Shell Conversion for the Parameters in the Stop Sector

In order to use the two-loop self-energies from `FeynHiggs` the parameters in the stop-sector have to be given as on-shell parameters, where the stop-masses are renormalised on-shell. In the public, MSSM-version of `FeynHiggs` the conversion of $\overline{\text{DR}}$-renormalised stop-parameters given at a specified scale into on-shell parameters is included. The formulas can be found in [108, 109] for the complex case. A discussion of the conversion for a possible extension to the NMSSM is given in this section.

For the top- and stop-sector the renormalisation transformation of the top- and stop-masses together with the mixing angle $\theta_{\tilde{t}}$ read

$$m_t \rightarrow m_t + \delta m_t, \quad m_{\tilde{t}_i}^2 \rightarrow m_{\tilde{t}_i}^2 + \delta m_{\tilde{t}_i}^2, \quad \theta_{\tilde{t}} \rightarrow \theta_{\tilde{t}} + \delta\theta_{\tilde{t}}. \tag{5.29}$$

The mass counterterms are obtained by on-shell renormalisation-conditions as described in sec. 3.2.1,

$$\delta m_t^{\text{OS}} = \frac{1}{2}\text{Re}\left[\Sigma_{tt}^{(\not{p},L)}(p) + \Sigma_{tt}^{(\not{p},R)}(p) + \Sigma_{tt}^{(S,L)}(p) + \Sigma_{tt}^{(S,R)}(p)\right]\Big|_{\not{p}=m_t} \tag{5.30}$$

$$\delta m_{\tilde{t}_i}^{2,\text{OS}} = \text{Re}\Sigma_{\tilde{t}_i\tilde{t}_i}\left(m_{\tilde{t}_i}^2\right), \tag{5.31}$$

while the counterterm for the mixing angle reads

$$\delta\theta_{\tilde{t}} = \frac{1}{2}\frac{\text{Re}\left[\Sigma_{\tilde{t}_1\tilde{t}_2}\left(m_{\tilde{t}_1}^2\right) - \Sigma_{\tilde{t}_1\tilde{t}_2}\left(m_{\tilde{t}_2}^2\right)\right]}{m_{\tilde{t}_1}^2 - m_{\tilde{t}_2}^2}. \tag{5.32}$$

The finite shifts for the conversion between the $\overline{\mathrm{DR}}$ and on-shell scheme for the top-quark and stop-squark masses and the mixing angle are given by the finite contributions of the renormalisation constants,

$$\Delta m_t = \delta m_t^{\mathrm{OS}} - \delta m_t^{\overline{\mathrm{DR}}}, \quad \Delta m_{\tilde{t}_i}^2 = \delta m_{\tilde{t}_i^{\mathrm{OS}}}^2 - \delta m_{\tilde{t}_i^{\overline{\mathrm{DR}}}}^2, \quad \Delta \theta_{\tilde{t}} = \delta \theta_{\tilde{t}}^{\mathrm{OS}} - \delta \theta_{\tilde{t}}^{\overline{\mathrm{DR}}} \qquad (5.33)$$

Thus the finite shifts for the conversion of the soft-breaking parameters of the stop-sector, $M_{\tilde{t}_{\mathrm{L}}}^2$, $M_{\tilde{t}}^2$ and A_t, from the $\overline{\mathrm{DR}}$ scheme into the on-shell scheme for the top-quark and stop-squark masses in the NMSSM with real parameters read

$$\Delta M_{\tilde{t}_{\mathrm{L}}}^2 = \left(\mathbf{U}_{\tilde{f}}\right)_{11}^2 \Delta m_{\tilde{t}_1}^2 + \left(\mathbf{U}_{\tilde{f}}\right)_{12}^2 \Delta m_{\tilde{t}_2}^2 - 2\frac{\left(\mathbf{U}_{\tilde{f}}\right)_{12}\left(\mathbf{U}_{\tilde{f}}\right)_{22}}{m_{\tilde{t}_1}^2 - m_{\tilde{t}_2}^2} \Delta \theta_{\tilde{t}} - 2 m_t \Delta m_t \quad (5.34\text{a})$$

$$\Delta M_{\tilde{t}}^2 = \left(\mathbf{U}_{\tilde{f}}\right)_{21}^2 \Delta m_{\tilde{t}_1}^2 + \left(\mathbf{U}_{\tilde{f}}\right)_{22}^2 \Delta m_{\tilde{t}_2}^2 - 2\frac{\left(\mathbf{U}_{\tilde{f}}\right)_{11}\left(\mathbf{U}_{\tilde{f}}\right)_{21}}{m_{\tilde{t}_1}^2 - m_{\tilde{t}_2}^2} \Delta \theta_{\tilde{t}} - 2 m_t \Delta m_t \quad (5.34\text{b})$$

$$\Delta A_t = \frac{1}{m_t}\left[\left(\mathbf{U}_{\tilde{f}}\right)_{11}\left(\mathbf{U}_{\tilde{f}}\right)_{12}\left(\Delta m_{\tilde{t}_1}^2 - \Delta m_{\tilde{t}_2}^2\right) + \left(m_{\tilde{t}_1}^2 - m_{\tilde{t}_2}^2\right)\Delta \theta_{\tilde{t}} - X_t \Delta m_t\right]. \tag{5.34c}$$

The corrections that have to be included in the top and stop self-energies for the Higgs-mass calculation depends on the considered two-loop contributions. If only two-loop corrections of $\mathcal{O}(\alpha_t \alpha_s)$ are considered, only corrections from (S)QCD have to be considered. If $\mathcal{O}(\alpha_t^2)$ corrections are included, contributions from the Higgs-sector have to be included as well, since they enter the calculation at the same order.

Differences between the MSSM and NMSSM Conversion

While the renormalisation constant of the top-quark mass δm_t is identical for the MSSM and NMSSM, the self-energies of the stops receive additional corrections from the scalar singlet-fields of the NMSSM. The contributions from the neutral Higgs- and the stop-fields to the stop-squark self-energy have the form

$$\tag{5.35}$$

with any neutral Higgs field Ψ_m in the mass basis. In the NMSSM the singlet component of Ψ_m couples to the stops only via the coupling of $\mathcal{O}(\lambda)$, while the MSSM-like doublet component couples to the sfermions via couplings of $\mathcal{O}(Y_t)$ and D-terms that are proportional to the gauge couplings g_1 and g_2. If the electroweak gauge-couplings are neglected the stop self-energies at one-loop order can be classified

as

$$\Sigma_{\tilde{t}_i\tilde{t}_i}\left(k^2\right) \approx \underbrace{\Sigma_{\tilde{t}_i\tilde{t}_i}^{(g,\tilde{g})}\left(k^2\right)}_{=\mathcal{O}(\alpha_s)} + \underbrace{\Sigma_{\tilde{t}_i\tilde{t}_i}^{(\Psi_m,\tilde{t})}\left(k^2\right)}_{=\mathcal{O}\left(Y_t^2\right)} + \underbrace{\Sigma_{\tilde{t}_i\tilde{t}_i}^{(\Psi_s)}\left(k^2\right)}_{=\mathcal{O}(\lambda^2)}. \tag{5.36}$$

The first term denotes the (S)QCD corrections, the second term denotes the MSSM-like contributions from the doublet-admixture of the Higgs fields denoted by Ψ_m and the third term denotes the corrections from the singlet admixture that are genuine to the NMSSM. The (S)QCD corrections are identical in both models. The MSSM-like contributions partially differ from the MSSM contributions by the mixing matrix elements of the Higgs sector.

In our result we incorporate MSSM-like two-loop corrections of $\mathcal{O}(\alpha_t\alpha_s, \alpha_t^2)$, while the genuine NMSSM corrections at two-loop order are neglected. These are correction from the stop-sector including at least one power of λ instead of Y_t in any coupling. Thus for a consistent $\overline{\text{DR}}$ to on-shell conversion in the stop-sector it is sufficient to include only MSSM-like contributions.

For scenarios where the singlet character is significantly attributed to one particular field in the $\mathcal{CP}$-even and -odd sector, the MSSM conversion represents a very good approximation for the MSSM-like contributions from the Higgs-sector.

5.5 Validating sample scenarios with `HiggsBounds`

For the purpose of investigating the result for scenarios that are not excluded by experimental probes of the Higgs sector the code `HiggsBounds` [110–114] was used to validate chosen scenarios. Thus the input parameters needed by `HiggsBounds` have to be derived from the definition of the scenario. This was done by a two-step procedure: First the scenario definition for the preliminary version of the `FeynHiggs` NMSSM-extension, which requires on-shell parameters in the stop-sector, was converted into a SUSY Les Houches Accord (SLHA) [115, 116] conform input file, which only contains $\overline{\text{DR}}$ parameters at a specified scale. After that the input was used to run `NMSSMTools` [17], which calculated all necessary input parameters in the effective coupling approximation as needed for `HiggsBounds`[3].

5.5.1 Conversion of the parameter X_t

The by far largest effect from the on-shell to $\overline{\text{DR}}$ conversion of the parameters in the sfermion-sector stems from X_t. Thus only the conversion of this parameter including only (S)QCD corrections at one-loop order was considered in this work. We follow the conversion as described in [105] for the case of real parameters. The relation

---

[3]For a more complete check of its experimental viability the scenario should be tested with `HiggsBounds` in conjunction with `HiggsSignals` [117]. However, for providing a first check for a sample scenario to test for the Higgs-mass prediction the check with `HiggsBounds` is considered sufficient.

between the on-shell and $\overline{\text{DR}}$ value for X_t is given by

$$X_t^{(\text{OS})} = X_t^{(\overline{\text{DR}})} \left(1 + \frac{\Delta m_t}{m_t} \right) - \frac{\Delta m_{\tilde{t}}^2}{2m_t}, \tag{5.37a}$$

where

$$\Delta m_t = \frac{\alpha_s}{6\pi m_t} \left[g_1^t + g_2^t + m_t^2 \left(6 \log \frac{m_t^2}{\mu_r^2} - 10 \right) + m_{\tilde{g}}^2 \left(\log \frac{m_{\tilde{g}}^2}{\mu_r^2} - 1 \right) \right], \tag{5.37b}$$

$$\Delta m_{\tilde{t}}^2 = \frac{2\alpha_s}{3\pi} \left(g_1^{\tilde{t}} - g_2^{\tilde{t}} \right), \tag{5.37c}$$

$$g_i^t = -m_{\tilde{t}_i}^2 \left(\log \frac{m_{\tilde{t}_i}^2}{\mu_r^2} - 1 \right) + f_i \text{Re} \left[B_0 \left(m_t^2, m_{\tilde{g}}^2, m_{\tilde{t}_i}^2 \right) \right]^{\text{fin}}, \tag{5.37d}$$

$$g_i^{\tilde{t}} = 2m_{\tilde{t}_i}^2 \left(\log \frac{m_{\tilde{t}_i}^2}{\mu_r^2} - 2 \right) - f_i \text{Re} \left[B_0 \left(m_{\tilde{t}}^2, m_{\tilde{g}}^2, m_t^2 \right) \right]^{\text{fin}}, \tag{5.37e}$$

$$f_i = m_{\tilde{g}}^2 + m_t^2 - m_{\tilde{t}_i}^2 - (-1)^i \, 2m_{\tilde{g}} m_t. \tag{5.37f}$$

Here $m_{\tilde{g}}$ denotes the gluino mass and B_0 denotes the one-loop standard integral as first defined in [118]. The conversion depends explicitly on the renormalisation scale μ_r. It also depends implicitly on the renormalisation schemes and scales of the parameters entering the conversion outlined in eqs. (5.37). This dependences, however, are of higher-orders and thus are neglected with the exception of the running of α_s. The numerical value of a running α_s can change significantly when calculated at different scales in both the $\overline{\text{DR}}$- and $\overline{\text{MS}}$-schemes. For the conversion of X_t the value of α_s at the scale μ_r in the $\overline{\text{MS}}$ scheme at one-loop order, given by

$$\alpha_s(\mu_r) \approx \frac{\alpha_s(M_Z)}{1 + \frac{\alpha_s(M_Z)}{4\pi} \beta_{\alpha_s}^{(1)} \log \frac{\mu_r^2}{M_Z^2}} , \quad \beta_{\alpha_s}^{(1)} = \frac{1}{4\pi} \left(11 - \frac{2}{3} N_c \right), \tag{5.38}$$

is used for five active flavours, $N_c = 5$, when evolving α_s from the scale M_Z to m_t. For the purposes of this work μ_r is set to the on-shell mass of the top-quark $m_t^{(\text{OS})} = 173.2$ GeV, which results in a change of the numerical value of α_s by $\approx 10\%$,

$$\alpha_s(M_Z) = 0.1184, \quad \alpha_s\left(m_t^{(\text{OS})} \right) = 0.1081, \tag{5.39}$$

where $\alpha_s(M_Z)$ was taken from the results of [119]. Any higher-order contribution in eq. (5.38) would lead to contributions that formally contribute to the Higgs-mass calculation as an effect of three-loop order. They are thus neglected in the result presented here which includes only one- and two-loop contributions.

6 Partial Contributions

The calculation of the one-loop corrections is performed in separate parts. Besides the full ons-loop calculation in the NMSSM also appropriate subsets of the one-loop corrections are identified and calculated to study the numerical impact of different partial one-loop contributions. With this approach the numerically leading higher-orders contributions can be identified. Four subsets are calculated for the one-loop Higgs masses, which are listed in tab. 6.1. The splitting of the m_t^4 approximation into

Approximation	Contributions
m_t^4-MSSM	$t/\tilde{t}$-sectors in gaugeless limit for $\lambda \to 0$
m_t^4-NMSSM	$t/\tilde{t}$-sectors in gaugeless limit
$f/\tilde{f}$	contributions from a complete fermion/sfermion doublet
HG Approximation	Higgs/higgsino/gauge/gaugino-sectors

Table 6.1: Overview over the different subsets considered for the one-loop corrections.

an MSSM and an NMSSM part is motivated by an upper bound on the NMSSM-parameters λ and κ, if one demands perturbativity of the NMSSM up to a high scale M_{GUT} [120]. In this case the relation

$$\lambda^2 + \kappa^2 \lesssim 0.5 \tag{6.1}$$

has to hold. Since the couplings between the singlet sector and the remaining fields are governed by λ, a "small" value for this parameter is expected to reduce the influence of the singlet sector. This effect can be quantified by calculating MSSM and NMSSM versions of approximations. The listed approximations will be described in this chapter and numerically studied chapter 8.

6.1 The m_t^4-Approximations

The m_t^4 Approximation accounts only for the contributions from the $t/\tilde{t}$-sectors in the electroweak gaugeless limit. It comes in two variants: The first, m_t^4-MSSM, only accounts for MSSM-like contributions, the second, m_t^4-NMSSM, also includes genuine NMSSM corrections. A comparison of both contributions reveals the impact of the genuine NMSSM corrections.

The approximation is a two-step procedure. The first step, which is common for both versions, consists of neglecting the momentum dependence of all present self-energies. The second step selects specific $t/\tilde{t}$-contributions, that are different for both versions of the m_t^4-approximations.

6.1.1 Common Approximations for Self-Energies

In both approximations the momentum-dependence of all appearing self-energies are neglected, since it is a sub-leading effect,

$$\Sigma_{\Psi_i^\dagger \Psi_j}\left(k^2\right) \approx \Sigma_{\Psi_i^\dagger \Psi_j}(0) \equiv \Sigma_{\Psi_i^\dagger \Psi_j} \tag{6.2}$$

Without momentum-dependence the self-energy becomes a real quantity. The momentum dependence of the self-energy will be suppressed for the rest of this section. Neglecting the momentum-dependence corresponds to neglecting the tree-level Higgs masses in the one-loop calculation. The renormalised two-point function reads

$$\mathrm{i}\hat{\Gamma}^{(m_t^4)}_{\Psi_i^\dagger \Psi_j}\left(k^2\right) = \mathrm{i}\left(k^2\mathbb{1} - \mathbf{M}_{\Psi\Psi} + \hat{\Sigma}_{\Psi\Psi}\right)_{ij} \tag{6.3}$$

with the renormalised self-energy matrices

$$\left(\hat{\Sigma}_{\Psi\Psi}\right)_{ij} = \hat{\Sigma}_{\Psi_i^\dagger \Psi_j} = \Sigma_{\Psi_i^\dagger \Psi_j} - (\delta V_{\mathrm{H}})_{\Psi_i \Psi_j} \tag{6.4}$$

The approximate one-loop corrections represent a finite, real shift to the pole of the propagator.

Since no Higgs fields appear within the loops in this approximation the mixing matrices from eq. (2.50), which transform the Higgs fields into the mass basis, appear only for the external Higgs fields. Thus the self-energy contributions in the mass basis can be written as linear combinations of the self-energies in the interaction basis in this approximation,

$$\hat{\Sigma}^{(m_t^4)}_{hh} = \mathbf{U}_{e(0)}\hat{\Sigma}^{(m_t^4)}_{\phi\phi}\mathbf{U}^\dagger_{e(0)}, \quad \hat{\Sigma}^{(m_t^4)}_{AA} = \mathbf{U}_{o(0)}\hat{\Sigma}^{(m_t^4)}_{\chi\chi}\mathbf{U}^\dagger_{o(0)}. \tag{6.5}$$

6.1.2 Classification of the leading Top/Stop-Contributions

For the two different m_t^4-approximations the Higgs self-energies can be classified by their couplings to the top quark and stop squarks in the electroweak gaugeless limit. These couplings will be given for the $\mathcal{CP}$-even sector in this section together with a list of the contributing topologies.

Only the doublet Higgs field ϕ_2 couples to the top-quark at lowest-order,

$$\mathrm{i}\Gamma_{\phi_2 t\bar{t}} = -\frac{1}{\sqrt{2}}Y_t, \quad \mathrm{i}\Gamma_{\phi_1 t\bar{t}} = \mathrm{i}\Gamma_{\phi_s t\bar{t}} = 0, \quad Y_t^2 = \frac{4\pi\alpha}{2s_w^2\sin^2\beta}\frac{m_t^2}{M_W^2}. \tag{6.6a}$$

The matrices for the couplings of the1 three $\mathcal{CP}$-even Higgs fields to the stop squarks

$\tilde{t}_1$ and $\tilde{t}_2$ in the electroweak gaugeless limit read

$$\mathrm{i}\Gamma_{\phi_1\tilde{t}\tilde{t}} = \mathrm{i}\mu_{\mathrm{eff}}Y_t \cdot \begin{pmatrix} \sqrt{2}\sin 2\theta_{\tilde{t}} & -\frac{1}{\sqrt{2}}\cos 2\theta_{\tilde{t}} \\ -\frac{1}{\sqrt{2}}\cos 2\theta_{\tilde{t}} & -\sqrt{2}\sin 2\theta_{\tilde{t}} \end{pmatrix} \tag{6.6b}$$

$$\mathrm{i}\Gamma_{\phi_2\tilde{t}\tilde{t}} = \mathrm{i}A_tY_t \cdot \begin{pmatrix} \sqrt{2}\sin 2\theta_{\tilde{t}} & -\frac{1}{\sqrt{2}}\cos 2\theta_{\tilde{t}} \\ -\frac{1}{\sqrt{2}}\cos 2\theta_{\tilde{t}} & -\sqrt{2}\sin 2\theta_{\tilde{t}} \end{pmatrix} + \mathrm{i}m_tY_t \cdot \begin{pmatrix} \sqrt{2} & 0 \\ 0 & -\sqrt{2} \end{pmatrix} \tag{6.6c}$$

$$\mathrm{i}\Gamma_{\phi_s\tilde{t}\tilde{t}} = \mathrm{i}m_t\lambda\cot\beta \cdot \begin{pmatrix} \sqrt{2}\sin\theta_{\tilde{t}}\cos\theta_{\tilde{t}} & \frac{1}{\sqrt{2}}\cos 2\theta_{\tilde{t}} \\ \frac{1}{\sqrt{2}}\cos 2\theta_{\tilde{t}} & -\sqrt{2}\sin\theta_{\tilde{t}}\cos\theta_{\tilde{t}} \end{pmatrix} \tag{6.6d}$$

and the non-vanishing coupling matrices between two stops and two $\mathcal{CP}$-even Higgs fields read

$$\mathrm{i}\Gamma_{\phi_2\phi_2\tilde{t}\tilde{t}} = -\mathrm{i}Y_t^2 \cdot \begin{pmatrix} 1 & 0 \\ 0 & 1 \end{pmatrix}, \quad \mathrm{i}\Gamma_{\phi_1\phi_s\tilde{t}\tilde{t}} = -\mathrm{i}\lambda Y_t \cdot \begin{pmatrix} \sin\theta_{\tilde{t}}\cos\theta_{\tilde{t}} & \frac{1}{2}\cos 2\theta_{\tilde{t}} \\ \frac{1}{2}\cos 2\theta_{\tilde{t}} & -\sin\theta_{\tilde{t}}\cos\theta_{\tilde{t}} \end{pmatrix}. \tag{6.6e}$$

Classifying the couplings in terms of the order of Y_t reveals that the singlet couplings to sfermions are of a lower order in Y_t than their counterparts with doublet fields. For each lower order in Y_t they gain a power in λ,

$$\Gamma_{\phi_i\tilde{t}\tilde{t}} = \mathcal{O}(Y_t) + \mathcal{O}(\alpha), \quad \Gamma_{\phi_s\tilde{t}\tilde{t}} = \mathcal{O}(\lambda) \tag{6.7a}$$

$$\Gamma_{\phi_2\phi_2\tilde{t}\tilde{t}} = \mathcal{O}(Y_t^2) + \mathcal{O}(\alpha), \quad \Gamma_{\phi_1\phi_s\tilde{t}\tilde{t}} = \mathcal{O}(\lambda Y_t). \tag{6.7b}$$

The reduced number of non-vanishing couplings between singlet Higgs and stop fields leads to a decreased number of topologies that can contribute to the unrenormalised Higgs one-loop self-energies with an external singlet field. They are given together with their order in Y_t and λ in tab. 6.2. The first column in this table shows diagrams that represent MSSM-like contributions in the NMSSM, while the second to forth column depict genuine NMSSM-corrections involving one ore two external singlet Higgs field. Applying the classification to the bare self-energies leads to

$$\Sigma_{\phi\phi}^{(m_t^4)} = \begin{pmatrix} \mathcal{O}(Y_t^2) & \mathcal{O}(Y_t^2) & \mathcal{O}(\lambda Y_t) \\ \mathcal{O}(Y_t^2) & \mathcal{O}(Y_t^2) & \mathcal{O}(\lambda Y_t) \\ \mathcal{O}(\lambda Y_t) & \mathcal{O}(\lambda Y_t) & \mathcal{O}(\lambda^2) \end{pmatrix}, \tag{6.8}$$

where the 2×2 sub-matrix contains MSSM-like contributions and the third row and column contain genuine NMSSM-corrections, involving the singlet Higgs field. For the $\mathcal{CP}$-odd sector the according classification leads to a similar result,

$$\Sigma_{\chi\chi}^{(m_t^4)} = \begin{pmatrix} \mathcal{O}(Y_t^2) & \mathcal{O}(\lambda Y_t) & 0 \\ \mathcal{O}(\lambda Y_t) & \mathcal{O}(\lambda^2) & 0 \\ 0 & 0 & 0 \end{pmatrix}, \tag{6.9}$$

with the MSSM-like self-energy for the doublet Higgs field. one-loop contributions to the Goldstone-boson are neglected here, since they contribute at sub-leading two-loop
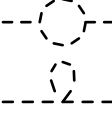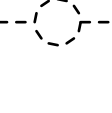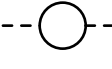
(i,j)	(1|2, 1|2)	(1, s)	(2, s)	(s, s)
order	$\mathcal{O}(Y_t^2)$	$\mathcal{O}(\lambda Y_t)$	$\mathcal{O}(\lambda Y_t)$	$\mathcal{O}(\lambda^2)$
fields	top/stop	stop	stop	stop
topologies				

Table 6.2: Diagrams and their order in terms of the couplings in the top-/stop-sector that contribute to the self-energies of the $\mathcal{CP}$-even fields ϕ_i at one-loop order in the gaugeless limit. The numbers 1 and 2 denote the doublet-states as external fields, while s denotes an external singlet. The internal lines depict either a top (solid) or a scalar top-partner (dashed).

order to the $\mathcal{CP}$-odd masses. For the one-loop tadpole-contributions the classification yields

$$T_{\phi_1}^{(1)} = \mathcal{O}(Y_t), \quad T_{\phi_2}^{(1)} = \mathcal{O}(Y_t), \quad T_{\phi_s}^{(1)} = \mathcal{O}(\lambda). \tag{6.10}$$

As a result from the classification by powers of the couplings λ and Y_t a possible suppression or enhancement of the genuine NMSSM-contributions by the parameter λ becomes apparent.

6.1.3 Analytic Relations between MSSM-like and genuine NMSSM Corrections

For the MSSM-like and genuine NMSSM diagrams in tab. 6.2 simple analytical relations exist. Due to the simple coupling structure, the genuine NMSSM-diagrams can be expressed by their MSSM-like counterparts and the ratio between the involved couplings.

Diagrams with a quartic Coupling

The third row diagrams in tab. 6.2 are related to each other by

$$\left(\phi_1 \cdots \overset{\tilde{t}_a}{\cdots} \phi_s \right) = \frac{\Gamma_{\phi_1 \phi_s \tilde{t}_a \tilde{t}_a}}{\Gamma_{\phi_2 \phi_2 \tilde{t}_a \tilde{t}_a}} \cdot \left(\phi_2 \cdots \overset{\tilde{t}_a}{\cdots} \phi_2 \right), \tag{6.11}$$

where the superscript a is the squark index in the mass basis. The coefficients are identical for both stop-fields and read

$$\frac{\Gamma_{\phi_1 \phi_s \tilde{t}_a \tilde{t}_a}}{\Gamma_{\phi_2 \phi_2 \tilde{t}_a \tilde{t}_a}} = \left| \frac{1}{2} \sin 2\theta_{\tilde{t}} \right| \frac{\lambda}{Y_t} \lesssim \frac{1}{2} \lambda \tag{6.12}$$

for $Y_t \approx 1$. This coefficient represents an upper limit for the size of each genuine NMSSM-diagram of this type relative to their MSSM-like counterparts. However, this upper limit only applies for a specific value of the mixing angle $\theta_{\tilde{t}} = \pi/4$ from the stop sector.

Diagrams with trilinear Couplings

The MSSM-like and genuine NMSSM diagrams involving trilinear scalar couplings differ only by the trilinear Higgs–stop couplings,

$$\phi_s \; \text{--}\!\bigcirc\!\text{--} \; \phi_{\{1,2\}} = \frac{\Gamma_{\phi_s \tilde{t}_a \tilde{t}_b}}{\Gamma_{\phi_i \tilde{t}_a \tilde{t}_b}} \cdot \phi_i \; \text{--}\!\bigcirc\!\text{--} \; \phi_{\{1,2\}} \tag{6.13a}$$

$$\phi_s \; \text{--}\!\bigcirc\!\text{--} \; \phi_s = \frac{\Gamma_{\phi_s \tilde{t}_a \tilde{t}_b}}{\Gamma_{\phi_i \tilde{t}_a \tilde{t}_b}} \frac{\Gamma_{\phi_s \tilde{t}_a \tilde{t}_b}}{\Gamma_{\phi_j \tilde{t}_a \tilde{t}_b}} \cdot \phi_i \; \text{--}\!\bigcirc\!\text{--} \; \phi_j \quad , \tag{6.13b}$$

where the superscripts a and b are the stop indices in the mass basis, and no summation over the indices i, j is intended. The relation holds for all choices for i and j. All non-vanishing ratios of the vertices read

$$\frac{\Gamma_{\phi_s \tilde{t}_a \tilde{t}_b}}{\Gamma_{\phi_1 \tilde{t}_a \tilde{t}_b}} = \lambda \frac{v}{\mu_{\text{eff}}} \cos \beta \tag{6.14a}$$

$$\frac{\Gamma_{\phi_s \tilde{t}_1 \tilde{t}_2}}{\Gamma_{\phi_2 \tilde{t}_1 \tilde{t}_2}} = \lambda \frac{v}{A_t} \cos \beta, \quad \frac{\Gamma_{\phi_s \tilde{t}_a \tilde{t}_a}}{\Gamma_{\phi_2 \tilde{t}_a \tilde{t}_a}} = \lambda \frac{v \sin 2\theta_{\tilde{t}}}{2 m_t \pm A_t \sin 2\theta_{\tilde{t}}} \cos \beta. \tag{6.14b}$$

where the indices a, b represent the stop-index in the mass basis and the value for the vacuum expectation-value of the doublet fields is $v \approx 177$ GeV in our conventions. The plus/minus sign in eq. (6.14) depends on the value of a.

The ratios in eq. (6.14) yield, that the graphs given in eq. (6.13) can be suppressed compared to the respective couplings from the doublet-sector not only by small values of λ and $\cos \beta$, but also by values of μ_{eff} larger than 177 GeV.

The ratio in eq. (6.14a) is applicable for all diagrams of this specific type, but yields a weaker upper limit than the ratios involving the trilinear breaking-parameter A_t in eq. (6.14b). Since small values < 100 GeV for μ_{eff} are disfavoured due to direct searches for charginos [41] the upper limit from the first ratio in eq. (6.14a) is given by

$$\frac{\Gamma_{\phi_s \tilde{t}_a \tilde{t}_b}}{\Gamma_{\phi_1 \tilde{t}_a \tilde{t}_b}} \lesssim 1.77 \lambda. \tag{6.15}$$

The remaining two ratios in eq. (6.14b) can yield stronger upper bound on the relative size of the genuine NMSSM-diagrams for large values of $A_t \gg \mu_{\text{eff}}$. However, the trilinear breaking-parameter A_t can be chosen such that one of the ratios diverges:

either $A_t = \mp 2m_t / \sin 2\theta_{\tilde{t}}$ or $A_t = 0$. In this case the corresponding MSSM-like diagram vanishes in the electroweak gaugeless limit, while the according genuine NMSSM-diagram does not. However, the NMSSM-diagram can still experience a relative suppression by the condition in eq. (6.14a). For the two extreme choices of A_t the ratios in eq. (6.14) without a pole read

$$A_t = 0 : \qquad \frac{\Gamma_{\phi_s \tilde{t}_a \tilde{t}_a}}{\Gamma_{\phi_2 \tilde{t}_a \tilde{t}_a}} \lesssim \frac{1}{2}\lambda \frac{v}{m_t} \sin 2\theta_{\tilde{t}} \cos\beta \approx \frac{1}{2}\lambda \qquad (6.16a)$$

$$A_t = \mp \frac{2m_t}{\sin 2\theta_{\tilde{t}}} : \frac{\Gamma_{\phi_s \tilde{t}_1 \tilde{t}_2}}{\Gamma_{\phi_2 \tilde{t}_1 \tilde{t}_2}} \lesssim \frac{1}{2}\lambda \frac{v}{m_t} \sin 2\theta_{\tilde{t}} \cos\beta \approx \frac{1}{2}\lambda. \qquad (6.16b)$$

We found that the effect of large values for these ratios is not severe even for the two extreme choices for A_t. This will be addressed in the discussion of numerical results in chapter 8.

6.1.4 Approximation in the Sbottom-Sector

If one restricts the self-energy contributions to the $t/\tilde{t}$-sectors all independent mass parameters from other sectors are neglected, in particular the bottom mass m_b is neglected

$$m_b \overset{m_t^4}{=} 0. \qquad (6.17)$$

In this approximation the Yukawa coupling of the bottom-quark Y_b vanishes and the left- and right-handed sbottom-fields do not mix at lowest-order (2.44). Only the left-handed sbottom field appears in the self-energy contributions for the charged Higgs due to the non-vanishing coupling-matrix between the charged Higgs-, the "left-handed" sbottom-field and any of the stop-fields,

$$\Gamma_{H^\pm \tilde{t} \tilde{b}_L} = (A_t \cos\beta_c + \mu_{\text{eff}} \sin\beta_c) Y_t \begin{pmatrix} \left(U_{\tilde{f}}\right)_{12} \\ \left(U_{\tilde{f}}\right)_{22} \end{pmatrix}. \qquad (6.18)$$

Since the left handed mass breaking parameter $M_{Q_L^3}$ contributes to both the stop and sbottom mass-matrices it cannot be neglected. Subsequently the sbottom fields can not both be massless The sbottom mass-matrix and the sbottom masses in the m_t^4-MSSM approximation read

$$\mathbf{M}_{\tilde{b}} \overset{m_t^4}{=} \begin{pmatrix} M_{\tilde{Q}_L}^2 & 0 \\ 0 & M_{\tilde{b}}^2 \end{pmatrix}, \quad m_{\tilde{b}_1}^2 \overset{m_t^4}{=} M_{\tilde{Q}_L}^2, \quad m_{\tilde{b}_2}^2 \overset{m_t^4}{=} M_{\tilde{b}}^2. \qquad (6.19)$$

In this case the sbottom mixing-matrix that is identical to the unity matrix. Expressing the soft mass-parameter for the third squark generation in terms of the top- and stop-masses and the stop mixing-matrix yields

$$m_{\tilde{b}_1}^2 \overset{m_t^4}{=} M_{\tilde{t}_L}^2 = m_{\tilde{t}_1}^2 \left(\mathbf{U}_{\tilde{t}}\right)_{11} + m_{\tilde{t}_2}^2 \left(\mathbf{U}_{\tilde{t}}\right)_{12} - m_t^2. \qquad (6.20)$$

Using this relation for one sbottom mass ensures the correct treatment of the sbottom sector in the m_t^4-approximation.

6.1.5 m_t^4-MSSM Approximation

In the m_t^4-MSSM approximation only MSSM-like $t/\tilde{t}$-contributions are taken into account. They are very well-known to be the numerically leading MSSM contributions [33, 121–124]: For the $\mathcal{CP}$-even sector this means the 2×2 submatrix in eq. (6.8), and for the $\mathcal{CP}$-odd sector this means the single matrix-element containing the self-energy for the doublet Higgs in eq. (6.9). These contributions are of $\mathcal{O}(Y_t^2)$ and they are usually denoted as corrections of order $\mathcal{O}(\alpha_t)$, where $\alpha_t = Y_t^2/(4\pi)$ and a factor m_t^2 is suppressed. These corrections yield the leading MSSM-contributions of $\mathcal{O}(m_t^4/M_W^2)$. The set of non-vanishing renormalisation constants necessary to properly renormalise the self-energies in this limit is reduced.

Throughout this section an overset m_t^4 will be used for the equal signs to express an equality that holds only in the m_t^4-MSSM approximation. Quantities in this approximation will be marked with a super- or subscript m_t^4.

Renormalisation Constants and Counterterms

Only the counterterm contributions to the Higgs potential that lead to terms are of $\mathcal{O}(Y_t^2)$ have to be considered. In the applied limit the only renormalisation constants with non-vanishing contributions are those for the charged Higgs mass and the doublet tadpoles,

$$\delta M_{H^\pm}^2, \ \delta T_{\phi_1}, \ \delta T_{\phi_2}. \tag{6.21}$$

The renormalisation constants of the gauge-boson masses vanish in the gaugeless limit.

Also the $\overline{\text{DR}}$ renormalisation constants

$$\delta\lambda, \ \delta\tan\beta, \ \delta\mu_{\text{eff}}, \ \delta v, \ \delta Z_{\mathcal{H}_2}. \tag{6.22}$$

do not contribute, although they can potentially lead to contributions that are of $\mathcal{O}(Y_t^2)$. However, not all of the renormalisation constants above contribute to $\mathcal{O}(Y_t^2)$ in the counterterms of the Higgs-mass matrices, given in eqs. (4.29) and (4.30). The constants stated in eq. (6.22) appear with a prefactor of v or v^2. This effectively changes their order in Y_t, since

$$vY_t = \frac{m_t}{\sin\beta} = \frac{m_t}{M_W}\frac{M_W}{\sin\beta}, \tag{6.23}$$

which results in a term that is neglected in the gaugeless limit. Accordingly, terms of this type These terms do not contribute in this approximation. The remaining

renormalisation constants vanish in the m_t^4-MSSM approximation,

$$\delta\kappa \stackrel{m_t^4}{=} \delta A_\kappa \stackrel{m_t^4}{=} \delta Z_{\mathcal{H}_2} \stackrel{m_t^4}{=} \delta Z_s \stackrel{m_t^4}{=} 0. \tag{6.24}$$

The reduced set of counterterms for the Higgs mass-matrix in this limit is identical for the $\mathcal{CP}$-even and -odd sectors. They read

$$\delta m_{\Psi_1\Psi_1}^{2,(m_t^4)} = \frac{1}{\sqrt{2}v}\left(-\frac{1-\sin^4\beta}{\cos\beta}\delta T_{\phi_1} + \cos^2\beta\sin\beta\ \delta T_{\phi_2}\right) + \delta M_{H^\pm}^2\sin^2\beta \tag{6.25a}$$

$$\delta m_{\Psi_2\Psi_2}^{2,(m_t^4)} = \frac{1}{\sqrt{2}v}\left(\sin^2\beta\cos\beta\ \delta T_{\phi_1} - \frac{1-\cos^4\beta}{\sin\beta}\delta T_{\phi_2}\right) + \delta M_{H^\pm}^2\cos^2\beta \tag{6.25b}$$

$$\delta m_{\Psi_1\Psi_2}^{2,(m_t^4)} = \frac{1}{\sqrt{2}v}\left(\sin^3\beta\ \delta T_{\phi_1} + \cos^3\beta\ \delta T_{\phi_2}\right) - \delta M_{H^\pm}^2\sin\beta\cos\beta \tag{6.25c}$$

$$\delta m_{\Psi_1\Psi_s}^{2,(m_t^4)} = \delta m_{\Psi_2\Psi_s}^{2,(m_t^4)} = \delta m_{\Psi_s\Psi_s}^{2,(m_t^4)} = 0, \tag{6.25d}$$

where Ψ denotes either ϕ or χ. Thus the renormalised self-energies in the m_t^4-MSSM approximation read

$$\hat{\Sigma}_{\Psi\Psi}^{(m_t^4)} = \begin{pmatrix} \Sigma_{\Psi_1\Psi_1}^{(m_t^4)} & \Sigma_{\Psi_1\Psi_2}^{(m_t^4)} & 0 \\ \Sigma_{\Psi_2\Psi_1}^{(m_t^4)} & \Sigma_{\Psi_2\Psi_2}^{(m_t^4)} & 0 \\ 0 & 0 & 0 \end{pmatrix} - \begin{pmatrix} \delta m_{\Psi_1\Psi_1}^{2,(m_t^4)} & \delta m_{\Psi_1\Psi_2}^{2,(m_t^4)} & 0 \\ \delta m_{\Psi_2\Psi_1}^{2,(m_t^4)} & \delta m_{\Psi_2\Psi_2}^{2,(m_t^4)} & 0 \\ 0 & 0 & 0 \end{pmatrix}. \tag{6.26}$$

While the self-energies in the interaction basis are exactly the self-energies as they would appear in the MSSM for the two Higgs doublets in the same limit, they are combined with the NMSSM tree-level Higgs mass-matrix and subsequently diagonalised.

6.1.6 m_t^4-NMSSM Approximation

In the m_t^4-NMSSM approximation the genuine NMSSM-corrections of order $\mathcal{O}(\lambda Y_t, \lambda^2)$, which are genuine to the NMSSM, are added to the m_t^4-MSSM approximation. In the literature, e.g. [109,125], these contributions are generally referred to as corrections of $\mathcal{O}(\alpha_t)$, although they include corrections beyond this order. For this work the order of genuine NMSSM-corrections will be spelled out in this section and whenever it is necessary to distinguish them from the MSSM-like corrections. For all other purposes they will be referred to together with their corresponding MSSM-like corrections as NMSSM-corrections of $\mathcal{O}(\alpha_t)$. Throughout this section the symbol $\widetilde{m}_t^4$ will be used in the same fashion as m_t^4 in the last section for the m_t^4-MSSM approximation.

Renormalisation Constants and Counterterms

All counterterm contributions to the Higgs potential that of $\mathcal{O}(Y_t^2)$ have to be considered. In the applied limit the only renormalisation constants with non-vanishing

contributions are those for the charged Higgs mass and the tadpoles,

$$\delta M_{H^\pm}^2, \ \delta T_{\phi_1}, \ \delta T_{\phi_2}, \ \delta T_{\phi_s}. \tag{6.27}$$

The renormalisation constants of the gauge-boson masses vanish in the gaugeless limit. Also the $\overline{\text{DR}}$ renormalisation constants

$$\delta\lambda, \ \delta\tan\beta, \ \delta\mu_{\text{eff}}, \ \delta v, \ \delta Z_{\mathcal{H}_2}. \tag{6.28}$$

have contributions that are of $\mathcal{O}(Y_t^2)$. Again, the remaining renormalisation constants vanish in this approximation

$$\delta\kappa \stackrel{\widetilde{m}_t^4}{=} \delta A_\kappa \stackrel{\widetilde{m}_t^4}{=} \delta Z_{\mathcal{H}_2} \stackrel{\widetilde{m}_t^4}{=} \delta Z_s \stackrel{\widetilde{m}_t^4}{=} 0. \tag{6.29}$$

In order to obtain a finite result the counterterms for the Higgs mass-matrix have to be extended. Spelling them out in detail is useful for understanding the genuine NMSSM-contributions. The counterterms for the $\mathcal{CP}$-even and -odd sectors read

$$\delta m_{\phi_1\phi_1}^{2,(\widetilde{m}_t^4)} = \delta m_{\phi_1\phi_1}^{2,(m_t^4)} + 2\lambda^2 v^2 \sin^2\beta \left(\frac{\delta\lambda}{\lambda} + 2\frac{\delta v}{v} \cos^2\beta \ \frac{\delta\tan\beta}{\tan\beta} \right) \tag{6.30a}$$

$$\delta m_{\phi_2\phi_2}^{2,(\widetilde{m}_t^4)} = \delta m_{\phi_2\phi_2}^{2,(m_t^4)} + 2\lambda^2 v^2 \cos^2\beta \left(\frac{\delta\lambda}{\lambda} + 2\frac{\delta v}{v} \sin^2\beta \ \frac{\delta\tan\beta}{\tan\beta} \right) \tag{6.30b}$$

$$\delta m_{\phi_1\phi_2}^{2,(\widetilde{m}_t^4)} = \delta m_{\phi_1\phi_2}^{2,(m_t^4)} - 2\lambda^2 v^2 \sin\beta\cos\beta \left[\frac{\delta\lambda}{\lambda} + 2\frac{\delta v}{v} + \left(\cos^2\beta - \sin^2\beta \right) \frac{\delta\tan\beta}{\tan\beta} \right] \tag{6.30c}$$

$$\delta m_{\phi_i\phi_s}^{2,(\widetilde{m}_t^4)} = \left[\delta m_{\phi_i\phi_s}^2 \right]_{\delta\kappa=\delta A_\kappa=0}, \quad i \in \{1,2,s\}, \tag{6.30d}$$

and for the $\mathcal{CP}$-odd sector

$$\delta m_{\chi_i\chi_j}^{2,(\widetilde{m}_t^4)} = \delta m_{\phi_i\phi_j}^{2,(m_t^4)}, \quad i,j \in \{1,2\} \tag{6.31a}$$

$$\delta m_{\chi_k\chi_s}^{2,(\widetilde{m}_t^4)} = \left[\delta m_{\chi_k\chi_s}^2 \right]_{\delta\kappa=\delta A_\kappa=0}, \quad k \in \{1,2,s\}. \tag{6.31b}$$

Here the counterterms for the singlet self-energies introduce non-vanishing contributions due to the counterterms for the tadpoles and the charged Higgs mass. In the m_t^4-NMSSM approximation the field renormalisation cannot be neglected in the $\overline{\text{DR}}$-scheme applied here. It gives a purely divergent contribution with a coefficient of $\mathcal{O}(\lambda Y_t)$. For the counterterms of the MSSM-like 2×2 submatrix they read

$$(\mathbf{M}_{\Psi\Psi})_{22} \ \delta Z_{\mathcal{H}_2} \stackrel{m_t^4}{=} \lambda^2 v^2 \sin^2\beta \ \delta Z_{\mathcal{H}_2} \equiv [((\mathbf{M}_{\Psi\Psi})_{22} \ \delta Z_{\mathcal{H}_2}]^{(\widetilde{m}_t^4)} \tag{6.32a}$$

$$\frac{1}{2}(\mathbf{M}_{\Psi\Psi})_{12} \ \delta Z_{\mathcal{H}_2} \stackrel{m_t^4}{=} -\frac{1}{2}\lambda^2 v^2 \sin\beta\cos\beta \ \delta Z_{\mathcal{H}_2}, \equiv [((\mathbf{M}_{\Psi\Psi})_{12} \ \delta Z_{\mathcal{H}_2}]^{(\widetilde{m}_t^4)}, \tag{6.32b}$$

where Ψ again denotes either ϕ or χ. For the counterterms of the genuine NMSSM-corrections the contributions read

$$
\frac{1}{2} \left(\mathbf{M}_{\phi\phi} \right)_{23} \delta Z_{\mathcal{H}_2} \stackrel{m_t^4}{=} \frac{1}{2} \frac{\lambda v}{\mu_{\text{eff}}} \lambda^2 v^2 \cos^2\beta \sin\beta \; \delta Z_{\mathcal{H}_2} + \frac{1}{2} \left(2\lambda v \mu_{\text{eff}} \sin\beta - \kappa v \mu_{\text{eff}} \cos\beta \right) \delta Z_{\mathcal{H}_2}
$$

$$
\equiv \left[\left((\mathbf{M}_{\phi\phi})_{23} \; \delta Z_{\mathcal{H}_2} \right) \right]^{(\widetilde{m_t^4})}
\tag{6.32c}
$$

$$
\frac{1}{2} \left(\mathbf{M}_{\chi\chi} \right)_{23} \delta Z_{\mathcal{H}_2} \stackrel{m_t^4}{=} \frac{1}{2} \frac{\lambda v}{\mu_{\text{eff}}} \lambda^2 v^2 \cos^2\beta \sin\beta \; \delta Z_{\mathcal{H}_2} - \frac{1}{2} 3\kappa v \mu_{\text{eff}} \cos\beta \; \delta Z_{\mathcal{H}_2}
$$

$$
\equiv \left[\left((\mathbf{M}_{\chi\chi})_{23} \; \delta Z_{\mathcal{H}_2} \right) \right]^{(\widetilde{m_t^4})} .
\tag{6.32d}
$$

Thus the finite contributions to the renormalised self-energies in the m_t^4-NMSSM approximation read

$$
\hat{\Sigma}_{\Psi\Psi}^{(\widetilde{m_t^4})} \Big|^{\text{fin}} = \left[\hat{\Sigma}_{\Psi\Psi}^{(m_t^4)} + \begin{pmatrix} 0 & 0 & \hat{\Sigma}_{\Psi_1\Psi_s}^{(\widetilde{m_t^4})} \\ 0 & 0 & \hat{\Sigma}_{\Psi_2\Psi_s}^{(\widetilde{m_t^4})} \\ \hat{\Sigma}_{\Psi_s\Psi_1}^{(\widetilde{m_t^4})} & \hat{\Sigma}_{\Psi_s\Psi_2}^{(\widetilde{m_t^4})} & \hat{\Sigma}_{\Psi_s\Psi_s}^{(m_t^4)} \end{pmatrix} \right]^{\text{fin}} ,
\tag{6.33}
$$

where Ψ denotes either ϕ or χ. While the finite contribution of the MSSM-like self-energies is identical to the m_t^4-MSSM approximation. Furthermore the renormalised, genuine NMSSM self-energies contribute in the m_t^4-NMSSM approximation. The renormalisation of the additional self-energies involves contributions from the field renormalisation constants.

6.1.7 Comparison with Results obtained in the effective Potential Approach

The m_t^4-NMSSM approximation has been calculated already in the effective potential [125–127]. This makes an analytic comparison of the obtained result possible.

The effective Higgs potential can be decomposed in the neutral Higgs sector as $V_{\text{eff}} = V_0 + \Delta V$, where ΔV contains higher-order corrections. Thus the Higgs mass matrices receive higher-order corrections,

$$
\mathbf{M}_{\Psi\Psi}^{\text{eff}} = \mathbf{M}_{\Psi\Psi} + \Delta\mathbf{M}_{\Psi\Psi}^{\text{eff}}.
\tag{6.34}
$$

The higher-order corrections $\Delta\mathbf{M}_{\Psi\Psi}^{\text{eff}}$ correspond to the renormalised self-energies in eq. (6.3). They are given by the derivatives of ΔV with respect to the fields taken in the classical minimum of V_{eff}, which corresponds to vanishing fields Ψ_i

$$
\left(\Delta\mathbf{M}_{\Psi\Psi}^{\text{eff}} \right)_{ij} = -\frac{1}{\sqrt{2}} \frac{\delta_{ij}}{v_i} \frac{\partial \Delta V}{\partial \Psi_i} \Big|^{\text{min.}} + \frac{\partial^2 \Delta V}{\partial \Psi_i \partial \Psi_j} \Big|^{\text{min.}} , \quad i,j \in \{1,2,s\},
\tag{6.35}
$$

where the short-hand notation $v_1 = v\cos\beta$ and $v_2 = v\sin\beta$ is used. The first term

corresponds to the diagrammatically obtained finite parts of the tadpole contributions, the the second to the $\overline{\text{DR}}$renormalised Higgs self-energy in the m_t^4-NMSSM approximation,

$$
\left.\frac{\partial \Delta V}{\partial \Psi_i}\right|^{\text{min}} = \delta T_{\Psi_i}|^{\text{fin}}, \qquad \left.\frac{\partial^2 \Delta V}{\partial \Psi_i \partial \Psi_j}\right|^{\text{min}} = \left(\Sigma_{\Psi\Psi}^{\widetilde{m_t^4}}\right)_{ij}^{\text{fin}}. \tag{6.36}
$$

The calculation in the effective potential approach corresponds to a Feynman-diagrammatic calculation in a pure $\overline{\text{DR}}$-scheme, where the only non-vanishing counterterm contributions are

$$
\left.\delta m_{\Psi_i \Psi_j}^{\text{eff}}\right|^{\text{fin}} = \frac{\delta_{ij}}{\sqrt{2}v_i}\, \delta T_{\phi_i}|^{\text{fin}}, \quad i \in \{1,2,s\}. \tag{6.37}
$$

These contributions stem from the expression of the soft-breaking Higgs-mass terms. The additional contributions from the tadpole counterterms to the Higgs-mass counterterms given in eqs. (4.29) and (4.30) are a result of the chosen on-shell renormalisation scheme for the charged Higgs-mass $M_{H^\pm}^2$. They are not present in the effective potential approach, that correlates to a calculation where the independent parameters are assumed to be $\overline{\text{DR}}$-renormalised. The identity between the result in the effective potential (left side) and the corresponding result obtained from the Feynman-diagrammatic calculation (right side),

$$
\left(\Delta \mathbf{M}_{\Psi\Psi}^{\text{eff}}\right)_{ij} = \left(\Sigma_{\Psi\Psi}^{\widetilde{m_t^4}}\right)_{ij}^{\text{fin}} - \left.\delta m_{\Psi_i \Psi_i}^{\text{eff}}\right|^{\text{fin}}, \tag{6.38}
$$

has been confirmed analytically.

6.2 Subsets of Fermion/Sfermion-Contributions

Amongst the fermion/sfermion-contributions ($f/\tilde{f}$-contribution) additional subsets can be formed by contributions of any fermion-doublet together with their superpartners, for example contributions that are proportional to the colour factor N_c of the third generation. These contributions stem from the top/bottom quarks and stop/sbottom-squarks. No additional approximation is applied in their evaluation, which means that the Higgs fields can couple to the squark fields via D-terms. Scalars that are gauge-singlets, however, do not obtain D-terms and thus no additional couplings between singlet Higgs fields and the squarks are introduced by D-terms. Hence all allowed diagrams for MSSM-like and genuine NMSSM self-energies are identical to the set in the m_t^4-approximation as shown in tab. 6.2. All renormalisation constants are required besides those that obtain only corrections from the Higgs- and gauge-sectors, which are δZ_{ϕ_s}, $\delta\kappa$ and δA_κ. In particular this means that the renormalisation constants for the gauge-boson masses contribute in this case.

6.3 Higgs- and Gauge-Sector Contributions

Finally we are considering the subset accounting1 only for the contributions from the Higgs- and gauge-sectors. All renormalisation constants and self-energies have to be considered.

For the contributions from gauge bosons and the gaugino fermions the couplings are identical to the MSSM-like Higgs fields and will not be discussed here. The focus of this section will be on the Higgs-higgsino and Higgs self-couplings genuine to the NMSSM. However, the contributions from the gauge bosons are necessary for a consistent renormalisation of the Higgs sector. Other than in the fermion/sfermion sector the number of contributing NMSSM diagrams in this sector is enhanced compared to the self-energies for the MSSM-like Higgs fields. In the MSSM the Higgs self-couplings and the couplings between Higgs and higgsino fields are determined purely by the gauge couplings, while the MSSM μ-term only contributes to the Higgs and higgsino masses. In the NMSSM, however, the Higgs self-couplings are determined by the gauge-couplings, λ and κ. The NMSSM Higgs-higgsino-couplings involving at least one singlet- or singlino-field are determined only by λ and κ and vanish in the MSSM-limit.

In this section the qualitative features of these contributions will be discussed in the interaction basis for simplicity. For the full calculation the diagrams have to evaluated in the mass basis. This means that the single diagrams have to be multiplied by the mixing matrix elements. The arguments then hold for the fields mixed into the mass states.

Higgsino Contributions

The genuine NMSSM higgsino contributions to the Higgs self-energies have the form

$$
\Psi_i(k) \ \text{--} \bigcirc \text{--} \ \Psi_j(k) = \mathcal{O}\Big(\Gamma_{\Psi_i \bar\psi_m \psi_n} \Gamma_{\Psi_i \bar\psi_n \psi_m}\Big) \qquad (6.39)
$$

In the MSSM no such diagram exists with purely higgsino-fields in the loop and thus they represent a genuine NMSSM-correction. If classified in terms of the couplings the self-energy corrections from these diagrams read

$$
\Sigma^{\tilde{h}_s}_{\Psi\Psi} = \begin{pmatrix} \mathcal{O}(\lambda^2) & \mathcal{O}(\lambda^2) & \mathcal{O}(\lambda\kappa) \\ \mathcal{O}(\lambda^2) & \mathcal{O}(\lambda^2) & \mathcal{O}(\lambda\kappa) \\ \mathcal{O}(\lambda\kappa) & \mathcal{O}(\lambda\kappa) & \mathcal{O}(\kappa^2) \end{pmatrix}. \qquad (6.40)
$$

Since the singlino-mass depends on the parameter κ the order of couplings must not represent the κ-dependency of the contributions. For example, after renormalisation the diagram in eq. (6.39) yields for neglected external momenta a self-energy

contribution that is proportional to

$$\kappa^2 m_{\tilde{h}_s}^2 \log \frac{m_{\tilde{h}_s}^2}{\mu_{\mathrm{r}}^2} \sim \frac{\kappa^4}{\lambda^2} \mu_{\mathrm{eff}}^2 \log \kappa^2, \tag{6.41}$$

where μ_{r} is the renormalisation scale, since the singlino mass grows linearly with κ, $m_{\tilde{h}_s} = \sqrt{2}\kappa/\lambda\mu_{\mathrm{eff}}$.

Higgs Contributions

The Higgs self-couplings stem from two diagrams,

$$\Psi_i(k) \, \text{---} \, \overset{\Psi_m}{\underset{\Psi_n}{\bigcirc}} \, \text{---} \, \Psi_j(k) = \Gamma_{\Psi_i\Psi_m\Psi_n}\Gamma_{\Psi_i\Psi_n\Psi_m}B_0\left(k^2, m_{\Psi_n}^2, m_{\Psi_m}^2\right) \tag{6.42a}$$

$$\Psi_i(k) \, \text{---} \, \overset{\Psi_m}{\diamond} \, \text{---} \, \Psi_j(k) = \Gamma_{\Psi_i\Psi_j\Psi_m\Psi_m}A_0\left(m_{\Psi_m}^2\right). \tag{6.42b}$$

The non-vanishing trilinear Higgs self-couplings are of the the orders

$$\Gamma_{\phi_i\phi_j\phi_k} = \mathcal{O}\left(\lambda^2\right), \quad \Gamma_{\phi_i\phi_j\phi_s} = \mathcal{O}(\lambda\kappa), \quad \Gamma_{\phi_i\phi_s\phi_s} = \mathcal{O}(\lambda\kappa), \quad \Gamma_{\phi_s\phi_s\phi_s} = \mathcal{O}\left(\kappa^2\right) \tag{6.43}$$

for the $\mathcal{CP}$-even fields without D-terms. For the $\mathcal{CP}$-odd fields any vertex with an even number of $\mathcal{CP}$-odd fields is allowed and of the same order as the vertex for $\mathcal{CP}$-even fields. For the quartic coupling the pattern is similar: A vertex that involves only $\mathcal{CP}$-even fields is proportional to λ^2, a mixed vertex is proportional to $\lambda\kappa$, and a pure singlet vertex is proportional to κ^2. The diagrams in eqs. (6.42) are thus of the orders

$$\Psi_i(k) \, \text{---} \, \overset{\Psi_m}{\underset{\Psi_n}{\bigcirc}} \, \text{---} \, \Psi_j(k) = \mathcal{O}\left(\lambda^{4-n}\kappa^n\right), \qquad \Psi_i(k) \, \text{---} \, \overset{\Psi_m}{\diamond} \, \text{---} \, \Psi_j(k) = \mathcal{O}\left(\lambda^{2-n}\kappa^n\right) \tag{6.44}$$

where n denotes by the number of involved singlet fields. As for the higgsino-contributions the order of the couplings might not reflect the λ- and κ-dependence of these contributions, since the masses of the internal fields depend on both parameters.

Comparison with the m_t^4-NMSSM Approximation

Both the magnitude of the genuine NMSSM-corrections from the stop-sector and from the Higgs-sector increase with λ. However, the Higgs-sector contributions

depend on higher powers of λ than the stop-contributions. Thus scenarios with an increased NMSSM-contributions from the stops are expected to have have also increased NMSSM-contributions from the Higgs-sector. These contributions are not genuine to the higher-order corrections to the mass of the singlet, since also doublet-fields couple with λ.

For increased values of κ only the contributions to the self-energies with an external singlet may yield a more sizeable contribution.

While the impact of the genuine stop-contributions is decreased for large values of μ_{eff} (6.14a), the Higgs-sector contributions can increase with μ_{eff} (6.41). Thus in scenarios with large values for λ or κ, and μ_{eff} the Higgs-sector contributions might be increased and have a larger impact than the genuine NMSSM-contributions from sfermions.

6.4 Two-Loop MSSM Approximation

Up to now the two-loop calculations for Higgs masses in the MSSM and NMSSM have mainly been performed in the electroweak gaugeless limit. In the previous sections the one-loop contributions were discussed in detail. The discussion can be used to estimate the numerical impact of genuine NMSSM-corrections at two-loop order. In the MSSM the leading two-loop contributions stem from QCD and SQCD corrections of $\mathcal{O}(\alpha_t \alpha_s)$, involving a gluon or a gluino, and the two-loop corrections of $\mathcal{O}(\alpha_t^2)$. The corresponding diagrams can be written as one-loop diagrams with an insertion as seen in tab. 6.3. The insertions are denoted by blobs. The blobs represent the topologies

(a1)   (a2)   (b1)   (b2)   (c1)   (c2)
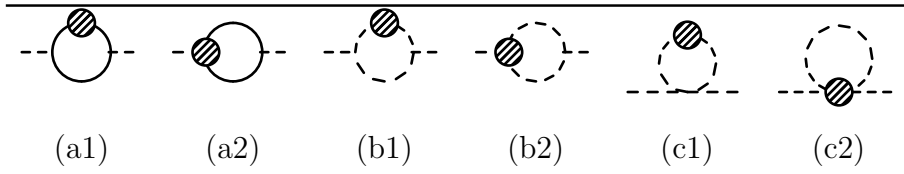
Table 6.3: Two-loop diagrams depicted as one-loop diagrams with insertions of a propagator correction, labelled (#1) , and a vertex correction, labelled (#2).

$$i \quad \begin{array}{c} o_2 \\ \\ o_1 \end{array} \quad : \quad \Gamma_{io_1o_2}^{f_1f_2f_3} = i \begin{array}{c} f_2 \quad o_2 \\ f_3 \\ f_1 \quad o_1 \end{array} , \quad \Gamma_{io_1o_2}^{f_1f_2} = i \begin{array}{c} f_1 \quad o_2 \\ \\ f_2 \quad o_1 \end{array} \qquad (6.45\text{a})$$

$$i \quad \begin{array}{c} \\ \end{array} \quad o : \quad \Gamma_{io}^{f_1f_2f_3} = i \begin{array}{c} f_1 \\ \\ f_2 \end{array} o, \quad \Gamma_{io}^{f} = i \begin{array}{c} f \\ \end{array} o, \qquad (6.45\text{b})$$

where the plain solid lines represent any field denoted by its label.

6.4.1 Corrections of $\mathcal{O}(\alpha_t\alpha_s)$

For this class corrections from a gluon, a gluino or a stop to the diagrams of the m_t^4-approximations are taken into account. We focus here on the diagrams involving the Higgs singlet field on one or both external lines.

The diagrams with a propagator-correction, any topology from eq. (6.45b) inserted into diagrams (#1), are suppressed by the same factors as the one-loop diagrams, since the Higgs fields couple directly to the fermion/sfermion fields in the outer loop.

For the diagrams with a vertex correction, any topology from eq. (6.45a) inserted into diagrams (#2), the number of diagrams with an external singlet is reduced. The singlet field does not couple to the top-quark in either the inner or outer loop, thus

$$\Gamma^{\bar{t}tg}_{\phi_s\bar{t}t} = 0. \tag{6.46}$$

The loop-induced singlet–top–top vertex gives rise to a contributions from the diagram (a1) to the singlet-doublet self-energy. However, it can be suppressed compared to the according diagram with a loop-induced vertex involving only Higgs doublet-fields,

$$\Gamma^{\tilde{t}_a\tilde{t}_a\tilde{g}}_{\phi_s\bar{t}t} = \frac{\Gamma_{\phi_s\tilde{t}_a\tilde{t}_b}}{\Gamma_{\phi_i\tilde{t}_a\tilde{t}_b}}\Gamma^{\tilde{t}_a\tilde{t}_a\tilde{g}}_{\phi_i\bar{t}t} \tag{6.47}$$

with the suppression factors given in eq. (6.14).

Since the vertex corrections of the diagrams (#2) for the singlet field receive a similar suppression as the corresponding one-loop diagrams, the two-loop self-energy corrections can be classified by the order of their couplings as

$$\Sigma_{\Psi\Psi} = \begin{pmatrix} \mathcal{O}(Y_t^2\alpha_s) & \mathcal{O}(Y_t^2\alpha_s) & \mathcal{O}(\lambda Y_t\alpha_s) \\ \mathcal{O}(Y_t^2\alpha_s) & \mathcal{O}(Y_t^2\alpha_s) & \mathcal{O}(\lambda Y_t\alpha_s) \\ \mathcal{O}(\lambda Y_t\alpha_s) & \mathcal{O}(\lambda Y_t\alpha_s) & \mathcal{O}(\lambda^2\alpha_s) \end{pmatrix}. \tag{6.48}$$

As for the m_t^4-NMSSM one-loop approximation the genuine two-loop NMSSM contributions of $\mathcal{O}(\alpha_t\alpha_s)$ are suppressed or enhanced compared to the MSSM-like contributions. Thus the relative size of the genuine NMSSM-corrections at one-loop order can be used as an estimate for the impact of the according two-loop corrections.

The genuine NMSSM-corrections of $\mathcal{O}(\alpha_t\alpha_s)$ have been calculated and implemented into the public code `NMSSMCalc`. This allows to test the MSSM-approximation for this set of contributions, see sect. 8.1.3.

6.4.2 Corrections of $\mathcal{O}(\alpha_t^2)$

For this class corrections to the diagrams of the m_t^4-approximations with insertion of $\mathcal{O}(Y_t^2, \lambda Y_t, \lambda^2)$ involving top/stop fields are taken into account. Both the external-and the sub-diagrams can contain a Higgs-singlet field and thus receive a suppression compared to the corresponding diagram in the MSSM. If the sub-diagram contains only stop-fields, it is always MSSM-like. Only the external diagram can be suppressed

in this case.

The two-loop self-energy contributions thus can be classified by the highest power in the coupling Y_t as

$$\Sigma_{\Psi\Psi} = \sum_{n=0}^{2} \begin{pmatrix} \mathcal{O}\left(Y_t^{4-n}\lambda^n\right) & \mathcal{O}\left(Y_t^{4-n}\lambda^n\right) & \mathcal{O}\left(\lambda^{1+n}Y_t^{3-n}\right) \\ \mathcal{O}\left(Y_t^{4-n}\lambda^n\right) & \mathcal{O}\left(Y_t^{4-n}\lambda^n\right) & \mathcal{O}\left(\lambda^{1+n}Y_t^{3-n}\right) \\ \mathcal{O}\left(\lambda^{1+n}Y_t^{3-n}\right) & \mathcal{O}\left(\lambda^{1+n}Y_t^{3-n}\right) & \mathcal{O}\left(\lambda^{2+n}Y_t^{2-n}\right) \end{pmatrix}. \tag{6.49}$$

For $n = 0$ only MSSM-like subdiagrams appear. The MSSM-like contributions for the doublet fields are recovered for this case in a 2×2 submatrix. They are identical to the MSSM-contributions up to mixing effects between the Higgs fields.

A calculation of the $\mathcal{O}(\alpha_t^2)$ corrections in the NMSSM in a mixed $\overline{\text{DR}}$/on-shell scheme is still missing. However, for $\overline{\text{DR}}$ calculations the contributions at this order have been obtained, see e.g. [39].

6.5 Conclusion

In this section partial one-loop contributions from appropriate subsets were determined. Analytic arguments for the expected numerical impact of these contributions have been provided for the genuine NMSSM contributions. The estimations based on these arguments will be tested for specific scenarios in the following chapters.

7 NMSSM-FeynHiggs: Predictions for NMSSM Higgs masses and mixing contributions

The results of this work will be part of the next major update for the code `Feyn-Higgs` [30–36]. This update will extend the calculation of the Higgs masses and the wave normalisation factors to NMSSM with real and complex parameters. The extension will include the full one-loop calculation including momentum-dependence, as outlined in this work. The MSSM approximation will be used for the two-loop contributions of $\mathcal{O}(\alpha_s\alpha_t, \alpha_t^2, \alpha_s\alpha_b, \alpha_t\alpha_b)$, for an overview see [32], and $\mathcal{O}(\alpha_s\alpha_t, \alpha_t^2)$ [31,35,36] for the MSSM with real and complex parameters, respectively. The resummation of large logarithms due to large SUSY-masses [30] will be included for the real and the complex as well as the momentum-dependence for the corrections of $\mathcal{O}(\alpha_t\alpha_s)$ in the real case [98].

In order to extend the one-loop calculation presented in this work to the NMSSM with complex parameters a new model file for `FeynArts` and `FormCalc` is created. It will contain all necessary counterterms for fully automated one-loop calculations, similar to the available model file for the MSSM with complex parameters [128]. The renormalisation scheme for the absolute values complex parameters will follow the scheme outlined in this work. Any additional $\overline{\text{DR}}$-counterterms for the phases of the complex parameters are obtained with the methods described in sec. 4.5. The model file for the NMSSM with complex parameters including one-loop counterterms will be published separately and included into future versions of `FeynArts` and `FormCalc`.

The new version of `FeynHiggs` will include an extended SLHA-conform interface, that allows to supply every $\overline{\text{DR}}$-parameter at its own scale. For the Higgs-mass calculation these parameters will be RGE-evolved to the renormalisation scale m_t, where the stop-parameters will be converted into the on-shell scheme for the top- and stop-masses with the MSSM routines as an approximation as discussed in sec. 5.4.3.

The obtained renormalised self-energies in the Higgs-sector will be used to calculate the wave function normalisation factors for the Higgs-fields, described in sec. 3.3, for the NMSSM with complex and real parameters.

The aforementioned implementations and developments are work in progress. For the studies in this work a preliminary version of `FeynHiggs` was used. In this version the one-loop calculation and the pole-determination was separated from `FeynHiggs`, which provides only the renormalised MSSM self-energies at the two-loop level as described in sec. 5.3. The calculation of wave normalisation factors will be available only in the final NMSSM-extension of `FeynHiggs`.

8 Study of the MSSM Approximations at one- and two-loop order

In this chapter the MSSM approximation implemented at the two-loop level will be tested. For this purpose a genuine NMSSM scenario will be studied, which gives rise to a SM-like Higgs with a predicted mass at the two-loop level of around 125 GeV and a lighter, singlet-like Higgs field. In order to investigate the influence of the extended Higgs- and higgsino sector of the NMSSM compared to the MSSM the study will start with one-dimensional variations of λ. The limit $\lambda \to 0$ and constant μ_{eff} leads to decoupled singlet fields with infinite mass and MSSM-like doublet fields in the Higgs- and neutralino sectors. Increasing the value of λ translates directly to increasing the influence of genuine NMSSM-effects. A detailed study of the one-loop result and the quality of approximations by partial contributions will be performed. In order to study the two-loop MSSM approximation the results obtained with the methods described in the previous chapters will compared with the public tool NMSSMCALC [29]. This tool offers a similar Higgs-mass calculation with diagrammatic methods in a hybrid $\overline{\text{DR}}$/on-shell renormalisation scheme and thus is well suited for a comparison.

In a subsequent study the behaviour of the mass of a singlet-like Higgs field under variations of A_t will be studied for different values of λ. It will be compared with the A_t-dependence of the masses of MSSM-like Higgs fields.

The chosen scenarios will always respect the relation

$$\lambda^2 + \kappa^2 \lesssim 0.5 \tag{8.1}$$

to ensure perturbative predictability of the NMSSM up to high scales [120].

8.1 MSSM-Approximation: A sample Scenario

The sample scenario for our study is defined by the parameters given in table 8.1. The parameter λ is varied if not stated otherwise. The derived tree-level masses of the stop-, chargino- and neutralino-fields are given in the appendix in sec. B.1 . For values $\lambda \gtrsim 0.32$ the mass of the lightest state becomes tachyonic at tree-level and therefore the analyses will be performed only for values of λ up to 0.32. The choice for the top-quark mass will be the pole mass m_t^{OS} for the comparison with `NMSSMCalc` and $m_t^{\overline{\text{MS}}}(m_t)$ for the remaining studies. Using the $\overline{\text{MS}}$ top-mass allows

to include the resummation of leading and next-to-leading logarithms implemented in `FeynHiggs`. The renormalisation scale for the studies in this chapter will be fixed at the used value of the top-quark mass. The discussed scenario is tested against the

<div align="center">Higgs sector parameters: heavy fermion masses:</div>

$M_{H^\pm}$	$\tan\beta$	μ_{eff}	A_κ	κ	m_t^{OS}	$m_t^{\overline{\text{MS}}}(m_t)$	$m_b^{\overline{\text{MS}}}(m_b)$	m_τ
1000	8	125	-300	0.2	173.2	167.48	4.2	1.78

<div align="center">sfermion- and gaugino-parameters:</div>

$M_{\tilde{q}}$	$M_{\tilde{l}}$	A_t	A_τ, A_b, A_q	A_l	$M_1^{(\text{GUT})}$	M_2	M_3
1500	200	-2000	-1500	-100	≈ 143	300	1500

Table 8.1: Definition of the analysed sample scenario. All dimensionful parameters are given in GeV. All $\overline{\text{DR}}$-parameters are defined at $m_t^{\overline{\text{MS}}}(m_t)$. All stop-parameters are on-shell parameters.

full set of experimental limits implemented in `HiggsBounds 4.1.3` [113]. To obtain the relevant quantities for `HiggsBounds` we made use of `NMSSMTools 4.4.0` [17] and linked it with `HiggsBounds`[1] as described in sec. 5.5.

8.1.1 Full Result

The full results for the tree-level, one- and two-loop Higgs-mass predictions in the sample scenario defined in tab. 8.1 are shown as a function of λ in fig. 8.1 for the $\mathcal{CP}$-even fields and in fig. 8.2 for the $\mathcal{CP}$-odd fields. The term 'full result' refers to all one-loop corrections in the NMSSM including momentum-dependence and reparametrisation, and all available contributions of $\mathcal{O}(\alpha_s\alpha_t, \alpha_s\alpha_b, \alpha_t^2, \alpha_t\alpha_b)$ from the MSSM including the resummation of large logarithms. For this study the parameter λ will be varied between 0.1 and 0.32. The lower limit of the parameter λ is chosen to depict only one point with a cross-over behaviour for the two smaller masses, m_{h_1} and m_{h_2}. For values $\lambda < 0.1$ there is another point with cross-over behaviour of the two larger masses. However, due to the small values of λ in this region it is less suitable to study the behaviour of the genuine NMSSM-corrections that scale with λ.

In order to understand the physical situation of the scenario it is important to determine the admixture of the genuine NMSSM-contributions to the plotted masses. Thus the squared mixing matrix elements determining the singlet admixture are given

---

[1]We thank Florian Domingo and Oskar Stål for providing a modified version of `NMSSMTools` including a link to `HiggsBounds`.
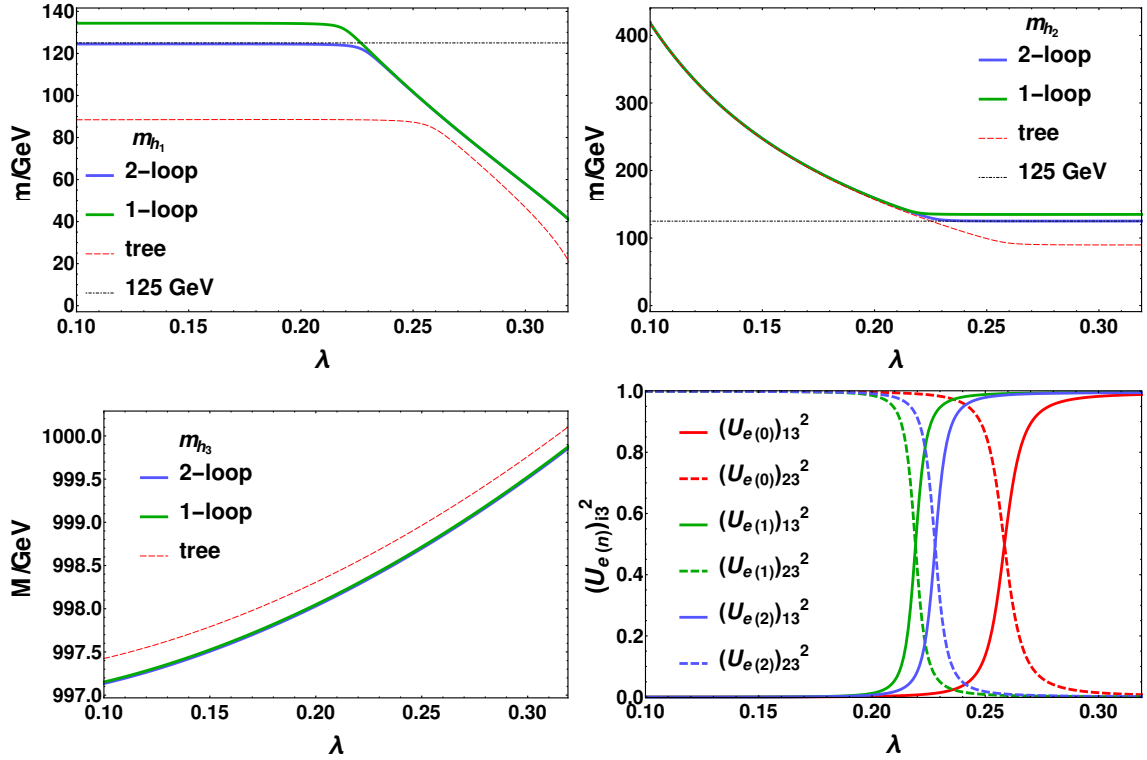
Figure 8.1: *Upper row and lower left*: Mass of the $\mathcal{CP}$-even Higgs-fields m_{h_i} at tree-level, full one- and two-loop order. All corrections from the NMSSM are calculated at one-loop order including momentum-dependence and reparametrisation. At two-loop order the MSSM-type corrections of $\mathcal{O}(\alpha_s\alpha_t, \alpha_s\alpha_b, \alpha_t^2, \alpha_t\alpha_b)$ without momentum-dependence are taken into account as well as the resummation of large logarithms. The dotted line represents 125 GeV. *Lower right*: Squared mixing-matrix elements that determine the singlet-admixture to the two lighter fields h_1 and h_2. The values for $\lambda_c^{(n)}$ at the intersection are $\lambda_c^{(0)} \approx 0.26$, $\lambda_i^{(1)} \approx 0.21$, and $\lambda_i^{(2)} \approx 0.23$ at the respective loop orders.

for the two lighter $\mathcal{CP}$-even fields. For the remaining fields no cross over behaviour appears in the depicted interval of λ, their mixing matrix elements are either ≈ 0 for doublet-like and ≈ 1 for singlet-like fields. The heaviest $\mathcal{CP}$-even and -odd fields, h_3 and A_2, are doublet-like, while the lighter $\mathcal{CP}$-odd field A_1 is singlet-like.

The lighter $\mathcal{CP}$-even masses switch their dominant admixture: For low values of λ the field h_2 is singlet- and the field h_1 is doublet-like and vice versa for large values of λ. Both fields are evenly mixed between a singlet and a doublet Higgs-field at the value $\lambda_c^{(n)}$ at the n-th loop-order with $n = 0$ denoting tree-level. The values $\lambda_c^{(n)}$ are different from each other. They can be determined from the plot on the lower right in fig. 8.1 as the intersection points between the squared mixing-matrix elements $[\mathbf{U}_{e(n)}^2]_{\{13,23\}}$, that are defined in sec. 3.3, that quantify the singlet-admixture of the fields h_1 and h_2. The (momentum-dependent) one-loop corrections cause the largest shift for $\lambda_c^{(1)}$ of $\lambda_c^{(1)} - \lambda_c^{(0)} \approx -0.05$, while the additional shift from the (momentum-independent) two-loop corrections is much smaller with $\lambda_c^{(2)} - \lambda_c^{(1)} \approx 0.01$. At $\lambda_c^{(n)}$ both
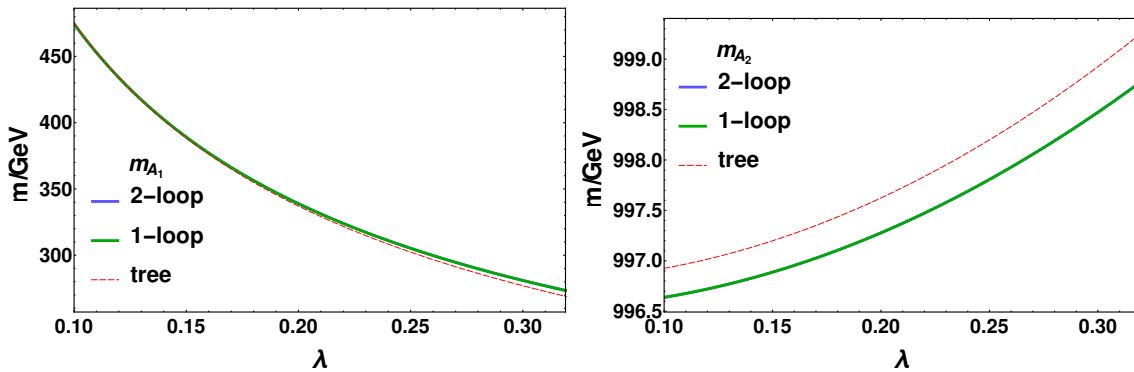
Figure 8.2: Mass of the $\mathcal{CP}$-odd Higgs fields m_{A_i} at tree-level, full one- and two-loop order with the same contributions as for the $\mathcal{CP}$-even sector given in fig. 8.1.

mixing-matrix elements are equal to 0.5 and thus higher-order corrections from both the singlet- and the doublet-sectors contribute equally to the mass prediction. Neither contribution is enhanced or suppressed by mixing effects. At $\lambda_c^{(2)}$ it is expected that the effect from neglecting genuine NMSSM-corrections as performed at the two-loop level is most severe.

The λ-dependence of the masses is dominated by tree-level and mixing effects: A strong singlet admixture leads to decreasing masses with increasing values of λ, while a small singlet-admixture leads to a slightly increasing masses. Generally the higher-order corrections for singlet-like fields grow faster with λ than their counterparts for doublet-like fields, since the Higgs singlet couples to the remaining field spectrum via λ. In the MSSM-approximation of the two-loop result singlet-like states receive no two-loop corrections. As in the MSSM the larger masses (of doublet-like fields) are affected by higher-order corrections to a lesser extent than the lighter states.

8.1.2 Numerically leading One-Loop Contributions

In this section the numerically leading one-loop contributions will be identified by studying the partial contributions defined in chapter 6. The ratios of Higgs–sfermion couplings defined in sec. 6.1.3, which can enhance or suppress the genuine NMSSM contributions, are plotted as a function of λ in fig. 8.3. All ratios are smaller than 1 and should suppress the genuine NMSSM-corrections.

The mass predictions for the MSSM- and NMSSM-versions of the m_t^4-approximation are depicted together with the tree-level and full one-loop results in fig. 8.4 as a function of λ. For all three masses the two different m_t^4-approximations are almost indistinguishable from each other for a wide range of λ. For the light singlet-light field at larger values of λ, however, a slight difference between both m_t^4-approximations can be observed together with a less accurate approximation of the full one-loop prediction. In order to study this effect in more detail the absolute differences between the partial and the full one-loop mass-predictions are plotted as a function of λ in fig. 8.5 together with the squared mixing-matrix elements that determine the singlet-
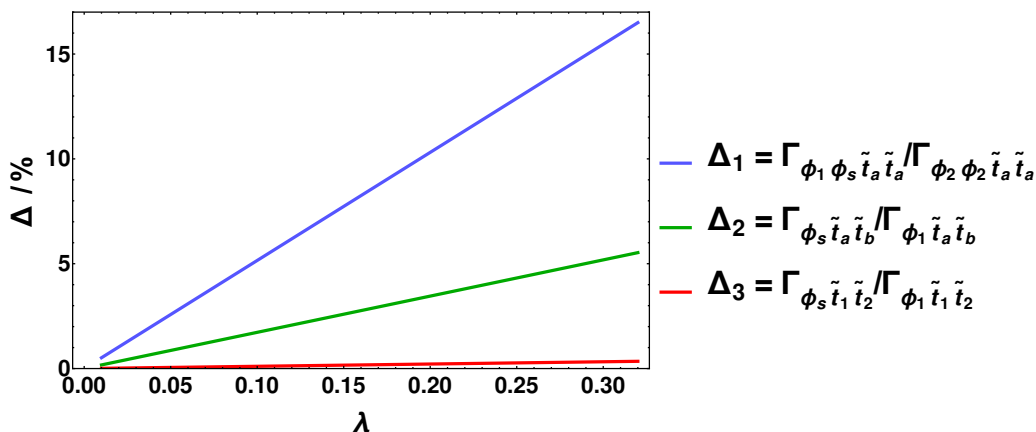
Figure 8.3: Suppression factors as defined in sec. 6.1.3. The omitted ratios of couplings remain smaller than the maximal value of Δ_3.

admixture to the lighter states h_1 and h_2.

In the first row of fig. 8.5 the squared mixing-matrix elements for the singlet-admixture are plotted for the three $\mathcal{CP}$-even fields as a function of λ. All plotted approximations reproduce the behaviour of the full one-loop result well. The difference between the points with cross-over behaviour between the two lighter fields, λ_c, never exceed the value of 0.01. However, for some approximations the shift can give rise to intersection points between the full one-loop and the approximate mass predictions as observed in the upper left plot for the mass of the lightest field in fig. 8.4. They result in discontinuous points in the plots of the mass-differences.

In the second row of fig. 8.5 the difference between the m_t^4-NMSSM approximation and the m_t^4-NMSSM approximation ($\Delta m = |m_{h_i}^{(m_t^4\text{-NMSSM})} - m_{h_i}^{(m_t^4\text{-MSSM})}|$) is plotted as a function of λ. The maximal difference between the approximations m_t^4-MSSM and m_t^4-NMSSM remains below 500 MeV for the mass of the lightest field h_1. For h_2 and h_3 the difference decreases by one and two orders of magnitude, respectively. The λ-dependence of Δm is different for the three masses depending strongly on the singlet admixture: The largest values for Δm are observed for singlet-like fields where it rises with λ. For doublet-like fields the difference remains below 10 MeV even for larger values of λ. At $\lambda_c^{(1)}$, the point of the cross-over behaviour between h_1 and h_2, a local maximum of the difference can be observed. However, it does not exceed 100 MeV. For the Higgs field with a mass around 125 GeV this represents an improvement an additional contribution of less than 1‰ by including genuine NMSSM-corrections of $\mathcal{O}(\lambda Y_t, \lambda^2)$. For the mass of the singlet-like field for larger values of λ a sharp increase of the difference between the approximations m_t^4-MSSM and -NMSSM can be observed. The corrections of $\mathcal{O}(\lambda Y_t, \lambda^2)$ account for a maximal contribution of $\approx 1\%$ for a singlet-like field with a mass below 40 GeV. For the heaviest field h_3 the difference is negligible but rises with its singlet admixture. This suggests that in scenarios where values $\lambda \gg 0.32$ are allowed, the genuine NMSSM-contributions could become more important and even dominant compared to the MSSM-like contributions. This, however, is not the case as will be discussed in the
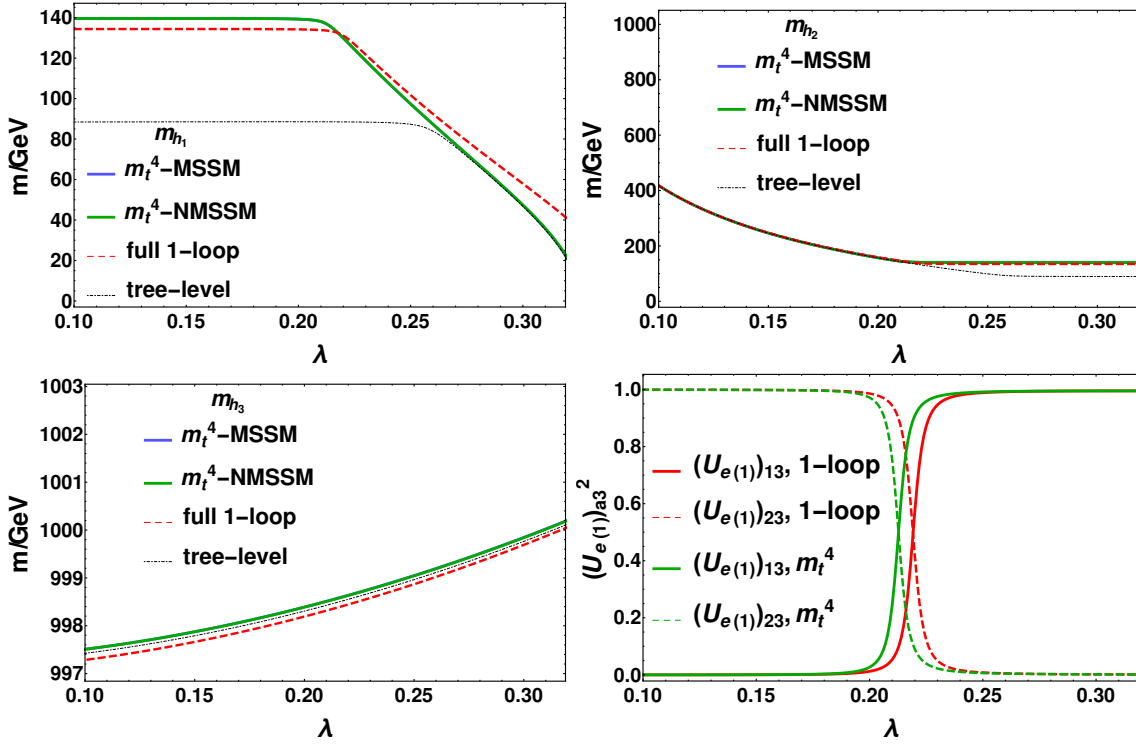
Figure 8.4: *Upper row and lower left*: Masses of the $\mathcal{CP}$-even Higgs-fields in the approximations m_t^4-MSSM and m_t^4-NMSSM approximations, at tree-level and at full one-loop order. *Lower right*: Squared mixing-matrix elements that determine the singlet-admixture to the two lighter fields h_1 and h_2 for partial one-loop contributions. The solid and dashed lines denote the singlet-admixture for h_1 and h_2, respectively. Lines with the same colour are calculated for the same set of partial contributions: full one-loop (red), m_t^4-MSSM and m_t^4-NMSSM (green). The approximations yield almost identical results for the singlet-admixture, thus only one of both is shown in this plot.

following.

In the third row of fig. 8.5 the difference between the m_t^4-NMSSM approximation and the full one-loop contribution ($\Delta m = |m_{h_i}^{(m_t^4\text{-NMSSM})} - m_{h_i}^{(1\text{L})}|$) is plotted as a function of λ. For the light doublet-like field, h_1 for $\lambda < \lambda_\mathrm{c}$ and h_2 for $\lambda > \lambda_\mathrm{c}$, the m_t^4-NMSSM approximation, which takes only leading top/stop-sector contributions into account, approximates the full one-loop result with an error of less than 5%. For the heaviest field the deviation remains far below 1 GeV and is negligible. For the singlet-like field, h_2 for $\lambda < \lambda_\mathrm{c}$ and h_1 for $\lambda > \lambda_\mathrm{c}$, the m_t^4-NMSSM contributions (and subsequently the MSSM version) approximates the full one-loop result very poorly. The error rises up to 50% of the full one-loop mass prediction of ≈ 40 GeV. This large deviation arises from contributions beyond the leading top/stop-sector contributions. These contributions can stem from either the remaining fermion/sfermion sectors or the Higgs- and gauge-sectors including their superpartners. Both sectors and their contributions are studied separately.
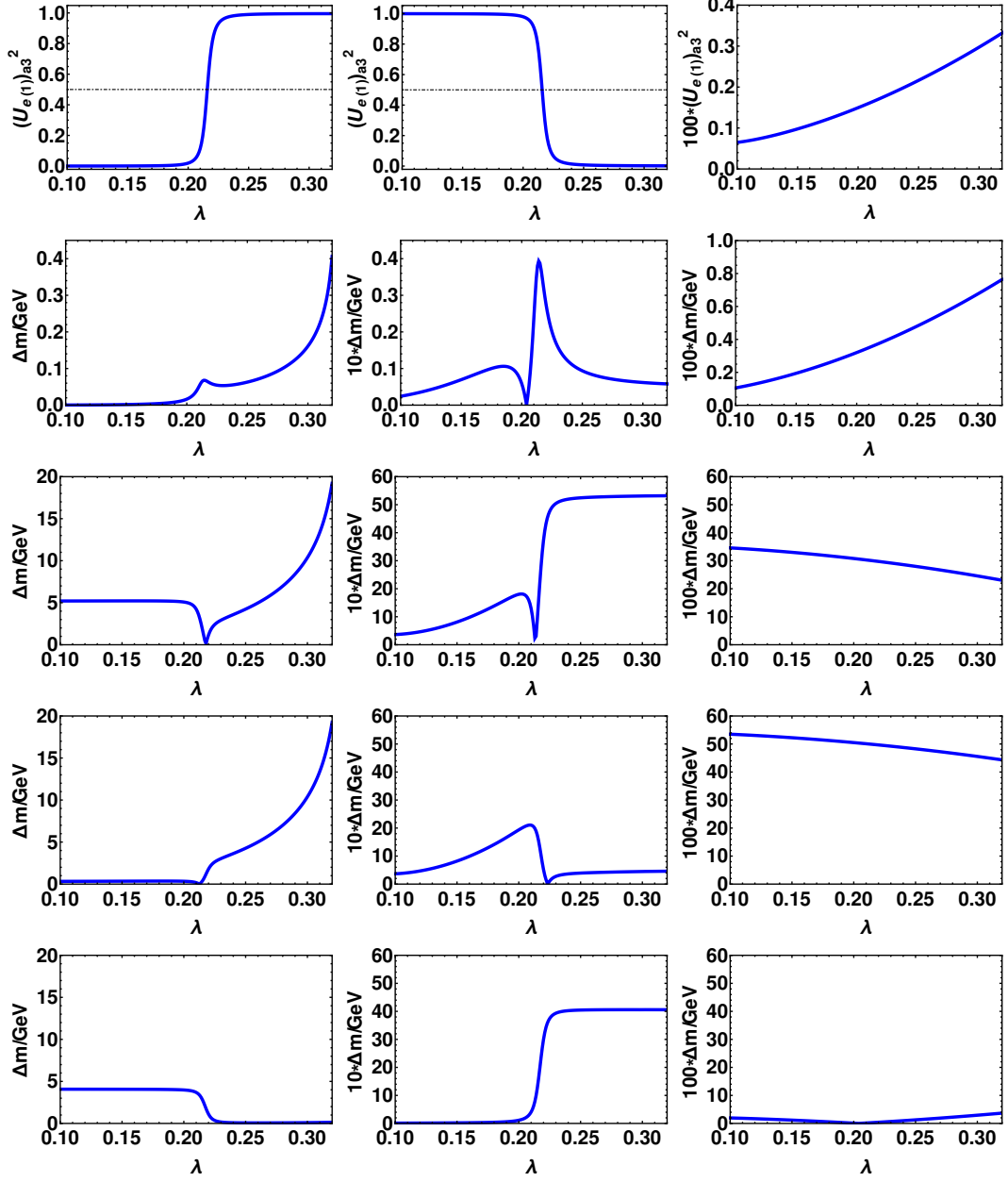
Figure 8.5: Partial one-loop contributions to the mass predictions and singlet admixture in the $\mathcal{CP}$-even sector. Each column shows the result for one of the fields h_1, h_2 and h_3 (from left to right). In the first row the result for h_3 is scaled by a factor 100. In the second to last row the mass axis is scaled by 10 and 100 for h_2 and h_3, respectively. *First row*: Squared mixing-matrix elements that determine the singlet admixture for the result in the m_t^4-approximation. The mixing is very similar for all depicted approximations. At $\lambda_c^{(1)}$, the vale for the cross-over behaviour between the two lighter fields, the squared mixing matrix-element is equal to 0.5 (dash-dotted black line). *Second to last row*: Absolute differences between partial one-loop mass predictions and the full one-loop result. For a detailed description and discussion see sec. 8.1.2.

In the fourth row of fig. 8.5 the difference between the prediction including the contributions from all fermions and sfermions including momentum-dependence and the full one-loop result ($\Delta m = |m_{h_i}^{(f/\tilde{f})} - m_{h_i}^{(1L)}|$) is plotted as a function of λ. While this subset provides a very accurate approximation for the light singlet-like field, it still provides only a bad approximation for the mass of a light singlet-like field. The heaviest field is approximated as well as in the m_t^4-NMSSM approximation. The comparison of the left plots in the third and fourth rows shows that the fermion/sfermion-sector contributions beyond the MSSM approximation, which are important for the MSSM-like doublet-fields have a negligible effect on the mass-prediction of singlet-like fields.

In the fifth (last) row of fig. 8.5 the difference between the m_t^4-NMSSM approximation supplemented with the momentum-dependent corrections from the Higgs- and gauge-sectors (HG) and the full one-loop result ($\Delta m = |m_{h_i}^{(m_t^4\text{-NMSSM+HG})} - m_{h_i}^{(1L)}|$) is plotted as a function of λ. The additional corrections in this approximation are found to cure the unsatisfactory behaviour of the previous approximations for the mass of a light singlet-like state at large values of λ, while the impact of the missing contributions from the fermion/sfermion sector beyond the m_t^4-NMSSM approximation is clearly visible for the doublet-like fields in the left plot. Even for the heaviest state, the mixed-in genuine NMSSM-contributions are well approximated. For the light MSSM-like fields the Higgs- and gauge-sector contributions improve the one-loop approximation by ≈ 1 GeV. The impact of the added contributions is less significant for the doublet-fields than for the singlet-like field and is comparable to its expected size in the MSSM [32].

As a result of the study outlined in this section the MSSM-like top/stop-sector contributions of $\mathcal{O}(Y_t)$ have been verified as the leading one-loop contributions to MSSM-like fields at the one-loop level. The genuine NMSSM top/stop-sector contributions of $\mathcal{O}(\lambda Y_t, \lambda^2)$ have the largest impact on singlet-like fields for large values of λ. For such large values of λ, however, the improvement of including those genuine NMSSM contributions is by far overshadowed by the fact that Higgs- and gauge-sector contributions become more and more important for a singlet-like Higgs field, so that the complete fermion/sfermion contributions no longer provide a good approximation for the full result in this region.

8.1.3 Comparison with `NMSSMCalc`

In order to test our results against available tools, we decided to compare with `NMSSMCalc` [29], since it is the only public tool performing the Higgs-mass calculation in a mixed $\overline{\text{DR}}$/on-shell renormalisation scheme. In this section the numerical differences between the results for the masses of the two lighter Higgs states of `NMSSMCalc` and our calculation will be discussed at different orders for the scenario given in tab 8.1. Both codes, `NMSSMCalc` and our calculation, labelled `NMSSM-FeynHiggs` in the following, are adapted. Both codes interpret the stop-sector parameters as defined for on-shell renormalised masses of the stops[2]. Since `NMSSMCalc` uses a different charge

---

[2]We thank Kathrin Walz for providing a modified version of `NMSSMCalc` for this feature.

renormalisation and the value $\alpha(M_Z)$ for the electromagnetic coupling constant, we reparametrised our result as described in sec. 4.4.2. The numerical values for $\alpha(M_Z)$ and $\Delta\alpha$ are taken directly from `NMSSMCalc`,

$$\Delta\alpha = \Delta\alpha^{(5)}_{\text{had}} + \Delta\alpha_{\text{lep}} = 5.89188 \cdot 10^{-2}, \quad \alpha(M_Z) = 1/128.962 \, . \tag{8.2}$$

After the reparametrisation is applied the only difference between the one-loop Higgs-mass predictions of `NMSSM-FeynHiggs` and `NMSSMCalc` stem from the finite contribution of δv. Furthermore only MSSM two-loop contributions of $\mathcal{O}(\alpha_t\alpha_s)$ calculated for on-shell renormalised top- and stop-masses are considered for this comparison as only their NMSSM-counterparts are implemented in `NMSSMCalc`. The resummation of logarithms is not included for the study in this section. For simplicity, we will refer to this reduced set of two-loop contributions as two-loop order throughout this section. The remaining differences between the Higgs-mass calculations of `NMSSMCalc` and `NMSSM-FeynHiggs` are summarised in tab. 8.2. The applied modifications ensure that the comparison between both codes will quantify the numerical impact of the genuine NMSSM two-loop corrections of $\mathcal{O}(Y_t\lambda\alpha_s, \lambda^2\alpha_s)$.

	NMSSMCalc		NMSSM-FeynHiggs
one-loop	$\alpha_{\text{em}}(M_Z)$ renormalised, $(\delta Z_{\text{e}} - \frac{1}{2}\Delta\alpha)$	$\leftrightarrow$	$\alpha_{\text{em}}(M_Z)$ reparametrised $(\delta Z_{\text{e}}^{\text{dep}}, \Delta_{\alpha(M_Z)})$
two-loop	NMSSM $\mathcal{O}(\alpha_t\alpha_s)$	$\leftrightarrow$	MSSM $\mathcal{O}(\alpha_t\alpha_s)$

Table 8.2: Main calculational differences between `NMSSMCalc` and our modified calculation (labelled `NMSSM-FeynHiggs`) used for the comparison in sec. 8.1.3. The difference at one-loop stems only from the dependent renormalisation of the electric charge, described in sec. 4.4.2. At two-loop order the codes differ only by the genuine NMSSM contributions of $\mathcal{O}(\lambda Y_t, \lambda^2)$, described in sec. 6.4. The two-loop MSSM corrections beyond $\mathcal{O}(\alpha_t\alpha_s)$ and the resummation are turned off in `NMSSM-FeynHiggs` for the comparison in sec. 8.1.3.

We used the SM parameters as specified in the built-in standard input files of `NMSSMCalc` for our calculation as given in the appendix in sec. B.2. We passed over the input values in the quark- and squark-sectors as on-shell parameters to `NMSSMCalc`. The pole mass for the top, $m_t^{(\text{OS})} = 173.2$ GeV, is used in this section, and the renormalisation scale is chosen as $m_t^{(\text{OS})}$. For the comparison both codes use the identical, value $\alpha_s^{\overline{\text{MS}}}(m_t^{(\text{OS})}) = 0.1069729$, which is evaluated by `NMSSMCalc` with the routines of [129].

As an initial test the one- and two-loop results of `NMSSMCalc` and NMSSM-FeynHiggs are compared in the MSSM-limit, where λ and κ vanish simultaneously. Both the effects of the different renormalisation schemes and the reparametrisation have to vanish in this limit and thus the results have to be identical. The one- and two-loop results for the mass of the lightest $\mathcal{CP}$-even field obtained with both codes, 140.742 GeV and 116.902 GeV, respectively, are in agreement with each other with

a precision of < 1 MeV. This confirms that the MSSM-contributions are treated identically in both calculations. Thus all observed differences between the results for non-vanishing values of λ and κ have to stem from the treatment of the genuine NMSSM-contributions and residual higher-order effects of the different renormalisation of v after the reparametrisation.
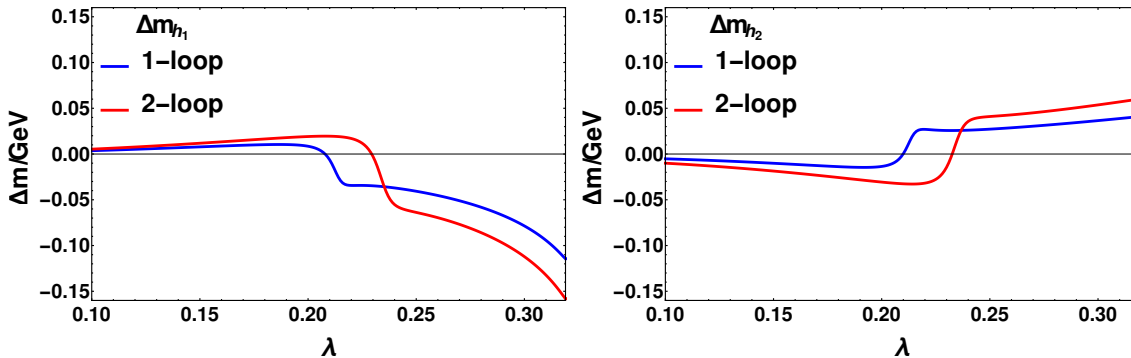

Figure 8.6: Difference between the mass predictions for the two lighter $\mathcal{CP}$-even fields h_1 and h_2 of `NMSSMCalc` and `NMSSM-FeynHiggs` at one- and two-loop order, $\Delta m_{h_i} = m_{h_i}^{\text{NMSSM-FH}} - m_{h_i}^{\text{NMSSMcalc}}$. The result of `NMSSM-FeynHiggs` has been reparametrised to $\alpha(M_Z)$. The point for the cross-over behaviour between the fields h_1 and h_2 at one- and two-loop order read $\lambda_c^{(1)} \approx 0.21$ and $\lambda_c^{(2)} \approx 0.24$, respectively. the value of Δm_{h_i} is negative for the singlet-like field and positive for the doublet-like field.

For the sample scenario defined in tab. 8.1 the absolute difference between the two mass predictions are plotted in fig. 8.6 as functions of λ for the two lighter $\mathcal{CP}$-even states at one- and two-loop order[3], $\Delta m_{h_i} = m_{h_i}^{\text{NMSSM-FH}} - m_{h_i}^{\text{NMSSMcalc}}$. The left plot in fig. 8.61 shows the mass for the lighter state h_1. It behaves doublet-like for values $\lambda \lesssim \lambda_c^{(n)}$ and singlet-like state for values $\lambda \gtrsim \lambda_c^{(n)}$. The behaviour of h_2 is the opposite. The relative influence of the genuine NMSSM-corrections compared to the MSSM-like corrections is expected to be large at $\lambda_c^{(n)}$, where neither the genuine NMSSM-corrections nor MSSM-like corrections are enhanced or suppressed due to mixing effects.

The difference between the two calculations is largest for regions with larger values of λ for the mass of the singlet-like state. The mass of the doublet-like state is effected to a lesser extent by the MSSM-approximation. For both fields Δm_{h_i} increase with λ, although the increase is more significant for the mass of the singlet-like field. At neither order a pronounced local extremum can be observed around $\lambda_i^{(n)}$ at each order. The impact on Δm_{h_i} around $\lambda_i^{(n)}$ is less significant than the impact of larger values of λ. The general shape of the one-loop difference, caused by the different renormalisation schemes, is still present for Δm_{h_i} at two-loop order. However, the point with cross-over behaviour between h_1 and h_2 is shifted by $\Delta\lambda_c = \lambda_c^{(2)} - \lambda_c^{(1)} \approx$

---

[3]The variation of the mass of the heaviest state is smaller than 2 MeV and thus not plotted in fig. 8.6.

0.03 between one- and two-loop order, which makes a point-wise comparison of each Δm_{h_i} between both orders difficult. However, it is possible to compare the local and global extrema, in particular at $\lambda_c^{(n)}$ and for the largest values of λ, to read off the numerical impact of the genuine two-loop NMSSM corrections implemented only in `NMSSMCalc`. For h_1 this yields $\Delta m_{h_1}(\lambda_c) \lesssim 50$ MeV, for h_2 we obtain $\Delta m_{h_2}(\lambda_c) \lesssim 30$ MeV. Both values are obtained for the $\lambda = 0.32$. The corresponding two-loop Higgs masses for this maximal differences are $m_{h_1} \approx 40$ GeV and $m_{h_2} \approx 125$ GeV, for the singlet- and doublet-like field, respectively.

These results confirm that the two-loop MSSM-approximation induced an uncertainty that is numerically small if $\lambda < Y_t$ as discussed in sec. 6.4.1. This is especially true for the masses of MSSM-like fields. The relative error induced by the two-loop MSSM-approximation remains in the region far below 1% even for the light singlet mass and larger values of λ. The different renormalisation schemes for δv and δZ_e, respectively, have a larger, but still small impact on the results in the given scenario.

8.1.4 Corrections beyond $\mathcal{O}(\alpha_t \alpha_s)$

While the genuine NMSSM two-loop corrections of $\mathcal{O}(\lambda Y_t \alpha_s, \lambda^2 \alpha_s)$ induce a very small effect below 50 MeV, the MSSM-corrections beyond $\mathcal{O}(\alpha_t \alpha_s)$ and the resummation of large logarithms can result in a shift for the mass of the light doublet-like field of several GeV. In order to quantify the impact of the additional MSSM-contributions of $\mathcal{O}(\alpha_t^2, \alpha_b \alpha_s, \alpha_t \alpha_b)$ and the resummation of logarithms the results with and without these corrections are plotted as functions of λ in fig. 8.7 using the $\overline{\text{MS}}$-value of the top-quark $m_t^{\overline{\text{MS}}}(m_t)$. A sizeable shift of about $3-4$ GeV can be observed for the mass of the doublet-like field. The mass prediction for the singlet-like field remains unaffected by the two-loop MSSM-corrections, since all singlet self-energies are neglected at two-loop order. The impact of the additional corrections beyond $\mathcal{O}(\alpha_t \alpha_s)$ exceed the
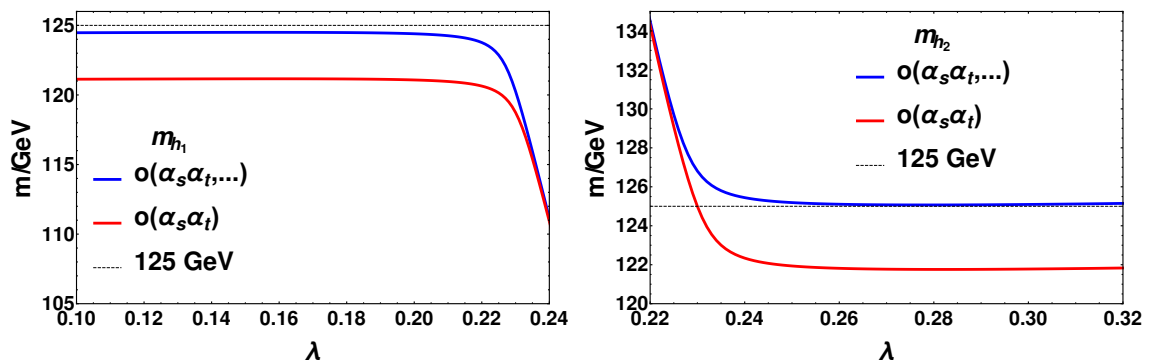
Figure 8.7: Mass predictions for the two lighter $\mathcal{CP}$-even fields h_1 and h_2 for different contributions at two-loop order. The blue lines include all MSSM-corrections of $\mathcal{O}(\alpha_t \alpha_s, \alpha_b \alpha_s, \alpha_t^2, \alpha_t \alpha_b)$, the red curves contain only MSSM-corrections of $\mathcal{O}(\alpha_t \alpha_s)$. Both include the resummation of large logarithms and the full NMSSM one-loop contributions. The thin, constant line marks 125 GeV.

numerical impact of the genuine NMSSM-corrections of $\mathcal{O}(\lambda Y_t \alpha_s, \lambda^2 \alpha_s)$ by several

orders of magnitude.

8.2 Stop-Mixing Dependence for a Singlet-like Higgs-field

The previous section was focused on the variation of λ, which couples or decouples the singlet Higgs-field and its superpartner from the remaining field spectrum of the NMSSM. In this section the influence of the trilinear breaking-parameter of the stop-sector, A_t, will be investigated for different values of λ in the sample scenario defined in tab. 8.1. In the MSSM the Higgs masses have a strong dependency on the value of A_t at one- and two-loop level, see for example [130] and references therein. While in the literature typically X_t is varied, that determines the mixing between the two stops, the studies presented in this section will focus on A_t due to its importance for the suppression-factors defined in sec. 6.1.3. For the sample scenario the relation between the X_t and A_t reads $X_t \approx A_t - 16$ GeV $\approx A_t$.

8.2.1 Mass-Prediction and Singlet-Admixture

The mass of the lightest $\mathcal{CP}$-even Higgs-field h_1 is plotted as a function of A_t for different values of λ together with their singlet-admixture in fig. 8.8. The singlet-admixture shows a strong dependence on A_t, especially for "maximal" stop-mixing around $A_t \approx \sqrt{6}M_{\tilde{q}} \approx 3700$ GeV at the one-loop level and around $A_t \approx 2M_{\tilde{q}} = 13000$ GeV at the two-loop level for on-shell parameters. In the investigated scenario the field h_1 remains doublet-like for $\lambda = 0.2$, while the singlet-admixture increases sharply at "maximal" stop-mixing for larger values of λ, until the field h_1 becomes dominantly singlet-like at $\lambda = 0.24$ for values of A_t between ± 4.5 TeV and ± 4 TeV at one- and two-loop order, respectively.

For the doublet-like field at $\lambda = 0.2$ the A_t-dependence resembles the situation in the MSSM: Significant maxima and minima for the mass m_{h_1} can be observed for for "maximal" and absent stop-mixing, respectively. The magnitude of the maxima are not identical for positive and negative values of A_t, the difference between the two maxima is more pronounced in the two-loop result. For an increased singlet-admixture to the field h_1 at higher values of λ these maxima are flattened out. Thus the minima for $A_t \approx 0$ become less pronounced for increased singlet-admixtures.

8.2.2 Singlet-Admixture for "maximal" Stop-Mixing

In order to study the behaviour of the maxima around "maximal" stop-mixing in dependence of λ the plots in 8.9 show the mass predictions of both lighter $\mathcal{CP}$-even fields h_1 and h_2 for different values of λ. The values of λ are chosen such that both fields h_1 and h_2 receive similar singlet-admixtures for "maximal" stop-mixing. For the lowest depicted values of λ the field h_2 is dominantly singlet- and for the largest values of λ doublet-like at "maximal" stop-mixing and vice versa for the field h_1. With increasing doublet-admixture for "maximal" stop-mixing the mass m_{h_2} 'inherits' the
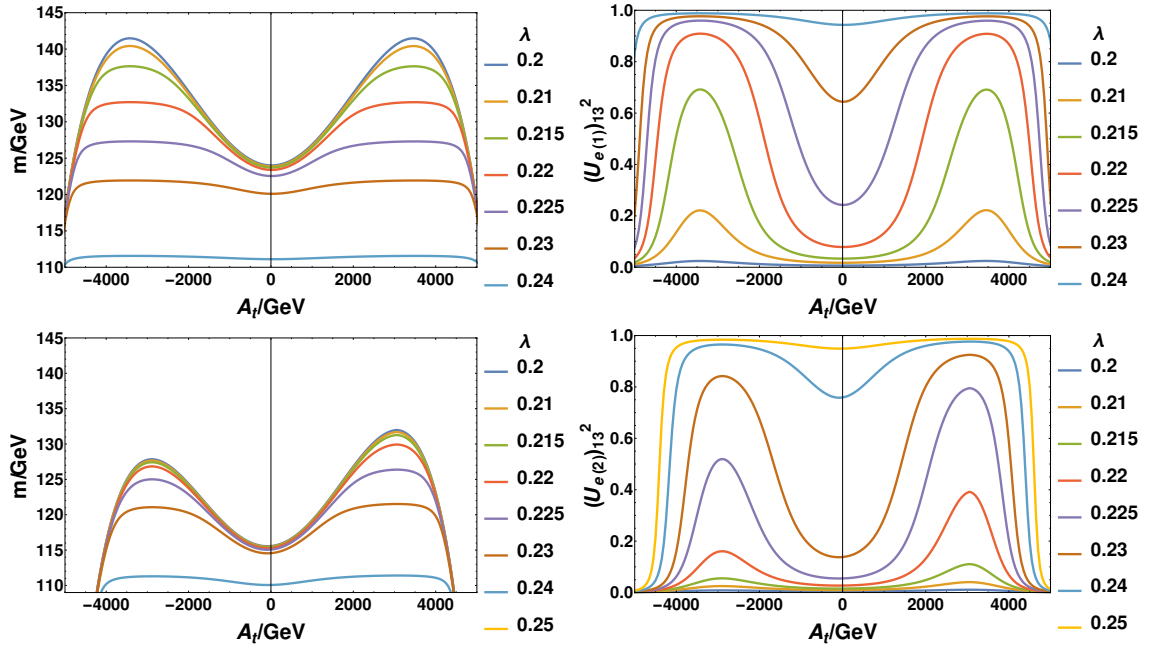
Figure 8.8: The left plots show the A_t-dependence of the mass m_{h_1} of the lightest $\mathcal{CP}$-even Higgs-field h_1 at one- and two-loop order in the upper and lower row, respectively, for different values of λ in the sample scenario defined in tab. 8.1. The right plots show the according A_t-dependences of the squared mixing-matrix elements that determine the singlet-admixture to h_1. The values for λ are chosen such that they are close to the one- and two-loop values of $\lambda_c^{(n)}$ of the sample scenario, where h_1 receives singlet- and doublet-contributions equally.

behaviour of the mass m_{h_1} of the former doublet-like field. At the same time the flattening observed for the maxima of the mass m_{h_1} resembles the behaviour of the mass m_{h_2} of the former singlet-like field.

8.2.3 Genuine NMSSM-Corrections to a dominantly Singlet-like Field

A more detailed study of the A_t-dependence for the mass m_{h_1} of the either dominantly singlet- and doublet-like field h_1 is shown in fig. 8.10. The mass is plotted in the MSSM and NMSSM version of the m_t^4-approximation at the one-loop order, which accounts for the dominant dependence on the stop-squark masses. For an increasing singlet-admixture the mass m_{h_1} exhibits a weaker dependence on A_t both in the m_t^4-MSSM and m_t^4-NMSSM approximations. The A_t-dependence is very similar for both approximations. This is quite remarkable since the m_t^4-MSSM approximation contains no higher-order corrections for the singlet-field ϕ_s. The additional genuine NMSSM-corrections included in the m_t^4-NMSSM approximation result in a mass-shift that depends only weakly on A_t. These contributions are shown in fig. 8.11 as the absolute difference between the two m_t^4-approximations. For all values of λ the A_t-dependence remains in the region of $10 \ldots 20$ MeV, several orders of magnitude below
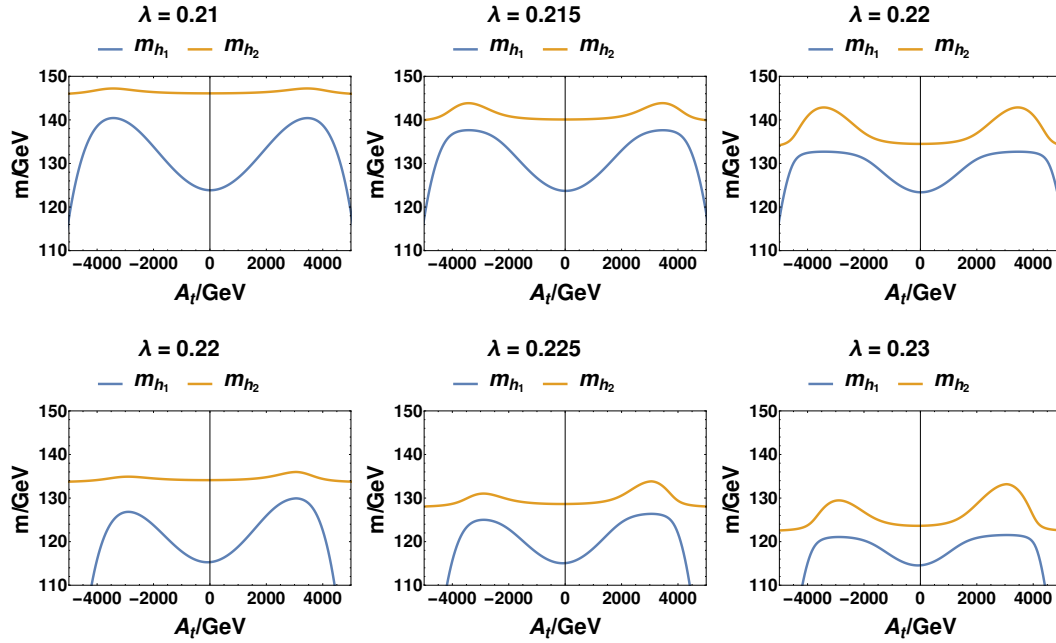
Figure 8.9: *Upper row*: One-loop mass-prediction for the lightest and next-to-lightest $\mathcal{CP}$-even Higgs-fields h_1 and h_2 for $\lambda = 0.21$, 0.215, 0.22, chosen close to $\lambda_c^{(n)}$, where the fields h_1 and h_2 receive a similar singlet-admixture close to "maximal" stop-mixing. *Lower row*: Two-loop version of the upper row for $\lambda = 0.21$, 0.215, 0.22.

the A_t-dependence of a doublet-like field. Since the singlet–sfermion–sfermion vertex is independent of A_t, the observed A_t-dependence thus stems from the stop-squark masses that enter the calculation logarithmically. The genuine NMSSM-corrections included in the m_t^4-NMSSM approximation have the strongest impact on the mass prediction for values of A_t where the singlet-admixture is shared between the two fields h_1 and h_2, e.g. around "maximal" stop-mixing for $\lambda = 0.2$ in this example. The apparent increase for larger values of A_t is an effect caused by the increasing doublet-admixture to h_1, that takes effect for slightly different values of A_t for both m_t^4-approximations.

As explained above the genuine NMSSM-corrections to the mass m_{h_1} have only a very weak dependence on A_t. However, extrema can be observed for the dominantly singlet-like states in fig. 8.10. Thus the A_t-dependence of the mass m_{h_1} for the dominantly singlet-like field h_1 is an effect driven by the residual doublet-admixture to h_1. Even for a singlet-like state with a doublet-admixture of $\lesssim 1\%$ the A_t-dependence of the genuine NMSSM-corrections from the top/stop-sectors can remain subleading to the residual A_t-dependence of the MSSM-like corrections.
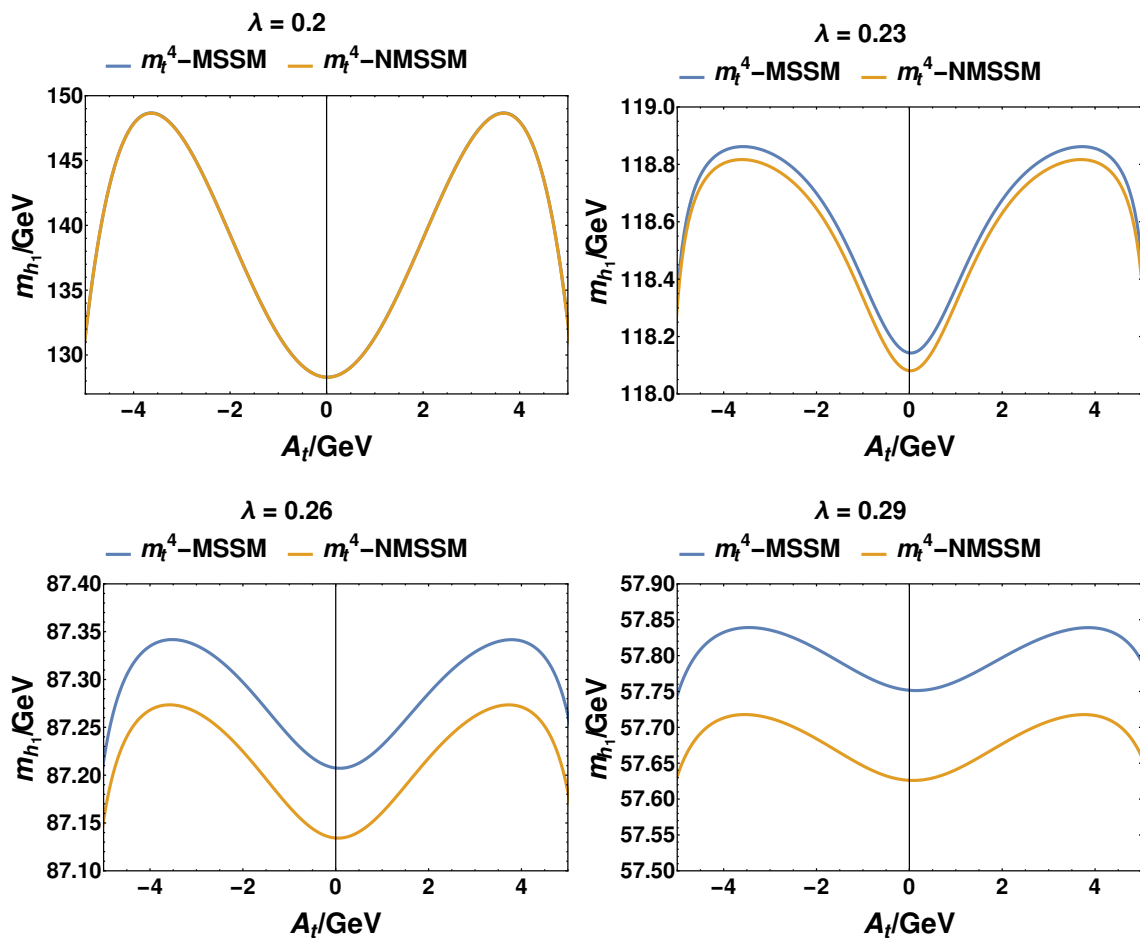
Figure 8.10: A_t-dependence of mass m_{h_1} of the field h_1 for selected values of λ at the one-loop level in the approximations m_t^4-MSSM and m_t^4-NMSSM. For $\lambda = 0.2$ the field is dominantly doublet-like. The singlet-admixture increases with λ as shown in the lower right plot in fig. 8.8 until h_1 is dominantly singlet-like for $\lambda = 0.29$.

8.3 Conclusion

In this section the two-loop MSSM-approximation employed in `NMSSM-FeynHiggs` and the partial one-loop corrections to the masses of the $\mathcal{CP}$-even fields in the NMSSM with real parameters were studied.

The MSSM-like one-loop contributions from the top/stop-sector have been identified as the leading fermion/sfermion-contributions at one-loop order in the NMSSM. However, for the mass of a (light) singlet-like field and larger values of λ these contributions can be subleading compared to the Higgs- and gauge-sector contributions.

For the MSSM-approximated two-loop corrections of $\mathcal{O}(\alpha_t \alpha_s)$ the result was compared against the full NMSSM-corrections of this order, yielding only very small deviations in the predictions for the masses of both doublet- and singlet-like fields. The MSSM-approximated contributions of $\mathcal{O}(\alpha_t^2)$ included in the prediction of NMSSM-
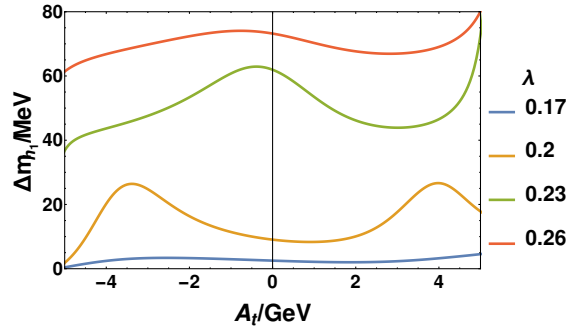
Figure 8.11: Absolute difference between the mass in both m_t^4-approximations, $\Delta m_{h_1} = |m_{h_1}^{(m_t^4-\mathrm{MSSM})} - m_{h_1}^{(m_t^4-\mathrm{NMSSM})}|$ for different values of λ. For $\lambda = 0.17$ the field is dominantly singlet-like. The singlet-admixture increases with λ as shown in the lower right plot in fig. 8.8 until h_1 is dominantly singlet-like for $\lambda = 0.29$

`FeynHiggs` so far have no counterpart in the NMSSM at this order in a mixed on-shell/$\overline{\mathrm{DR}}$ renormalisation scheme. However, the same reasoning that successfully motivated the MSSM-approximation of $\mathcal{O}(\alpha_t\alpha_s)$ can be applied for the MSSM-approximated corrections of $\mathcal{O}(\alpha_t^2)$. One can expect that they are dominant relative to their genuine NMSSM-counterparts as well.

For the two-loop corrections beyond the fermion/sfermion-contributions potentially large one-loop corrections from the Higgs- and gauge-sector suggest an increased effect of Higgs- and gauge-sector contributions also at the two-loop level. An increased importance of these contributions has already been observed for pure $\overline{\mathrm{DR}}$-calculations for similar scenarios [131], while a full calculation of these contributions in a mixed on-shell/$\overline{\mathrm{DR}}$renormalisation scheme is still missing.

9 Theoretical Uncertainties for NMSSM Higgs-mass predictions

The experimental value of the mass of the detected Higgs signal [12],

$$m_H = 125.09 \pm 0.21(\text{stat.}) \pm 0.11(\text{syst.}) \text{ GeV}, \tag{9.1}$$

has an error of only several permil. It is thus already three years after its discovery an (electroweak) precision observable. In order to make full use of this high-precision measurement every model that provides a prediction for this quantity should ideally provide a result with a similar precision. If a prediction with similar precision is unavailable it is important to provide a solid estimate for the theoretical uncertainties of the available prediction. This is the situation for both the MSSM and the NMSSM, the experimental error of the mass of the SM-like Higgs-boson is significantly smaller than the theoretical uncertainties of the current predictions. Two different sources for theoretical uncertainties exist in these predictions. One are the experimental errors of the input parameters, the other are unknown higher-order corrections.

For the MSSM detailed estimates for theoretical uncertainties of the Higgs-mass predictions are available, see e.g. [32, 38]. At least one tool, `FeynHiggs`, provides routines for an automated estimate of the theoretical uncertainties of its Higgs-mass prediction.

For the NMSSM several public spectrum generators are available that offer an automated calculation of Higgs-masses: `FlexibleSUSY` [23], `NMSSMCALC` [29], `NMSSMTools` [24, 132, 133], `SOFTSUSY` [26–28] and `SPheno` [20, 21]. The results obtained by the different codes for the same set of input parameters can differ by several GeV.

A first step towards investigating the theoretical uncertainties for NMSSM Higgs-mass predictions using $\overline{\text{DR}}$-methods has been performed in [39]. In this publication the tools mentioned before were used to calculate NMSSM Higgs-masses for six sample scenarios with different physical properties. The sources for the differences between the codes have been identified. After they have been modified to address the differences, an agreement at the level of $\mathcal{O}(10 \text{ MeV})$ for the same set of higher-order corrections has been achieved. However, this comparison did not account derivatives resulted by use of different renormalisation schemes. Among the tested tools only `NMSSMCalc` offered the option to use a mixed $\overline{\text{DR}}$/on-shell scheme , but a comparison between different $\overline{\text{DR}}$/on-shell schemes was not considered in [39]. In order to improve on this situation a comparison between `NMSSMCalc` and the NMSSM-extended version of `FeynHiggs` developed in this work, called `NMSSM-FeynHiggs` in the following, is currently performed. It follows closely the comparison performed in [39] with necessary adaptions and extensions for the on-shell calculation as described below.

	Q	$\tan\beta(M_Z)$	λ	κ	A_λ	A_κ	μ_{eff}	M_1	M_2	M_3	A_t	A_b	$M_{\tilde{t}_1}$	$M_{\tilde{t}}$
TP1	1500	10	0.1	0.1	-10	-10	900	500	1000	3000	3000	0	1500	1500
TP2	1500	10	0.05	0.1	-200	-200	1500	1000	2000	2500	-2900	0	2500	500
TP3	1000	3	0.67	0.1	650	-10	200	200	400	2000	1000	1000	1000	1000
TP4	750	2	0.67	0.2	405	0	200	120	200	1500	1000	1000	750	750
TP5	1500	3	0.67	0.2	570	-25	200	135	200	1400	0	0	1500	1500
TP6	1500	3	1.6	1.61	375	-1605	614	200	400	2000	0	0	1500	1500

Table 9.1: Definition of the TP scenarios. All parameters are given $\overline{\text{DR}}$ parameters at the scale Q besides $\tan\beta$, which is defined at M_Z. All dimensionful parameters are given in GeV. The remaining soft SUSY breaking-parameters, common to all points, are $M_{\tilde{f}_{\text{L}}} = M_{\tilde{f}} = 1500$ GeV, $A_f = 0$.

In a subsequent step a comparison between the $\overline{\text{DR}}$/on-shell and the $\overline{\text{DR}}$ calculations of the codes mentioned above is necessary. After these steps an estimate of theory uncertainties can be obtained.

This section focuses on the comparison of the predictions for Higgs-masses implemented in `NMSSMCalc` and `NMSSM-FeynHiggs`. It aims at an identification of all sources for differences in their mass-predictions and eliminating all differences beside those that are caused by the different renormalisation scheme. Since this task requires thorough knowledge about both codes it is performed in close collaborations between the authors of `NMSSMCalc` and `NMSSM-FeynHiggs` and is currently work in progress. The results for modified versions of `NMSSMCalc` have been obtained by its authors.

First a brief description of the studied scenarios will be given followed by a short classification of the possible sources of uncertainties Subsequently a short description of the differences between the codes `NMSSMCalc` and `NMSSM-FeynHiggs` will be provided together with the means to identify those that are unrelated to the renormalisation-scheme dependence. Finally the present status of the ongoing comparison will be presented.

9.1 Description of Scenarios

The test-point (TP) scenarios discussed in [39] for the comparison of the calculations with $\overline{\text{DR}}$-methods will also be used for the comparison between `NMSSMCalc` and `NMSSM-FeynHiggs`. They are defined in tab. 9.1. The TP-scenarios correspond to the following different physical situations:

- MSSM-like point (TP1)

- MSSM-like point with large stop splitting (TP2)

- Point with light singlet and λ close to the perturbativity limit (TP3)

- Point with heavy singlet and λ close to the perturbativity limit (TP4)

- Point with slightly lighter singlet. Additional matter needed for perturbativity; inspired by [134] (TP5)

- Point with huge λ (TP6)

All points feature an (MS)SM-like Higgs-field with a mass around 125 GeV at the two-loop level for $\overline{\text{DR}}$ calculations. For the comparison of the $\overline{\text{DR}}$/on-shell codes the scenarios will be evaluated once at the high scale Q and once at the on-shell value of the top-quark mass $m_t^{\text{OS}} = 172.9$ GeV, called the low scale in the following. No evaluation for TP2 at the low scale was possible, since the RGE-evolved parameters at the low scale yield tachyonic stops. Since `NMSSM-FeynHiggs` is designed with the intent of calculating Higgs-masses at the top-quark mass m_t, only the comparison at the low scale will be considered for the final estimate of the intrinsic uncertainties. At this scale hybrid $\overline{\text{DR}}$/on-shell calculations are expected to provide a more accurate mass prediction compared to pure $\overline{\text{DR}}$-calculations. The calculation at the high scales will be included for completeness to enable a later comparison with the results of [39].

9.2 Classifying Uncertainties

Uncertainties of the Higgs-mas prediction can be divided into two types: Parametric and intrinsic uncertainties. Parametric uncertainties are all uncertainties related to the input-parameters of the calculation . Intrinsic uncertainties denote all uncertainties that are related to unknown higher-order corrections. Calculations differ by higher-order effects in particular because of differences in the renormalisation scheme and scale of the calculation and further differences like the RGE-evolution of $\overline{\text{DR}}/\overline{\text{MS}}$-renormalised input parameters together with their on-shell conversion.

For this comparison we will divide the theory uncertainties slightly differently into all uncertainties that are caused by input parameters and uncertainties that are caused by differences of the Higgs-mass calculations themselves. The input uncertainties include the parametric uncertainties for the SM-quantities together with higher-order effects due to the RGE-evolution and conversion of input parameters. The remaining uncertainties are caused only by the renormalisation scheme and scale dependence of the calculation.

9.2.1 Parametric Uncertainties

Amongst the parametric uncertainties the experimental error of the top-quark mass m_t has the by far the largest influence on the MSSM Higgs-mass predictions, since the leading MSSM one-loop corrections are of $\mathcal{O}(m_t^4/M_W^2)$. In the NMSSM this also holds for an (MS)SM-like Higgs-field. The experimental errors of remaining heavier fermions, the bottom-quark m_b and the τ-lepton m_τ, can have a minor influence on the Higgs-mass prediction in the TP-scenarios. Since the two-loop (S)QCD contributions to the Higgs-mass are proportional to α_s, its experimental error also can have a visible effect on result depending on the total size of the two-loop corrections. A detailed study of the parametric uncertainties in the MSSM can be found in [38]. For the investigation of the intrinsic uncertainties of `NMSSMCalc` and `NMSSM-FeynHiggs` both codes get the identical input values for measured quantities. They are listed in the appendix under sec. B.3.

9.2.2 SUSY Input Parameters

The TP-scenarios are defined by a complete set of independent parameters, where all $\overline{\text{DR}}$-quantities are given at the scale Q besides $\tan\beta$, which is given at M_Z. In principle these parameters can be defined in any renormalisation scheme at any scale. The SUSY Les Houches Accord (SLHA) has been defined in [116,135] as a well-defined interface between different codes. In this input format all SUSY parameters have to be given as $\overline{\text{DR}}$-parameters together with the scale at which they are defined. Any code reading the SLHA input-file has to transform the $\overline{\text{DR}}$-parameters $M_l^{\overline{\text{DR}}}(M_{\text{in}}^j)$ defined at their individual input scale M_{in}^j into the form necessary for the calculations carried out by the code. This can include both the RGE-evolution of $M_l^{\overline{\text{DR}}}$ to the scale M_{calc} of the calculation as well as the conversion into another renormalisation scheme, typically the on-shell scheme,

$$M_l^{\overline{\text{DR}}}(M_{\text{in}}^j) \quad \xrightarrow{\text{RGE}-\text{evolution}} \quad M_l^{\overline{\text{DR}}}(M_{\text{calc}}) \quad \xrightarrow{\text{conversion}} \quad M_l^{\text{OS}}. \tag{9.2}$$

The order at which either the RGE-evolution or the conversion is performed can give rise to higher-order effects in the comparison of different codes.

9.2.3 Theoretical uncertainties from unknown higher-order Corrections

Unknown higher-order corrections contribute to the intrinsic uncertainties of the Higgs-mass prediction. Parts of them can be studied by comparing the mass predictions that employ different renormalisation schemes that account for different higher-order contributions. The predictions of `NMSSMCalc` and `NMSSM-FeynHiggs` use a different renormalisation and reparametrisation of the electromagnetic coupling-constant α. Since the reparametrisation for α only accounts for on-loop order effects of the renormalisation to a non-standard value for α, residual two-loop effects are expected as additional higher-order corrections that appear in the comparison. These higher-order corrections should be studied separately, since their leading contributions can be of the order of potentially non-negligible two-loop correction from the Higgs-sector.

9.3 Differences between `NMSSMCalc` and `NMSSM-FeynHiggs`

The implemented functionalities in `NMSSMCalc` and `NMSSM-FeynHiggs` are different. `NMSSMCalc` allows one to calculate Higgs-masses and branching-ratios in the NMSSM with complex parameters. The currently unpublished version of `NMSSM-FeynHiggs` calculates only Higgs-masses in the NMSSM with real parameters with the MSSM-approximation at the two-loop level.

    `NMSSM-FeynHiggs` was intended for the calculation of MSSM and NMSSM Higgs-masses at or close to the electroweak scale for SUSY-masses up to several TeV.

Although `NMSSMCalc` uses a similar calculation with Feynman-diagrammatic methods, the codes is designed to calculate the Higgs masses at a common scale that is given in the input file. However, for purely Feynman-diagrammatic calculations the reliability for very large SUSY masses above ≈ 5 TeV is questionable. The higher-order corrections can become potentially large due to logarithms of the ratio of the electroweak and the SUSY scale. Partially the problem can be remedied by the resummation of such large logarithms, which are included in `FeynHiggs` and `NMSSM-FeynHiggs` see [37] and references therein.

 `NMSSMCalc` provides the calculation of NMSSM Higgs-masses with on-shell or $\overline{\text{DR}}$ renormalised top- and stop-masses, while `NMSSM-FeynHiggs` provides only the on-shell renormalisation of these sectors is implemented, with the option to reparametrise the on-shell top-quark mass m_t^{OS} to the $\overline{\text{MS}}$- or $\overline{\text{DR}}$-scheme. For the comparison described in this sections the options for on-shell renormalised top- and stop-masses will be considered if not stated otherwise.

In this section we will focus on the differences affecting the implemented Higgs-mass prediction for these options in the $\mathcal{CP}$-conserving (real) NMSSM. The relevant differences between the two codes stem from the employed renormalisation scheme for electromagnetic coupling-constant α, the included higher-order corrections, and the treatment of the strong coupling constant α_s for both the Higgs-mass prediction and the on-shell conversion of the stop-sector parameters.

Treatment of $\overline{\text{DR}}$ input-parameters

According to the SLHA-conventions all soft-breaking parameters are provided in the $\overline{\text{DR}}$-scheme together with their respective scale.

 `NMSSMCalc` accepts all soft-breaking parameters at the same scale Q, which serves as the renormalisation scale for the Higgs-mass calculation. No RGE-evolution for the soft-breaking parameters is necessary.

In `NMSSM-FeynHiggs` a conversion from $\overline{\text{DR}}$ input-parameters to on-shell parameters, which are used internally, is performed in the stop-/sbottom-sector. In the present version of the code no RGE-evolution for the remaining soft-breaking parameters is performed. Their effects are treated as higher-order effects and are neglected. In the public version of `NMSSM-FeynHiggs`, the necessary routines needed for a proper treatment of SLHA input files will be implemented.

Both `NMSSMCalc` and `NMSSM-FeynHiggs` perform the on-shell conversion at the one-loop level. The conversion is performed at the one-loop level to account for the on-shell renormalisation at the two-loop level.

Included higher-order Corrections

The two-loop corrections in `NMSSM-FeynHiggs` are approximated by the MSSM contributions, while in `NMSSMCalc` a complete NMSSM-calculation of only the $\mathcal{O}(\alpha_t \alpha_s)$ is implemented while all further contributions at the two-loop level are neglected. Within of the MSSM-approximation `NMSSM-FeynHiggs` contains contributions beyond $\mathcal{O}(\alpha_t \alpha_s)$ and the resummation of large logarithms. It also includes higher-order

corrections to the bottom Yukawa-coupling summed up in Δ_b. These additional contributions and features that are not (yet) included in `NMSSMCalc` and thus will not be considered for the comparison of the two codes.

Renormalisation Scheme of α

The renormalisation schemes employed in `NMSSMCalc`and `NMSSM-FeynHiggs` are almost identical to each other, with the notable exception of the renormalisation of the vacuum expectation-value v or the electromagnetic coupling constant α. While in `NMSSM-FeynHiggs` v is renormalised as an independent parameter in the $\overline{\text{DR}}$-scheme, in `NMSSMCalc` α is renormalised and $\alpha(M_Z)$ is chosen as input parameter instead. In the standard version of `NMSSM-FeynHiggs` α is reparametrised in terms of Fermi's constant, yielding the value α_{G_F}. In contrast to the MSSM calculation the charge renormalisation is of particular importance for the determination of the theoretical uncertainty for the NMSSM calculation. In the MSSM different choices for α are an effect of two-loop order, that formally is of the same order as two-loop corrections from the Higgs- and electroweak gauge-sector. However, the two-loop corrections of $\mathcal{O}(\alpha_t \alpha_s)$ have been obtained in the electroweak gaugeless limit and thus the higher-order effects related to the renormalisation of α are neglected for the contributions of $\mathcal{O}(\alpha_t \alpha_s)$. In the NMSSM, however, the charge renormalisation appears already at one-loop order and the numerical value of α has either to be chosen according to the renormalisation scheme or has to be reparametrised.

Treatment of α_s: Two-Loop Higgs Self-Energies

In `NMSSM-FeynHiggs` α_s is always evolved to the scale of the on-shell top-quark mass m_t^{OS} from the input-value for $\alpha_s^{\overline{\text{MS}}}(M_Z)$. In `NMSSMCalc` $\alpha_s^{\overline{\text{MS}}}(M_Z)$ is evolved to a scale Q and subsequently converted into its $\overline{\text{DR}}$-value. The employed RGE-evolution of α_s is described in [129]. It represents the running in the SM. The $\overline{\text{MS}}$ to $\overline{\text{DR}}$ conversion for α_s can be found in [136].

Treatment of α_s: On-Shell Conversion of stop-sector Parameters

Since only corrections of $\mathcal{O}(\alpha_t \alpha_s)$ are considered, both codes use the MSSM-conversion of $\mathcal{O}(\alpha_s)$ as described in see sec. 5.4.3. However, the calculation of the relevant top and stop self-energies differs by the used value for α_s: While `NMSSM-FeynHiggs` always uses $\alpha_s^{\overline{\text{MS}}}(m_t^{\text{OS}})$, `NMSSMCalc` uses $\alpha_s^{\overline{\text{DR}}}(Q)$. While α_s does not enter the one-loop calculation explicitly, different choices for α_s cause a higher-order effect within the on-shell conversion for the stop-sector parameters.

9.4 Identification of Input-Uncertainties

The initial task for the comparison in this section is to identify the input uncertainties in order to isolate the intrinsic uncertainties from higher-order corrections. This is

done by separating any treatment of the provided input parameters from the Higgs-mass calculation and by providing adapted versions of both codes for the comparison.

9.4.1 RGE-Evolution and On-Shell Conversion of the Input Parameters

For the calculation in the TP-scenario at the low scale the input parameters have to be evolved from Q to $m_t^{\rm OS}$. The RGE-evolution is performed by `FlexibleSUSY 1.2.2` [23], which includes the two-loop RGE-evolution in the NMSSM for the soft-breaking parameters.

After the input parameters have been evaluated at either the high or the low scale, all necessary input-parameters are calculated by the built-in routines of `NMSSMCalc`. The parameters obtained by `NMSSMCalc` include the on-shell values for the trilinear breaking parameter A_t and the soft-breaking masses $M_{\tilde{t}_L}$ and $M_{\tilde{t}}$ in the stop-sector as well as the on-shell mass of the charged Higgs $M_{H^\pm}$. The on-shell value for $M_{H^\pm}$ is calculated with one-loop corrections for the one-loop Higgs-mass predictions and two-loop corrections for the two-loop Higgs-mass predictions, respectively. By this procedure of using the same input parameters in both codes possible higher-order effects from the RGE-evolution and on-shell conversion are avoided.

9.4.2 Adapted Versions of `NMSSMCalc` and `NMSSM-FeynHiggs`

In order to address the different treatments of α_s in the Higgs self-energies at the two-loop level, the two codes will be adjusted such that they use an identical, fixed value for α_s. Further adaptions are provided for the treatment of the renormalisation of the electromagnetic coupling constant α in order to separate this effect from the influence of α_s. The different settings are listed together with their abbreviations in tab. 9.2. A more detailed explanation of the adaptions will be given together with the obtained numerical results in the following section 9.5.

9.5 Numerical Results

In this section the Higgs-mass predictions for the (MS)SM-like field in the TP-scenarios will be discussed. The scenario TP6 will be omitted, since the MSSM-approximation is not expected to be viable for its "extreme" value of $\lambda \approx 1.6$. While the complete results for all $\mathcal{CP}$-even Higgs-masses can be found in the appendix B.3, this section will focus on the differences between the mass-predictions for the (MS)SM-like Higgs-field of `NMSSMCalc` and `NMSSM-FeynHiggs`. Each scenario

	α	Δ_α	α_s	comments
`NMSSM-FH` α_{G_F}	α_{G_F}	✓	$\alpha_s^{\overline{\text{MS}}}(m_t)$	vanilla
`NMSSM-FH` $\alpha(M_Z)$	$\alpha(M_Z)$	✓	$\alpha_s^{\overline{\text{MS}}}(m_t)$	
`NMSSM-FH` $\alpha(M_Z)(-)$	$\alpha(M_Z)$	–	$\alpha_s^{\overline{\text{MS}}}(m_t)$	unphysical
`NMSSMCalc`	$\alpha(M_Z)$	–	$\alpha_s^{\overline{\text{DR}}}(Q)$	vanilla
`NMSSMCalc` α_s^{mod}	$\alpha(M_Z)$	–	$\alpha_s^{\overline{\text{MS}}}(m_t)$	
`NMSSMCalc` $(-)$	$\alpha(M_Z)$	–	$\alpha_s^{\overline{\text{MS}}}(m_t)$	uses $\delta v^{\overline{\text{DR}}}$

Table 9.2: The headings specify the used value for the electromagnetic coupling constant α, whether the reparametrisation Δ_α for the used value of α has been applied and which value for the strong coupling constant α_s is used. In the versions marked with "$(-)$" the chosen value for α does neither fit the renormalisation scheme nor has a reparametrisation been applied (see text). They represent inconsistent and thus unphysical calculations created only for the purpose of this comparison.

will be evaluated at the high scale Q and the low scale m_t^{OS}. Additionally a "rough"[1] MSSM-limit of each scenario was evaluated.

In the following a short discussion of the singlet-admixture will be provided before the numerical results are presented. Subsequently the theoretical uncertainties caused by the input parameters and the MSSM-approximation of `NMSSM-FeynHiggs` are presented together with an explanation of the adapted versions of the codes outlined in tab. 9.2. In the last section the two codes will be compared for their standard mass-predictions.

9.5.1 Singlet-admixture

The singlet-admixture to the fields h_i beyond lowest-order is defined by the wave function normalisation matrix $\hat{\mathbf{Z}}$ and the tree-level mixing matrix $\mathbf{U}_{e(0)}$ as defined in eq. (3.34). However, in this section we use the approximation for the matrix $\mathbf{U}_{e(n)}$ as described in sec. 3.3.1. The approximate matrices $\mathbf{U}_{e(n)}$ are obtained by the eigenvalue decomposition from the iterative pole determination as an approximation for the wave renormalisation factors. The quantities $\mathbf{U}_{e(n)}$ are approximately unitary matrices with a unitarity violation of typically less than 1‰, if the obtained mass from from the iterative procedure is of the order of $\mathcal{O}(100 \text{ GeV})$. Since at lowest-

---

[1]The input parameters evaluated at either scale will be fixed after the RGE-evolution with non-vanishing values for λ and κ, and subsequently the MSSM-limit, involving λ, $\kappa \to 0$, is taken. For a future comparison with $\overline{\text{DR}}$-calculations the MSSM-limit should be applied before any RGE-evolution takes place, to ensure that both codes calculate results in the same scenario. Since λ and κ have the largest effect on genuine NMSSM-parameters, the error of this approach is expected to be minor for the present calculation. Also for the purpose of the presented results the "rough" MSSM-limit is sufficient since no RGE-evolution is implemented in either `NMSSMCalc` or `NMSSM-FeynHiggs`.

order the singlet-admixture to the fields h_i is determined by the squared matrix-elements $|\mathbf{U}_{e(0)}|^2_{i3}$, we will assume that at higher-orders the matrix-elements $|\mathbf{U}_{e(n)}|^2_{i3}$ approximate the singlet-admixture to $h_i{}^2$.

For the TP-scenarios numerical values for the $|\mathbf{U}_{e(0)}|^2_{i3}$ and $|\mathbf{U}_{e(n)}|^2_{i3}$ are presented in tab. 9.3. The depicted values for $|\mathbf{U}_{e(n)}|^2_{i3}$ are obtained by the pole determination for the mass of the the lightest $\mathcal{CP}$-even Higgs-field.

		Comparison I			Comparison II		
		$|\mathbf{U}_{e(n)}|^2_{13}$	$|\mathbf{U}_{e(n)}|^2_{23}$	$|\mathbf{U}_{e(n)}|^2_{33}$	$|\mathbf{U}_{e(n)}|^2_{13}$	$|\mathbf{U}_{e(n)}|^2_{23}$	$|\mathbf{U}_{e(n)}|^2_{33}$
	$n=0$	0	1	0	0	1	0
TP1	$n=2$	0	1	0	0	1	0
	$n=0$	0	1	0	–	–	–
TP2	$n=2$	0	1	0	–	–	–
	$n=0$	0.84	0.14	0.02	0.95	0.03	0.02
TP3	$n=2$	0.92	0.06	0.02	0.96	0.02	0.02
	$n=0$	0	0.97	0.03	0	0.97	0.03
TP4	$n=2$	0.17	0.80	0.03	0.02	0.95	0.03
	$n=0$	0.03	0.95	0.02	0.13	0.84	0.02
TP5	$n=2$	0.31	0.67	0.02	0.28	0.69	0.02

Table 9.3: Singlet-admixture $|\mathbf{U}_{e(0)}|^2_{i3}$ at lowest order and approximate two-loop singlet-admixture $|\mathbf{U}_{e(2)}|^2_{i3}$ to the fields h_i for the high scale Q (comparison I) and the low scale m_t^{OS} (comparison II). The mass hierarchy $m_{h_1} < m_{h_2} < m_{h_3}$ is assumed.

At two-loop order in each scenario TP1 ... 4 one field can be identified to be dominantly singlet-like. For TP5 the singlet-admixture is significant for both lighter Higgs-fields. For TP4 the singlet-admixture to h_1 at the low scale m_t^{OS} is an order of magnitude smaller than at the high scale Q. This may lead to smaller higher-order effects from the genuine NMSSM corrections.

9.5.2 Higher-order effects from α_s

The codes `NMSSMCalc` and `NMSSM-FeynHiggs` have a different standard value that is used internally for the strong coupling-constant α_s: In `NMSSMCalc` the $\overline{\mathrm{DR}}$ renormalised value for α_s is evaluated at the scale specified in the SLHA-Input file, while `NMSSM-FeynHiggs` always uses the $\overline{\mathrm{MS}}$-value of α_s at the pole mass of the top-quark. The value for α_s is fixed intentionally, since `NMSSM-FeynHiggs` is designed to calculate the Higgs-mass at the electroweak scale. The strong scale dependence

---

[2]In [39] the dominantly singlet- and the (MS)SM-like fields are identified primarily by the matrix $\mathbf{U}_{e(n)}$.

of α_s can lead to vastly different two-loop results for the Higgs-masses, since all two-loop contributions of $\mathcal{O}(\alpha_t \alpha_s)$ are directly proportional to α_s. In fig. 9.1 the absolute differences between the two mass-predictions for the dominantly (MS)SM-like Higgs-field obtained by the standard (vanilla) version of `NMSSMCalc` and `NMSSM-FeynHiggs` are shown in orange for all TP-scenarios at the high and low scale. In order to eliminate the influence of different values for the electromagnetic coupling constants, the used `NMSSM-FeynHiggs`-modification includes the reparametrisation for $\alpha(M_Z)$ if not stated otherwise. It is abbreviated with "`NMSSM-FH` $\alpha(M_Z)$". The comparison for TP2 at the low scale is unphysical, since the scenario yields negative squared masses for the stop-squarks after the RGE-evolution. Throughout this chapter it will be treated as if the difference between the codes were zero to allow an easy comparison between charts depicting the low- and high-scale results.

For the calculation at the high scale the differences between the mass-predictions can exceed 5 GeV, while at the low scale the difference generally remains below 1 GeV. This behaviour is a pure MSSM-effect, since also TP2 with a very small value for λ is significantly affected. It can be directly traced back to the scale dependence of α_s. The values at the different scales Q in the TP-scenarios are shown in the $\overline{\text{DR}}$- and $\overline{\text{MS}}$-scheme in tab. 9.4. The shown values for $\alpha_s^{\overline{\text{MS}}}$ were obtained with the

Q	$\alpha_s^{\overline{\text{MS}}}(Q)$	$\alpha_s^{\overline{\text{DR}}}(Q)$
m_t^{OS}	0.10697	0.10789
750 GeV	0.09065	0.09131
1000 GeV	0.08803	0.08865
1500 GeV	0.08458	0.08515

Table 9.4: The strong coupling constant at the different scales Q of the TP-scenarios and the top-quark mass m_t^{OS}. As starting value $\alpha_s(M_Z) = 0.1184$ [119] was used.

results of [129] including corrections up to partial four-loop order as implemented in `NMSSMCalc`, while the values for $\alpha_s^{\overline{\text{DR}}}$ were obtained with the two-loop result of [136]. The scale variation has a larger effect on α_s than the $\overline{\text{MS}}$ to $\overline{\text{DR}}$ conversion.

In tab. 9.5 the two-loop shifts to the (MS)SM-like Higgs-boson masses,

$$m_{h_i}^{(2L)} = m_{h_i}^{(\text{tree})} + \Delta m_{h_i}^{(1L)} + \Delta m_{h_i}^{(2L)} = m_{h_i}^{(1L)} + \Delta m_{h_i}^{(2L)} \tag{9.3}$$

with

$$\Delta m_{h_i}^{(2L)} = m_{h_i}^{(2L)} - m_{h_i}^{(1L)}, \tag{9.4}$$

are given for the vanilla version of `NMSSMCalc` and `NMSSM-FeynHiggs` reparametrised to $\alpha(M_Z)$ together with the change of the strong coupling constant at the high scale $\alpha_s^{\overline{\text{DR}}}(Q)$, that is used in `NMSSMCalc`, relative to its $\overline{\text{MS}}$ value at m_t^{OS}, that is used in `NMSSM-FeynHiggs`. The majority of the difference between the two-loop shifts
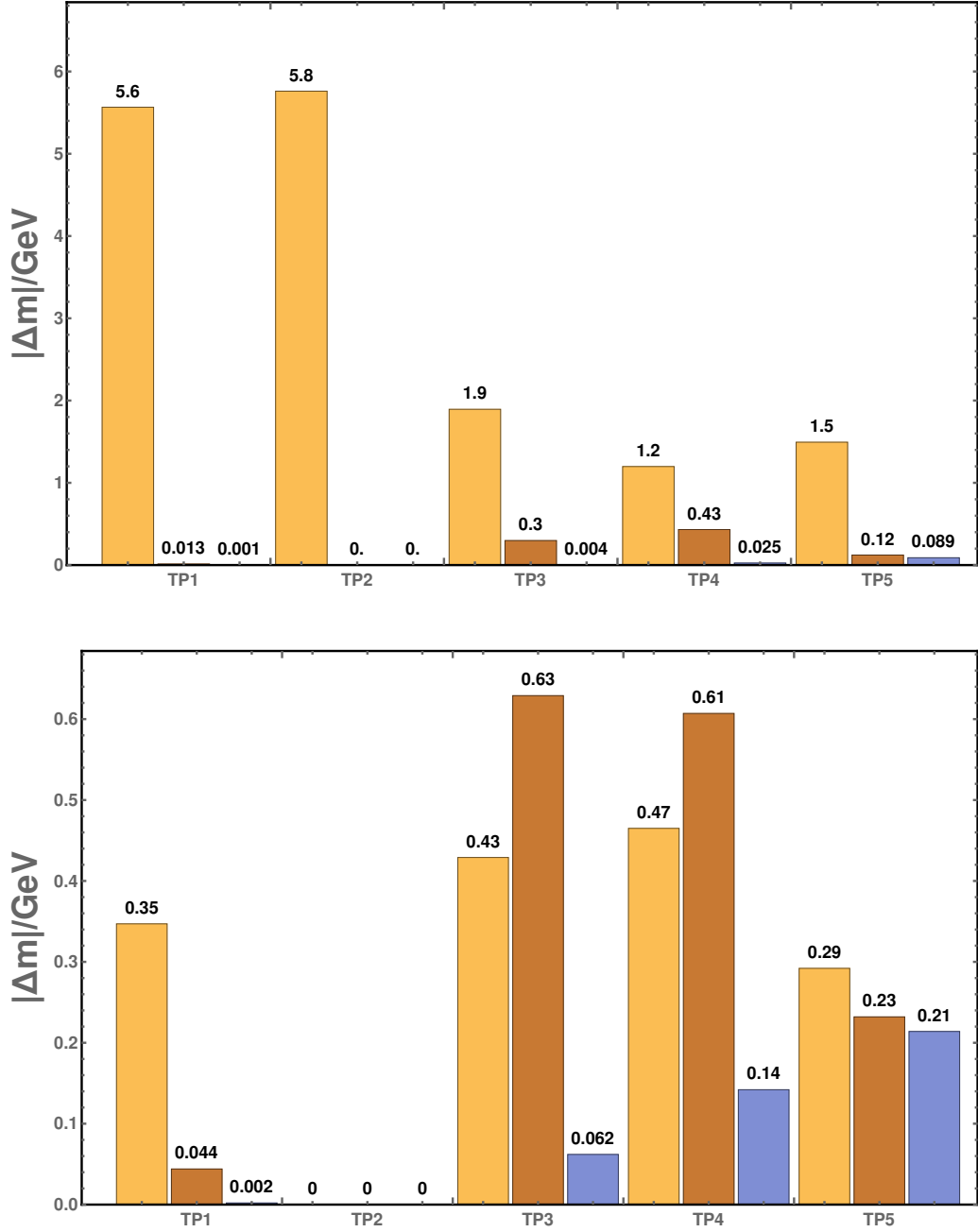
Figure 9.1: Absolute difference between the two-loop predictions for the mass of the dominantly (MS)SM-like Higgs-field of `NMSSMCalc` and "NMSSM-Feyn-Higgs $\alpha(M_Z)$" (orange, $\Delta m = |m_{h_i}^{(\text{NC})} - m_{h_i}^{(\text{N-FH }\alpha(M_Z))}|$), "NMSSMCalc$\alpha_s^{\text{mod}}$" and "NMSSM-FeynHiggs $\alpha(M_Z)$" (brown, $\Delta m = |m_{h_i}^{(\text{NC }\alpha_s^{\text{mod}})} - m_{h_i}^{(\text{N-FH }\alpha(M_Z))}|$), and "NMSSMCalc$\alpha_s^{\text{mod}}$" and "NMSSM-FeynHiggs $\alpha(M_Z)(-)$" (blue, $\Delta m = |m_{h_i}^{(\text{NC }\alpha_s^{\text{mod}})} - m_{h_i}^{(\text{N-FH }\alpha(M_Z)(-))}|$). The upper chart shows the comparison at the high scale, the lower chart at the low scale.

	Q/GeV	$\Delta m^{(2\mathrm{L})}$/GeV		$\Delta\alpha_{s\mathrm{rel}}$
		NMSSMCalc	NMSSM-FH	
TP1	1500	19.692	25.263	$\approx 20\%$
TP2	1500	20.253	26.014	$\approx 20\%$
TP3	1000	10.896	13.196	$\approx 17\%$
TP4	750	4.571	5.675	$\approx 15\%$
TP5	1500	11.603	13.875	$\approx 20\%$

Table 9.5: Two-loop shifts $\Delta m = |m^{(2\mathrm{L})} - m^{(1\mathrm{L})}|$ for `NMSSMCalc` and `NMSSM-FeynHiggs` with $\alpha(M_Z)$ and relative difference between the values of the strong coupling constant in the $\overline{\mathrm{MS}}$-scheme at the top-quark pole mass $m_t^{(\mathrm{OS})}$ and in the $\overline{\mathrm{DR}}$-scheme at the high scale Q, $\delta\alpha_{\mathrm{rel}} = (\alpha_s(m_t^{(\mathrm{OS})}) - \alpha_s(Q))/\alpha_s(m_t^{(\mathrm{OS})})$

of `NMSSMCalc` (abbreviated as `NC`) and `NMSSM-FeynHiggs` (abbreviated as `N-FH`) in tab. 9.5 at the high scale can be explained by $\Delta\alpha_{s\mathrm{rel}}$, since

$$\Delta m^{\mathrm{N\text{-}FH}}\,(1 - \Delta\alpha_{s\mathrm{rel}}) \approx \Delta m^{\mathrm{NC}}. \tag{9.5}$$

The calculation at the low scale is only influenced by the $\overline{\mathrm{MS}}$ to $\overline{\mathrm{DR}}$ conversion, and the low-scale mass-predictions are in much better agreement with each other than the high-scale mass-predictions, that are also affected also by the RGE-evolution of α_s.

In order to eliminate the influence of an RGE-evolving α_s and its renormalisation scheme conversion, `NMSSMCalc` was modified such that it uses the same value $\alpha_s^{\overline{\mathrm{MS}}}(m_t^{\mathrm{OS}})$ as `NMSSM-FeynHiggs`. This version is labelled "`NMSSMCalc` α_s^{mod}". The difference between the two-loop mass predictions of this modified version and "`NMSSM-FH` $\alpha(M_Z)$" is shown in brown in fig. 9.4. For the calculation at the high scale both codes show much more similar results with a difference of at most 430 MeV. At the low scale the modified version "`NMSSMCalc` α_s^{mod}" yields a more similar mass prediction for the MSSM-like scenario TP1 and TP5. For TP3 and TP4 the differences between the two predictions are slightly increased compared the comparison with the unmodified version of `NMSSMCalc` and can be attributed to the $\overline{\mathrm{MS}}$–$\overline{\mathrm{DR}}$-conversion of α_s and the two-loop MSSM-approximation of `NMSSM-FeynHiggs`.

The residual differences are increased for larger singlet-admixtures and increased difference between the mass-scale of the stops and the renormalisation scale. These behaviours can be observed in both charts in fig. 9.1: The residual differences between the predictions of "`NMSSM-FH` $\alpha(M_Z)$" and "`NMSSMCalc` α_s^{mod}", that are depicted in brown in fig. 9.1, are smaller at the high scale, where the renormalisation scheme μ_{r} is chosen close to the stop-masses (tab. 9.6). They are somewhat enhanced for the scenarios with larger mass-splitting in the stop-sector, most notably for TP3 and TP4. The extreme mass-splitting for TP2 is mitigated by the small values of λ, which suppress genuine NMSSM-corrections.

In order to eliminate the theoretical uncertainty induced by α_s for all subsequent

	Comparison I		Comparison II	
	$m_{\tilde{t}_1}$	$m_{\tilde{t}_2}$	$m_{\tilde{t}_1}$	$m_{\tilde{t}_2}$
TP1	1360.25	1656.14	1547.21	1564.19
TP2	2553.68	507.225	–	–
TP3	941.474	1085.45	941.784	1085.16
TP4	669.224	855.688	760.14	549.379
TP5	1547.21	1564.19	1503.75	1468.22

Table 9.6: Stop-squark masses in GeV at tree-level for the calculation at the high scale Q (comparison I) and low scale m_t^{OS} (comparison II).

studies both `NMSSMCalc` and `NMSSM-FeynHiggs` will use the same fixed value for $\alpha_s^{\overline{\mathrm{MS}}}(m_t^{(\mathrm{OS})}) = 0.10697$. For all following studies this modification is considered to be included if not stated otherwise. Hence, the addition "α_s^{mod}" for the α_s-modified version of `NMSSMCalc` will be dropped in the following.

9.5.3 Effects of the MSSM-Approximation

The residual differences between `NMSSMCalc` and "NMSSM-FH $\alpha(M_Z)$", depicted in brown in fig. 9.1, are caused by the different renormalisation schemes for δv and δZ_{e}, respectively, and the two-loop MSSM-approximation of `NMSSM-FeynHiggs`. They correlate to the difference studied in sec. 8.1.3, but have a generally somewhat larger impact than the effects observed in that section. Scenario TP3 bares the closest resemblance of the physical situation in the sample scenario from section 8.1.3. Both scenarios feature a light singlet-like state (tab. B.1) with relatively small mass-splitting in the stop-sector and a large gluino-mass.

In order to disentangle the effects from the renormalisation scheme and the approximation a further comparison is performed, where `NMSSMCalc` and `NMSSM-FeynHiggs` were modified such that both codes use a $\overline{\mathrm{DR}}$ renormalisation scheme for the vacuum expectation-value v while using $\alpha(M_Z)$ *without* applying a reparametrisation. These versions are labelled "`NMSSMCalc` $(-)$" and "NMSSM-FH $\alpha(M_Z)(-)$". These modified versions do not reflect a physical calculation, since they use a value for α that does not fit the applied renormalisation condition without applying a reparametrisation. However, the residual two-loop difference between the these versions, that is depicted in blue in fig. 9.1, provides an insight into the size of the genuine NMSSM two-loop corrections. For the calculation at the high scale they remain below 90 MeV in all TP-scenarios and are largest for TP5, where the singlet-admixture to the dominantly (MS)SM-like field is largest. For the calculation at the low scale the residual differences are slightly larger, up to 210 MeV, for TP5.

Thus the MSSM-approximation can be expected to lead to an effect that is minor compared to the effect of the different renormalisation schemes. The effect of the differences in the renormalisation scheme is enhanced compared to the effect observed earlier in section 8.1.3 for the sample scenario that is similar to TP3. This enhance-

	$\mathcal{O}(\alpha_t \alpha_s)$	$\mathcal{O}(\alpha_t \alpha_s, \alpha_b \alpha_s)$ + MSSM	'full'	Δm_1	Δm_2
TP1	124.84	123.84	123.84	< 0.01	< 0.01
TP2	123.81	123.08	123.05	0.73	0.03
TP3	127.55	126.59	126.10	0.96	0.49
TP4	128.23	127.52	126.33	0.71	1.19
TP5	126.12	125.12	124.85	1.00	0.27

Table 9.7: Results for the (MS)SM-like Higgs-mass for the high scale as obtained with `SPHENO` from [39]. The orders of the included two-loop NMSSM-contributions are stated, where "MSSM" refers to the $\overline{\text{DR}}$ results for the corrections that are included in `FeynHiggs` and 'full' denotes the corresponding NMSSM-contributions plus the correction from the Higgs-sector in the gaugeless limit, that means corrections including the couplings λ and κ. The differences Δm_i denote the impact of the MSSM corrections, Δm_1, and the Higgs-sector contributions, Δm_2. The corrections of $\mathcal{O}(\alpha_b \alpha_s)$ alone are negligible for all scenarios.

ment is driven by the larger values of λ. The uncertainty arising from employing the MSSM-approximation can be seen to be insignificant compared to the other theoretical uncertainties for all TP-scenarios. The largest (but still numerically small) effect occurs to TP5, where the increased singlet-admixture to the (MS)SM-like field accounts for a larger impact of the MSSM-approximation.

9.5.4 Higher-order effects from the Reparametrisation

In `NMSSM-FeynHiggs` the reparametrisation procedure for α is applied at the tree-level, leading to a reparametrised result at one-loop order. Beyond one-loop order the reparametrisation shifts are considered to be negligible higher-order effects. However, a reparametrisation for the genuine NMSSM one-loop Higgs-contributions would result in contributions that are formally of the same order as the two-loop contributions from the Higgs-sector. The impact of these contributions can be estimated for the TP-scenarios. For the comparison of $\overline{\text{DR}}$-calculations in [39] the code `SPheno` includes two-loop corrections from the Higgs-sector in the gaugeless limit. The corresponding numerical results are given in tab. 9.7 for convenience[3].

While the Higgs-sector contributions at the two-loop level give rise to a small mass-shift for the MSSM-like scenarios TP1 and TP2, their effect on the mass of the (MS)SM-like fields reside between 0.3 and 1.2 GeV for TP3-5. As mentioned above, a change in the parametrisation of $\alpha 1$ at the one-loop level induces a shift that is of the order of the two-loop contributions from the Higgs-m and gauge-sector. It can therefore give an indication of possible effects of unknown higher-order effects of this

---

[3]While the two-loop MSSM-corrections seem to have a very small effect on the results in all TP-scenarios, they have been found to yield a larger effect for the calculation with mixed on-shell/$\overline{\text{DR}}$ renormalisation schemes in certain scenarios.

order.

9.5.5 Higher-order effects from α

In fig. 9.2 the differences Δm between the two-loop mass-predictions using the values $\alpha(M_Z)$ and α_{G_F}, and the corresponding renormalisation schemes are depicted. In order to disentangle the effects that are genuine to the NMSSM, the difference between the corresponding Higgs-mass predictions in the MSSM are depicted in orange. For the original TP-scenarios two results are presented. In brown the difference between the `NMSSM-FeynHiggs` versions with the reparametrisations to α_{G_F} and to $\alpha(M_Z)$ are depicted, while the difference between the vanilla versions of `NMSSM-FeynHiggs` with corrections up to $\mathcal{O}\alpha_t\alpha_s$ only and `NMSSMCalc` is depicted in blue.

Both for the calculation at the high and the low scale the difference between the MSSM-results ranges between 500 and 700 MeV, with marginally larger differences for the calculation at the low scale.

For the MSSM-like scenarios TP1 and TP2 the genuine NMSSM-effects are small at both scales. They remain below 50 MeV for both the results obtained with only one or two different codes.

For TP3-5 the difference between the reparametrised versions of `NMSSM-FeynHiggs` is generally smaller than the difference in the MSSM-limit. The comparison of the vanilla versions of `NMSSMCalc` and `NMSSM-FeynHiggs` yields larger differences, since it accounts also for the different renormalisation schemes. The size of this additional difference between the two comparisons for the TP-scenarios (brown and blue bars in fig. 9.2) closely resembles the differences obtained for the comparison between `NMSSMCalc` and "`NMSSM-FH` $\alpha(M_Z)$" (brown bars in fig. 9.1). For an estimate of the remaining theoretical uncertainties from unknown higher-order corrections all the above effects have to be taken into account.

The genuine NMSSM-effects are more important for scenarios with rather large values for λ (TP3-5), where the difference can be altered by up to 500 MeV compared to the MSSM-result at the high scale. For TP5 that means that the MSSM-difference (orange) is almost completely absorbed by genuine NMSSM-effects. For scenarios with large mass-splitting in the stop-sector the genuine NMSSM-effects are somewhat enhanced (TP3, TP4) as well as for a larger singlet-admixture (TP5).

For the calculation at the low scale the genuine NMSSM-effects alter the MSSM-result by at most 200 MeV. From the obtained results neither at the high nor at the low scale a tendency can be deduced that indicates a general increase or a decrease of the differences due to genuine NMSSM-effects. However, the difference between the calculation using only one and both codes (brown and blue bars in fig. 9.2) is increased for large mass-splitting in the stop-sector (TP3, TP4) and a larger singlet-admixture (TP5).

The presented results indicate that the renormalisation scheme of the electromagnetic coupling constant α can have a significant numerical impact on the mass-prediction even for a (MS)SM-like Higgs-field of up to 1 GeV from the combined MSSM-like and genuine NMSSM-effects. The comparison between the two codes
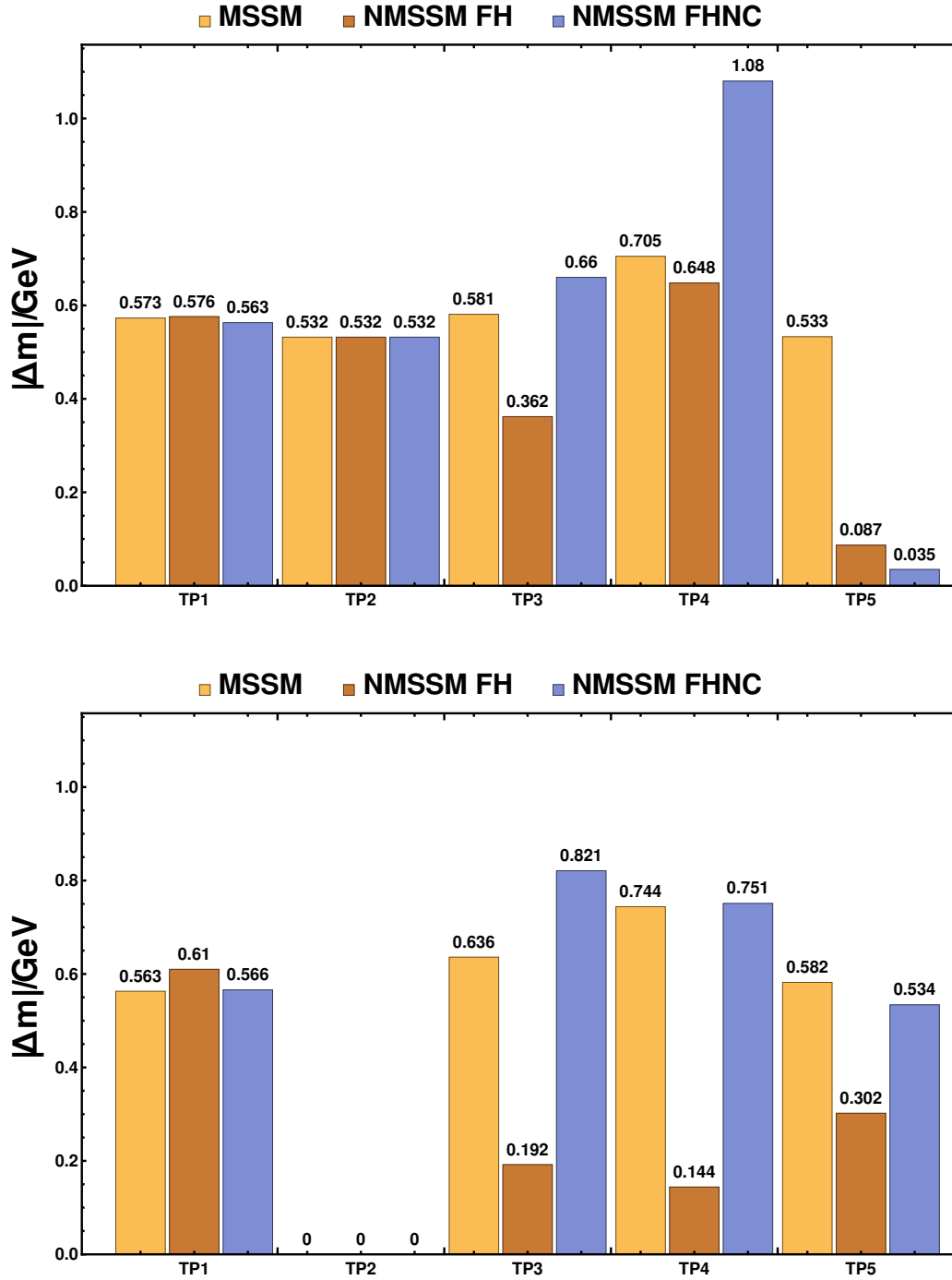
Figure 9.2: Absolute difference between the two-loop mass-prediction parametrised in terms of $\alpha(M_Z)$ and α_{G_F} for the MSSM-limit (orange, $\Delta m = \left| m_{h_i}^{(\text{NC})} - m_{h_i}^{(\text{N-FH})} \right|$), between the two reparametrisations in NMSSM-FeynHiggs (brown, $\Delta m = \left| m_{h_i}^{(\text{N-FH}\alpha(M_Z))} - m_{h_i}^{(\text{N-FH})} \right|$), and between the original versions with corrections up to $\mathcal{O}(\alpha_t\alpha_s)$ (blue, $\Delta m = \left| m_{h_i}^{(\text{NC})} - m_{h_i}^{(\text{N-FH})} \right|$), of the TP-scenarios.

based on somewhat different schemes reveals differences that go beyond the ones obtained from changing the parametrisation in a single code.

9.5.6 Higher-order effects from the Top-/Stop-sector

In this section results for the comparison of "NMSSMCalc α_s^{mod}" with $\overline{\mathrm{DR}}$-renormalised masses in the top-/stop-sector and the standard version of NMSSM-FeynHiggs with on-shell renormalised masses in the top-/stop-sector are presented in tab. 9.8. The scenarios were evaluated at the scale m_t^{OS}. The results are preliminary, in the sense that the $\overline{\mathrm{DR}}$-option in NMSSMCalc only accounts for the conversion of the top-mass and stop-sector parameters, but not for the determination of the on-shell mass for the charged Higgs. In NC the on-shell charged Higgs mass is determined with top- and stop-masses in the chosen renormalisation scheme, while the results for NMSSM-FeynHiggs are obtained for the on-shell mass for the charged Higgs obtained with on-shell top- and stop-masses. The differences between the two codes for contributions

	TP1	TP2	TP3	TP4	TP5
NMSSMCalc α_s^{mod}	116.94	–	128.34	132.29	123.84
NMSSM-FH $\mathcal{O}(\alpha_t\alpha_s)$	113.19	–	123.39	128.25	121.78
NMSSM-FH	121.70	–	126.30	131.13	123.48

Table 9.8: Results for the (MS)SM-like Higgs-field obtained in the TP-scenarios from the codes "NMSSMCalc α_s^{mod}" with $\overline{\mathrm{DR}}$-renormalised masses in the top-/stop-sector and NMSSM-FeynHiggs evaluated once including only the corrections up to $\mathcal{O}(\alpha_t\alpha_s)$ and once including all corrections of $\mathcal{O}(\alpha_s\alpha_t, \alpha_t^2, \alpha_s\alpha_b, \alpha_t\alpha_b)$ with on-shell renormalised masses in the top-/stop-sector.

up to $\mathcal{O}(\alpha_t\alpha_s)$ employing a $\overline{\mathrm{DR}}$ and the on-shell renormalisation of the stop-sector are found to be sizeable, reaching up to 5 GeV for TP3. The inclusion for the additional MSSM corrections result in a sizeable shift compared to the results including only correction of $\mathcal{O}(\alpha_t\alpha_s)$, reaching up to 8.5 GeV for TP1. For all TP-scenarios the results including the additional MSSM contributions in the on-shell scheme for the top-/stop-sector are generally closer to the result with a $\overline{\mathrm{DR}}$ scheme in the same sector including only corrections up to $\mathcal{O}(\alpha_t\alpha_s)$.

9.6 Conclusion

In order to asses theoretical uncertainties from unknown higher-order corrections, in a first step the theoretical uncertainties related to the input parameters in NMSSMCalc and NMSSM-FeynHiggs have been identified. Different modified versions of both codes have been developed to disentangle different sources for higher-order effects:

- Higher-order effects from the soft-breaking input-parameters have been disentangled by separating their RGE-evolution and on-shell conversion of $\overline{\mathrm{DR}}$

input-parameters from the actual Higgs-mass calculations.

- Higher-order effects from α_s have been identified. For comparison purposes a modified version of `NMSSMCalc` has been provided by its authors, where the fixed value $\alpha_s^{\overline{\text{MS}}}(m_t^{\text{OS}})$ is used.

- Higher-order corrections from the renormalisation scheme of α have been addressed by adapting both codes such that both use the identical renormalisation scheme for α.

With these modified versions it was possible to isolate the uncertainty related to the MSSM-approximation in `NMSSM-FeynHiggs`. For the points TP1-4 the uncertainty remains very small and does not exceed 140 MeV, while the larger singlet-admixture to the (MS)SM-like Higgs-field for TP5 slightly increases the uncertainty to ≈ 210 MeV.

Furthermore the uncertainties estimated by different renormalisation prescriptions for α the top-/stop-sector have been quantified for the evaluation at the low scale m_t^{OS}:

- Higher-order effects from the top-/stop-sector induced by either choosing the $\overline{\text{DR}}$ or the on-shell scheme for the top- and stop-masses together with different renormalisation prescriptions for α yield a effects between 2-5 GeV. Their total size is similar to the expected MSSM-effects [38].

- Higher-order effects from different renormalisation prescriptions for α yield no significant differences to the corresponding effect in the MSSM. The genuine NMSSM-effect remains $\lesssim 200$ MeV for all studied scenarios. Thus it remains small compared to the studied higher-order effects from the top-/stop-sector.

The comparison of different renormalisation prescriptions has been used to study the order of unknown higher-order correction. The investigation at the one-loop level revealed that genuine NMSSM-contributions from the Higgs- and gauge-sector can be sizeable. However, only the $\overline{\text{DR}}$ results in the gaugeless limit are available so far for the Higgs-sector contributions at the two-loop level. The resummation of large logarithms, which is only contained in `NMSSM-FeynHiggs`, can yield additional contributions in the range of several GeV for SUSY masses of more than 2 TeV [37]. Appropriate estimates of theoretical uncertainties are necessary for for different parameter regions taking into account the type of corrections implemented in different codes.

10 Conclusion

The goal of the work presented in this thesis was to provide precise predictions for the Higgs-masses and related quantities in the Next-to-Minimal Supersymmetric Standard Model (NMSSM). Such precise predictions are important for an accurate interpretation of the Higgs signal discovered in 2012 at the LHC and the already very precise determination of its mass.

We presented a detailed discussion of the Higgs-mass prediction in the NMSSM for the full and partial contributions at the one-loop level, while at two-loop order the result was approximated with the known corrections from the Minimal Supersymmetric Standard Model (MSSM). The applied MSSM approximation was motivated by a detailed study of analytic and numeric properties of the one-loop contributions and numeric properties of the two-loop contributions in Chapters 6 and 8.

The status of automated higher-order calculations in the NMSSM with real and complex parameters for the tools `FeynHiggs`, `FeynArts` and `FormCalc` and upcoming improvements as a consequence of this work were briefly discussed in Chapter 7.

Furthermore, we presented first results for an estimation of theoretical uncertainties in the NMSSM from genuine NMSSM-effects in Chapter 9.

NMSSM Higgs-mass prediction

The Higgs-masses in the Next-to-Minimal Supersymmetric Standard Model (NMSSM) can receive potentially large higher-order corrections. In order to provide a precise prediction for the Higgs-masses, these higher-order contributions have to be calculated and included. We provided Higgs-mass predictions for the $\mathcal{CP}$-even and -odd sectors, that contain a full calculation of the momentum-dependent one-loop correction and added the known, momentum-independent MSSM two-loop corrections of $\mathcal{O}(\alpha_s\alpha_t, \alpha_t^2, \alpha_s\alpha_b, \alpha_t\alpha_b)$ to the result. The terms neglected by the MSSM approximation are genuine contributions for the gauge-singlet Higgs-field and its mixing with the remaining Higgs-fields at higher-orders. Our approximation is intended for the use in scenarios where the NMSSM remains predictive up to the GUT-scale M_{GUT}.

For the one-loop contributions from the sfermions the genuine MMSSM contributions are sub-leading to the corresponding MSSM-like contributions, if one demands perturbativity of the theory up to the scale M_{GUT}, which implies that $\lambda \lesssim 0.7$. The suppression of the genuine NMSSM-contributions is caused by a relative suppression of the singlet–sfermion couplings compared to the according doublet–sfermion couplings by small values of λ and large values of μ_{eff}. For large values of λ the genuine NMSSM one-loop corrections from sfermions become larger. However, we found that for such cases the genuine NMSSM-contribution from the Higgs-sector, that grow faster with λ can be more important, especially for the mass of a singlet-like state.

The behaviour of the genuine NMSSM contributions at the one-loop level suggests a similar behaviour of the genuine NMSSM contributions at the two-loop level. We have tested this assumption by comparing the result including contributions of $\mathcal{O}(\alpha_t\alpha_s)$ between the MSSM approximation and the NMSSM contributions available in the code `NMSSMCalc` in a genuine NMSSM scenario where the second lightest state is responsible for the Higgs signal at around 125 GeV. We found that they were still sub-leading to their MSSM-counterparts at two-loop order, especially for the mass of a (MS)SM-like Higgs-field. These results suggest that the MSSM-approximation is applicable for two-loop corrections beyond $\mathcal{O}(\alpha_t\alpha_s)$. However, the $\overline{\text{DR}}$-results for the NMSSM two-loop contributions from the Higgs-sector imply that the genuine NMSSM corrections from the fermions are in comparison also sub-leading as they are at the one-loop level.

The dependence of the mass of a singlet-like state on the trilinear breaking parameter of the stop sector, A_t, has been investigated. We found that even for a doublet-admixture of less than 1% the dependence on A_t can be dominated by the A_t-dependence of the admixed doublet-like fields.

Automated higher-order calculations

The renormalisation scheme developed in this work forms the basis for a `FeynArts` model file for the NMSSM with complex parameters. It will include all one-loop counterterms to allow automatic higher-order calculations. Based on the presented results the code `FeynHiggs` will be extended to provide NMSSM Higgs-mass predictions and the calculation of the wave function normalisation matrix $\hat{\mathbf{Z}}$ with renormalised self-energy contributions up to the two-loop level in the applied MSSM approximation.

Theoretical Uncertainties for NMSSM Higgs-mass Predictions

As a first step for estimating the intrinsic theoretical uncertainties of NMSSM Higgs-mass predictions, the comparison of different renormalisation prescriptions implemented in the codes `NMSSMCalc` and `NMSSM-FeynHiggs` has been used to study the order of unknown higher-order corrections.

We compared our results of `NMSSM-FeynHiggs` with the code `NMSSMCalc` for contributions of up to $\mathcal{O}(\alpha_t\alpha_s)$. We found that higher-order effects induced by different renormalisation prescriptions for the electromagnetic coupling α and the top-/stop-masses are of similar size to the according difference in the MSSM calculation. The higher-order effects induced by different renormalisation prescriptions for the strong coupling α_s are minor compared to higher-order effects induced by a possible RGE-evolution of α_s, that can be induced by choosing a non-standard renormalisation scale for the Higgs-mass calculation implemented in `FeynHiggs`. The standard renormalisation scale for the Higgs-mass predictions in `FeynHiggs` is either the on-shell, $\overline{\text{MS}}$ or $\overline{\text{DR}}$ mass of the top-quark, that is used in the calculation. By including MSSM corrections beyond $\mathcal{O}(\alpha_t\alpha_s)$ an additional sizeable higher-order effect is induced that reaches up to 8 GeV. The investigation at the one-loop level revealed that genuine NMSSM-contributions from the Higgs- and gauge-sector can be sizeable. However,

only the $\overline{\mathrm{DR}}$ results in the gaugeless limit are available so far for the Higgs-sector contributions at the two-loop level and can yield a sizeable effect for the studied scenarios between 1 and 2 GeV. The resummation of large logarithms, which is only contained in `NMSSM-FeynHiggs`, can yield additional contributions in the range of several GeV for SUSY masses of more than 2 TeV. For appropriate estimates of theoretical uncertainties in the NMSSM are necessary for different parameter regions taking into account the type of corrections implemented in different codes.

A Appendix: Theory

A.1 Conventions and Notation

A.1.1 Conventions

The metric tensor is defined as follows

$$g_{\mu\nu} = \text{diag}\,(1, -1, -1, -1).\qquad\text{(A.1)}$$

The γ-matrices are given in the Weyl representation by

$$\gamma^\mu = \begin{pmatrix} 0 & \sigma^\mu \\ \bar{\sigma}^\mu & 0 \end{pmatrix} \text{ where } \sigma^\mu = (\mathbb{1}, \vec{\sigma})\,,\ \bar{\sigma}^\mu = (\mathbb{1}, -\vec{\sigma})\qquad\text{(A.2)}$$

with the three dimensional Pauli matrices $\vec{\sigma}$. From these matrices the left- and right-chiral projectors for Dirac fermions,

$$P_{\mathrm{L}} = \frac{1}{2}\left(1 - \gamma^5\right) \text{ and } P_{\mathrm{R}} = \frac{1}{2}\left(1 + \gamma^5\right),\qquad\text{(A.3)}$$

can be formed with $\gamma^5 = \mathrm{i}\gamma^0\gamma^1\gamma^2\gamma^3$. The elementary charge e is defined positive in this work, $e > 0$.

A.1.2 Grassmann Numbers

The left-sided derivative of Grassmann coordinates from chapter A.3.1 can be defined by

$$\partial^\alpha \vartheta_\beta \equiv \frac{\partial}{\partial \vartheta_\alpha} \vartheta_\beta := \delta^\alpha_\beta,\ \bar{\partial}^{\dot\alpha}\vartheta_{\dot\beta} \equiv \frac{\partial}{\partial\bar{\vartheta}_{\dot\alpha}}\bar{\vartheta}_{\dot\beta} := \delta^{\dot\alpha}_{\dot\beta}.\qquad\text{(A.4)}$$

The integral over a Grassman variable can be defined by its application to a general superfield (A.38),

$$\int \mathrm{d}\vartheta_\alpha F(x, \vartheta, \bar{\vartheta}) := \sqrt{2}\xi_\alpha(x),\qquad\text{(A.5)}$$

$$\int \mathrm{d}\bar{\vartheta}_\alpha F(x, \vartheta, \bar{\vartheta}) := \sqrt{2}\chi_\alpha(x),\qquad\text{(A.6)}$$

$$\int \mathrm{d}^2\vartheta F(x, \vartheta, \bar{\vartheta}) := M(x),\qquad\text{(A.7)}$$

$$\int \mathrm{d}^2\bar{\vartheta} F(x, \vartheta, \bar{\vartheta}) := N(x),\qquad\text{(A.8)}$$

$$\int \mathrm{d}^2\vartheta \mathrm{d}^2\bar{\vartheta} F(x,\vartheta,\bar{\vartheta}) := \frac{1}{2} D(x). \tag{A.9}$$

A.1.3 $SU(2)_\mathrm{L}$-invariant Product

The product of two $SU(2)_\mathrm{L}$-doublets Φ_1 and Φ_2 is defined by

$$\Phi_1 \cdot \Phi_2 = \epsilon_{\alpha\beta}\Phi_1^\alpha\Phi_2^\beta, \quad \epsilon_{\alpha\beta} = \begin{pmatrix} 0 & -1 \\ 1 & 0 \end{pmatrix}_{\alpha\beta}. \tag{A.10}$$

A.2 $SU(N)$ invariant Yang–Mills Theory

The invariant action S of a field theory is given by

$$S = \int \mathrm{d}^4x\ \mathcal{L}. \tag{A.11}$$

Invariance of the measure under Poincaré- and local $SU(N)$ gauge-transformations leads to an invariant Lagrangian under the same transformations. Its parts will be outlined in the following section. For an abelian group the relations in this section hold for vanishing structure functions.

A.2.1 Poincaré Invariance and allowed kinetic Terms

The fields of a relativistic invariant quantum field theory (QFT) transform under a representation of the Poincaré-group, which is formed by the Lie algebra

$$[P^\mu, P^\nu] = 0\ , \tag{A.12a}$$

$$[P^\mu, J^{\rho\sigma}] = \mathrm{i}\,(g^{\mu\rho}P^\sigma - g^{\mu\sigma}P^\rho)\ , \tag{A.12b}$$

$$[J^{\mu\nu}, J^{\rho\sigma}] = \mathrm{i}\,(-g^{\mu\rho}J^{\nu\sigma} + g^{\nu\rho}J^{\mu\sigma} - g^{\nu\sigma}J^{\mu\rho} + g^{\mu\sigma}J^{\nu\rho}) \tag{A.12c}$$

of its generators P^μ and $J^{\mu\nu}$. This invariance determines the structure of all possible terms in the Lagrangian density. All so far observed elementary particles in nature carry either spin 0, 1/2 or 1. The allowed kinetic terms for complex scalar (ϕ, spin 0), fermion (ψ, spin 1/2) and vector (A^μ, spin 1) fields are[1]

$$\begin{aligned} \mathcal{L}_\mathrm{kin} &= \mathcal{L}_\mathrm{kin,scalar} + \mathcal{L}_\mathrm{kin,fermion} + \mathcal{L}_\mathrm{kin,vector} \\ &= -\phi^\dagger\partial_\mu\partial^\mu\phi + \bar{\psi}\slashed{\partial}\psi - \frac{1}{4}F^{\mu\nu}F_{\mu\nu}, \end{aligned} \tag{A.13}$$

where $\bar{\psi} = \psi^\dagger\gamma^0$, $\slashed{\partial} = \gamma^\mu\partial_\mu$ and $F^{\mu\nu}$ denotes the total antisymmetric field-strength tensor. The kinetic term (A.13) describes massless, non-interacting, relativistic fields.

---

[1]Terms involving the dual field strength tensor lead to total derivatives that do not contribute to the action.

A.2.2 Gauge Invariance

The choice of the gauge group under which the Lagrangian of the theory remains invariant determines the described interaction. All fields of the theory that are charged under a specific generator have to be given in a specific multiplet representation of the according gauge group. For this work only the (anti-)fundamental and adjoint representations are necessary.

A field F that is charged under a gauge group $SU(N)$ is given in the fundamental representation, the corresponding anti field $\bar{F}$ is given in the anti-fundamental representation. The field F transforms under $SU(N)$ as

$$F(x) \rightarrow \exp\left[-\mathrm{i}\boldsymbol{\alpha}(x)\right]F(x). \tag{A.14}$$

Fields uncharged under the gauge group transform trivially as a singlet. The bold faced $\boldsymbol{\alpha}$ is given in the adjoint representation of $SU(N)$ and can be written with its generators $\boldsymbol{T}_a$

$$\boldsymbol{\alpha}(x) = g \sum_{a=1}^{N^2-1} \alpha_a(x)\boldsymbol{T}_a \tag{A.15}$$

Here g is the real valued coupling constant of the theory. Since fields in the adjoint representation are of matrix value, they are bold faced in the following. The $N^2 - 1$ generators for $SU(N)$ fulfil the commutation relations

$$[\boldsymbol{T}_a, \boldsymbol{T}_b] = \mathrm{i}g f_{abc}\boldsymbol{T}_c \tag{A.16}$$

with the structure constants f_{abc}. The spin-one fields $\boldsymbol{V}^\mu$ of the theory are given in the adjoint representation of $SU(N)$,

$$\boldsymbol{V}_\mu = g \sum_{a=1}^{N^2-1} V_\mu^a \boldsymbol{T}^a \tag{A.17}$$

and transform as

$$\boldsymbol{V}_\mu \rightarrow \boldsymbol{V}_\mu + \partial_\mu \boldsymbol{\alpha} + \mathrm{i}\left[\boldsymbol{\alpha}, \boldsymbol{V}_\mu\right], \tag{A.18a}$$

which reads in components

$$V_{\mu,a} \rightarrow V_{\mu,a} + \partial_\mu \alpha_a + g f_{abc} V_\mu^b \alpha^c. \tag{A.18b}$$

To maintain gauge invariance of the kinetic terms given in (A.13), the transition from the derivative to the covariant derivative has to be performed for the fermions and scalars of the the theory,

$$\mathbb{1}\partial_\mu \rightarrow \boldsymbol{D}_\mu = \mathbb{1}\partial_\mu + \mathrm{i}\boldsymbol{V}_\mu = \mathbb{1}\partial_\mu + \mathrm{i}g \sum_{a=1}^{N^2-1} V_\mu^a \boldsymbol{T}^a. \tag{A.19}$$

The field-strength tensor for the spin-one fields is now given by the covariant derivative

$$\boldsymbol{V}_{\mu\nu} = \frac{\mathrm{i}}{g}\left[\boldsymbol{D}_\mu, \boldsymbol{D}_\nu\right] = \frac{1}{g}\left(\partial_\mu \boldsymbol{V}_\nu - \partial_\nu \boldsymbol{V}_\mu - \left[\boldsymbol{V}_\mu, \boldsymbol{V}_\nu\right]\right) \tag{A.20a}$$

which reads in components

$$V^a_{\mu\nu} = \partial_\mu V^a_\nu - \partial_\nu V^a_\mu - \mathrm{i}g f_{abc} V^b_\mu V^c_\nu. \tag{A.20b}$$

The component fields V^a_μ are called gauge bosons. For more than one gauge group the transformations for the fields (A.14) and the covariant derivative (A.19) can be extended by additional transformations.

The kinetic terms for the fermions and gauge bosons in a gauge theory with an $SU(N)$ invariance read

$$\mathcal{L}_{\mathrm{kin}} = \sum_i \bar{\psi}^i \slashed{D} \psi^i - \mathrm{Tr}\left[\boldsymbol{V}^{\mu\nu} \boldsymbol{V}_{\mu\nu}\right], \tag{A.21}$$

where the index i sums over all fermion multiplets and singlets and the trace is understood over the component fields

$$\mathrm{Tr}\left[\boldsymbol{V}^{\mu\nu}\boldsymbol{V}_{\mu\nu}\right] = \sum_{a=1}^{N^2-1} V^{a,\mu\nu} V^a_{\mu\nu}. \tag{A.22}$$

A.2.3 Spontaneous Symmetry-Breaking

Mass terms for gauge bosons violate gauge invariance explicitly. To maintain a description of vector bosons within a framework of gauge theories the mechanism of spontaneous symmetry-breaking can be used. In order to generate mass terms for gauge bosons by spontaneous symmetry breaking a Lorentz-scalar, the Higgs field Φ, in the fundamental representation of $SU(N)$ can be introduced to the theory. The Lagrangian for this field is given by

$$\mathcal{L}_{\mathrm{Higgs}} = \left(\boldsymbol{D}_\mu \Phi\right)^\dagger \left(\boldsymbol{D}^\mu \Phi\right) - V_{\mathrm{H}}(\Phi) \tag{A.23}$$

with the Higgs potential V_H. The Higgs field can be decomposed as

$$\Phi = \underline{v} + \underline{\phi} = \underline{v} + \underline{\varphi} + \underline{\chi} \tag{A.24}$$

into multiplets in the fundamental representation of $SU(N)$ for the constant vacuum expectation-value $\underline{v}$ and fields $\underline{\phi}$. To avoid confusion between symbols the underlined quantities in the decomposition are multiplets in the fundamental representation of $SU(N)$. The component fields are distinguished by an index. The fields $\underline{\phi}$ can be further decomposed into the physical Higgs fields $\underline{\varphi}$ and the massless Goldstone bosons $\underline{\chi}$, that accompany spontaneous breaking of continuous symmetries [137–139]. These Goldstone modes can be absorbed into the gauge bosons by a gauge transformation

and thus the vector bosons gain a longitudinal degree of freedom. Demanding the decomposition of (A.24) breaks the $SU(N)$ symmetry spontaneously. The explicit form of $\underline{v}$ is determined by requiring that $V_H(\underline{v})$ is minimal at the classical level.

The mass terms for the gauge bosons are obtained by inserting the vacuum-expectation value into the kinetic term of the Higgs field,

$$\left(\boldsymbol{D}_\mu v\right)_i^\dagger \left(\boldsymbol{D}^\mu v\right)_i = g^2 \left[v_j^* \left(T_{ji}^a\right)^\dagger T_{ik}^b v_k\right] V_\mu^a V^{b,\mu} \equiv \left(M_V^2\right)_{ab} V_\mu^a V^{b,\mu}. \tag{A.25}$$

Here M_V^2 is the squared mass matrix for the gauge bosons.

A.2.4 Quantisation

It is not possible to quantise the Lagrangian (A.13) naively, since one would quantise unphysical degrees of freedom of the gauge bosons. Gauge invariance is a symmetry of the classical (unquantised) theory and alone is not sufficient to construct quantised vector fields that suffice the commutation relations of canonical quantisation. A generalisation of the gauge symmetry that holds for the quantised theory provides a way to circumvent these problems. This symmetry is called Becchi–Rouet–Stora—Tyutin (BRST) symmetry [140–143]. It allows to add BRST-invariant terms that violate gauge invariance explicitly. Additionally, new, unphysical degrees of freedom, the so called ghost fields, are introduced for each of the vector fields.

With the BRST operator s [69] the gauge fixing and ghost terms reads

$$\mathcal{L}_{\text{fix+ghost}} = \mathcal{L}_{\text{ghost}} + \mathcal{L}_{\text{fix}} = s \left(\bar{u}^a F^a\right). \tag{A.26}$$

The implicit sum over the group indices is understood here and in the following. Here $\bar{u}^a$ is the antighost field and F^a the gauge fixing functional, which can be written as

$$F^a = \frac{\xi_A}{2} B^a + C^a[\boldsymbol{A}_\mu], \quad B^a = -\frac{1}{\xi} C^a. \tag{A.27}$$

The real parameter ξ_A is called a gauge-fixing parameter. Here B^a is an auxiliary field, the Nakanishi–Lautrup field that can be eliminated by its equation of motion, and C^a is a functional depending of the vector field itself. The C^a can be chosen arbitrarily. A convenient choice for C^a is the R_ξ-gauge,

$$C^a = \partial^\mu A_\mu^a + \mathrm{i}g\xi_A' v_i T_{ij}^a \phi_j, \tag{A.28}$$

which avoids gauge boson–Goldstone mixing propagators at tree-level. Here g is the coupling constant of the gauge group. Inserting (A.27) and (A.28) into (A.26) yields for the kinetic terms of the ghost fields u^a

$$\mathcal{L}_{\text{ghost}} = \mathrm{i}\bar{u}^a \left[\partial^\mu D_\mu^{ab} - \xi_A' (M_{\text{ghost}}^2)^{ab} - \xi_A' g^2 v_i^* \left(T_{ij}^a\right)^\dagger T_{jk}^b \phi_k\right] u^b, \tag{A.29}$$

with the covariant derivative D_μ and the ghost mass matrix

$$(M_{\text{ghost}}^2)^{ab} = g^2 v_i^* \left(T_{ij}^a\right)^\dagger T_{jk}^b v_k. \tag{A.30}$$

The kinetic term gives rise to couplings of the ghosts to gauge bosons and Higgs fields of the theory. The mass of the ghost fields depends on the choice of the gauge-fixing parameter ξ_A. The result for the gauge-fixing term is

$$\mathcal{L}_{\text{fix}} = -\frac{1}{2\xi_A} \left|C^a\right|^2 = -\frac{1}{2\xi_A} \left|\partial^\mu A_\mu^a + \mathrm{i}g\xi_A' v_i T_{ij}^a \chi_j\right|^2. \tag{A.31}$$

It leads to mass terms for the Goldstone bosons

$$\left(M_\chi^2\right)_{ij} \chi_i \chi_j = -\frac{(\xi_A')^2}{\xi_A} g^2 \left(\chi_i T_{ij}^a v_j^*\right)\left(v_k T_{kj}^b \chi_j\right), \tag{A.32}$$

that are also dependent of the gauge-fixing parameters.

A.2.5 Lagrangian

The Lagrangian from eq. (A.11) for a spontaneously broken Yang–Mills theory is given by the sum of the aforementioned parts,

$$\mathcal{L} = \mathcal{L}_{\text{kin}} + \mathcal{L}_{\text{Higgs}} + \mathcal{L}_{\text{fix + ghost}}. \tag{A.33}$$

A.3 $SU(N)$ invariant Super-Yang–Mills Theory

A Super-Yang–Mills theory is the supersymmetric extension of a Yang–Mills theory. The Poincaré-invariance is extended in the only non-trivial way, which leads to an increase of the number of degrees of freedom. Super gauge invariance, the supersymmetric version of gauge invariance, generates furthermore additional interactions that are not present without supersymmetry.

A.3.1 Super-Poincaré Invariance and allowed kinetic Terms

According to the theorem of Haag, Łopuszański and Sohnius [144] the Poincaré group (A.12) can only be extended nontrivially by fermionic operators. The N new fermionic generators $Q_{i,\alpha}$ ($i \in \{1, \ldots, N\}$) form together with the generators from (A.12) the Super-Poincaré group. The new generators fulfil the anticommutation relations

$$\{Q_{i,\alpha}, Q_{i,\alpha}\} = 0, \quad \{\bar{Q}_i^{\dot{\alpha}}, \bar{Q}_i^{\dot{\alpha}}\} = 0. \tag{A.34}$$

In the supersymmetric extensions discussed in the following only one additional fermionic generators is added ($N = 1$). The Lie algebra of the Super-Poincaré group

is thus formed by

$$\{Q_\alpha, \bar{Q}_{\dot\beta}\} = 2\,(\sigma^\mu)_{\alpha\dot\beta}\,P_\mu\,, \qquad \{Q_\alpha, Q_\beta\} = \{\bar{Q}^{\dot\alpha}, \bar{Q}^{\dot\beta}\} = 0\,, \qquad \text{(A.35a)}$$

$$[Q_\alpha, P^\nu] = 0\,, \qquad\qquad [Q_\alpha, J^{\mu\nu}] = -\,(\sigma^{\mu\nu})_\alpha{}^\beta Q_\beta\,. \qquad \text{(A.35b)}$$

With the extension of the Poincaré algebra it is necessary to change the field degrees of freedom of the theory. Additionally to the four space-time coordinates x^μ two more two-dimensional fermionic coordinates ϑ_α and $\bar{\vartheta}_{\dot\alpha}$ ($\alpha, \dot\alpha \in \{1,2\}$) are introduced. All tupels $(x, \vartheta, \bar{\vartheta})$ together form the superspace. With them the fermionic generators are given by

$$Q_\alpha = -\mathrm{i}\left(\partial_\alpha + \mathrm{i}\,(\sigma^\mu)_{\alpha\dot\beta}\,\bar{\vartheta}^{\dot\beta}\partial_\mu\right) \quad \text{and} \quad \bar{Q}^{\dot\alpha} = -\mathrm{i}\left(\bar{\partial}^{\dot\alpha} + \mathrm{i}\,(\bar{\sigma}^\mu)^{\dot\alpha\beta}\,\vartheta_\beta\partial_\mu\right). \qquad \text{(A.36)}$$

Due to the extension of the space-time coordinates to the superspace, the covariant derivative D_μ (A.19) needs to be extended. The extension describing the derivative with respect to the new Grassman variables ϑ_α and $\bar{\vartheta}^{\dot\alpha}$ read

$$D_\alpha = \partial_\alpha - \mathrm{i}\,(\sigma^\mu)_{\alpha\dot\beta}\,\bar{\vartheta}^{\dot\beta}\partial_\mu \quad \text{and} \quad \bar{D}^{\dot\alpha} = \bar{\partial}^{\dot\alpha} - \mathrm{i}\,(\bar{\sigma}^\mu)^{\dot\alpha\beta}\,\vartheta_\beta\partial_\mu\,. \qquad \text{(A.37)}$$

These fermionic derivatives transform covariantly on the superspace. They anticommute with the new Grassmann variables and the new generator (A.36). The field degrees of freedom are described as fields on superspace. They are polynomials in ϑ and $\bar{\vartheta}$ up to the order $\vartheta^4 = \vartheta_\alpha\vartheta^\alpha\bar{\vartheta}_{\dot\beta}\bar{\vartheta}^{\dot\beta}$, where the sum over the indices on the right side is understood,

$$\begin{aligned} F(x, \vartheta, \bar{\vartheta}) =&\, f(x) + \sqrt{2}\vartheta\xi(x) + \sqrt{2}\bar{\vartheta}\bar{\chi}(x) + \vartheta\vartheta M(x) + \bar{\vartheta}\bar{\vartheta}N(x) \\ &+ \vartheta\sigma^\mu\bar{\vartheta}A_\mu(x) + \vartheta\vartheta\bar{\vartheta}\bar{\lambda}(x) + \bar{\vartheta}\bar{\vartheta}\vartheta\zeta(x) + \frac{1}{2}\vartheta\vartheta\bar{\vartheta}\bar{\vartheta}D(x)\,. \end{aligned} \qquad \text{(A.38)}$$

The fields described in A.13 appear as complex component fields, but not all of them have a physical meaning. To describe physical fields, special cases of this general superfield are needed.

Chiral Superfields

To describe the SM fermions and their superpartners chiral and antichiral superfields Φ and $\Phi^\dagger$ are used. They are defined by

$$\begin{aligned} \bar{D}^\alpha\Phi = 0 \quad \Leftrightarrow \quad \Phi(x, \vartheta, \bar{\vartheta}) &= \exp\left(-\mathrm{i}\vartheta\sigma^\mu\bar{\vartheta}\right)\phi(x, \vartheta) \\ &= A(y) + \sqrt{2}\vartheta\xi(y) + \vartheta\vartheta F(y) \\ &= \phi(y, \vartheta) \end{aligned} \qquad \text{(A.39)}$$

with $y = x + \mathrm{i}\vartheta\sigma^\mu\bar{\vartheta}$. A chiral superfield contains a complex scalar field A, a Weyl-spinor field and a complex auxiliary field F without dynamic terms. Thus the chiral superfield contains the same number of fermionic and bosonic degrees of freedom.

Vector Superfields

To describe the gauge vector-fields, general superfields V with the property

$$V = V^\dagger \tag{A.40}$$

are used. This condition constrains the component fields from the general superfield (A.38): The fields f, A_μ and D have to be real and $M = N^\dagger$, $\xi = \chi$, $\lambda = \zeta$. The definitions of the vector superfield in a gauge theory allows another constraint using a chiral superfield Λ in the form of a super gauge-transformation,

$$V \to V' = V + i\left(\Lambda - \Lambda^\dagger\right) \,, \tag{A.41}$$

Under this transformation the vector field transforms analogous to a classical gauge transformation, $A_\mu \to A_\mu - 2\partial_\mu \operatorname{Im} f$. In the Wess–Zumino gauge [145] a special choice for Λ gauges the component fields f, ξ and M to zero. Thus the form of the vector superfield in this gauge reads

$$V_{\mathrm{WZ}} = \vartheta\sigma^\mu\bar\vartheta A_\mu(x) + \vartheta\vartheta\bar\vartheta\bar\lambda(x) + \bar\vartheta\bar\vartheta\vartheta\lambda(x) + \frac{1}{2}\vartheta\vartheta\bar\vartheta\bar\vartheta D(x). \tag{A.42}$$

The field D is an auxiliary field without an own dynamic. The resulting field contains three real, bosonic degrees of freedom with A_μ and four fermionic degrees of freedom with λ and $\bar\lambda$.

Kinetic Terms

By introducing a left- and right-chiral field strength

$$\mathcal{W}_\alpha = -\frac{1}{4}\bar D_{\dot\beta}\bar D^{\dot\beta}D_\alpha V_{\mathrm{WZ}}, \quad \bar{\mathcal{W}}^{\dot\alpha} = -\frac{1}{4}D^\beta D_\beta \bar D^{\dot\alpha}V_{\mathrm{WZ}}, \tag{A.43}$$

the kinetic terms for a chiral superfield and a vector superfield in the Wess–Zumino gauge read

$$\mathcal{L}_{\mathrm{kin}} = \int \mathrm{d}^2\vartheta\,\mathrm{d}^2\bar\vartheta\ \Phi^\dagger\Phi + \left(\int \mathrm{d}^2\vartheta\,\mathcal{W}_\alpha\mathcal{W}^\alpha + \mathrm{h.c.}\right). \tag{A.44}$$

This term contains the kinetic as given in (A.13) for all component fields according to their spin.

A.3.2 Super Gauge-Invariance

A (anti-)chiral superfield that is charged under a gauge group $SU(N)$ is given in the (anti-)fundamental representation of the gauge group. A vector superfield V containing the gauge bosons of $SU(N)$ as component fields is given in the adjoint representation. They transform under a super-gauge transformation as

$$\Phi \longrightarrow e^{-i\boldsymbol{\Lambda}}\Phi, \quad \Phi^\dagger \longrightarrow \Phi^\dagger e^{i\boldsymbol{\Lambda}^\dagger}, \quad e^{2\boldsymbol{V}} \longrightarrow e^{-i\boldsymbol{\Lambda}}e^{2\boldsymbol{V}}e^{i\boldsymbol{\Lambda}^\dagger}. \tag{A.45}$$

Here the bold faced fields are given in the adjoint representation of $SU(N)$,

$$\boldsymbol{V} = gV^a\frac{T^a}{2}, \quad \boldsymbol{\Lambda} = g\Lambda^a\frac{T^a}{2}. \tag{A.46}$$

The left- and right-chiral field strength is derived from the component fields,

$$\mathcal{W}^a_\alpha = -\frac{1}{4}\bar{D}_{\dot\beta}\bar{D}^{\dot\beta}D_\alpha V^a, \quad \bar{\mathcal{W}}^{\dot\alpha}_a = -\frac{1}{4}D^\beta D_\beta \bar{D}^{\dot\alpha}V_a. \tag{A.47}$$

With these transformations the super-gauge invariant kinetic term for one chiral and one vector superfields reads

$$\mathcal{L}_{\text{kin}} = \int \mathrm{d}^2\vartheta\mathrm{d}^2\bar\vartheta \ \Phi^\dagger\mathrm{e}^{2\boldsymbol{V}}\Phi + \left(\int \mathrm{d}^2\vartheta \ \mathcal{W}^a_\alpha\mathcal{W}^\alpha_a + \text{h.c.}\right). \tag{A.48}$$

The kinetic terms for a vector superfield as given in (A.44) remain invariant under a super-gauge transformation (A.41). Together the terms (A.48) are known as the Kähler potential. The Kähler potential gives rise to quartic interactions between the scalar components of chiral and anti-chiral superfields that are defined by the gauge-couplings. They stem from the auxiliary component fields.

A.3.3 SUSY electroweak Symmetry-Breaking and Soft SUSY-Breaking Terms

Demanding Super-Poincaré invariance of the action implies additional interaction terms between chiral superfields. The renormalisable terms that can be written down are polynomials in either chiral or anti-chiral superfields up to the third power,

$$W = a_i\Phi_i + b_{ij}\Phi_i\Phi_j + c_{ijk}\Phi_i\Phi_j\Phi_k \tag{A.49}$$

with the complex coupling matrices a, b, and c. These terms can be used to implement mass terms for the superfields by the BEH-mechanism as described in section 2.1.2. Since the superpotential has to be a polynomial in either chiral or antichiral superfields, at least two Higgs superfields are necessary to create mass terms for leptons, up- and down-type quarks. These mass terms stem from the trilinear terms in eq. (A.49).

Soft Supersymmetry-Breaking

With the superpotential of eq. (A.49) the mass term generates an identical mass for all components of a fermion/sfermion superfield. The same happens also for the masses of the gauge bosons and their superpartners, although their mass terms are generated in the Kähler potential. However, no superpartners have been observed until today [41]. To allow for different superpartner masses while conserving gauge invariance and renormalisability of the theory soft-breaking terms have to be introduced. These are additional terms of the supersymmetric Lagrangian involving only

superpartner fields. They can have the form

$$\mathcal{L}_{\text{soft}} = \mathcal{L}_{\text{soft}}^{\text{scalar}} + \mathcal{L}_{\text{soft}}^{\text{fermion}}, \quad \mathcal{L}_{\text{soft}}^{\text{scalar}} = a_i A_i + b_{ij} A_i A_j + c_{ijk} A_i A_j A_k,$$
$$\mathcal{L}_{\text{soft}}^{\text{fermion}} = M_{ij} \operatorname{Tr} \bar{\boldsymbol{\lambda}}_i \boldsymbol{\lambda}_j = M_{ij} \bar{\lambda}_i^a \lambda_j^a. \tag{A.50}$$

The breaking parameter matrices a, b, c and M can be complex. Soft-breaking terms break supersymmetry while keeping gauge invariance intact.

A.3.4 Quantisation

The quantisation described in sec. A.2.4 for the non-supersymmetric case is not applicable directly to supersymmetric theories. The BRST-symmetry sector has to be extended to a supersymmetric form in order to define supersymmetric BRST-invariant gauge-fixing terms. The extended gauge fixing term can give rise to additional parameters that need to be renormalised. The additional counterterms of this sector are finite and can be used to restore supersymmetric properties of a calculation if they are violated due to a regularisation procedure. Their explicit form has to be derived directly from the symmetry-relations of the theory, the Slavnov–Taylor-identities [66, 146].

For Higgs-mass calculations in the Minimal and Next-to-Minimal Supersymmetric Standard Models as described in this work the extended, supersymmetric gauge-fixing sector can be neglected. It has been shown that the applied dimensional reduction conserves supersymmetry for the full one-loop calculation and the used two-loop calculations in the electroweak gaugeless limit [68]. For the one-loop calculation the non-supersymmetric gauge-fixing term as described in [68] is sufficient.

B Appendix: Numerical Results

B.1 Derived Masses in the Sample Scenario

The chargino- and stop-masses are independent of λ. They read

$$m^2_{\chi^\pm_1} = 110.1 \text{ GeV}, \quad m^2_{\chi^\pm_2} = 326.2 \text{ GeV}, \quad m^2_{\tilde{t}_1} = 1388.8 \text{ GeV}, \quad m^2_{\tilde{t}_2} = 1620.8 \text{ GeV}. \tag{B.1}$$

The neutralino masses are λ-dependent due to the λ-dependent singlino mass-terms. They are plotted as a function of λ in fig. B.1. For $\lambda \lesssim 0.14$ the heaviest neutralino field χ^0_5 is singlet-like, for values $\lambda \gtrsim 0.14$ the second-heaviest field χ^0_4 is singlet-like. For large values of λ all fields besides χ^0_5 obtain a singlet component and thus a λ-dependent mass.
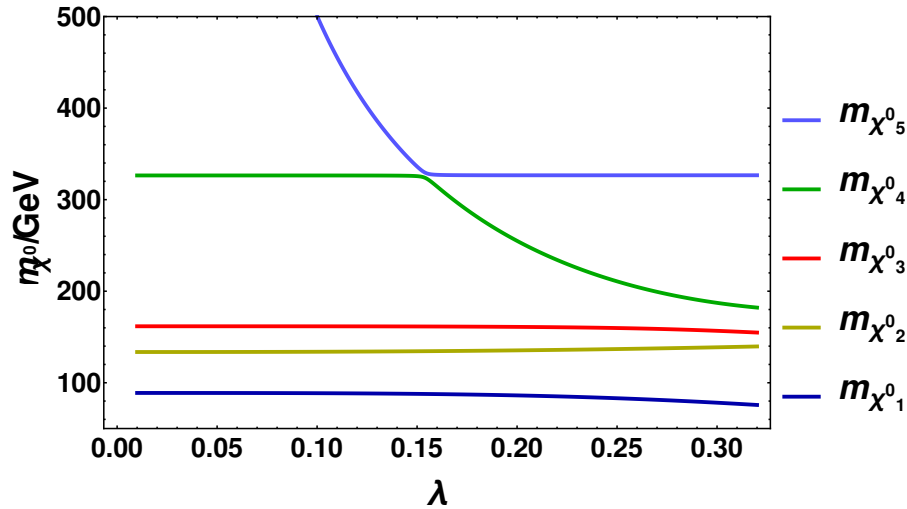

Figure B.1: Neutralino masses in the sample scenario of chap. 8.

B.2 Input Parameters for the Comparison with `NMSSMCalc`

The SM input parameters for the comparison are taken from the built-in SLHA input file,

$$\alpha(M_Z) = 128.962 \cdot 10^2 \tag{B.2a}$$

$$\alpha_s^{\overline{\text{MS}}}(M_Z) = 0.1190 \tag{B.2b}$$

$$m_t^{\text{OS}} = 172.5 \text{ GeV} \tag{B.2c}$$

$$m_b^{\overline{\text{MS}}}(m_b) = 4.19 \text{ GeV} \tag{B.2d}$$

$$m_\tau^{\text{OS}} = 1.77684 \text{ GeV}. \tag{B.2e}$$

B.3 Numerical results for Comparison with `NMSSMCalc`

The tree-level Higgs-masses are given in tab. B.1. The masses of the $\mathcal{CP}$-even Higgs-

	Comparison I			Comparison II		
	m_{h_1}	m_{h_2}	m_{h_3}	m_{h_1}	m_{h_2}	m_{h_3}
TP1	**88.23**	*1797.49*	2768.59	**88.41**	*1795.71*	2842.02
TP2	**89.22**	*5949.75*	6369.10	–	–	–
TP3	*76.34*	**105.78**	653.62	*58.70*	**108.70**	665.17
TP4	**107.35**	*138.05*	466.69	**100.03**	*135.15*	475.25
TP5	**100.64**	*120.03*	625.57	**94.76**	*109.46*	631.22

Table B.1: Tree-level Higgs-masses for the TP-scenarios at the high and the low scale. The bold numbers refer to the (MS)SM-like Higgs-field, the italic numbers refer to the dominantly singlet like field.

fields for the comparison with `NMSSMCalc` are depicted in the following for the TP-scenarios together with the value for the on-shell mass for the charged Higgs as obtained with `NMSSMCalc` at the respective order are depicted in tab. B.2. The corresponding results in the MSSM-limit are given in tab. B.3.

TP1

Comparison I at scale Q, $M_{H\pm} = 2751.09$

NMSSMCalc vanilla	$\{121.843, 1797.457, 2747.997\}$
NMSSMCalc α_s^{mod}	$\{116.264, 1797.451, 2747.834\}$
NMSSMCalc $(-)$	$\{116.261, 1797.450, 2747.834\}$
NMSSM-FH α_{G_F}	$\{115.701, 1797.451, 2747.909\}$
NMSSM-FH $\alpha(M_Z)$	$\{116.277, 1797.451, 2747.838\}$
NMSSM-FH $\alpha(M_Z)(-)$	$\{116.262, 1797.451, 2747.840\}$

Comparison II at scale m_t^{OS}, $M_{H\pm} = 2695.70$

NMSSMCalc vanilla	$\{113.452, 1797.462, 2694.140\}$
NMSSMCalc α_s^{mod}	$\{113.755, 1797.543, 2692.842\}$
NMSSMCalc CT mod	$\{113.781, 1797.543, 2692.839\}$
NMSSM-FH α_{G_F}	$\{113.189, 1797.596, 2692.842\}$
NMSSM-FH $\alpha(M_Z)$	$\{113.799, 1797.596, 2692.753\}$
NMSSM-FH $\alpha(M_Z)(-)$	$\{113.783, 1797.596, 2692.755\}$

TP2

Comparison I at scale Q, $M_{H\pm} = 6376.48$

NMSSMCalc vanilla	$\{120.416, 5951.364, 6374.602\}$
NMSSMCalc α_s^{mod}	$\{114.655, 5951.362, 6374.514\}$
NMSSMCalc $(-)$	$\{114.655, 5951.362, 6374.514\}$
NMSSM-FH α_{G_F}	$\{114.123, 5951.363, 6374.593\}$
NMSSM-FH $\alpha(M_Z)$	$\{114.655, 5951.363, 6374.523\}$
NMSSM-FH $\alpha(M_Z)(-)$	$\{114.655, 5951.363, 6374.524\}$

Comparison II at scale m_t^{OS}, $M_{H\pm} = 6343.78$

NMSSMCalc vanilla	$\{-, -, -\}$ (tanchyonic stops)
NMSSMCalc K. Walz	$\{-, -, -\}$ (tanchyonic stops)
NMSSM-FeynHiggs	$\{-, -, -\}$ (tanchyonic stops)
NMSSM-FH α_{G_F}	$\{-, -, -\}$ (tanchyonic stops)
NMSSM-FH $\alpha(M_Z)$	$\{-, -, -\}$ (tanchyonic stops)
NMSSM-FH $\alpha(M_Z)(-)$	$\{-, -, -\}$ (tanchyonic stops)

TP3

Comparison I 1at scale Q, $M_{H\pm} = 639.815$

NMSSMCalc vanilla	$\{91.141, 125.674, 650.870\}$
NMSSMCalc α_s^{mod}	$\{90.240, 123.482, 650.798\}$
NMSSMCalc $(-)$	$\{90.376, 123.664, 650.915\}$
NMSSM-FH α_{G_F}	$\{89.933, 124.142, 650.177\}$
NMSSM-FH $\alpha(M_Z)$	$\{90.178, 123.780, 650.517\}$
NMSSM-FH $\alpha(M_Z)(-)$	$\{90.481, 123.668, 650.900\}$

Comparison II at scale m_t^{OS}, $M_{H\pm} = 634.538$

NMSSMCalc vanilla	$\{89.370, 124.008, 645.337\}$
NMSSMCalc α_s^{mod}	$\{90.195, 124.208, 645.369\}$
NMSSMCalc $(-)$	$\{89.640, 123.479, 644.877\}$
NMSSM-FH α_{G_F}	$\{90.549, 123.387, 645.191\}$
NMSSM-FH $\alpha(M_Z)$	$\{89.813, 123.579, 644.45\}$
NMSSM-FH $\alpha(M_Z)(-)$	$\{90.151, 123.417, 644.818 \}$

TP4

Comparison I at scale Q, $M_{H\pm} = 453.502$

NMSSMCalc vanilla	$\{127.681, 142.370, 465.721\}$
NMSSMCalc α_s^{mod}	$\{126.051, 141.856, 465.572\}$
NMSSMCalc $(-)$	$\{126.226, 141.982, 465.641\}$
NMSSM-FH α_{G_F}	$\{127.131, 141.951, 464.905\}$
NMSSM-FH $\alpha(M_Z)$	$\{126.483, 141.852, 465.231\}$
NMSSM-FH $\alpha(M_Z)(-)$	$\{126.251, 142.095, 465.600\}$

Comparison II at scale m_t^{OS}, $M_{H\pm} = 449.349$

NMSSMCalc vanilla	$\{128.857, 139.075, 461.312\}$
NMSSMCalc α_s^{mod}	$\{128.999, 139.752, 461.348\}$
NMSSMCalc $(-)$	$\{128.001, 139.176, 460.963\}$
NMSSM-FH α_{G_F}	$\{128.248, 139.961, 461.312\}$
NMSSM-FH $\alpha(M_Z)$	$\{128.392, 139.184, 460.487\}$
NMSSM-FH $\alpha(M_Z)(-)$	$\{128.143, 139.433, 460.846\}$

TP5

Comparison I at scale Q, $M_{H\pm} = 614.300$

NMSSMCalc vanilla	$\{120.559, 123.698, 626.088\}$
NMSSMCalc α_s^{mod}	$\{118.168, 122.326, 626.020\}$
NMSSMCalc $(-)$	$\{118.441, 122.538, 625.288\}$
NMSSM-FH α_{G_F}	$\{119.039, 122.291, 625.468\}$
NMSSM-FH $\alpha(M_Z)$	$\{118.841, 122.204, 625.600\}$
NMSSM-FH $\alpha(M_Z)(-)$	$\{118.528, 122.449, 626.283\}$

Comparison II at scale m_t^{OS}, $M_{H\pm} = 614.981$

NMSSMCalc vanilla	$\{118.842, 122.372, 626.460\}$
NMSSMCalc α_s^{mod}	$\{118.800, 122.312, 626.431\}$
NMSSMCalc $(-)$	$\{118.472, 121.811, 625.944\}$
NMSSM-FH α_{G_F}	$\{119.011, 121.778, 626.481\}$
NMSSM-FH $\alpha(M_Z)$	$\{118.277, 122.080, 627.677\}$
NMSSM-FH $\alpha(M_Z)(-)$	$\{119.107, 121.597, 625.869\}$

Table B.2: Two-loop masses of the $\mathcal{CP}$-even Higgs-fields in the TP-scenarios. The masses are given in GeV in the form $\{m_{h_1}, m_{h_2}, m_{h_3}\}$.

TP1 MSSM-limit

Comparison I at scale Q, $M_{H^\pm} = 2751.161$	
NMSSMCalc vanilla	{122.497, 1797.498, 2747.993}
NMSSMCalc α_s^{mod}	{116.951, 1797.498, 2747.830}
NMSSM-FH $\alpha(M_Z)$	{116.951, 1797.498, 2747.835}
NMSSM-FH α_{G_F}	{116.378, 1797.498, 2747.965}

Comparison II at scale m_t^{OS}, $M_{H^\pm} = 2695.188$	
NMSSMCalc vanilla	{114.165, 1771.217, 2694.188}
NMSSMCalc α_s^{mod}	{114.466, 1771.217, 2692.894}
NMSSM-FH $\alpha(M_Z)$	{114.466, 1771.217, 2692.900}
NMSSM-FH α_{G_F}	{113.903, 1771.217, 2962.980}

TP2 MSSM-limit

Comparison I at scale Q, $M_{H^\pm} = 4345.769$	
NMSSMCalc vanilla	{120.401, 2949.576, 4344.175}
NMSSMCalc α_s^{mod}	{114.639, 2949.576, 4344.113}
NMSSM-FH α_{G_F}	{114.107, 2949.576, 4344.161}
NMSSM-FH $\alpha(M_Z)$	{114.639, 2949.576, 4344.119}

Comparison II at scale m_t^{OS}, $M_{H^\pm} =$	
NMSSMCalc vanilla	{−, −, −} (tanchyonic stops)
NMSSMCalc α_s^{mod}	{−, −, −} (tanchyonic stops)
NMSSM-FH α_{G_F}	{−, −, −} (tanchyonic stops)
NMSSM-FH $\alpha(M_Z)$	{−, −, −} (tanchyonic stops)

TP3 MSSM-limit

Comparison I at scale Q, $M_{H^\pm} = 738.595$	
NMSSMCalc vanilla	{102.796, 397.492, 736.464}
NMSSMCalc α_s^{mod}	{99.945, 397.492, 736.360}
NMSSM-FH α_{G_F}	{99.365, 397.492, 736.362}
NMSSM-FH $\alpha(M_Z)$	{99.946, 397.492, 736.360}

Comparison II at scale m_t^{OS}, $M_{H^\pm} = 718.245$	
NMSSMCalc vanilla	{101.680, 379.520, 715.785}
NMSSMCalc α_s^{mod}	{101.823, 379.520, 715.842}
NMSSM-FH α_{G_F}	{101.187, 379.520, 715.851}
NMSSM-FH $\alpha(M_Z)$	{101.823, 379.520, 715.846}

TP4 MSSM-limit

Comparison I at scale Q, $M_{H^\pm} = 541.156$	
NMSSMCalc vanilla	{91.606, 400.000, 541.721}
NMSSMCalc α_s^{mod}	{89.304, 400.000, 541.539}
NMSSM-FH $\alpha(M_Z)$	{89.304, 400.000, 541.539}
NMSSM-FH α_{G_F}	{88.599, 400.000, 541.510}

Comparison II at scale m_t^{OS}, $M_{H^\pm} = 528.181$	
NMSSMCalc vanilla	{90.738, 386.446, 528.400}
NMSSMCalc α_s^{mod}	{90.878, 386.446, 528.459}
NMSSM-FH $\alpha(M_Z)$	{90.878, 386.447, 528.459}
NMSSM-FH α_{G_F}	{90.134, 386.447, 528.433}

TP5 MSSM-limit

Comparison I at scale Q, $M_{H^\pm} = 705.613$	
NMSSMCalc vanilla	{101.848, 393.700, 703.381}
NMSSMCalc α_s^{mod}	{97.633, 393.700, 703.286}
NMSSM-FH $\alpha(M_Z)$	{97.632 393.700, 703.286}
NMSSM-FH α_{G_F}	{97.099, 393.700, 703.287}

Comparison II at scale m_t^{OS}, $M_{H^\pm} = 687.785$	
NMSSMCalc vanilla	{98.794, 372.606, 684.680}
NMSSMCalc α_s^{mod}	{98.977, 372.606, 684.626}
NMSSM-FH $\alpha(M_Z)$	{98.977, 372.606, 684.626}
NMSSM-FH α_{G_F}	{98.395, 372.606, 684.633}

Table B.3: One-loop masses of the $\mathcal{CP}$-even Higgs-fields in the TP-scenarios. The masses are given in GeV in the form $\{m_{h_1}, m_{h_2}, m_{h_3}\}$. The mass that is unaffected by the change of codes is the mass of the decoupled singlet-field.

Bibliography

[1] ATLAS, G. Aad *et al.*, Observation of a new particle in the search for the Standard Model Higgs boson with the ATLAS detector at the LHC, *Phys. Lett.* **B716**, 1 (2012), 1207.7214.

[2] CMS, S. Chatrchyan *et al.*, Observation of a new boson at a mass of 125 GeV with the CMS experiment at the LHC, *Phys. Lett.* **B716**, 30 (2012), 1207.7235.

[3] S. Glashow, Partial Symmetries of Weak Interactions, *Nucl.Phys.* **22**, 579 (1961).

[4] S. Weinberg, A Model of Leptons, *Phys.Rev.Lett.* **19**, 1264 (1967).

[5] A. Salam, Weak and Electromagnetic Interactions, *Conf.Proc.* **C680519**, 367 (1968).

[6] F. Englert and R. Brout, Broken Symmetry and the Mass of Gauge Vector Mesons, *Phys.Rev.Lett.* **13**, 321 (1964).

[7] P. W. Higgs, Broken symmetries, massless particles and gauge fields, *Phys.Lett.* **12**, 132 (1964).

[8] P. W. Higgs, Broken Symmetries and the Masses of Gauge Bosons, *Phys.Rev.Lett.* **13**, 508 (1964).

[9] P. W. Higgs, Spontaneous Symmetry Breakdown without Massless Bosons, *Phys.Rev.* **145**, 1156 (1966).

[10] H. E. Haber and G. L. Kane, The Search for Supersymmetry: Probing Physics Beyond the Standard Model, *Phys. Rept.* **117**, 75 (1985).

[11] H. P. Nilles, Supersymmetry, Supergravity and Particle Physics, *Phys. Rept.* **110**, 1 (1984).

[12] CMS, C. Collaboration, Measurements of the Higgs boson production and decay rates and constraints on its couplings from a combined ATLAS and CMS analysis of the LHC pp collision data at sqrt s = 7 and 8 TeV, (2015).

[13] P. Fayet, Supergauge Invariant Extension of the Higgs Mechanism and a Model for the electron and Its Neutrino, *Nucl. Phys.* **B90**, 104 (1975).

[14] J. R. Ellis, J. F. Gunion, H. E. Haber, L. Roszkowski, and F. Zwirner, Higgs Bosons in a Nonminimal Supersymmetric Model, *Phys. Rev.* **D39**, 844 (1989).

[15] M. Drees, Supersymmetric Models with Extended Higgs Sector, *Int. J. Mod. Phys.* **A4**, 3635 (1989).

[16] C. Panagiotakopoulos and A. Pilaftsis, Higgs scalars in the minimal nonminimal supersymmetric standard model, *Phys. Rev.* **D63**, 055003 (2001), hep-ph/0008268.

[17] U. Ellwanger, C. Hugonie, and A. M. Teixeira, The Next-to-Minimal Supersymmetric Standard Model, *Phys. Rept.* **496**, 1 (2010), 0910.1785.

[18] J. P. Hall and S. F. King, NMSSM+, *JHEP* **01**, 076 (2013), 1209.4657.

[19] M. Maniatis, The Next-to-Minimal Supersymmetric extension of the Standard Model reviewed, *Int. J. Mod. Phys.* **A25**, 3505 (2010), 0906.0777.

[20] W. Porod, SPheno, a program for calculating supersymmetric spectra, SUSY particle decays and SUSY particle production at e+ e- colliders, *Comput. Phys. Commun.* **153**, 275 (2003), hep-ph/0301101.

[21] W. Porod and F. Staub, SPheno 3.1: Extensions including flavour, CP-phases and models beyond the MSSM, *Comput. Phys. Commun.* **183**, 2458 (2012), 1104.1573.

[22] S. P. Martin, Two loop effective potential for a general renormalizable theory and softly broken supersymmetry, *Phys. Rev.* **D65**, 116003 (2002), hep-ph/0111209.

[23] P. Athron, J.-h. Park, D. Stöckinger, and A. Voigt, FlexibleSUSY - A spectrum generator generator for supersymmetric models, *Comput. Phys. Commun.* **190**, 139 (2015), 1406.2319.

[24] U. Ellwanger and C. Hugonie, NMSPEC: A Fortran code for the sparticle and Higgs masses in the NMSSM with GUT scale boundary conditions, *Comput. Phys. Commun.* **177**, 399 (2007), hep-ph/0612134.

[25] F. Domingo, A New Tool for the study of the CP-violating NMSSM, (2015), 1503.07087.

[26] B. C. Allanach, SOFTSUSY: a program for calculating supersymmetric spectra, *Comput. Phys. Commun.* **143**, 305 (2002), hep-ph/0104145.

[27] B. C. Allanach, P. Athron, L. C. Tunstall, A. Voigt, and A. G. Williams, Next-to-Minimal SOFTSUSY, *Comput. Phys. Commun.* **185**, 2322 (2014), 1311.7659.

[28] B. C. Allanach, A. Bednyakov, and R. Ruiz de Austri, Higher order corrections and unification in the minimal supersymmetric standard model: SOFTSUSY3.5, *Comput. Phys. Commun.* **189**, 192 (2015), 1407.6130.

[29] J. Baglio *et al.*, NMSSMCALC: A Program Package for the Calculation of Loop-Corrected Higgs Boson Masses and Decay Widths in the (Complex) NMSSM, *Comput.Phys.Commun.* **185**, 3372 (2014), 1312.4788.

[30] T. Hahn, S. Heinemeyer, W. Hollik, H. Rzehak, and G. Weiglein, High-Precision Predictions for the Light CP -Even Higgs Boson Mass of the Minimal Supersymmetric Standard Model, *Phys. Rev. Lett.* **112**, 141801 (2014), 1312.4937.

[31] M. Frank *et al.*, The Higgs Boson Masses and Mixings of the Complex MSSM in the Feynman-Diagrammatic Approach, *JHEP* **02**, 047 (2007), hep-ph/0611326.

[32] G. Degrassi, S. Heinemeyer, W. Hollik, P. Slavich, and G. Weiglein, Towards high precision predictions for the MSSM Higgs sector, *Eur. Phys. J.* **C28**, 133 (2003), hep-ph/0212020.

[33] S. Heinemeyer, W. Hollik, and G. Weiglein, The Masses of the neutral CP -even Higgs bosons in the MSSM: Accurate analysis at the two loop level, *Eur. Phys. J.* **C9**, 343 (1999), hep-ph/9812472.

[34] S. Heinemeyer, W. Hollik, and G. Weiglein, FeynHiggs: A Program for the calculation of the masses of the neutral CP even Higgs bosons in the MSSM, *Comput. Phys. Commun.* **124**, 76 (2000), hep-ph/9812320.

[35] W. Hollik and S. Paßehr, Higgs boson masses and mixings in the complex MSSM with two-loop top-Yukawa-coupling corrections, *JHEP* **10**, 171 (2014), 1409.1687.

[36] W. Hollik and S. Paßehr, Two-loop top-Yukawa-coupling corrections to the charged Higgs-boson mass in the MSSM, *Eur. Phys. J.* **C75**, 336 (2015), 1502.02394.

[37] T. Hahn, S. Heinemeyer, W. Hollik, H. Rzehak, and G. Weiglein, Prediction of the light CP-even Higgs-Boson Mass of the MSSM: Towards the ILC Precision, in *International Workshop on Future Linear Colliders (LCWS13) Tokyo, Japan, November 11-15, 2013*, 2014, 1404.0186.

[38] B. C. Allanach, A. Djouadi, J. L. Kneur, W. Porod, and P. Slavich, Precise determination of the neutral Higgs boson masses in the MSSM, *JHEP* **09**, 044 (2004), hep-ph/0406166.

[39] F. Staub *et al.*, Higgs mass predictions of public NMSSM spectrum generators, (2015), 1507.05093.

[40] C.-N. Yang and R. L. Mills, Conservation of Isotopic Spin and Isotopic Gauge Invariance, *Phys.Rev.* **96**, 191 (1954).

[41] Particle Data Group, K. Olive *et al.*, Review of Particle Physics, *Chin.Phys.* **C38**, 090001 (2014).

[42] A. Denner, Techniques for calculation of electroweak radiative corrections at the one loop level and results for W physics at LEP-200, *Fortsch.Phys.* **41**, 307 (1993), 0709.1075.

[43] S. Weinberg, *The Quantum Theory of Fields*The Quantum Theory of Fields 3 Volume Hardback Set (Cambridge University Press).

[44] U. Amaldi, W. de Boer, and H. Furstenau, Comparison of grand unified theories with electroweak and strong coupling constants measured at LEP, *Phys. Lett.* **B260**, 447 (1991).

[45] Planck, P. A. R. Ade *et al.*, Planck 2013 results. XVI. Cosmological parameters, *Astron. Astrophys.* **571**, A16 (2014), 1303.5076.

[46] Super-Kamiokande, Y. Fukuda *et al.*, Evidence for oscillation of atmospheric neutrinos, *Phys. Rev. Lett.* **81**, 1562 (1998), hep-ex/9807003.

[47] B. T. Cleveland *et al.*, Measurement of the solar electron neutrino flux with the Homestake chlorine detector, *Astrophys. J.* **496**, 505 (1998).

[48] L. Bergstrom, Saas-Fee Lecture Notes: Multi-messenger Astronomy and Dark Matter, (2012), 1202.1170.

[49] A. D. Sakharov, Violation of CP Invariance, c Asymmetry, and Baryon Asymmetry of the Universe, *Pisma Zh. Eksp. Teor. Fiz.* **5**, 32 (1967), [Usp. Fiz. Nauk161,61(1991)].

[50] S. Dimopoulos and S. Raby, Supercolor, *Nucl. Phys.* **B192**, 353 (1981).

[51] E. Witten, Dynamical Breaking of Supersymmetry, *Nucl. Phys.* **B188**, 513 (1981).

[52] M. Dine, W. Fischler, and M. Srednicki, Supersymmetric Technicolor, *Nucl. Phys.* **B189**, 575 (1981).

[53] S. Dimopoulos and H. Georgi, Softly Broken Supersymmetry and SU(5), *Nucl. Phys.* **B193**, 150 (1981).

[54] N. Sakai, Naturalness in Supersymmetric Guts, *Z. Phys.* **C11**, 153 (1981).

[55] R. K. Kaul and P. Majumdar, Cancellation of Quadratically Divergent Mass Corrections in Globally Supersymmetric Spontaneously Broken Gauge Theories, *Nucl. Phys.* **B199**, 36 (1982).

[56] L. Girardello and M. T. Grisaru, Soft Breaking of Supersymmetry, *Nucl. Phys.* **B194**, 65 (1982).

[57] J. Wess and J. Bagger, *Supersymmetry and supergravity* (, 1992).

[58] H. Goldberg, Constraint on the Photino Mass from Cosmology, *Phys. Rev. Lett.* **50**, 1419 (1983), [Erratum: Phys. Rev. Lett.103,099905(2009)].

[59] J. R. Ellis, J. S. Hagelin, D. V. Nanopoulos, K. A. Olive, and M. Srednicki, Supersymmetric Relics from the Big Bang, *Nucl. Phys.* **B238**, 453 (1984).

[60] G. Gamberini, G. Ridolfi, and F. Zwirner, On Radiative Gauge Symmetry Breaking in the Minimal Supersymmetric Model, *Nucl. Phys.* **B331**, 331 (1990).

[61] S. Dimopoulos and D. W. Sutter, The Supersymmetric flavor problem, *Nucl. Phys.* **B452**, 496 (1995), hep-ph/9504415.

[62] G. D. Kribs, E. Poppitz, and N. Weiner, Flavor in supersymmetry with an extended R-symmetry, *Phys. Rev.* **D78**, 055010 (2008), 0712.2039.

[63] W. Siegel, Supersymmetric Dimensional Regularization via Dimensional Reduction, *Phys. Lett.* **B84**, 193 (1979).

[64] D. Stöckinger, Regularization by dimensional reduction: consistency, quantum action principle, and supersymmetry, *JHEP* **03**, 076 (2005), hep-ph/0503129.

[65] G. 't Hooft and M. J. G. Veltman, Regularization and Renormalization of Gauge Fields, *Nucl. Phys.* **B44**, 189 (1972).

[66] W. Hollik and D. Stöckinger, Regularization and supersymmetry restoring counterterms in supersymmetric QCD, *Eur. Phys. J.* **C20**, 105 (2001), hep-ph/0103009.

[67] D. Stöckinger and P. Varso, FeynArts model file for MSSM transition counterterms from DREG to DRED, *Comput. Phys. Commun.* **183**, 422 (2012), 1109.6484.

[68] W. Hollik and D. Stöckinger, MSSM Higgs-boson mass predictions and two-loop non-supersymmetric counterterms, *Phys. Lett.* **B634**, 63 (2006), hep-ph/0509298.

[69] M. Böhm, A. Denner, and H. Joos, *Gauge Theories of the Strong and Electroweak Interaction* (Vieweg+Teubner Verlag, 2001).

[70] H. Lehmann, K. Symanzik, and W. Zimmermann, On the formulation of quantized field theories, *Nuovo Cim.* **1**, 205 (1955).

[71] P. H. Chankowski, S. Pokorski, and J. Rosiek, Complete on-shell renormalization scheme for the minimal supersymmetric Higgs sector, *Nucl. Phys.* **B423**, 437 (1994), hep-ph/9303309.

[72] S. Heinemeyer, W. Hollik, J. Rosiek, and G. Weiglein, Neutral MSSM Higgs boson production at e+ e- colliders in the Feynman diagrammatic approach, *Eur. Phys. J.* **C19**, 535 (2001), hep-ph/0102081.

[73] E. Fuchs, *Interference effects in new physics processes at the LHC*, PhD thesis, U. Hamburg, Dept. Phys., 2015.

[74] A. Petermann, La normalisation des constantes dans la théorie des quantaNormalization of constants in the quanta theory, *Helv. Phys. Acta* **26**, 499 (1953).

[75] M. Gell-Mann and F. E. Low, Quantum electrodynamics at small distances, *Phys. Rev.* **95**, 1300 (1954).

[76] K. Ender, T. Graf, M. Muhlleitner, and H. Rzehak, Analysis of the NMSSM Higgs Boson Masses at One-Loop Level, *Phys. Rev.* **D85**, 075024 (2012), 1111.4952.

[77] SLD Electroweak Group, DELPHI, ALEPH, SLD, SLD Heavy Flavour Group, OPAL, LEP Electroweak Working Group, L3, S. Schael *et al.*, Precision electroweak measurements on the Z resonance, *Phys. Rept.* **427**, 257 (2006), hep-ex/0509008.

[78] CDF, D0, T. A. Aaltonen *et al.*, Combination of CDF and D0 W-Boson Mass Measurements, *Phys. Rev.* **D88**, 052018 (2013), 1307.7627.

[79] DELPHI, OPAL, LEP Electroweak, ALEPH, L3, S. Schael *et al.*, Electroweak Measurements in Electron-Positron Collisions at W-Boson-Pair Energies at LEP, *Phys. Rept.* **532**, 119 (2013), 1302.3415.

[80] M. Frank *et al.*, Charged Higgs Boson Mass of the MSSM in the Feynman Diagrammatic Approach, *Phys. Rev.* **D88**, 055013 (2013), 1306.1156.

[81] A. Brignole, Radiative corrections to the supersymmetric neutral Higgs boson masses, *Phys. Lett.* **B281**, 284 (1992).

[82] M. Frank, S. Heinemeyer, W. Hollik, and G. Weiglein, FeynHiggs1.2: Hybrid MS-bar / on-shell renormalization for the CP even Higgs boson sector in the MSSM, (2002), hep-ph/0202166.

[83] A. Freitas and D. Stöckinger, Gauge dependence and renormalization of tan beta in the MSSM, *Phys. Rev.* **D66**, 095014 (2002), hep-ph/0205281.

[84] M. Sperling, D. Stöckinger, and A. Voigt, Renormalization of vacuum expectation values in spontaneously broken gauge theories: Two-loop results, *JHEP* **01**, 068 (2014), 1310.7629.

[85] M. Sperling, D. Stöckinger, and A. Voigt, Renormalization of vacuum expectation values in spontaneously broken gauge theories, *JHEP* **07**, 132 (2013), 1305.1548.

[86] A. Brignole, G. Degrassi, P. Slavich, and F. Zwirner, On the O(alpha(t)**2) two loop corrections to the neutral Higgs boson masses in the MSSM, *Nucl. Phys.* **B631**, 195 (2002), hep-ph/0112177.

[87] W. Hollik and S. Paßehr, Two-loop top-Yukawa-coupling corrections to the Higgs boson masses in the complex MSSM, *Phys. Lett.* **B733**, 144 (2014), 1401.8275.

[88] O. Stål, G. Weiglein, and L. Zeune, Improved prediction for the mass of the W boson in the NMSSM, *JHEP* **09**, 158 (2015), 1506.07465.

[89] F. Domingo and T. Lenz, W mass and Leptonic Z-decays in the NMSSM, *JHEP* **07**, 101 (2011), 1101.4758.

[90] T. Hahn, Generating Feynman diagrams and amplitudes with FeynArts 3, *Comput. Phys. Commun.* **140**, 418 (2001), hep-ph/0012260.

[91] F. Staub, SARAH 4 : A tool for (not only SUSY) model builders, *Comput. Phys. Commun.* **185**, 1773 (2014), 1309.7223.

[92] R. Benbrik *et al.*, Confronting the MSSM and the NMSSM with the Discovery of a Signal in the two Photon Channel at the LHC, *Eur. Phys. J.* **C72**, 2171 (2012), 1207.1096.

[93] S. F. King and P. L. White, Resolving the constrained minimal and next-to-minimal supersymmetric standard models, *Phys. Rev.* **D52**, 4183 (1995), hep-ph/9505326.

[94] M. Masip, R. Munoz-Tapia, and A. Pomarol, Limits on the mass of the lightest Higgs in supersymmetric models, *Phys. Rev.* **D57**, R5340 (1998), hep-ph/9801437.

[95] M. E. Machacek and M. T. Vaughn, Two Loop Renormalization Group Equations in a General Quantum Field Theory. 1. Wave Function Renormalization, *Nucl. Phys.* **B222**, 83 (1983).

[96] M. E. Machacek and M. T. Vaughn, Two Loop Renormalization Group Equations in a General Quantum Field Theory. 2. Yukawa Couplings, *Nucl. Phys.* **B236**, 221 (1984).

[97] M. E. Machacek and M. T. Vaughn, Two Loop Renormalization Group Equations in a General Quantum Field Theory. 3. Scalar Quartic Couplings, *Nucl. Phys.* **B249**, 70 (1985).

[98] S. Borowka, T. Hahn, S. Heinemeyer, G. Heinrich, and W. Hollik, Momentum-dependent two-loop QCD corrections to the neutral Higgs-boson masses in the MSSM, *Eur. Phys. J.* **C74**, 2994 (2014), 1404.7074.

[99] S. Agrawal, T. Hahn, and E. Mirabella, FormCalc 7.5, (2012), 1210.2628, [PoSLL2012,046(2012)].

[100] B. Chokoufe Nejad, T. Hahn, J. N. Lang, and E. Mirabella, FormCalc 8: Better Algebra and Vectorization, *J. Phys. Conf. Ser.* **523**, 012050 (2014), 1310.0274.

[101] C. Groß *et al.*, New Developments in FormCalc 8.4,   (2014), 1407.0235, [PoSLL2014,035(2014)].

[102] S. Agrawal, T. Hahn, and E. Mirabella, FormCalc 7, *J. Phys. Conf. Ser.* **368**, 012054 (2012), 1112.0124.

[103] `Mathematica`, http://www.wolfram.com/mathematica/ .

[104] T. Hahn and M. Perez-Victoria, Automatized one loop calculations in four-dimensions and D-dimensions, *Comput. Phys. Commun.* **118**, 153 (1999), hep-ph/9807565.

[105] K. E. Williams, *The Higgs Sector of the Complex Minimal Supersymmetric Standard Model*, PhD thesis, Institute of Particle Physics Phenomenology, Durham University, 2008.

[106] L. Hofer, U. Nierste, and D. Scherer, Resummation of tan-beta-enhanced supersymmetric loop corrections beyond the decoupling limit, *JHEP* **10**, 081 (2009), 0907.5408.

[107] D. Noth and M. Spira, Higgs Boson Couplings to Bottom Quarks: Two-Loop Supersymmetry-QCD Corrections, *Phys. Rev. Lett.* **101**, 181801 (2008), 0808.0087.

[108] S. Heinemeyer, W. Hollik, H. Rzehak, and G. Weiglein, The Higgs sector of the complex MSSM at two-loop order: QCD contributions, *Phys. Lett.* **B652**, 300 (2007), 0705.0746.

[109] M. Mühlleitner, D. T. Nhung, H. Rzehak, and K. Walz, Two-loop contributions of the order $\mathcal{O}(\alpha_t\alpha_s)$ to the masses of the Higgs bosons in the CP-violating NMSSM, *JHEP* **05**, 128 (2015), 1412.0918.

[110] P. Bechtle, O. Brein, S. Heinemeyer, G. Weiglein, and K. E. Williams, HiggsBounds: Confronting Arbitrary Higgs Sectors with Exclusion Bounds from LEP and the Tevatron, *Comput. Phys. Commun.* **181**, 138 (2010), 0811.4169.

[111] P. Bechtle, O. Brein, S. Heinemeyer, G. Weiglein, and K. E. Williams, Higgs-Bounds 2.0.0: Confronting Neutral and Charged Higgs Sector Predictions with Exclusion Bounds from LEP and the Tevatron, *Comput. Phys. Commun.* **182**, 2605 (2011), 1102.1898.

[112] P. Bechtle *et al.*, Recent Developments in HiggsBounds and a Preview of HiggsSignals, *PoS* **CHARGED2012**, 024 (2012), 1301.2345.

[113] P. Bechtle *et al.*, `HiggsBounds − 4`: Improved Tests of Extended Higgs Sectors against Exclusion Bounds from LEP, the Tevatron and the LHC, *Eur. Phys. J.* **C74**, 2693 (2014), 1311.0055.

146

[114] P. Bechtle, S. Heinemeyer, O. Stal, T. Stefaniak, and G. Weiglein, Applying Exclusion Likelihoods from LHC Searches to Extended Higgs Sectors, *Eur. Phys. J.* **C75**, 421 (2015), 1507.06706.

[115] Beyond the Standard Model Working Group, B. C. Allanach *et al.*, Les Houches 'Physics at TeV Colliders 2003' Beyond the Standard Model Working Group: Summary report, in *Physics at TeV colliders. Proceedings, Workshop, Les Houches, France, May 26-June 3, 2003*, pp. 171–289, 2004, hep-ph/0402295.

[116] B. C. Allanach *et al.*, SUSY Les Houches Accord 2, *Comput. Phys. Commun.* **180**, 8 (2009), 0801.0045.

[117] P. Bechtle, S. Heinemeyer, O. Stål, T. Stefaniak, and G. Weiglein, *HiggsSignals*: Confronting arbitrary Higgs sectors with measurements at the Tevatron and the LHC, *Eur. Phys. J.* **C74**, 2711 (2014), 1305.1933.

[118] G. 't Hooft and M. J. G. Veltman, Scalar One Loop Integrals, *Nucl. Phys.* **B153**, 365 (1979).

[119] C. McNeile, C. T. H. Davies, E. Follana, K. Hornbostel, and G. P. Lepage, High-Precision c and b Masses, and QCD Coupling from Current-Current Correlators in Lattice and Continuum QCD, *Phys. Rev.* **D82**, 034512 (2010), 1004.4285.

[120] D. J. Miller, R. Nevzorov, and P. M. Zerwas, The Higgs sector of the next-to-minimal supersymmetric standard model, *Nucl. Phys.* **B681**, 3 (2004), hep-ph/0304049.

[121] H. E. Haber and R. Hempfling, Can the mass of the lightest Higgs boson of the minimal supersymmetric model be larger than m(Z)?, *Phys. Rev. Lett.* **66**, 1815 (1991).

[122] Y. Okada, M. Yamaguchi, and T. Yanagida, Upper bound of the lightest Higgs boson mass in the minimal supersymmetric standard model, *Prog. Theor. Phys.* **85**, 1 (1991).

[123] J. R. Ellis, G. Ridolfi, and F. Zwirner, On radiative corrections to supersymmetric Higgs boson masses and their implications for LEP searches, *Phys. Lett.* **B262**, 477 (1991).

[124] R. Barbieri and M. Frigeni, The Supersymmetric Higgs searches at LEP after radiative corrections, *Phys. Lett.* **B258**, 395 (1991).

[125] G. Degrassi and P. Slavich, On the radiative corrections to the neutral Higgs boson masses in the NMSSM, *Nucl. Phys.* **B825**, 119 (2010), 0907.4682.

[126] U. Ellwanger, Radiative corrections to the neutral Higgs spectrum in supersymmetry with a gauge singlet, *Phys. Lett.* **B303**, 271 (1993), hep-ph/9302224.

[127] T. Elliott, S. F. King, and P. L. White, Radiative corrections to Higgs boson masses in the next-to-minimal supersymmetric Standard Model, *Phys. Rev.* **D49**, 2435 (1994), hep-ph/9308309.

[128] T. Fritzsche *et al.*, The Implementation of the Renormalized Complex MSSM in FeynArts and FormCalc, *Comput. Phys. Commun.* **185**, 1529 (2014), 1309.1692.

[129] K. G. Chetyrkin, J. H. Kuhn, and M. Steinhauser, RunDec: A Mathematica package for running and decoupling of the strong coupling and quark masses, *Comput. Phys. Commun.* **133**, 43 (2000), hep-ph/0004189.

[130] A. Djouadi, The Anatomy of electro-weak symmetry breaking. II. The Higgs bosons in the minimal supersymmetric model, *Phys. Rept.* **459**, 1 (2008), hep-ph/0503173.

[131] M. D. Goodsell, K. Nickel, and F. Staub, Two-loop corrections to the Higgs masses in the NMSSM, *Phys. Rev.* **D91**, 035021 (2015), 1411.4665.

[132] U. Ellwanger, J. F. Gunion, and C. Hugonie, NMHDECAY: A Fortran code for the Higgs masses, couplings and decay widths in the NMSSM, *JHEP* **02**, 066 (2005), hep-ph/0406215.

[133] U. Ellwanger and C. Hugonie, NMHDECAY 2.0: An Updated program for sparticle masses, Higgs masses, couplings and decay widths in the NMSSM, *Comput. Phys. Commun.* **175**, 290 (2006), hep-ph/0508022.

[134] S. F. King, M. Muhlleitner, and R. Nevzorov, NMSSM Higgs Benchmarks Near 125 GeV, *Nucl. Phys.* **B860**, 207 (2012), 1201.2671.

[135] P. Z. Skands *et al.*, SUSY Les Houches accord: Interfacing SUSY spectrum calculators, decay packages, and event generators, *JHEP* **07**, 036 (2004), hep-ph/0311123.

[136] H. Baer, J. Ferrandis, K. Melnikov, and X. Tata, Relating bottom quark mass in DR-BAR and MS-BAR regularization schemes, *Phys. Rev.* **D66**, 074007 (2002), hep-ph/0207126.

[137] Y. Nambu, Quasiparticles and Gauge Invariance in the Theory of Superconductivity, *Phys.Rev.* **117**, 648 (1960).

[138] J. Goldstone, Field Theories with Superconductor Solutions, *Nuovo Cim.* **19**, 154 (1961).

[139] J. Goldstone, A. Salam, and S. Weinberg, Broken Symmetries, *Phys.Rev.* **127**, 965 (1962).

[140] C. Becchi, A. Rouet, and R. Stora, The Abelian Higgs-Kibble Model. Unitarity of the S Operator, *Phys.Lett.* **B52**, 344 (1974).

[141] C. Becchi, A. Rouet, and R. Stora, Renormalization of the Abelian Higgs-Kibble Model, *Commun.Math.Phys.* **42**, 127 (1975).

[142] C. Becchi, A. Rouet, and R. Stora, Renormalization of Gauge Theories, *Annals Phys.* **98**, 287 (1976).

[143] L. Faddeev and V. Popov, Feynman Diagrams for the Yang-Mills Field, *Phys.Lett.* **B25**, 29 (1967).

[144] R. Haag, J. T. Lopuszanski, and M. Sohnius, All Possible Generators of Supersymmetries of the s Matrix, *Nucl.Phys.* **B88**, 257 (1975).

[145] J. Wess and B. Zumino, Supergauge Invariant Extension of Quantum Electrodynamics, *Nucl.Phys.* **B78**, 1 (1974).

[146] W. Hollik, E. Kraus, and D. Stöckinger, Renormalization of supersymmetric Yang-Mills theories with soft supersymmetry breaking, *Eur. Phys. J.* **C23**, 735 (2002), hep-ph/0007134.

[147] W. Hollik *et al.*, Renormalization of the minimal supersymmetric standard model, *Nucl. Phys.* **B639**, 3 (2002), hep-ph/0204350.

[148] D. R. T. Jones, Asymptotic Behavior of Supersymmetric Yang-Mills Theories in the Two Loop Approximation, *Nucl. Phys.* **B87**, 127 (1975).

[149] D. R. T. Jones and L. Mezincescu, The Beta Function in Supersymmetric Yang-Mills Theory, *Phys. Lett.* **B136**, 242 (1984).

[150] P. C. West, The Yukawa beta Function in N=1 Rigid Supersymmetric Theories, *Phys. Lett.* **B137**, 371 (1984).

[151] N. N. Bogoliubov and D. V. Shirkov, *Introduction to the Theory of Quantized Fields* (Interscience Publishers, 1959), Volume 3, S. 225.

[152] K. Melnikov and T. v. Ritbergen, The Three loop relation between the MS-bar and the pole quark masses, *Phys. Lett.* **B482**, 99 (2000), hep-ph/9912391.

[153] G. Degrassi, P. Slavich, and F. Zwirner, On the neutral Higgs boson masses in the MSSM for arbitrary stop mixing, *Nucl. Phys.* **B611**, 403 (2001), hep-ph/0105096.

Acknowledgements

First I would like to thank my supervisor Georg Weiglein for his support, encouragement, detailed explanations and motivating discussions during the years of my PhD.

I thank Géraldine Servant, who kindly agreed to review my dissertation, and Jan Louis, Peter Schleper and Thomas Konstandin for being the referees in my examination committee.

I also thank Sven Heinemeyer for regular support and discussions about the subject of my thesis. For a fruitful (and ongoing) collaboration I thank the team of `NMSSMCalc` and especially Ramona Gröber, who provided the many necessary adaptions and results of `NMSSMCalc` that were needed to facilitate a detailed comparison between both our codes.

During the years at DESY it was a pleasure to work alongside many inspiring colleagues. I gratefully acknowledge helpful physics discussions with Stefan Liebler (aka "The good-hearted Soul of Building 1"), Alexander Voigt, Florian Domingo, Lisa Zeune, Sebastian Paßehr, Emanuele Bagnaschi, Wolfgang Hollik (jr.), Martin Vollmann, Gregor Mittag, Alessandra Cagnazzo and Elina Fuchs. During the years I enjoyed the social and professional contact to my fellow PhD students in and around my office, amongst them Shireen Gangal, Marco Tonini, Christian Weiss, Ibrahim Akal, Markus Ebert, So Young Shim and Shruti Patel. Special thanks are also deserved by Pa-Olo Gunnellini.

Also, I thank the QCD-community amongst my former and present colleagues that provides a competitive environment for any researcher interested in physics beyond the standard model as well as a different point of view to the field, amongst them Frank Tackmann, Jonathan Gaunt, Andrew Papanastasiou and Maximilian Stahlhofen.

My heartfelt thanks go to my grandfather and my father for their constant support and to my sister. It is a great pleasure for me to be able to thank all of you together in my thesis. Last but definitely not least I thank Zarah for seemingly endless conversations and moral support as well as the insight that Z denotes so much more than a fundamental particle in nature.

Erklärung

Hiermit erkläre ich an Eides statt, dass ich die vorliegende Dissertationsschrift selbst verfasst und keine anderen als die angegebenen Quellen und Hilfsmittel benutzt habe.

Peter Drechsel
Hamburg, den 27.11.2015